

AD \_\_\_\_\_

Award Number: W81XWH-10-1-0767

TITLE: A Partnership Training Program: Studying Targeted Drug  
Delivery Using Nanoparticles in Breast Cancer Diagnosis and Therapy

PRINCIPAL INVESTIGATOR: Paul C. Wang, Ph.D.

CONTRACTING ORGANIZATION: Howard University  
Washington, DC 20059

REPORT DATE: October 2014

TYPE OF REPORT: Annual Summary Report 09/15/13-09/14/14

PREPARED FOR: U.S. Army Medical Research and Materiel Command  
Fort Detrick, Maryland 21702-5012

DISTRIBUTION STATEMENT:

X Approved for public release; distribution unlimited

The views, opinions and/or findings contained in this report are those of the author(s) and should not be construed as an official Department of the Army position, policy or decision unless so designated by other documentation.

REPORT DOCUMENTATION PAGE				Form Approved OMB No. 0704-0188	
Public reporting burden for this collection of information is estimated to average 1 hour per response, including the time for reviewing instructions, searching existing data sources, gathering and maintaining the data needed, and completing and reviewing this collection of information. Send comments regarding this burden estimate or any other aspect of this collection of information, including suggestions for reducing this burden to Department of Defense, Washington Headquarters Services, Directorate for Information Operations and Reports (0704-0188), 1215 Jefferson Davis Highway, Suite 1204, Arlington, VA 22202-4302. Respondents should be aware that notwithstanding any other provision of law, no person shall be subject to any penalty for failing to comply with a collection of information if it does not display a currently valid OMB control number. <b>PLEASE DO NOT RETURN YOUR FORM TO THE ABOVE ADDRESS.</b>					
1. REPORT DATE October 2014		2. REPORT TYPE Annual Summary		3. DATES COVERED 15 Sep 2013 - 14 Sep 2014	
4. TITLE AND SUBTITLE A Partnership Training Program: Studying Targeted Drug Delivery Using Nanoparticles in Breast Cancer Diagnosis and Therapy				5a. CONTRACT NUMBER	
				5b. GRANT NUMBER W81XWH-10-1-0767	
				5c. PROGRAM ELEMENT NUMBER	
6. AUTHOR(S) Paul C. Wang, Ph.D.  E-Mail: pwang@howard.edu				5d. PROJECT NUMBER	
				5e. TASK NUMBER	
				5f. WORK UNIT NUMBER	
7. PERFORMING ORGANIZATION NAME(S) AND ADDRESS(ES)  Howard University  Washington, DC 20059				8. PERFORMING ORGANIZATION REPORT NUMBER	
9. SPONSORING / MONITORING AGENCY NAME(S) AND ADDRESS(ES)  U.S. Army Medical Research and Materiel Command Fort Detrick, Maryland 21702-5012				10. SPONSOR/MONITOR'S ACRONYM(S)	
				11. SPONSOR/MONITOR'S REPORT NUMBER(S)	
12. DISTRIBUTION / AVAILABILITY STATEMENT  Approved for Public Release; Distribution Unlimited					
13. SUPPLEMENTARY NOTES					
14. ABSTRACT In the fourth year of this training grant, 11 faculty, 6 postdocs, 9 graduate and 1 undergraduate students from 7 departments at the Howard University have been trained in using nanoparticles as targeted drug delivery vehicles for cancer diagnosis and therapy. 25 seminars and workshops in cancer, molecular imaging, and nanomedicine have been offered. The trainees have received hands-on training in nanotechnology, MRI and optical imaging, cell biology lab techniques, and small animal handling. We implemented a new NMR method to measure kinetics of chemical exchange of ligand-target complex in solid tumor for pharmacokinetic modeling. We generated a humanized bivalent scFv-derived, DT390-based recombinant immunotoxin, which exhibited high cytotoxicity and anti-tumor efficacy against cancer cells. 16 research projects utilized the Nanomedicine Core. We published 7 research papers and review articles on nanotechnology in cancer research. Nanomedicine Core users have submitted 10 grant applications, and received two new NIH grants. The Core continued to be a synergy center drawing multidisciplinary research using nanotechnology for cancer research.					
15. SUBJECT TERMS Training, Nanotechnology, Breast Cancer, Diagnosis, Therapy, Imaging, Drug Delivery					
16. SECURITY CLASSIFICATION OF:			17. LIMITATION OF ABSTRACT	18. NUMBER OF PAGES	19a. NAME OF RESPONSIBLE PERSON
a. REPORT	b. ABSTRACT	c. THIS PAGE			USAMRMC
U	U	U	UU	128	19b. TELEPHONE NUMBER (include area code)

## Table of Contents

	<u>Page</u>
Cover.....	1
SF 298.....	2
Table of Contents.....	3
Introduction.....	4
Body.....	4
Key Research Accomplishments.....	16
Reportable Outcomes.....	17
Conclusion.....	19
References.....	21
Appendices.....	22

## **A Partnership Training Program – Studying Targeted Drug Delivery Nanoparticles in Breast Cancer Diagnosis and Therapy**

### **I. INTRODUCTION**

In this program, we proposed to establish a Nanomedicine Core to train faculty and students at Howard University to pursue molecular imaging of breast cancer using nanoparticles as targeted drug delivery vehicles. This is a partnership with the Johns Hopkins University In Vivo Cellular Molecular Imaging Center and the Nanotechnology Characterization Lab at NCI-Frederick. At Howard University, this partnership involves a multidisciplinary consortium of four departments: Radiology, Radiation Oncology, Molecular Biology and Biochemistry, and Electrical Engineering. The program has two components, a research component and a broad training component. The Howard University trainees will obtain training through collaborative research and by participation in a broad based training program. Renowned experts in nanomedicine and molecular imaging will participate in the training through mentoring research, seminars, workshops, and by offering laboratory internships. This transfer of nanomedicine techniques will support ongoing, long-term breast cancer research at Howard University. The major goal is to provide faculty trainees and their students at Howard with updated nanomedicine techniques to apply to independent breast cancer research, thus enhancing their ability to educate the next generation of scientists. The program objectives are:

1. Train new researchers in breast cancer using modern nanomedicine techniques.
2. Offer lectures, seminars, workshops, and laboratory internships in nanotechnology and molecular imaging.
3. Conduct two proposed research projects.
4. Establish a Nanomedicine Core to support long-term sustainable research.
5. Research concept development and submission of competitive grants in breast cancer imaging.

### **II. BODY**

Molecular imaging and functional MRI continue to provide new insights into the etiology, diagnosis, and treatment of breast cancer. In clinic, these methods have made a significant impact in breast cancer diagnosis and in monitoring response to therapy. As our understanding of breast cancer advances, we further recognize the complexities of this disease and the urgent need for individualized characterization and treatment. Recent exciting advances in the application of MR methods for breast cancer research have resulted from the development of contrast agents (CAs) that generate receptor-targeted or molecular-targeted contrast. Targeted CAs can be directed to cell surface receptors using antibodies [1, 2] or ‘smart’ agents activated by specific enzymes, or based on the expression of detectable reporters [3, 4]. These molecular imaging capabilities, in combination with the strong functional imaging capabilities of MR methods, allow molecular-functional characterization of cancer and the physiological microenvironment of tumors [5]. Non-invasive MR can play an important role in the molecular-functional characterization of breast cancer for detection, drug delivery, development of therapeutics, and monitoring of treatment response. Lately, the development of nanotechnology has also had a dramatic impact on diagnosis and treatment [6-8]. Among many possible applications of nanotechnology in medicine, the use of various nanomaterials as pharmaceutical delivery systems for drugs, DNA, and imaging agents has gained increasing attention. Many nanoparticle-based drug delivery and drug targeting systems have been approved by FDA or are under development [9-11]. Their use aims to minimize drug degradation, prevent undesirable side effects, and increase drug bioavailability and the fraction of drug dosage delivered to the pathological area.

In order to achieve the goals of this training program, we have proposed conducting two research projects and a broad-based training program to train researchers at Howard University in the field of the application of nanotechnology in targeted drug delivery. In conjunction with these activities, we also proposed establishing a University Nanomedicine Core to promote and facilitate campus-wide research and training. The following progress report is a summary of the accomplishments for the third year in the areas: (i) research, (ii) training, (iii) establishment of Nanomedicine Core, and (iv) alignment with the Statement of Work.

## **II.1. Research Projects**

**Project 1:** Study the physicochemical characteristics of nanoparticles as MR contrast agent delivery system with the dynamic contrast enhancement pattern for clinical applications

In the first three years of this grant, we have made liposome (Lip) with transferrin (Tf) as ligand on the surface. This transferrin labeled liposome (Tf-Lip) has demonstrated to be preferentially targeted to MD-MB-231 breast cancer cells both in vitro and in vivo. We have used these liposomes loaded with gadolinium (Gd) based MRI contrast agent (CA) in a dynamic contrast enhancement (DCE) study of solid tumor. The MRI image of tumors using transferrin targeted liposome (Tf-Lip-CA) versus liposome without transferrin (Lip-CA) showed very distinct image enhancement patterns. The MRI image enhancement by Tf-Lip-CA is much faster than by Lip-CA. The enhancement pattern is heterogeneous throughout the solid tumor and correlates well with the level of transferrin receptor expression in the cancer cells, shown by histological findings. Cancer cells with high levels of transferrin receptors, such as the fast proliferating cancer cells usually located at the outer regions of tumor showed faster and stronger enhancement. The enhancement pattern and liposome endocytosis process varies depending on liposome size. In order to study the endocytosis process of the liposome, we have implemented a pharmacokinetic model to analyze the MRI image enhancement pattern.

Pharmacokinetic parameters often used in DCE-MRI pharmacokinetic analysis include extracellular extravascular space (EES), volume transfer constant between EES and blood plasma, EES volume, blood plasma volume, rate constant from EES to blood plasma, rate constant from blood plasma to EES, rate constant from EES to cancer cells, and rate constant from cancer cells to EES. However, the methodological implementation in pharmacokinetics analysis has been highly variable, leading to multiple challenges in data quality. One of the challenges is the size distribution of liposome used in the study. This year, we have made great efforts to perfecting the liposome fabrication method in order to construct well characterized liposomes with a narrow size distribution for targeted drug delivery. Utilizing the well-defined liposomes of different sizes, we will study the differences in cell uptake of Tf-Lip-CA in solid tumor.

### **Liposome Preparation and Reduction of Size Distribution**

#### **Liposome Preparation**

We have used a thin-film hydration method for liposome preparation [12]. Various lipid components (DPPC, DSPE-PEG, and cholesterol) were first mixed in chloroform. The chloroform was then removed by nitrogen gas using a rotary evaporator resulting in a thin lipid film. The lipid film was hydrated with buffer under agitation to form liposomes. The liposomes at this stage were large and had a wide distribution of sizes. The heterogeneous liposomes were repeatedly extruded through a series of 200, 100, 80, 50, and 30 nm polycarbonate membrane filters to create smaller liposomes, with the size of the resulting liposome depending on the combination of filters used. Sonification was applied to

further break down liposomes to smaller sizes before 50 and 30 nm extrusion. The liposomes were then conjugated with PEG to prolong blood circulation [13].

The size of the liposomes was determined by dynamic light scattering (DLS). For an example, five different groups of liposomes, varying in size from 50 to 170 nm, were produced using the extrusion method (Figure 1). The relative standard deviation (RSD) of liposome size was in the range of 20-30%, suggesting a relatively large size distribution in each group, which may lead to poor quality DCE data and mask the subtle differences in image enhancement patterns of different size liposomes. A narrow size distribution will be critical for studying the size dependence of targeted liposome uptake in solid tumors.

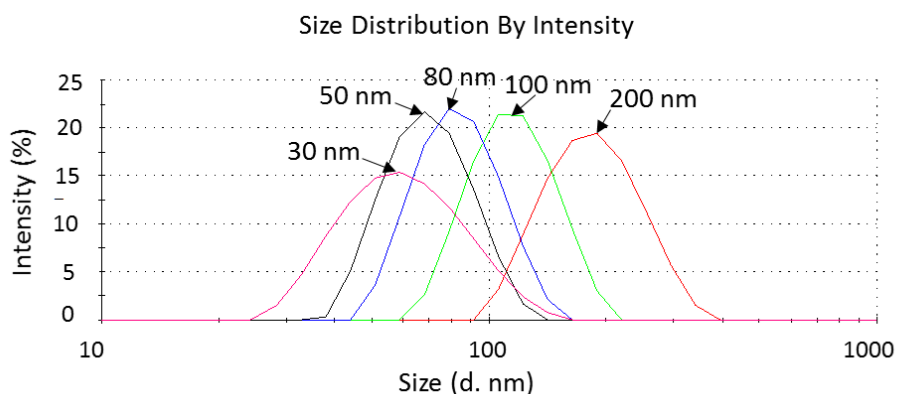


**Figure 1.** Liposome size measurement. Liposomes were made using the extrusion method. Each group of liposomes is labeled with membrane filter size. The size measurement is intensity weighted.

DLS is a commonly used technique for measuring particle size in colloidal suspensions [14]. The DLS-measured particle size, known as z-average size, is a scattered light intensity weighted mean size of the particle ensemble. The measured size is biased toward the larger-size particles in the distribution. In order to confirm the size distribution measurement of our liposomes, we are planning to use cryo-transmission electron microscopy (cryo-TEM) at the University of Maryland College Park to confirm the liposome size distribution and to check the accuracy of DLS measurement.

### Reduction of Size Distribution

In order to narrow down the size distribution of liposomes created with the extrusion method, we are developing a size exclusion chromatography (SEC) method to separate liposome of different sizes. This method has been shown effectively producing liposomes with well-defined size [15]. In the meantime, we are also implementing a relatively new microfluidic flow-focusing method to produce liposomes with a very narrow size distribution [16]. This method consists of a fast central flow containing lipid in an alcohol solution, which intersects from both sides by aqueous buffer solutions (Figure 2). When these three flows merge into a central microchannel, the alcohol and lipids diffuse into the aqueous buffer solution. As the alcohol solution is diluted to a critical concentration, the lipids assemble spontaneously to form liposomes. This microfluidic method enables a controlled formation of liposomes size ranging from about 50 to 150 nm in diameter, with RSDs from ~10% for smaller liposome to ~20% for larger liposome [17]. These liposome size distribution will be much narrower than the size distribution currently acquired using the extrusion method.

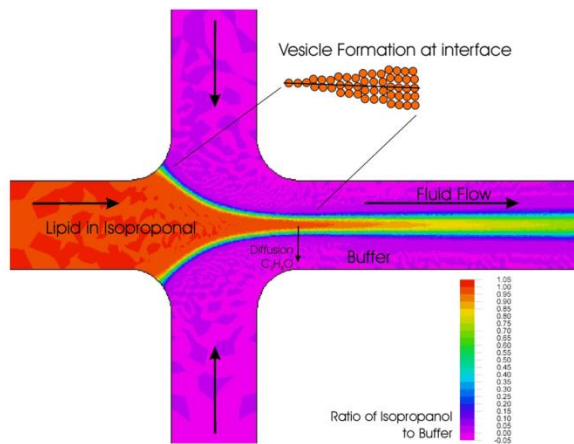


**Figure 2.** Schematic of liposome formation in a microfluidic channel. Andreas Jahn. 2008. *Controlled liposome formation and solute encapsulation with continuous-flow microfluidic hydrodynamic focusing*. (Doctoral dissertation)

## NMR Study of Tf Binding Process in Solid Tumor

Nuclear magnetic resonance (NMR) has long been used in drug discovery to study ligand-target binding process. The methods of detection of ligand binding fall into two main categories: probing the NMR chemical shift signals of protein, and probing the relaxation rates of ligand in the free or bound states. These NMR methods are capable of probing the dynamic properties of ligand-target binding in solution on a defined timescale. However, these methods are not applicable to study ligand-target binding in solid tumor due to the lack of notable differences in NMR chemical shift between the bound and free states, resulting in overlapping peaks caused by broad line widths.

We proposed a new NMR method that utilizes a distinguished compartmental model to measure chemical exchange kinetics in a complex in vivo solid tumor environment. This method involves acquiring a series of Carr-Purcell-Meiboom-Gill (CPMG) measurements and processing the data using two different analyses (nonnegative least squares (NNLS), and transverse relaxation dispersion). The combined strategy allows investigating dynamic ligand binding processes that are inaccessible to conventional NMR methods. To test the validity of this approach, we have used a simple tryptophan binding to serum albumin model to detect the interconversion in a two-site exchange system. 6-fluoro-DL-tryptophan (6F-TRP) was dissolved in 0.05M HCl at room temperature to make a 45-mM stock solution. Bovine serum albumin (BSA) was then dissolved in the 6F-TRP stock to prepare a 1.13-mM BSA/ 45-mM 6F-TRP mixed solution for characterization of chemical exchange process between the free and BSA-bound states of 6F-TRP. To mimic a condition in which macromolecules cannot penetrate cellular barriers, such as cytoplasmic membranes, semi-permeable dialysis membranes (8-10 kD MWCO) were implemented to separate the BSA/6F-TRP mixed solution from the 6F-TRP solution. All the samples were separately placed in 5-mm NMR tubes for  $^{19}\text{F}$  transverse relaxation experiments.  $^{19}\text{F}$  NMR data were measured with a 9.4T Bruker NMR.  $T_2$  relaxation data were collected using a spectroscopic CPMG pulse sequence. The  $^{19}\text{F}$   $T_2$  relaxation decays were acquired with a sufficient number of transients, repetition time of 10s, and echo-spacing  $2\tau_{\text{CPMG}}$  varying from 0.2 to 25 ms in 19 steps. The acquired  $^{19}\text{F}$  transverse relaxation decays were introduced into the multiexponential  $T_2$  relaxation analysis by using the NNLS algorithm equipped with the Tikhonov regularization (detailed in the submitted manuscript):

$$\sum_{n=1}^N \left| \sum_{m=1}^M A_{nm} S_m - y_n \right|^2 + \mu \left| \sum_{m=1}^M S_m \right|^2 \quad [1]$$

The NNLS approach makes no *a priori* assumptions about the number of relaxation components present. A minimum energy constraint, i.e. a Tikhonov regularization of second kind in our study, is imposed into

the function to lessen the impact of noise on the curve fitting and to permit generation of a continuous  $T_2$  distribution. Given the  $\chi^2$  misfit defined as

$$\chi^2 = \sum_{n=1}^N (\sum_{m=1}^M A_{nm} S_m - y_n)^2 / \sigma_n^2 \quad [2]$$

, which is the sum of variances of the prediction errors divided by the standard deviation of  $y_n$ , a nonnegative set of  $S_m$  was obtained by performing regularization of NNLS fits, in which an appropriate value of the regularizer  $\mu$  was selected for an optimal condition that the  $\chi^2$  misfit value from the regularized fit was 100.5% of the non-regularized  $\chi^2$ .

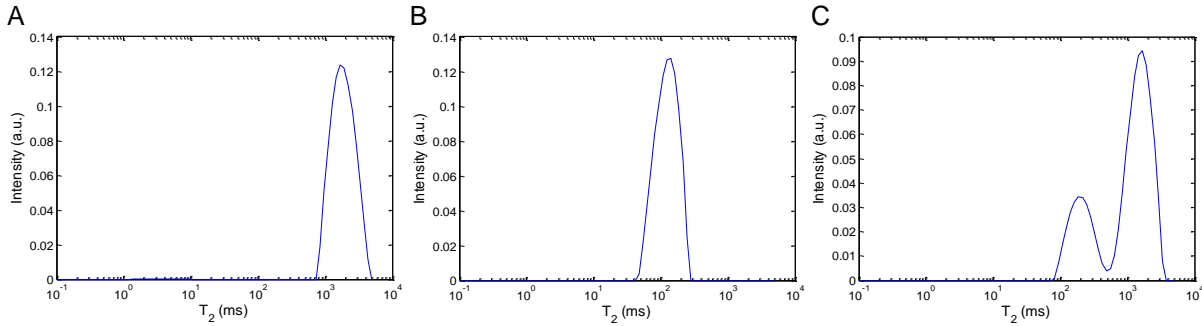


**Figure 3.**  $T_2$  distributions obtained from NNLS analysis of  $^{19}\text{F}$  transverse relaxation curves measured in the (A) 6F-Trp, (B) BSA/ 6F-Trp mixed, and (C) 6F-Trp and BSA/ 6F-Trp mixed bilayer solutions.

The typical  $T_2$  distribution result shown in Fig. 3 demonstrated that the NNLS analysis is capable of detecting signals from the intracellular and extracellular compartments, which was mimicked by using the dialysis membrane to separate the protein-ligand mixture from the ligand-only solution in this study (Fig. 3C). The  $T_2$  distributions containing two distinct peaks in Fig. 3C were identified and verified through examining the  $T_2$  distributions of 6F-TRP solution (Fig. 3A) and BSA/6F-TRP mixed solution (Fig. 3B), respectively. Figure 4 shows the transverse relaxation dispersions collected in the free 6F-Trp, the free/bound exchanging 6F-Trp and their associated fitted curves. The curves fitted to the relaxation dispersion data using the slow exchange model (Eq. 1) are displayed in dashed lines, while those using the skewed population approximation model (Eq. 2) are solid lines. The slow exchange model depicting the blue, dashed curve estimated  $\delta\omega = 1231 \pm 155$  Hz (or  $3.27 \pm 0.41$  ppm) in the BSA/6F-Trp mixed solution, compared with the BSA-bound 6F-Trp resonance of a 3.45-ppm drift from the free peak observed in the  $^{19}\text{F}$  spectra. In addition, the skewed population approximation depicting the blue, solid curve provided the estimates of  $k_{\text{ex}} = 249.8 \text{ s}^{-1}$ , spin populations = 97.54% (free 6F-Trp) and 2.46% (BSA-bound 6F-Trp), respectively, for the BSA/6F-Trp mixed solution, referring to the dissociation constant  $K_D = 912 \text{ }\mu\text{M}$ , compared with spin population = 97.49 to 97.65% (free 6F-Trp) and 2.51 to 2.35% (BSA-bound 6F-Trp) calculated from the dissociation constants  $K_D = \sim 10$  to  $3000 \text{ }\mu\text{M}$  reported in literature. Here we have demonstrated that the fitting of the multiexponential- $T_2$ -analysis-derived CPMG relaxation dispersions were sensibly comparable to the results in previous studies using other different methods.



This work, accomplished by using the analysis of multicomponent  $T_2$  relaxation data as well as the CPMG relaxation dispersion analysis, demonstrates the ability to initiate the study of the targeting efficiency of liposome in vivo and the examination of Tf-liposome biodistribution under the same physiological condition as the DCE MRI study. By monitoring the  $^{31}\text{P}$  NMR relaxation radiating from the cationic lipid 1,2-dioleoyl-*sn*-glycero-3-phosphoethanolamine, we expect to see a change in the  $T_2$  relaxation time of  $^{31}\text{P}$  nuclei when Tf-liposome nanoparticles attach TfR.

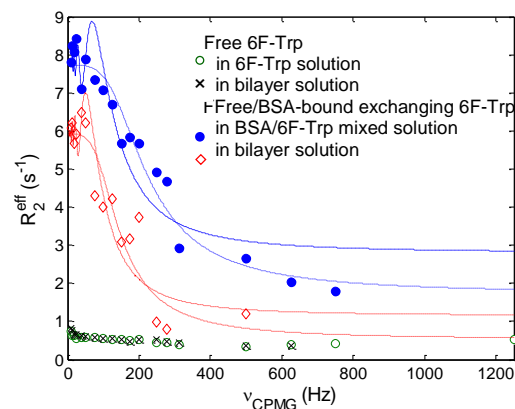


**Figure 4:** The transverse relaxation dispersions collected in the free 6F-Trp and the free/bound exchanging 6F-Trp

**Project 2:** Development of Multifunctional Nanoparticles for Breast Cancer Diagnosis and Treatment – Using Anti-VEGFR-2 Immunotoxin as Dual Purpose Ligand and Chemotherapeutics as Encapsulated payload

Angiogenesis is a vital process for tumor development, growth and metastasis and this process involves various proangiogenic factors, forming a complex interacting network. Among these factors are vascular endothelial growth factor receptor (VEGFR), epidermal growth factor receptor (EGFR), and prostate-specific membrane antigen (PSMA). Studies have shown that EGFR is overexpressed and mutated (EGFR variant III or EGFRvIII) in almost all types of cancer, especially in those arising from the brain, breast, head and neck, lung and prostate. EGFR signaling promotes not only cancer cell growth, but also angiogenesis by inducing other proangiogenic factors such as VEGF and interleukin-8. PSMA has also been shown to be universally expressed in the neovasculature of most types of nonprostate cancers including breast cancer. PSMA regulates angiogenesis by modulating integrin signal transduction. High expression of EGFR, EGFRvIII, and PSMA and their critical roles in tumor growth and angiogenesis make them extremely attractive targets to develop targeted imaging and therapy against tumor angiogenesis and tumor growth.

### Generation of a Bispecific Bivalent Recombinant Immunotoxin (RIT) against Tumors with EGFR and EGFRvIII Expression

Anti-EGFR monoclonal antibodies (mAbs) and tyrosine kinase inhibitors (TKIs) have been developed and investigated intensively in an attempt to develop EGFR-targeted therapy of various types of cancer. However, only mAbs have to date demonstrated a certain degree of survival improvement for a small subset of patients. Results with reversible and irreversible TKIs are generally disappointing. Continued development of mAbs is facing formidable challenges, especially with the dose-limiting side effects induced by their binding with the EGFR expressed in normal tissues, and with the innate and acquired resistance associated with up-regulation of ligands to compete with mAbs for receptor binding, persistent activation of downstream signaling through multiple interacting pathways, and EGFR mutations.

Table 1. IC<sub>50</sub> of DT390-BiscFv806

Cell lines	Tumor type	IC <sub>50</sub> (M)
U87	GMB	1.5 × 10 <sup>-9</sup>
U87-ED4	GMB	4.6 × 10 <sup>-14</sup>
JHU-29	HNSCC	1.2 × 10 <sup>-9</sup>
JHU-13	HNSCC	3.8 × 10 <sup>-10</sup>
JHU-11	HNSCC	1.9 × 10 <sup>-8</sup>
JHU-19	HNSCC	1.0 × 10 <sup>-9</sup>
JHU-22	HNSCC	1.3 × 10 <sup>-7</sup>
JHU-6	HNSCC	2.1 × 10 <sup>-8</sup>

GMB: glioblastoma multiforme; HNSCC: head and neck squamous cell carcinoma

By capitalizing on the unique specificity to the overexpressed EGFR and EGFRvIII in cancer, and humanization-derived benefits of the mAb806, we generated a bivalent RIT, designated as DT390-BiscFv806, by fusing an engineered diphtheria toxin (DT) fragment (DT390) with the humanized mAb806-derived bivalent single-chain variable fragment (biscFv) *via* amino acid linkers. DT390-BiscFv806 was produced with a DT-resistant *Pichia* expression system. They were purified following a four-step scheme: diafiltration, capture by hydrophobic chromatography, borate anion exchange chromatography, and anion exchange chromatography. The purity of the final product was >95%. NuPAGE 4-12% gel electrophoresis and Superdex 200 size-exclusion chromatography revealed a single band and a major peak, respectively, with a size of ~97 kDa.

We then tested the cytotoxicity of DT390-BiscFv806 against a group of cancer cell lines (Table 1). Cytotoxicity studies showed that DT390-BiscFv806 was highly cytotoxic although the half maximal inhibitory concentration (IC<sub>50</sub>) was different against different cancer cell lines (Table 1). The IC<sub>50</sub> of DT390-BiscFv806 was measured to be 1.5 × 10<sup>-9</sup> M and 4.6 × 10<sup>-14</sup> M for U87 and EGFRvIII-transfected U87-EGFRvIII cells, respectively. Notably, DT390-BiscFv806 had four orders of magnitude more potency against the U87-EGFRvIII cells than against the parental U87 cells.

The IC<sub>50</sub> of DT390-BiscFv806 varied among the six HNSCC cell lines and there was a good correlation between the IC<sub>50</sub> and the EGFR expression levels. The HuBiscFv-DT390 exhibited the highest cytotoxicity against the JHU-13 cells with an IC<sub>50</sub> of 3.8 × 10<sup>-10</sup> M (Table 1). The JHU-6 cells that had the least EGFR expression showed the least sensitivity to the HuBiscFv-DT390 with an IC<sub>50</sub> of 2.4 × 10<sup>-7</sup> M.

We further evaluated the antitumor efficacy of DT390-BiscFv806 in established U87-EGFRvIII and U87 animal xenograft tumor models (Fig. 5). The tumor growth was inhibited significantly by systemic administration of DT390-BiscFv806 with a mean percentage tumor growth inhibition (%TGI) of 76.3% (ranging from 59.8%-96.2%) and 59.4% (ranging from 31.5%-76.0%), respectively.

A manuscript regarding the generation of DT390-BiscFv806 and studies on its anti-tumor efficacy has been prepared and submitted to the journal, Clin Cancer Res, for publication.

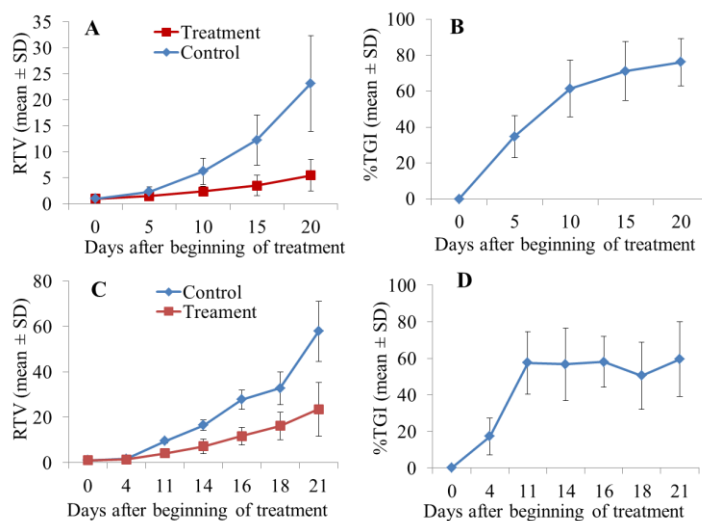


**Figure 5** Growth inhibition of established tumor xenografts by DT390-BiscFv806. 1A and 1C represent the changes of the relative tumor volume (RTV) of U87-EGFRvIII and U87 tumor xenografts, respectively, at different times after beginning of treatment. 1B and 1D show the changes of the %TGI of U87-EGFRvIII and U87 xenografts, respectively, at different times after beginning of treatment.

## Engineered Antibody Fragments for PSMA-targeted Imaging

The high specificity of antibodies, along with the potential of imparting molecular specificity into existing imaging modalities, makes them extremely attractive for molecular imaging. Because of their dependence on a specific antigen target, antibodies are more suitable for imaging cancers with slow growth rate and low metabolic activity such as prostate cancer. However, two major issues form a critical barrier for their use in tumor imaging. One is the long circulation time (few days to weeks in blood), which requires at least 1-2 days after administration to reach a clear and specific tumor/background tissue contrast. Another is the poor tumor tissue penetration, imposed by the large molecular size of antibodies, binding-site barrier, and high tumor interstitial pressure. As a result, the contrast enhancement is suboptimal, same-day imaging is unachievable, and to date, only a small group of antibodies have been approved for clinical imaging.

Because of the common issues of antibodies, great efforts have been made to generate antibody fragments. The most critical aspect in antibody engineering is generating antibody fragments with high functional activity in high quantity and purity. This project is designed to develop a novel PSMA-specific platform of engineered antibody fragments for molecular imaging of prostate cancer. The project is formulated on the hypotheses: 1) engineered fragments could serve as a platform to develop imaging agents, such as PET and optical imaging agents, with high sensitivity and specificity to cancers that overexpress PSMA; and 2) engineered fragments will enable imaging on the same day as administration, in contrast to antibodies.

In the initial studies, we engineered three formats of PSMA-targeted antibody fragments: a single-chain variable fragment (scFv, 27 kDa), a bivalent tandem scFv (biscFv, 54.6 kDa), and a bivalent scFv fold-back diabody (scfbDb, 54.6 kDa), capitalizing on the high specificity of J591 antibody against the extracellular domain of PSMA. The scFv contained one  $V_L$  and one  $V_H$  joined by a 15 amino acid linker ((G<sub>4</sub>S)<sub>3</sub>), while the biscFv had two identical scFvs. The long linker allows for proper folding and dimerization of the  $V_L/V_H$  within the same scFv to form the binding sites. Different from the scFv and biscFv, the scfbDb consisted of two scFvs bridged by optimized lengths of GS linkers. The fold-back structure of scfbDb was formed by preventing dimer formation between the  $V_L/V_H$  within the same scFv by reducing the  $V_L/V_H$  linker to five residues (G<sub>4</sub>S), while permitting interactions between the distal and proximal  $V_L/V_H$  domains from different scFv by placing a longer linker ((G<sub>4</sub>S)<sub>3</sub>) between the two scFv.

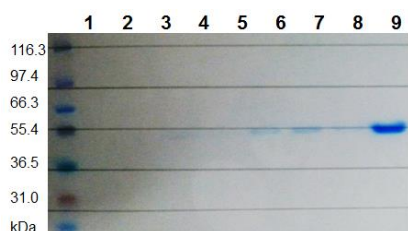


**Figure 6** shows the non-reducing SDS-PAGE electrophoresis of the fold-back diabody as a representative of the fragments. Each lane represents the eluted scfbDb with different concentrations of NaCl from an anion exchange column. The scfbDb in lane 9 is the product used for studies.

Competition assay showed that the binding affinity of scfbDb was 7-fold and 2.5-fold higher than that of biscFv and scFv, respectively. The scfbDb was confirmed for its ability to efficiently mediate the entry of the toxin moiety, DT390, to the cytosol of PSMA-expressing LNCaP cells, but not to PSMA-absent PC-3 cells under confocal microscopy. Optical imaging studies with the fluorescently labeled scfbDb are ongoing in animal models of cancer.

## II.2. Broad Based Training Components

The Molecular Imaging Laboratory has regular bi-weekly group meetings, journal clubs, and

seminars. Some seminars have been arranged through webinars sponsored by imaging vendors, giving the Howard University community the opportunity to attend seminars given by experts from around the world, followed by very productive and fruitful local discussions. The group meetings engage participants in discussing the current status of research projects, analyzing any experimental issues of the current research, reviewing progress, and exchanging ideas, and have been the primary mode of interaction between Howard researchers and collaborating experts. The faculty trainees have also attended seminars at JHU ICMIC. The HU and JHU partnership leaders have been coordinating the training efforts through meetings and emails. Through participation in the Imaging Core-sponsored seminars and workshops, and interaction with Imaging Core staff, a multidisciplinary nanomedicine research community has been established and many fruitful exchanges of research ideas generated. Significant common synergies of interests have been identified, and much multidisciplinary research collaboration has developed. This year, the Molecular Imaging Lab has continued to provide didactic training for Howard researchers. The Molecular Imaging Lab has offered a series of NMR/MRI Lectures and Hands-on Training, and also has supported staff to attend a NIH FAES graduate nanomedicine course and a NIST workshop on standards for the advancement of optical medical imaging.

This year, there were two new faculty members using the facility to conduct research in the nanomedicine field due to the establishment of the Nanomedicine Core through this funding support. In total, there were 11 faculty members from 7 departments and 11 scientists from the other institutions, including Children's National Medical Center, Johns Hopkins, Fu Jen University, and Angimmune, who used the core facility to conduct 16 research projects. Six postdoctoral fellows, 9 graduate students and 1 undergraduate student worked with principle investigators on various research projects. Two graduate students graduated this year and received PhD degrees. The faculty trainees and postdocs of the program have submitted grants to NIH, CDMRP, and NSF together with partnership leaders. We believe that trainees engaged in this training program gain the interdisciplinary knowledge and skills they need to lead multidisciplinary research in the area of nanomedicine. The seminars and workshops organized at Howard University, as well as at other institutions, are listed as following:

#### Seminars and workshops

1. RTRN Research Resources Spotlight Webinar Series - Howard University Imaging Core Facility: Molecular Imaging Laboratory. Paul Wang, September 26, 2013
2. Molecular Fluorescent Imaging Guided Cancer Resection – From Bench to Bedside. Sammuel Achlefu, Johns Hopkins/Radiology, October 9, 2014
3. Measuring Renal Oxygenation in a Mouse Model of Volume-Dependent Hypertension using BOLD MRI. Darah Wright, November 20, 2013
4. Utilizing Multispectral Optoacoustic Tomography (MOST) for Imaging and Assessment of Tumor Growth, Angiogenesis and Therapeutic Intervention (webinar). Neal Burton , January 28, 2014
5. Understanding Underlying Mechanism of ICP-OES and ICP-MS (Thermo Scientific webinar). Anneorie Bogerts, January 29, 2014
6. Maglib Quantification by MRI. Zhenjiang Zhang, February 28, 2014
7. Glioblastoma Multiform – Building the Gap Diagnosis and Treatment (Bruker Biospin Corp webinar), March 18, 2014
8. Nanomedicine. NIH FAES Graduate course, weekly classes, March 24 – May 25, 2014
9. Targeting Vasculature in Inflammatory Bowel Disease (VisualSonics webinar), March 27, 2014
10. Multifunctional Nanoparticles: Applications in Cancer Therapy and Diagnostics. Mohanmmed Shukoor, May 19, 2014
11. PMSA-Based Imaging and Therapy. Ying Chen, Johns Hopkins/Radiology, May 28, 2014
12. Water Exchange – Key Parameter for MRI Contrast Agent Design. Yunkou Wu, June 23, 2014

13. ICP-MS Techniques in Nanoparticle Analysis: Fundamentals, Challenges, and Prospectives (Spectroscopy Magazine webinar), Jorg Bettmer, June 25, 2014
14. Basic NMR Theory, PC Lin, July 23, 2014
15. Chemical Shifts and Coupling Constants, PC Lin, July 25, 2014
16. NMR Instrumentation, PC Lin, July 28, 2014
17. NMR Data Acquisition and Processing, PC Lin, July 31, 2014
18. NMR Dynamics, PC Lin, August 4, 2014
19. NMR Lab – Practice, Stephen Lin, August 7, 2014
20. Fourier Transform and MR Imaging Principles, PC Lin, August 11
21. Post-Imaging Processing Practice, PC Lin, August 14, 2014
22. MRI Imaging Lab Practice (I), P Wang, August 21, 2014
23. Advanced Imaging Techniques, P Wang, August 25, 2014
24. MRI Imaging Practice (II), P Wang, August 28, 2014
25. NIST Workshop on Standards for the Advancement of Optical Medical Imaging. NIST, Gaithersburg, August 26-26, 2014

### **II.3. Nanomedicine Core**

It is essential for Howard University to establish a basic infrastructure that is capable of supporting a sustainable long-term research program in the field of molecular imaging of breast cancer and nanomedicine. In continuing to improve its infrastructure, the University Imaging Core has obtained a NIH Supplement grant, which will be used to pay for installation and moving costs associated with replacing an aging 4.7T MRI machine with a newer 7T MRI machine. In order to seek support beyond the current grant, the University Imaging Core, together with Computational Biology and Bioinformatics Core, and Proteomics Core, has applied for and received new funding from the NIH/RCMI (Research Centers for Minority Institutions) program. The Nanomedicine Core is part of the University Imaging Core facility. This funding will support a major portion of the operation costs and staff salary for the Imaging Core for the next 5 years. This year, a presentation on the Nanomedicine Core and University Imaging Core facility was given at the National Academies' Review of Army Research Laboratory (ARL) Programs that Support Historically Black Colleges and Universities and Minority Institutions (HBCU/MI), sponsored by the ARL. The Core's equipment and research activities were presented to provide the committee feedback on how HBCU/MI have used ARL funds to enhance science, technology, engineering and mathematics (STEM) programs in their institutions.

Howard University Health Sciences has implemented a Research Strategy Plan that sets the direction of the university biomedical research with emphasis on health disparities research. This plan embraces new research disciplines such as proteomics, computational biology, nanomedicine and genomics. To execute the University Research Strategy Plan and its commitment to nanomedicine research, the University is constructing a new Interdisciplinary Research Building, to be completed in late 2014, in which there will be a designated space for Nano biomedical imaging research. The designated lab space is for nanomaterial fabrication with ultrastructure imaging and analytical instrument for physicochemical characterization of nanoparticles, molecular biology labs with incubators and hoods for cell culture and flow cytometry, and imaging suites for confocal microscope. The University has also budgeted funds for purchasing a PET/SPECT/CT machine for small animal imaging research. These new lab space and facilities will further enhance nanomedicine and breast cancer research capabilities at Howard University.

While maintaining state-of-the-art infrastructure is critical to providing researchers with tools to perform the proposed researched projects, it is equally important to provide a broader research training experience for faculty and students. The Nanomedicine Core continues to offer training opportunities through seminar series, instrumentation workshops, and didactic lectures. The Nanomedicine Core staff has helped researchers in experimental design, conducting imaging experiments, and analyzing data. In the 4<sup>th</sup> year of this training program, we continued to expand the user base of the Nanomedicine Core to pursue multidisciplinary biomedical research. There are 16 research projects that have been supported by the Nanomedicine Core, including projects in the initial phase of research. This year, we added one new project, liposome as drug delivery vehicle for head and neck cancer. We have recruited Dr. Zhenjiang Zhang, a chemist, from Chinese National Center for Nanosciences and Nanotechnology as a postdoc trainee. Dr. Zhang has a strong background in biochemistry and medicinal chemistry. He has developed mesoporous silica nanorods coated with gold (Au@SiO<sub>2</sub>) as a multifunctional platform for cancer diagnosis and treatment. He is working on perfecting the liposome fabrication and liposome-ligand conjugation processes.

#### **II.4. Statement of Work Summary**

The accomplishments aligned with the Statement-of-Work occurred in this reporting period is listed as following:

##### Research Component

- Task 1. To conduct Research Project 1 “Study the physicochemical characteristics of nanoparticles as MR contrast agent delivery system with the dynamic contrast enhancement pattern for clinical applications” (months 1-48).
- a. Purchase supplies for cell culture and materials for nanoparticles (months 1-2) (completed).
  - b. Construct liposome (Lip) nanoparticles with transferrin (Tf) as the ligand and encapsulated Gd-based MRI contrast agent (CA) inside as payload (months 3-9) (completed).
  - c. Characterize the physicochemical properties of nanoparticles, including size distribution, surface charge, encapsulation efficiency, and Tf linkage on the surface. Some of the measurements will be done at NCL, NCI-Frederick (months 6-12) (in progress).
  - d. Study targeting efficiency of the liposome nanoparticle using MDA-MB-231 cells. Study the interactions of nanoparticles with breast cancer cells (months 13-24) (completed).
  - e. Study the correlation of the dynamic contrast enhancement (DCE) pattern with the distribution of Tf-liposome nanoparticles in tumor xenografts. Both MR and optical imaging will be used (30 mice) (months 25-36) (in progress).
  - f. Evaluate the potential clinical applications of the DCE pattern, focusing on the relationship between the DCE pattern and the tumor features of TfR expression level, permeability of neovasculatures, vascular density, tumor growth and necrosis (months 25-40) (in progress).
  - g. Data analysis and preparation of manuscripts for publication (months 40-48) (in progress).
- Task 2. To conduct Research Project 2 “Develop multifunctional nanoparticles for breast cancer diagnosis and treatment – using anti-VEGFR-2 immunotoxin as dual purpose ligand and chemotherapeutics as encapsulated payload” (months 1-48).
- a. Purchase supplies and prepare for the study (months 1-2) (completed).

- b. Define the efficacy of the anti-murine anti-VEGFR-2 immunotoxin in endothelial cell killing and vascular permeability increase in animal models (months 3-18) (completed).
  - c. Construct and characterize the targeted anti-VEGFR-2 immunotoxin multifunctional nanoparticles. Some of the work will be done at NCL (months 13-18) (completed).
  - d. Determine the biodistribution, pharmacokinetics and toxicity of the nanoparticles in healthy mice (8) and mice bearing with tumor xenografts (22). Optical imaging will be used. Measurements of biodistribution will be done at NCL and HNF (months 19-40) (completed).
  - e. Define the synergistic effects of the targeted delivery, anti-angiogenics and chemotherapeutics in breast cancer animal models. Histological staining will be used to study the tumor vasculature (months 25-40) (in progress).
  - f. Data analysis and preparation of manuscripts for publication (months 40-48) (in progress).
- Task 3. Research concept development and submission of competitive grants in breast cancer targeted imaging and therapy (months 37-48) (in progress).

#### Broad Training Component

- Task 4. Provide opportunities to the faculty trainees in Howard University to update knowledge of nanomedicine (months 1-48) (in progress for all tasks).
- a. Biweekly group meetings at the Molecular Imaging Lab (months 1-48)
  - b. Monthly Seminar series at Howard University Cancer Center to be presented by the mentors and invited speakers (months 1-48).
  - c. Johns Hopkins University ICMIC Seminar Series organized by Dr. Bhujwalla (months 1-48).
  - d. To attend the biweekly Nanobiology Program Seminar Series at NCI-Frederick organized by Dr. Blumenthal (months 1-48).
  - e. Annual scientific meetings with mentors and trainees.
- Task 5. Train Howard faculty in advanced nanomedicine lab techniques (in progress for all tasks).
- a. Laboratory internships at the Johns Hopkins University and NCL, topics include molecular imaging and nano characterization techniques, 2-4 days each (months 1-36).
  - b. Workshop series. Topics include MR and optical imaging, SEM/TEM/AFM, optical instrumentation, drug design and liposome (months 1-48).
- Task 6. Administrative and communication affairs (coordinated by Drs. Wang and Bhujwalla) (Months 1-48) (in progress for all tasks).
- a. Status reports (quarterly and annual reports)
  - b. Research progress review (quarterly)
  - c. Administrative meetings (biannually meetings)
  - d. Coordination of seminars, workshops, and laboratory internships

### III. KEY RESEARCH ACCOMPLISHMENTS

- Constructed liposomes ranging in size from 50 to 170 nm using thin film hydration with polycarbonate membrane filters. The liposome size relative standard deviation was 20-30%.
- Implemented a new NMR method that utilizes a distinguished compartmental model to measure chemical exchange kinetics in a complex in vivo solid tumor environment.
- Generated a humanized bivalent scFv-derived, DT390-based recombinant immunotoxin, DT390-BiscFv806, capitalizing the unique specificity of antibody mAb806 against EGFR and EGFRvIII overexpressed in cancer but not the EGFR in normal tissue.
- Demonstrated that our novel recombinant immunotoxin DT390-BiscFv806 exhibited high cytotoxicity and anti-tumor efficacy against the cancer cells either with EGFR expression alone or with EGFR and EGFRvIII co-expression, indicating that DT390-BiscFv806 is highly promising for treatment of cancers arising from the brain, head and neck, lung, breast, and prostate.
- Construct three formats of J591 antibody fragments: single-chain variable fragment (scFv), bivalent tandem scFv (biscFv), and bivalent scFv diabody (scfbDb) in fold-back structure for cancer imaging.
- Demonstrated that the fold-back structure of scfbDb has an increased efficiency of target binding and toxin delivery to target cells, compared with other formats.
- Designed a simple and highly sensitive sensing nanosystem for the detection of Hg<sup>2+</sup> and Cu<sup>2+</sup> based on fluorescence quenching of ultrasmall DNA-Ag NCs.
- Constructed small gold nanoparticles to study size-dependent penetration ability and the potential applications of for intranucleus delivery.
- Found that gold nanoparticles smaller than 10 nm can enter the nucleus, whereas larger ones (10 - 16 nm) can only be found in the cytoplasm.
- Reviewed the evolution of immunotoxin development, the challenges of immunotoxin therapy for human solid tumors, and the potential strategies to overcome these challenges in literature.
- Reviewed literature pertaining to the development, characterization and applications of nanoparticles in cancer imaging and therapy.
- Reviewed literature pertaining to mechanisms of membrane trafficking in drug-resistant cancer cells and the development of nanoparticles as drug delivery platforms to overcome drug resistance. Published a review article.



#### IV. REPORTABLE OUTCOMES

##### Publications

1. Xue X, Hall HD, Zhang Q, Wang PC, Gottesman MM, Liang XJ. Nanoscale Drug Delivery Platforms Overcome Platinum-Based Resistance in Cancer Cells Due to Abnormal Membrane Protein Trafficking. *ACS Nano* vol.7 (12)10452-10464, 2013.
2. Shan L, Liu Y, Wang PC. Recombinant Immunotoxin Therapy of Solid Tumors: Challenges and Strategies. *J. Basic Clin Med* 2(2):1-6, 2013.
3. Lin PC, Lin S, Wang PC, Sridhar R. Techniques for Physicochemical Characterization of Nanomaterials. *Biotechnol Adv.* (4):711-726, 2014.
4. Li SL, Cao WP, Kumar A, Jin SB, Zhao YY, Zhang CQ, Zou GZ, Wang PC, Li F, Liang XJ. Highly Sensitive Simultaneous Detection of Mercury and Copper Ions by Ultrasmall Fluorescent DNA-Ag Nanoclusters *New J. Chem* 38(4):1546-1550, 2014
5. Jin SB, Li SL, Wang CX, Liu J, Yang XL, Wang PC, Zhang X, Liang XJ. Biosafe Nanoscale Pharmaceutical Adjuvant Materials. *J Biomed Nanotechnology* (10)1-27, 2014
6. Huo S, Jin S, Ma X, Xue X, Yang K, Kumar A, Wang PC, Zhang J, Hu Z, Liang XJ. Ultrasmall Gold Nanoparticles as Carriers for Nucleus-Based Gene Therapy Due to Size-Dependent Nuclear Entry. *ACS Nano* 8(6):5852-5862, 2014.
7. Yang KN, Zhang CQ, Wang W, Wang PC, Zhou JP, Liang XJ. pH-Responsive Mesoporous Silica Nanoparticles Applied in Controlled Drug Delivery Systems for Cancer Treatment. *Cancer Biol Med.* 11(1):34-43, 2014.

##### Presentations

1. Wright D, Lin S, Lin PC, Wu CS, Zhang D, Duerinckx A, Wang PC, Lee DL. Measuring Renal Oxygenation in a Mouse Model of Volume-Dependent Hypertension using BOLD MRI. Radiological Society of Northern America, Chicago, IL, Dec 1-6, 2013.
2. Wang PC. Molecular Imaging and Nanoparticles as Drug Delivery Vehicles. Industrial Technology Research Institute, HsiChu, Taiwan, Dec.10. 2013.
3. Wang PC, Magnetic Resonance Imaging: Principles and Instrumentation. Fu Jen University Department of Electrical Engineering, Taipei, Taiwan, Dec. 11, 2013
4. Wang PC. Introduction of Howard University Molecular Imaging laboratory. Fu Jen University Medical School, Taipei, Taiwan, Dec 13, 2013.
5. Wang PC. Howard University Imaging Core Facility. The National Academies Committee on Review of Army Research Laboratory (ARL) Programs Support Historically Black Colleges and Universities and Minority Institutions (HBCUs/MIs), Washington, DC, Feb 24, 2014.
6. Zhang Z, Wang J, Nie X, Chen C, Wang PC. Near Infrared Laser Mediated Targeted Tumor Thermo-chemotherapy Using Thermosensitive Polymer Coated Gold Nanoparticles. Howard University Research Day 2014. Washington DC. April 4, 2014.
7. Shan L, Lin S, Lin PC, Zhang Z, Liu Y, Wang PC. Engineered Antibody Fragments and Immunotoxin for Targeted Imaging and Therapy of Prostate Cancer. Howard University Research Day 2014. Washington DC. April 4, 2014.
8. Lin S, Shan L, Lin PC, Zhang Z, Gu X, Wang PC. Construction of Transferrin Receptor-targeted Multimodality Agents for Cancer Imaging. Howard University Research Day 2014. Washington DC. April 4, 2014.
9. Wang PC. Howard University Biomedical Core Facility. Howard University Research Day 2014. Washington DC. April 4, 2014

10. Zhang Z, Wang J, Nie X, Chen C, Wang PC. Near Infrared Laser Mediated Targeted Tumor Thermo-chemotherapy Using Thermosensitive Polymer Coated Gold Nanoparticles. Howard University Radiology Imaging Symposium. Washington DC. May 6, 2014.
11. Shan L, Lin S, Lin PC, Zhang Z, Liu Y, Wang PC. Engineered Antibody Fragments and Immunotoxin for Targeted Imaging and Therapy of Prostate Cancer. Howard University Radiology Imaging Symposium. Washington DC. May 6, 2014.
12. Lin S, Shan L, Lin PC, Zhang Z, Gu X, Wang PC. Construction of Transferrin Receptor-targeted Multi-modality Agents for Cancer Imaging. Howard University Radiology Imaging Symposium. Washington DC. May 6, 2014.
13. Wang PC. Molecular Imaging Laboratory. Howard University Radiology Imaging Symposium. Washington DC. May 6, 2014.

## Grants

- |     |  |   |                                |
|-----|--|---|--------------------------------|
| 1.  | NIH/NCRR/RCMI/2  | G12RR003048   | 03/01/14-05/31/19              |
|     | Biomedical Infrastructure for Health Disparities Research  |   | Southerland (PI); Wang (co-PI) |
|     | Biomedical Imaging Care Facility (Role: Core Facility PI)  |   | \$ 2,009,920                   |
| 2.  | NIH/NCRR/RCMI – Administrative Supplement  |   | 04/01/14-03/31/15              |
|     | Biomedical Infrastructure for Health Disparities Research  |   | Southerland (PI); Wang (co-PI) |
|     | Request Support of Moving and Reinstallation Charges for a 7 T MRI Machine   |   | \$ 193,826                     |
| 3.  | NIH/NIBIB  | Mentored Clinical Scientist Development Award (K08) |                                |
|     | Prussian blue nanoconstructs for imaging and therapy of aggressive pediatric brain tumors  |   |                                |
|     | Rohan Fernandes (Children’s Nat Med Centr, PI) Paul Wang (mentor) (10/01/13 submitted, not funded)   |   |                                |
| 4.  | DoD University Research Instrumentation Program (DURIP)  |   |                                |
|     | Enhancement of STEM research and training through multiphoton confocal imaging   |   |                                |
|     | Eva Polston (PI, Howard/Physiology and Biophysics); Wang (co-PI) (10/20/13 submitted, not funded)  |   |                                |
| 5.  | NSF  |   |                                |
|     | pH-Sensitive Nanoparticulate MRI Agent with Enhanced Contrast and Reduced Side Effects   |   |                                |
|     | Tongxin Wang (PI, Howard/School of Engineering), Paul Wang (co-PI) (10/21/13 submitted; not funded)  |   |                                |
| 6.  | NIH  |   |                                |
|     | Novel Nanotechnology Platform for Breast Cancer Treatment  |   |                                |
|     | Emmanuel Akala (PI, Howard/Pharmaceutical Science). Paul Wang (co-PI) (1/14/14 submitted; not funded)  |   |                                |
| 7.  | NIH  |   |                                |
|     | Engineered Antibody Fragments for PSMA-targeted Imaging and Therapy  |   |                                |
|     | Liang Shan (PI, Howard/Radiology), Paul Wang (co-PI) (02/15/14 submitted; not funded)  |   |                                |
| 8.  | NIH  |   |                                |
|     | Howard University Blueprint Program for Enhancing Neuroscience Diversity through Undergraduate Research Education Experiences (HU BP-ENDURE) |   |                                |
|     | Evaristus Nwulia (Howard/Psychiatry, PI), Paul Wang (co-PI) (05/23/14 submitted, not funded)   |   |                                |
| 9.  | NSF  |   |                                |
|     | pH-Sensitive Nanoparticulate MRI Agent with Enhanced Contrast and Reduced Side Effects   |   |                                |
|     | Tongxin Wang (PI, Howard/ Engineering), Paul Wang (co-PI) (10/21/13 submitted; not funded)   |   |                                |
| 10. | DoD W81XWH-14-L  |   |                                |
|     | A humanized bivalent fold-back recombinant immunotoxin for prostate cancer therapy   |   |                                |

Liang Shan (PI, Howard/Radiology), (09/15/21014 submitted, pending)

### Degrees

1. Belinda Hauser (Nanomedicine Core predoctoral trainee) received a Ph.D. degree in Genetics. Thesis title: Epidermal Growth Factor Receptor (EGFR) Associated Head and Neck Squamous Cell Carcinoma (HNSCC) Tumorigenesis.
2. Whitney Barfield (Nanomedicine Core predoctoral trainee) received a Ph.D. degree in Microbiology. Thesis title: Osteopontin Genotype as a Determinant of Skeletal Muscle Remodeling – In vivo and in vitro studies show complex transcriptional regulation influencing muscle inflammation.

## **V. CONCLUSIONS**

This year, we have made liposomes ranging in size from 50 to 170 nm using a thin film hydration combined with membrane filter method. The relative standard deviation of liposome size was in the 20-30% range. In the coming year, we will use a microfluidic channel device to improve the liposome size distribution. A narrow size distribution will be critical for studying the size dependence of targeted liposome uptake in solid tumors. For studying pharmacokinetics and targeting efficiency of liposome in solid tumor using DCE imaging data, we have implemented a distinguished compartmental model to measure ligand-target chemical exchange kinetics in a complex in vivo environment.

By capitalizing on the unique specificity of antibody mAb806 against EGFR and EGFRvIII overexpressed in cancer but not the EGFR in normal tissue, and by further taking the mAb806 humanization-derived benefits, we generated a humanized bivalent scFv-derived, DT390-based recombinant immunotoxin, DT390-BiscFv806. This novel RIT exhibited high cytotoxicity and anti-tumor efficacy against the cancer cells either with EGFR expression alone or with EGFR and EGFRvIII co-expression. The results indicate that DT390-BiscFv806 is highly promising for treatment of cancers arising from the brain, head and neck, lung, breast, prostate, and others. To develop a PSMA-targeted platform of engineered antibody fragments for cancer imaging, we constructed three formats of antibody fragments including single-chain variable fragment (scFv), bivalent tandem scFv (biscFv), and bivalent scFv diabody (scFvDb) in fold-back structure, leveraging the high specificity of J591 antibody against the extracellular domain of PSMA. Initial studies showed that the fold-back structure of scFvDb resulted in an increased efficiency of target binding and toxin delivery to target cells, compared with other formats. The favorable properties of the fold-back diabody in pharmacology make it attractive as a springboard to develop imaging agents for cancer and cancer angiogenesis imaging.

We have designed a simple and highly sensitive sensing nanosystem for the detection of Hg<sup>2+</sup> and Cu<sup>2+</sup> based on fluorescence quenching of ultrasmall DNA-Ag NCs. We have constructed small gold nanoparticles to study size-dependent penetration ability and the potential applications of for intranuclear delivery. We found gold nanoparticles smaller than 10 nm can enter the nucleus, whereas larger ones (10 - 16 nm) can only be found in the cytoplasm. We have reviewed literature and written an article on the development, characterization and applications of nanoparticles in cancer imaging and therapy. We have also written a review on the challenges of immunotoxin therapy for human solid tumors, and the potential strategies to overcome these challenges (Appendix 2).

For the broad training component, faculty members, and graduate and undergraduate students from different departments at Howard University have been trained in the use of nanoparticles as targeted drug delivery vehicles for cancer diagnosis and therapy. A total of 25 seminars and webinars, workshops and symposia in cancer, molecular imaging and nanomedicine have been offered in addition to the biweekly group meetings. The Imaging Core also has offered a series of NMR/MRI Lectures and

hands-on training for the trainees. Training activities were coordinated by partnership leaders from Howard and John Hopkins Universities to help participants gain useful interdisciplinary knowledge and skills to conduct breast cancer research using nanotechnology. There are 11 faculty members from 7 departments and 11 scientists from the other institutions, including Children's National Medical Center, Johns Hopkins, Fu Jen University, and Angimmune, who use the core facility to conduct these research projects. There is 1 undergraduate student, 9 graduate students and 6 postdoctoral fellows working with principle investigators on various research projects. Two graduate students graduated this year and received PhD degrees. We have recruited a new chemist postdoc trainee to work on perfecting liposome fabrication and liposome-ligand conjugation processes. This year, we added one new project that uses liposome as drug delivery vehicle for head and neck cancer.

The faculty trainees and postdocs of the program have submitted grants to NIH, CDMRP, and NSF together with the partnership leaders. We have received a new five years NIH/RCMI grant to support the University Imaging Core. We also have received a NIH Supplement grant for installing a new 7T MRI machine. The university has designated a lab space in a new Interdisciplinary Research Building for nanomedicine research. The university has budgeted fund to purchase a PET/SPECT/CT machine to support small animal imaging research. These new lab space and facilities will further enhance nanomedicine and breast cancer research capability at Howard University.

This is the 4th year of the grant. There are a few tasks that remain to be completed. We have yet to construct liposomes with a sufficiently narrow size distribution to properly study size dependence of targeted liposome uptake in solid tumors. The relative large size distribution currently generated leads to poor DCE data quality, which masks subtle differences in MR image enhancement patterns resulting from liposome size difference. We would also like to complete testing of a new NMR method to study ligand binding process in vivo. The results from this NMR method will improve the pharmacokinetic modeling analysis of DCE data. In order to finish these incomplete tasks, we have submitted a one year extension from U.S. Army Medical Research Acquisition Activity. The request for extension has been granted. During this extension, we will continue to refine our liposome fabrication method to achieve a more narrow size distribution to improve the results from the DCE study in solid tumor model. We will implement the NMR T2 relaxation rate measurement to improve pharmacokinetic modeling to analyze the DCE image data. We will continue to support faculty and to train graduate students working on this research project.

## VI. REFERENCES

1. Pourtau L, Oliveira H, Thevenot J, Wan Y, Brisson AR, Sandre O, Miraux S, Thiaudiere E, Lecommandoux S. Antibody-Functionalized Magnetic Polymersomes: In vivo Targeting and Imaging of Bone Metastases using High Resolution MRI. *Advanced Healthcare Materials* 2013. Doi: 10.1002/adhm.201300061.
2. Gallo J, Long NJ, Aboagye EO. Magnetic nanoparticles as contrast agents in the diagnosis and treatment of cancer. *Chemical Society Reviews* 42(19): 7816-7833, 2013.
3. Gulaka PK, Yu JX, Liu L, Mason RP, Kodibagkar VD. Novel S-Gal analogs as <sup>1</sup>H MRI reporters for in vivo detection of  $\beta$ -galactosidase. *Magnetic Resonance Imaging* 31(6): 1006-1011, 2013.
4. Geninatti Crich S, Alberti D, Szabo I, Aime S, Djanashvili K. MRI visualization of melanoma cells by targeting overexpressed sialic acid with a Gd(III)-dota-en-pba imaging reporter. *Angewandte Chemie International Edition* 52(4): 1161-1164, 2013.
5. Penet MF, Glunde K, Jacobs MA, Pathak AP, Bhujwalla ZM. Molecular and functional MRI of the tumor microenvironment. *Journal of Nuclear Medicine* 49(5): 687-690, 2008.
6. Lammers T, Rizzo LY, Storm G, Kiessling F. Personalized nanomedicine. *Clinical Cancer Research* 18(18): 4889-4894, 2012.
7. Caruso F, Hyeon T, Rotello VM. Nanomedicine. *Chemical Society Reviews* 41(7): 2537-2538, 2012.
8. Lammers T, Aime S, Hennink WE, Storm G, Kiessling F. Theranostic nanomedicine. *Accounts of Chemical Research* 44(10): 1029-1038, 2011.
9. Kwon IK, Lee SC, Han B, Park K. Analysis on the current status of targeted drug delivery to tumors. *Journal of Controlled Release* 164(2): 108-114, 2012.
10. Sultana S, Khan MR, Kumar M, Kumar S, Ali M. Nanoparticles-mediated drug delivery approaches for cancer targeting: a review. *Journal of Drug Targeting* 21(2): 107-125, 2013.
11. Cheng Z, Al Zaki A, Hui JZ, Muzykantov VR, Tsourkas A. Multifunctional nanoparticles: cost versus benefit of adding targeting and imaging capabilities. *Science* 338(6109): 903-1020, 2012.
12. Laouini, A., Jaafar-Maalej, C., Limayem-Blouza, I., Sfar, S., Charcosset, C., & Fessi, H. (2012). Preparation, characterization and applications of liposomes: state of the art. *Journal of Colloid Science and Biotechnology*, 1(2), 147-168.
13. Immordino, M. L., Dosio, F., & Cattel, L. (2006). Stealth liposomes: review of the basic science, rationale, and clinical applications, existing and potential. *International journal of nanomedicine*, 1(3), 297-315.
14. Kato, H., et al. (2012). Accurate Size and Size-Distribution Determination of Polystyrene Latex Nanoparticles in Aqueous Medium Using Dynamic Light Scattering and Asymmetrical Flow Field Flow Fractionation with Multi-Angle Light Scattering. *Nanomaterials*, 2(1): 15-30.
15. Edwards, K. A., & Baeumner, A. J. (2006). Analysis of liposomes. *Talanta*, 68(5), 1432-1441.
16. Jahn, A., Vreeland, W. N., Gaitan, M., & Locascio, L. E. (2004). Controlled vesicle self-assembly in microfluidic channels with hydrodynamic focusing. *Journal of the American Chemical Society*, 126(9), 2674-2675.
17. Jahn, A., Stavis, S. M., Hong, J. S., Vreeland, W. N., DeVoe, D. L., & Gaitan, M. (2010). Microfluidic mixing and the formation of nanoscale lipid vesicles. *Acs Nano*, 4(4), 2077-2087.

## **VII. APPENDICES**

1. Dr. Zhenjiang Zhang's CV
2. Proof of No-Cost Extension (First Three Pages)
3. Research Projects Supported by the Nanomedicine Core
4. Personnel Who Received Pay for the Research
5. Students Who Participated in Nanomedicine Core Supported Research Projects
6. Reprints of Publication
5. Reprints of Abstracts

**Appendix 1** Dr. Zhenjiang Zhang's CV

**BIOGRAPHICAL SKETCH**

Provide the following information for the Senior/key personnel and other significant contributors in the order listed on Form Page 2.  
Follow this format for each person. **DO NOT EXCEED FOUR PAGES.**

NAME Zhenjiang Zhang		POSITION TITLE Research Associate	
eRA COMMONS USER NAME (credential, e.g., agency login)			
EDUCATION/TRAINING <i>(Begin with baccalaureate or other initial professional education, such as nursing, include postdoctoral training and residency training if applicable.)</i>			
INSTITUTION AND LOCATION	DEGREE <i>(if applicable)</i>	MM/YY	FIELD OF STUDY
Shandong University, Jinan, China	B.S.	07/99	Chemistry
University of Arizona, Tucson, AZ	Visiting Student	09/09	Bio-macromolecular NMR
Peking University, Beijing, China	Ph.D.	07/11	Chemical Biology
National Center for Nanoscience and Technology, Beijing, China	Post-doc	09/13	Nanomedicine
Howard University, Washington, DC	Post-doc	now	Nanomedicine

Please refer to the application instructions in order to complete sections A, B, C, and D of the Biographical Sketch.

**A. Personal Statement**

As a postdoctoral research associate in the Department of Radiology, Howard University, I have the knowledge, skills and motivation necessary to successfully conduct research based on my broad background in nanomedicine, NMR/MRI, and organic/medicinal chemistry. At the Molecular Imaging Laboratory, I am responsible for the preparation and characterization of nanoscale MRI contrast agents such as liposomes loaded with gadopentetate dimeglumine or superparamagnetic iron oxide nanoparticles (SPION). In addition, I am also responsible for protein-dye labeling for optical imaging studies.

Before pursuing my Ph.D., I worked as an organic synthesis chemist for pharmaceutical companies and developed excellent skills in synthesis, purification and characterization of small organic compounds. During my Ph.D. study at Peking University, Beijing, China, my research is about molecular recognition of G-quadruplex DNA, a promising cancer-specific molecular target. I designed and successfully achieved two peptide macrocycles as new G-quadruplex ligands. I also solved a novel intramolecular G-quadruplex structure using high-field NMR during my visit to the University of Arizona, AZ. As a postdoctoral research associate at the National Center for Nanoscience and Technology, Beijing, China, I started to explore nanomedicine for cancer theranostics, and successfully developed two gold nanorods (AuNRs) based nanoplateforms, mesoporous silica-coated AuNRs and thermo-responsive polymer encapsulated AuNRs. These research experiences expanded my expertise to include nanoscale fabrication and characterization, and how to evaluate the bioeffects and efficacies of multifunctional nanoconstructs using cancer cell lines and mouse tumor models. Currently, my research is focused on development of multifunctional magnetoliposomes for cancer theranostics. Specifically, it includes preparation of liposomes with narrow size distribution, tumor targeting ligand conjugation, encapsulation of MRI contrast and therapeutic agents, and efficacies evaluation for tumor targeting and MRI-guided tumor therapy.

**B. Positions and Honors****Positions and Employment**

2004-2005 Organic Synthesis Chemist, Beijing Orlytech Technology Limited Co./Pharmaron Beijing Limited



Co., Beijing, China

2011-2013 Res. Associate, National Center for Nanoscience and Technology, Beijing, China

2013- Res. Associate, Department of Radiology, College of Medicine, Howard University, DC

### **Honors**

2012 Kuancheng Wang Postdoctoral Fellowship (Chinese Academy of Sciences, Beijing, China)

2008 Scholarship for Chinese Ph.D. Students to Study Overseas (China Scholarship Council, Beijing, China)

1999 Excellent Undergraduate Thesis of Shandong University (Shandong University, Jinan, China)

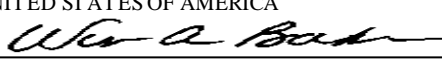
### **C. Selected Peer-reviewed Publications**

1. **Zhang, Z.**, Wang, J., Chen, C., "Near-infrared light-mediated nanoplatfoms for cancer thermo-chemotherapy and optical imaging", *Adv Mater.* **2013**, 25(28), 3869-80.
2. **Zhang, Z.**, Wang, J., Chen, C., "Gold nanorods based platforms for light-mediated theranostics", *Theranostics* **2013**, 3(3), 223-38.
3. **Zhang, Z.**, Wang, L., Wang, J., Jiang, X., Li, X., Hu, Z. Ji, Y., Wu, X., Chen, C., "Mesoporous silica-coated gold nanorods as a light-mediated multifunctional theranostic platform for cancer treatment", *Adv Mater.* **2012**, 24(11), 1418-23.
4. **Zhang, Z.**, He, X., Yuan, G., "Formation and recognition of G-quadruplex relevant for pilin antigenic variation in neisseria gonorrhoeae", *Can J Chem.* **2012**, 90(1), 34-8.
5. **Zhang, Z.**, Yuan, G., "A convenient method for synthesis of tetraoxazole peptide macrocycles", *ARKIVOC* **2011**, x, 368-78.
6. **Zhang, Z.**, He, X., Yuan, G., "Regulation of the equilibrium between G-quadruplex and duplex DNA in promoter of human c-myc oncogene by a pyrene derivative", *Int J Biol Macromol.* **2011**, 49(5), 1173-6.
7. **Zhang, Z.**, Dai, J., Veliath, E., Jones, R. A., Yang, D., "Structure of a two-G-tetrad intramolecular G-quadruplex formed by a variant human telomeric sequence in K<sup>+</sup> solution: insights into the interconversion of human telomeric G-quadruplex structures", *Nucleic Acids Res.* **2010**, 38(3), 1009-21.
8. He, X., **Zhang, Z.**, Zhang, Q., Yuan, G., "Selective recognition of G-quadruplex in vascular endothelial growth factor gene with small molecule natural products by ESI mass spectrometry and CD spectroscopy", *Can J Chem.* **2012**, 90(1), 55-9.
9. Sidell, N., Mathad, R. I., Shu, F., **Zhang, Z.**, Kallen, C. B., Yang, D., "Intercalation of XR5944 with the estrogen response element is modulated by the tri-nucleotide spacer sequence between half-sites", *J Steroid Biochem Mol Biol.* **2011**, 124(3-5), 121-7.
10. Lin, J., Huang, G., Zhang, Z., Hao, A., "Synthesis and Amination of 3-Chloropropylalkyldiethoxysilanes", *Synth Commun.* **2000**, 30(19), 3633-8.

### **D. Research Support**

None

**Appendix 2**      Proof of No-Cost Extension (First Three Pages)

<b>AMENDMENT OF SOLICITATION/MODIFICATION OF CONTRACT</b>				1. CONTRACT ID CODE <b>S</b>		PAGE OF PAGES <b>1   11</b>	
2. AMENDMENT/MODIFICATION NO. <b>P00001</b>		3. EFFECTIVE DATE <b>23-Sep-2014</b>		4. REQUISITION/PURCHASE REQ. NO. <b>W91ZSQ0133N602</b>		5. PROJECT NO.(If applicable)	
6. ISSUED BY USA MED RESEARCH ACQ ACTIVITY 820 CHANDLER ST FORT DETRICK MD 21702-5014		CODE <b>W81XWH</b>		7. ADMINISTERED BY (If other than item 6)  <b>See Item 6</b>		CODE	
8. NAME AND ADDRESS OF CONTRACTOR (No., Street, County, State and Zip Code) HOWARD UNIVERSITY, INC. 2400 6TH ST NW WASHINGTON DC 20059-0002				9A. AMENDMENT OF SOLICITATION NO.			
				9B. DATED (SEE ITEM 11)			
				X 10A. MOD. OF CONTRACT/ORDER NO. <b>W81XWH-10-1-0767</b>			
				X 10B. DATED (SEE ITEM 13) <b>15-Sep-2010</b>			
CODE <b>4B806</b>		FACILITY CODE					
<b>11. THIS ITEM ONLY APPLIES TO AMENDMENTS OF SOLICITATIONS</b>							
<input type="checkbox"/> The above numbered solicitation is amended as set forth in Item 14. The hour and date specified for receipt of Offer <input type="checkbox"/> is extended, <input type="checkbox"/> is not extended. Offer must acknowledge receipt of this amendment prior to the hour and date specified in the solicitation or as amended by one of the following methods: (a) By completing Items 8 and 15, and returning _____ copies of the amendment; (b) By acknowledging receipt of this amendment on each copy of the offer submitted; or (c) By separate letter or telegram which includes a reference to the solicitation and amendment numbers. FAILURE OF YOUR ACKNOWLEDGMENT TO BE RECEIVED AT THE PLACE DESIGNATED FOR THE RECEIPT OF OFFERS PRIOR TO THE HOUR AND DATE SPECIFIED MAY RESULT IN REJECTION OF YOUR OFFER. If by virtue of this amendment you desire to change an offer already submitted, such change may be made by telegram or letter, provided each telegram or letter makes reference to the solicitation and this amendment, and is received prior to the opening hour and date specified.							
<b>12. ACCOUNTING AND APPROPRIATION DATA (If required)</b>							
<b>13. THIS ITEM APPLIES ONLY TO MODIFICATIONS OF CONTRACTS/ORDERS. IT MODIFIES THE CONTRACT/ORDER NO. AS DESCRIBED IN ITEM 14.</b>							
A. THIS CHANGE ORDER IS ISSUED PURSUANT TO: (Specify authority) THE CHANGES SET FORTH IN ITEM 14 ARE MADE IN THE CONTRACT ORDER NO. IN ITEM 10A.							
B. THE ABOVE NUMBERED CONTRACT/ORDER IS MODIFIED TO REFLECT THE ADMINISTRATIVE CHANGES (such as changes in paying office, appropriation date, etc.) SET FORTH IN ITEM 14, PURSUANT TO THE AUTHORITY OF FAR 43.103(B).							
C. THIS SUPPLEMENTAL AGREEMENT IS ENTERED INTO PURSUANT TO AUTHORITY OF:							
X D. OTHER (Specify type of modification and authority) Unilateral Modification IAW, USAMRAA General Terms & Conditions							
E. IMPORTANT: Contractor <input checked="" type="checkbox"/> is not, <input type="checkbox"/> is required to sign this document and return _____ copies to the issuing office.							
<b>14. DESCRIPTION OF AMENDMENT/MODIFICATION (Organized by UCF section headings, including solicitation/contract subject matter where feasible.)</b> Modification Control Number: <b>jbrzell145536</b> <b>PROPOSAL TITLE:</b> A Partnership Training Program: Studying Targeted Drug Delivery Using Nanoparticles In Breast Cancer Diagnosis and Therapy <b>PRINCIPAL INVESTIGATOR:</b> Paul Wang <b>PERIOD OF PERFORMANCE:</b> 15 September 2010 – 14 September 2015 <b>AWARD AMOUNT:</b> \$1,412,749 <b>OBLIGATED AMOUNT:</b> \$1,412,749  The purpose of this modification is to extend the period of performance by 12 months at no additional cost to the Government, per the recipient's request dated 14 August 2014. The annual technical report is due no later than 14 October 2014. The final technical report is due no later than 14 December 2015. Submissions of the financial reports (SF425s) shall continue during the no-cost extension period. Additionally, administrative changes have been made throughout the award document. These changes are highlighted in yellow.							
Except as provided herein, all terms and conditions of the document referenced in Item 9A or 10A, as heretofore changed, remains unchanged and in full force and effect.							
15A. NAME AND TITLE OF SIGNER (Type or print)				16A. NAME AND TITLE OF CONTRACTING OFFICER (Type or print) WENDY A. BAKER / GRANTS OFFICER TEL: 301-619-2034 EMAIL: wendy.a.baker.civ@mail.mil			
15B. CONTRACTOR/OFFEROR  (Signature of person authorized to sign)		15C. DATE SIGNED		16B. UNITED STATES OF AMERICA BY  (Signature of Contracting Officer)		16C. DATE SIGNED <b>23-Sep-2014</b>	

## SECTION SF 30 BLOCK 14 CONTINUATION PAGE

## SUMMARY OF CHANGES

## SECTION 00010 - SOLICITATION CONTRACT FORM

The 'issued by' organization has changed from  
US ARMY MEDICAL RESEARCH ACQUISITION ACT  
DIRECTOR  
820 CHANDLER STREET  
FORT DETRICK MD 21702-5014  
to  
USA MED RESEARCH ACQ ACTIVITY  
820 CHANDLER ST  
FORT DETRICK MD 21702-5014

The 'administered by' organization has changed from  
USA MED RESEARCH ACQ ACTIVITY  
ATTN: MONICA PILEGGI  
301-619-2268  
MONICA.PILEGGI  
FORT DETRICK MD 21702  
to  
USA MED RESEARCH ACQ ACTIVITY  
820 CHANDLER ST  
FORT DETRICK MD 21702-5014

## CLIN 0001

The CLIN extended description has changed from Period of Performance: 15 September 2010 through 14 October 2014 (Research ends 14 September 2014). to Period of Performance: 15 September 2010 through 14 September 2015.

## DELIVERIES AND PERFORMANCE

The following Delivery Schedule item for CLIN 0001 has been changed from:

DELIVERY DATE	QUANTITY	SHIP TO ADDRESS	UIC
POP 15-SEP-2010 TO 14-OCT-2014	N/A	USA MED RESEARCH MAT CMD 1077 PATCHEL STREET BLDG 1056 FORT DETRICK MD 21702 FOB: Destination	W91ZSQ

To:

DELIVERY DATE	QUANTITY	SHIP TO ADDRESS	UIC
---------------	----------	-----------------	-----

POP 15-SEP-2010 TO N/A  
14-SEP-2015

USA MED RESEARCH MAT CMD  
1077 PATCHEL STREET BLDG 1077  
FORT DETRICK MD 21702  
FOB: Destination

W91ZSQ

The following have been modified:

PI NAME AND TITLE

**Proposal Title:** A Partnership Training Program: Studying Targeted Drug Delivery Using Nanoparticles In Breast Cancer Diagnosis and Therapy

**Principal Investigator:** Mr. Paul Wang

**ADMINISTERED BY:**

Jamie Shortall

Contract Specialist

US Army Medical Research Acquisition Activity

Phone: 301-619-2393

Email: [jamie.a.shortall.civ@mail.mil](mailto:jamie.a.shortall.civ@mail.mil)

SECTION 00800 - SPECIAL CONTRACT REQUIREMENTS

The following have been modified:

**A.** This award is made under the authority of 31 U.S.C. 6304 and 10 U.S.C. 2358. The recipient's statement of work and the revised budget dated 8 September 2010 for this proposal submitted in response to the Fiscal Year 2009 Department of 2009 Breast Cancer Research Program, HBCU/MI Partnership Training Award Announcement, which closed 8 April 2009, are incorporated herein by reference. The Catalog of Federal Domestic Assistance Number relative to this award is CFDA 12.420.

**B. ACCEPTANCE OF AWARD:** The recipient is not required to countersign this assistance award. In case of disagreement, the recipient shall notify the Grants Officer and not assess the award any costs until such disagreement(s) is resolved.

**C. USAMRAA GENERAL TERMS AND CONDITIONS:** This assistance agreement is subject to the USAMRAA General Terms and Conditions and to any special considerations as contained in the below mentioned Section titled "Special Terms and Conditions". These USAMRAA General Terms and Conditions are incorporated by reference with the same force and effect as if they were given in full text. The full text of the USAMRAA General Terms and Conditions may be accessed electronically at <http://www.usamraa.army.mil>.

**D. SPECIAL TERMS AND CONDITIONS**

**1. TRAINING TECHNICAL REPORTING REQUIREMENTS (DEC 2008) (USAMRAA)**

**ANNUAL SUMMARY**

A 2-5 page annual summary in electronic format (PDF or Word file only), presenting a description of the training and research accomplishments to date, shall be submitted within 30 calendar days after the anniversary date of the award

### Appendix 3      Research Projects Supported by the Nanomedicine Core

1. Physicochemical Characteristics of Nanoparticles as MR Contrast Agent Delivery System with the Dynamic Contrast Enhancement Pattern for Clinical Applications (Wang PC, Ping-Chang Lin/Radiology; Sridhar R/ Radiation Oncology; Bhujwalla Z/Radiology/Johns Hopkins)
2. Develop multifunctional nanoparticles for breast cancer diagnosis and treatment – using anti-VEGFR-2 immunotoxin as dual purpose ligand and chemotherapeutics as encapsulated payload (Shan L/Radiology; Liu YY, Naville D/ NIH and Angimmune LLC).
3. Relativity simulation vs. 2D HSQC measurements of multiple fluorine compounds mixture (Ping-Chang Lin/Radiology)
4. Design of Multifunctional Polymeric Nanoparticles for Breast Cancer Diagnosis and Treatment (Akala E/Pharmacy)
5. Use of MRI/MRS to Assess for a Gamma-Glutamylcysteine Mediated in vivo Reduction in Hypoxic Stress-Induced Oxidative White Matter Injury in Mice (Costello J, Nath D, Jonas R/Children's National Medical Center)
6. Use of MRI in Mouse brain tumor model and drug delivery (Nazarian J/Children's National Medical Center)
7. A Fluorescence Imaging Approach to Visualizing peripherally inserted central catheters (Shekhar, Raj/Children's National Medical Center)
8. SPIOs with modified polymer-pHLIP peptide surface as an effective MRI-contrast agent for diagnosis of pancreatic tumor (Qibing Zhou/ Huazhong University of Science and Technology, Shan L/Radiology)
9. Neural Mechanisms of Age-Related Decline in Olfaction and Associated Cognitive Abilities (Nwulia E/Psychiatry, Obisesan T/Medicine/Howard, Casella N/Psychiatry/Johns Hopkins)
10. Efficiency of Brain Delivery of Novel Therapeutics Through the Olfactory Neuroepithelium (Nwulia E/Psychiatry)
11. Parallel computing in bioinformatics (Yayin Fan/Biochemistry, Joseph Arul/Fu Jen University)
12. Renal Oxygenation levels are Decreased in Peroxisome Proliferator Activated Receptor –  $\alpha$  Knockout Mice during Angiotensin II Hypertension (Darah Wright, Dexter Lee/Physiology, Biophysics; Ping-Chang Lin, Stephen Lin/Radiology)
13. Anti-PSMA Diphtheria Immunotoxin for Prostate Cancer Imaging and Therapy (Shan L, /Radiology; Liu YY/ Angimmune LLC)
14. Osteopontin Genotype as a Determinant of Muscle Remodeling: A Study of African-American Young Adult Volunteers (Barfield W, Bond V/ Health and Human Performance, Wang PC, Williams L/Radiology, Hoffman EP/Children's National Medical Center)
15. Liposomal Formulation of BTZQ for Head and Neck Cancer (YL Lin/Fu Jen University)
16. Using Permanent Magnet to Guide Diffusion of Magnetic Nanoparticles in Brain Tissue Samples (Partam Manalai/Psychiatry and Behavioral Sciences)

#### **Appendix 4**      Personnel Receiving Pay in This Research Effort

- Paul C. Wang, Ph.D (PI)
- Ping-Chang, Lin, Ph.D.
- Liang Shan, Ph.D.
- Zhenjiang Zhang, Ph.D.

## **Appendix 5**      Students Who Participated in Nanomedicine Core Supported Research Projects

### Postdoctoral Fellows:

- Rohan Fernandes (Children's National Medical Center)
- Jie Meng (Chinese Academy of Medical Sciences)
- Shimelis Hailu (Chemistry)
- Javad Nazarian (Children's National Medical Center)
- Shuang Shi (Dentistry)
- Zhenjiang Zhang (Chemistry/Radiology)

### Predoctoral M.D./Ph.D./Dental Students:

- Philipe Auguste (Medicine)
- Whitney Barfield (Microbiology, received PhD degree)
- Kenisha Ford (Physics)
- Belinda Hauser (Genetics, received PhD degree)
- Eyob Hulu (Pharmaceutical Sciences)
- Ermias Tilahun (Pharmaceutical Sciences)
- Darah White (Physiology and Biophysics)
- Brian B Wu (Medicine)
- Jie Xia (Pharmaceutical Sciences)

### Undergraduate students:

- Taylor Williams (Biology)



## Appendix 6      Reprints of Publications

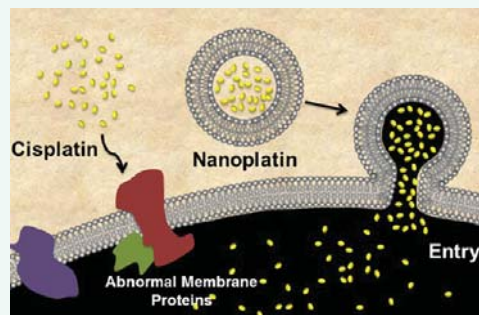
1. Xue X, Hall HD, Zhang Q, Wang PC, Gottesman MM, Liang XJ. Nanoscale Drug Delivery Platforms Overcome Platinum-Based Resistance in Cancer Cells Due to Abnormal Membrane Protein Trafficking. *ACS Nano* vol.7 (12)10452-10464, 2013.
2. Shan L, Liu Y, Wang PC. Recombinant Immunotoxin Therapy of Solid Tumors: Challenges and Strategies. *J. Basic Clin Med* 2(2):1-6, 2013.
3. Lin PC, Lin S, Wang PC, Sridhar R. Techniques for Physicochemical Characterization of Nanomaterials. *Biotechnol Adv.* (4):711-726, 2014.
4. Li SL, Cao WP, Kumar A, Jin SB, Zhao YY, Zhang CQ, Zou GZ, Wang PC, Li F, Liang XJ. Highly Sensitive Simultaneous Detection of Mercury and Copper Ions by Ultrasmall Fluorescent DNA-Ag Nanoclusters *New J. Chem* 38(4):1546-1550, 2014
5. Jin SB, Li SL, Wang CX, Liu J, Yang XL, Wang PC, Zhang X, Liang XJ. Biosafe Nanoscale Pharmaceutical Adjuvant Materials. *J Biomed Nanotechnology* (10)1-27, 2014
6. Huo S, Jin S, Ma X, Xue X, Yang K, Kumar A, Wang PC, Zhang J, Hu Z, Liang XJ. Ultrasmall Gold Nanoparticles as Carriers for Nucleus-Based Gene Therapy Due to Size-Dependent Nuclear Entry. *ACS Nano* 8(6):5852-5862, 2014.
7. Yang KN, Zhang CQ, Wang W, Wang PC, Zhou JP, Liang XJ. pH-Responsive Mesoporous Silica Nanoparticles Applied in Controlled Drug Delivery Systems for Cancer Treatment. *Cancer Biol Med.* 11(1):34-43, 2014.

# Nanoscale Drug Delivery Platforms Overcome Platinum-Based Resistance in Cancer Cells Due to Abnormal Membrane Protein Trafficking

Xue Xue,<sup>†,\*</sup> Matthew D. Hall,<sup>§</sup> Qiang Zhang,<sup>‡</sup> Paul C. Wang,<sup>⊥</sup> Michael M. Gottesman,<sup>§,\*</sup> and Xing-Jie Liang<sup>†,\*</sup>

<sup>†</sup>CAS Key Laboratory for Biomedical Effects of Nanomaterials and Nanosafety, National Center for Nanoscience and Technology of China, Beijing 100190, People's Republic of China, <sup>‡</sup>Department of Pharmaceutics, School of Pharmaceutical Science, Peking University, Beijing 100191, People's Republic of China, <sup>§</sup>Laboratory of Cell Biology, Center for Cancer Research, National Cancer Institute, National Institutes of Health, Bethesda, Maryland 20892, United States, and <sup>⊥</sup>Molecular Imaging Laboratory, Department of Radiology, Howard University, Washington DC 20060, United States

**ABSTRACT** The development of cellular resistance to platinum-based chemotherapies is often associated with reduced intracellular platinum concentrations. In some models, this reduction is due to abnormal membrane protein trafficking, resulting in reduced uptake by transporters at the cell surface. Given the central role of platinum drugs in the clinic, it is critical to overcome cisplatin resistance by bypassing the plasma membrane barrier to significantly increase the intracellular cisplatin concentration enough to inhibit the proliferation of cisplatin-resistant cells. Therefore, rational design of appropriate nanoscale drug delivery platforms (nDDPs) loaded with cisplatin or other platinum analogues as payloads is a possible strategy to solve this problem. This review will focus on the known mechanism of membrane trafficking in cisplatin-resistant cells and the development and employment of nDDPs to improve cell uptake of cisplatin.



**KEYWORDS:** cancer · cisplatin · drug resistance · nanoscale drug delivery platforms · membrane trafficking · nanotechnology · chemotherapy · abnormal membrane proteins

Platinum (Pt)-based chemotherapeutic drugs, principally cisplatin ( $\text{cis-[PtCl}_2\text{-(NH}_3\text{)}_2\text{]}$ ) and carboplatin ( $[\text{Pt}(\text{O},\text{O}'\text{-cdbc})(\text{NH}_3)_2]$ , cdbc = cyclobutane-1,1-dicarboxylate) are widely employed in the clinic to treat malignancies such as cancer of the testis, lung, ovary, breast, bladder, head and neck, colon, and rectum.<sup>1–3</sup> Clinically, the chemotherapeutic effect of platinum-based drugs presents a satisfactory response when tumors are first exposed to the drugs.<sup>4</sup> However, after repeated treatments, most malignancies sooner or later become resistant to even unrelated anticancer agents, in spite of different chemical structures or different mechanisms of intracellular activity.<sup>5</sup> The exception to this is testicular cancer, for which platinum therapy provides an approximately 99% cure rate. Thus, intrinsic and/or acquired resistance, as well as the formidable side effects of accumulating platinum in normal tissues, often hampers Pt-based treatment of

cancer.<sup>6,7</sup> Movement of chemotherapeutic agents through the cellular lipid bilayer membrane was first thought to occur predominantly by passive diffusion.<sup>8,9</sup> However, emerging evidence in the literature indicates that active processes are more likely the major determinant of cellular uptake of cisplatin.<sup>6,10</sup> Evidence suggests that various membrane proteins collectively regulate the uptake and efflux of drugs. The reduction of platinum accumulation as a pivotal factor influencing the effectiveness of tumor chemotherapy is therefore mediated by down-regulation of these facilitative transporters and alteration in membrane protein trafficking.<sup>11–13</sup> Understanding the role of abnormal membrane proteins in the development of platinum drug resistance can serve as a basis for selecting drug targets and promoting drug development.

Many studies have been published concerning the role of active transport of platinum drugs across biological membranes.<sup>14–16</sup>

\* Address correspondence to mgottesman@nih.gov, liangxj@nanoctr.cn.

Received for review September 25, 2013 and accepted November 12, 2013.

Published online November 12, 2013  
10.1021/nn405004f

© 2013 American Chemical Society

However, in order to achieve successful and effective drug delivery in cases of resistant cancer, new therapeutic strategies still need to be developed.<sup>17–19</sup> Newer, more targeted agents have not displaced shotgun therapeutics such as cisplatin. In recent years, nanotechnology, through an amalgamation of chemistry, engineering, biology, and medicine, has provided potential solutions to some of the daunting challenges associated with cancer therapy. Furthermore, although the feasibility and efficacy of reversing drug resistance have been studied in the clinic, ways to use nanotechnology to circumvent the resistant phenotype have not been clarified or fully explored. This review examines the reduced drug accumulation that occurs in resistant cancer cells caused by abnormal membrane transporter expression and unusual protein-related metabolic modulation and introduces nanotechnology formulations and current nanomedical approaches to address platinum-based resistance, with a specific focus on the effort to overcome abnormal membrane protein trafficking and increase cellular uptake of chemotherapeutic agents.

## ABNORMAL MEMBRANE PROTEINS PLAY PIVOTAL ROLES IN PLATINUM-BASED RESISTANCE

### Modulation of Membrane Transporters in Resistant Cells.

Membrane transporters are a group of integral membrane proteins that facilitate the movement of a variety of endogenous and exogenous substrates across cellular and organelle membranes, including the movement of ions, small molecules, and macromolecules. An increasing number of membrane transporters have been identified as contributing to cancer resistance. These transporters govern the movement of drugs and their secondary metabolites, thereby determining their pharmacodynamics and adverse drug reactions. Changes in several transporters, such as in the ATP-binding cassette (ABC) transporters, solute carriers (SLCs), and ATPase membrane protein superfamilies have been implicated as determinants of the pharmacology of cisplatin, oxaliplatin, carboplatin, and related investigational compounds.<sup>11,20,21</sup> Changes in membrane transporters affect the accumulation of platinum drugs in resistant cells or tissues by increasing drug efflux or decreasing drug uptake, by metabolic modifications or by detoxification.<sup>22,23</sup>

Of these transporter-related resistance mechanisms, overexpression of ABC transport molecules is generally considered the most frequent. ABC transporters are transmembrane proteins that use the energy of ATP hydrolysis to shuttle various substrates against the concentration gradient outward or into intracellular organelles. To date, there are 48 known human transporters in the ABC family, classified into seven subfamilies A through G. At least 13 of them have been recognized as drug transporters when drugs share physiochemical characteristics with

**VOCABULARY:** **nDDPs** - nanoscale drug delivery platforms; **Pt** - platinum; **ABC** - ATP-binding cassette; **SLCs** - solute carriers; **MRP** - multidrug resistance-associated protein; **BCRP** - breast cancer resistance protein; **RFC** - reduced folate carrier; **CNT** - concentrative nucleoside transporter; **ENT** - equilibrative nucleoside transporter; **CTR** - copper transporter; **DCA** - dichloroacetate; **CDKs** - cyclin-dependent kinases; **PDK** - pyruvate dehydrogenase; **MDR** - multidrug resistance; **EGFR** - epidermal growth factor receptor; **FDA** - Food and Drug Administration; **PE-Glylated** - poly(ethylene glycol)-conjugated; **P-gp** - P-glycoprotein; **SWNTs** - single-walled carbon nanotubes; **MWNTs** - multiwalled carbon nanotubes; **iNOS** - inducible nitric oxide synthase; **NSCLC** - non-small-cell lung cancer; **FR** - folate receptor;

certain endogenous substrates,<sup>21,24,25</sup> and three, ABCB1 (P-glycoprotein), ABCC1 (MRP, or multidrug resistance-associated protein), and ABCG2 (BCRP, or breast cancer resistance protein), are broad spectrum multidrug efflux pumps.<sup>24</sup>

The solute carrier (SLC) family of transporters is another superfamily of membrane proteins that mediates the cellular uptake of anticancer agents, including SLC19A1 (RFC1) and SLC1B1 (SLC21A6). SLC transporters play a critical role in multiple cellular physiological processes and traffic specific substrates such as amino acids, oligopeptides, sugars, monocarboxylic acids, organic cations, anions, phosphates, nucleosides, metals, and vitamins. SLCs also mediate drug absorption, distribution, metabolism, and elimination, particularly in the case of uptake of hydrophilic anticancer drugs that cannot rely solely on passive diffusion, including cisplatin, carboplatin, and oxaliplatin.<sup>26,27</sup> Structurally, members of the SLC19 family (the reduced folate carrier (RFC) family), SLC28 and 29 families (concentrative and equilibrative nucleoside transporter proteins (CNT and ENT, respectively)), SLC7A and 3A families (amino acid transporters), and SLC31A (the copper transporter family (CTR)) are associated with uptake of anticancer drugs.<sup>10,20</sup> CTR1 has been identified as a mediator that increases drug accumulation and cytotoxic properties.<sup>28</sup> For instance, CTR1-deficient mouse embryonic fibroblasts have been shown to demonstrate reduced influx of cisplatin, carboplatin, and oxaliplatin.<sup>29</sup> In addition, studies have indicated that platinum accumulation is partly mediated by different energy-dependent cellular proteins that use ATP hydrolysis as an energy source. In resistant cancer cells, ATP levels tend to be depleted, leading to metabolic dysfunction and decreased drug accumulation.<sup>28</sup>

**Modulation of Membrane Content and Potential in Resistant Cells.** The plasma membrane itself also plays a role in drug resistance, especially through abnormal membrane protein trafficking. A number of studies have pointed to abnormal membranes as contributing to

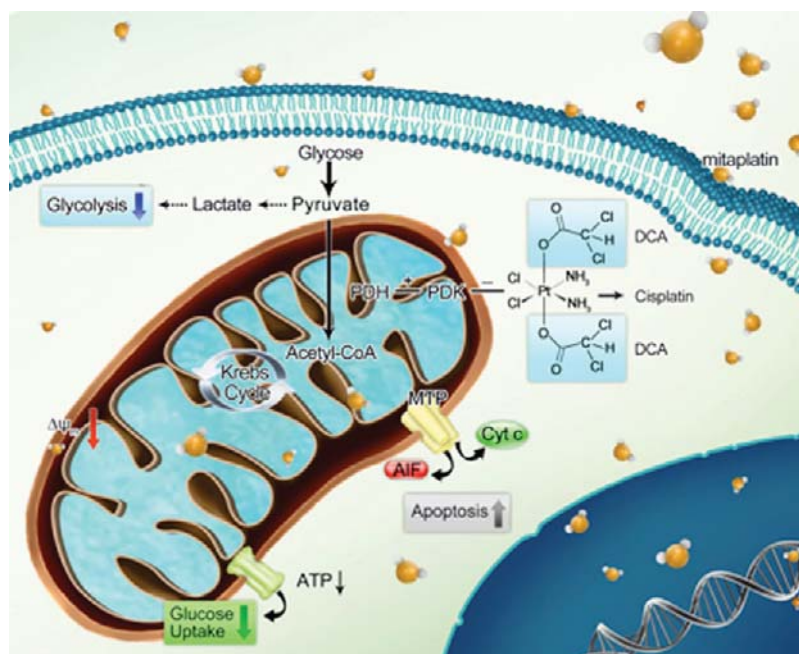


**Figure 1.** Mitaplatin circumvents cancer resistance to cisplatin by targeting mitochondria. In cancer cells, oxidative phosphorylation is inhibited, and cancer cells rely on cytoplasmic glycolysis to produce energy. This metabolic shift induces apoptosis resistance. After crossing the membrane, mitaplatin targets mitochondria, inhibits the activity of mitochondrial PDK, and leads to activation of PDH, which promotes the influx of acetyl-CoA into mitochondria and increases the Krebs cycle. With triggering hyperpolarized  $\Delta\psi/m$  in resistant cells, mitaplatin also results in reduced glucose utilization. Similar to cisplatin, mitaplatin also enters the nuclei and targets DNA to form 1,2-intrastrand d(GpG) cross-links. Adapted from Figure 7 of ref 31. Copyright 2012 American Chemical Society.

resistance in cancer cells. These abnormalities include higher membrane potentials, abnormal fluidity of the plasma membrane, and changes in competency. Altered membrane protein trafficking results in a lowered level of transporters at the cell surface, therefore reducing the potential capacity of cells to facilitate the uptake of drugs (and nutrients).

Previous studies by us found that the biophysical status of cellular membranes was associated with cisplatin resistance. Compared to sensitive cells, resistant cells had higher plasma membrane potentials<sup>30</sup> and mitochondrial membrane potentials,<sup>31</sup> which would be dependent on differences in the structure or function of fatty acid composition, resistance-related membrane protein expression, ion conductivity, or metabolic regulation.<sup>32</sup> One study indicated that the change of lipid content in cisplatin-resistant cells could mediate the modulation of membrane fluidity, which was determined by cholesterol, total lipids, and phospholipid content.<sup>33</sup> The study pointed out that, compared to sensitive cells, the cholesterol and cholesterol ether content was significantly higher, while diacylglycerol and triacylglycerol content was apparently lower in the resistant cells. These differences provide potential opportunities for drugs designed to selectively target resistant tumor cells. For instance, the orphan drug dichloroacetate (DCA) reverses the Warburg effect by inhibiting pyruvate dehydrogenase kinase (PDK), providing a mitochondrial target to influence

the unique cellular metabolism of cancer cells and promote their apoptosis.<sup>34,35</sup> Mitaplatin, a platinum(IV) complex containing cisplatin and two DCA molecules bound as ligands that are released when the complex is reduced, alters the mitochondrial membrane potential and selectively kills cancer cells by targeting both nuclear DNA *via* cisplatin and mitochondria *via* DCA.<sup>36</sup> In cancer-sensitive cells, oxidative phosphorylation is inhibited to force cancer cells to rely on cytoplasmic glycolysis to produce energy. This metabolic shift induces apoptosis resistance. The enhanced lipophilicity of mitaplatin increases its ability to cross the plasma membrane and thus be further employed to overcome tumor resistance by modulating abnormal glycolysis and by rendering resistant cancer cells more vulnerable to hyperpolarized mitochondrial membrane potentials (Figure 1).<sup>31</sup> Subsequently, other platinum(II) and platinum(IV) complexes containing DCA incorporated as a ligand have been reported.<sup>37</sup>

**Modulation of Intracellular pH in Resistant Cells.** In addition, an acidic pH-activated mechanism to overcome efflux-dependent resistance has been explored.<sup>38–41</sup> This has been driven by observations that cells resistant to cisplatin have acidified intracellular compartments. Furthermore, the influence of pH on the cytotoxicity of cisplatin in mouse mammary tumor cells can be exploited, as tumor cells are more sensitive to cisplatin when cultured in pH 6.0 medium rather than physiologic pH.<sup>42</sup> Given this, the expectation is that an

acid-labile linker would release its payload at a greater rate inside the more acidic cisplatin-resistant cells. By way of example, Kievit *et al.* demonstrated that doxorubicin tethered to iron oxide NPs by an acid-labile hydrazone linkage was released to a greater extent at acidic pH.<sup>39</sup>

**Modulation of Cell Cycle in Resistant Cells.** The cell life cycle is the sequence of events that occur during DNA replication and cell division, which is divided into four successive phases: G<sub>1</sub>, S (synthesis), G<sub>2</sub> (collectively known as interphase), and M (mitosis). During G<sub>1</sub>, S, and G<sub>2</sub>, cells accumulate nutrients needed for mitosis. After mitosis, cells enter a state of quiescence called the G<sub>0</sub> phase and stop dividing temporarily.<sup>43,44</sup> Cell cycle arrest is coordinated with the production of membrane phospholipids, the major cellular constituents required for the assembly of biological membranes. A doubling of membrane phospholipids is required for cell proliferation. Previous studies have demonstrated that phospholipids accumulate when cells enter S phase<sup>45</sup> and are synthesized in the G<sub>2</sub>/M phase,<sup>46</sup> which are controlled by a series of cell cycle regulators.<sup>47,48</sup> The cell cycle can be disturbed or delayed by various molecular events, including the intertwined actions of cyclin-dependent kinases (CDKs)<sup>49</sup> and specific proteolytic mechanisms,<sup>50</sup> as well as chemotherapeutic agents.<sup>51,52</sup> Cisplatin is well-known to arrest cells at G<sub>2</sub>,<sup>53</sup> a process mediated by checkpoint kinases<sup>54</sup> and the miRNAs that control them.<sup>55</sup> In cells that have acquired multidrug resistance, cell cycle distribution and cell cycle arrest is often altered as a result of this cycle-specific toxin. For example, cisplatin-resistant hepatocellular carcinoma cells have been shown to spend more time in the G<sub>2</sub>/M and S phases (allowing them to spend greater time recognizing and repairing DNA damage).<sup>56</sup> Interfering with cell cycle arrest, by inhibiting or down-regulating checkpoint kinases, can resensitize cisplatin-resistant cells by forcing the cells to continue through the G<sub>2</sub> checkpoint into mitosis, enforcing apoptosis.<sup>55,57</sup> However, gene silencing technologies are limited in their efficiency, and small molecules face challenges associated with pharmacokinetics and unwanted side effects.

As such, NP-mediated interference with the cell cycle state has received attention. In fact, bare liposomes not loaded with drug have been shown to arrest cells in G<sub>0</sub>/G<sub>1</sub> phase and induce apoptosis, though obviously the delivery of a drug by liposomes results in altered cellular responses.<sup>58–60</sup> Roa *et al.*<sup>61</sup> reported that glucose-capped gold nanoparticles accelerate cells through the G<sub>0</sub>/G<sub>1</sub> phase and arrest them in G<sub>2</sub>/M (much like cisplatin). Increasing evidence has been reported that metal-based nanomaterials such as iron NPs,<sup>62</sup> silver NPs,<sup>63–65</sup> albumin NPs,<sup>66,67</sup> ENREF 60 ZnO NPs,<sup>68</sup> and Au NPs<sup>61,69</sup> can affect the cell cycle in different phases. While modification of the cell cycle state of cells may alter cell fate by sensitizing chemotherapy,

further study of the mechanisms of interaction between nanoparticles and phospholipid cell membranes is required, as drugs that arrest cells can inhibit each other's efficacy.<sup>70</sup>

## SUCCESSFUL APPLICATIONS OF NANOTECHNOLOGY AS THERAPY FOR DRUG-RESISTANT CANCER

**Nanoscale Drug Delivery Platforms That Target Membrane Transporters.** Drugs are often internalized by diffusion across the cellular membrane or by transport-facilitated processes. The drug efflux pumps (such as P-glycoprotein (P-gp; ABCB1)) on the cell membrane can recognize free drug molecules, capture, and efflux them when they attempt to cross the membrane.

Nanoscale drug delivery platforms (nDDPs, not to be confused with the often-used acronym for cisplatin, DDP) based on biodegradable, biocompatible, and FDA-approved components are taken up by endocytosis, preventing the drugs from being recognized by efflux pumps. The drugs are covalently bound to the nDDP, which results in a higher intracellular accumulation unaffected by transport processes.<sup>71–73</sup> This increase is achieved partly because of circumvention of membrane-crossing events and partly because each nDDP nanoparticle can deliver many drug molecules (the analogy being that of a Trojan horse).

Because of the side effects of platinum-based chemotherapeutic drugs, efforts to design targeted and/or controlled-release drug delivery systems is ongoing, with various modifications and accommodations for multiple types of drug payloads. At a chemical level, controlled release is achieved by installing linkers between the nanoparticle and drug containing functional groups that are susceptible to either enzymatic (*e.g.*, esterase) or nonenzymatic (*e.g.*, hydrolysis) cleavage.

The main objective of nDDPs is to localize the therapeutic agent at its site of action for maximal effect without resulting in a toxic distribution of the agent at nontarget sites. After careful consideration of their size, toxicity, absorbance, distribution, and elimination, most nanostructure platforms derive their effectiveness from adequate delivery systems, including polymers, liposomes, micelles, dendrimers, nanoshells, and nanotubes, as well as magnetic or metal nanoparticles.<sup>74–76</sup> Some of them are promising applications or becoming realities in healthcare. For instance, it has been reported that poly(ethylene glycol)-conjugated (PEGylated) multiwalled carbon nanotubes (MWCNTs) act as drug efflux modulators. They accumulate in resistant cancer cells as well as in sensitive cancer cells without damaging the plasma membrane, indicating that they are efficient drug carriers able to overcome drug resistance.<sup>77</sup> This is likely achieved because the nanoparticle itself is either not recognized by, or is too large to be extruded by, multidrug resistance efflux pumps. Moreover, ligand-mediated



interaction between nanoparticles and the surface of resistant cancer cells is one of the most popular strategies. Properly designed nanoparticles can focus on active targets at specific targeting sites with therapeutic payloads, taking advantage of markers on the membranes of resistant cancer cells, reducing the dispersal of the drug and enhancing its therapeutic potential.<sup>78,79</sup>

Defective endocytosis causes less intracellular accumulation of drugs such as cisplatin. Metallofullerene nanoparticles have been successfully designed to repair receptor-mediated endocytosis in resistant cells, resulting in more efficient formation of cisplatin–DNA adducts to sensitize the resistant cells both *in vitro* and *in vivo*.<sup>80</sup> In addition, active nanocarrier endocytosis has been accomplished by other ligands such as transferrin,<sup>80</sup> epidermal growth factor receptor (EGFR), peptides,<sup>81,82</sup> and siRNA<sup>83</sup> via receptor-mediated endocytosis.

**Other Modification Strategies Related to Abnormal Membrane Protein Trafficking.** *nDDPs That Modify the Phospholipids of Resistant Cells.* Alterations in the composition of the cell membranes of resistant tumor cells have been observed.<sup>84–86</sup> For example, a study based on virtual screening found a novel phospholipid named phosphatidylinositol-(1,2-dioctanoyl) sodium salt, identified with transmembrane P-gp transportation inhibitory activity. Further tests showed that the phosphatidylinositol derivative increased the bioactivity of drugs in several tumor cell lines, due to P-gp inhibition.<sup>87</sup> Another study indicated that MCF-7 cisplatin-resistant cells accumulated more 3,3'-dioctadecyloxacyanine perchlorate (DiO) dye from dye-loaded liposomes than sensitive cells.<sup>88</sup>

Among different kinds of drug carriers, such as polymeric micelles, niosomes, liposomes, microspheres, immunoglobulins, peptides, and small proteins, liposomes are considered as suitable lipophilic carriers due to their natural lipid components. Liposomes are nanosized artificial vesicles composed of one or more phospholipid-enriched bilayers containing mixed lipid chains that are employed to attach to unhealthy tissue.<sup>89,90</sup> Liposomes afford a unique opportunity to deliver drugs due to their attractive composition, including fluidity, permeability, stability, and structure, which makes them biocompatible and biodegradable. On the other hand, liposomes sometimes alter the pharmacokinetic parameters and dynamic interactions between tumor cells and encapsulated drugs: strongly lipophilic drugs are entrapped almost completely in the lipid bilayer; strongly hydrophilic drugs are located exclusively in the aqueous compartment, and drugs with intermediate log *P* partition between the lipid and aqueous phases, both in the bilayer and in the aqueous core. Furthermore, liposomes can easily be loaded with different drugs for combination chemotherapy. Ye *et al.* showed that cationic liposome-mediated

inducible nitric oxide synthase (iNOS) gene therapy is effective with low dose cisplatin treatment in lung cancer. Systemic delivery of the liposome–pVAX-iNOS complex enhanced cisplatin-mediated suppression of tumors by inhibition of cell proliferation, invasion, migration, and promotion of cell apoptosis both *in vitro* and *in vivo*.<sup>91</sup> Because lipid-based nanoparticles have the advantage of minimum toxicity for *in vivo* applications, their potential success in the clinic has been apparent. Lipoplatin, a liposomal encapsulation of cisplatin into tumor-targeted 110 nm nanoparticles (Figure 2A), shown to be effective in non-small-cell lung cancer (NSCLC) both in phase II and III trials, combines a reduction in the toxicity associated with antitumor activity similar to the free drug.<sup>92,93</sup> Lipoplatin infusion in tumor cells exhibited 10–50 times higher activity than in the adjacent normal specimens, with less general toxicity and nephrotoxicity, no significant weight gain reduction, and fewer renal and liver impairments than cisplatin administration.<sup>93,94</sup> The direct fusion of lipoplatin with the membrane allows for a therapeutic effect even after the development of cisplatin resistance (Figure 2B).<sup>95</sup>

**nDDPs That Modify Cellular Metabolism.** An alternative to traditional ways to treat cancer resistance is to decrease intracellular ATP levels by inhibiting mitochondrial function, which can significantly reduce the activity of drug efflux pumps. The pluronic block copolymer (P85) is an important and promising example of a modifying agent for P-gp, the best-known and most thoroughly studied multidrug resistance membrane transporter, which was discovered in 1986.<sup>96,97</sup> Membrane fluidization by P85 treatment inhibits the P-gp ATPase drug efflux system and interferes with metabolic processes. Therefore, both energy depletion and increased permeability and fluidization of a broad spectrum of drugs are critical factors contributing to the activity of the block copolymer for reversion of multidrug resistance (MDR).<sup>98,99</sup>

As an alternative approach to the use of biological nanoparticles, anticancer peptide therapy focuses on the development of therapeutic peptides to kill resistant cells. A novel peptide, CT20p, derived from a helical unit of the pro-apoptotic protein Bax, is an example of a peptide that is an effective killer both *in vitro* and in a murine breast cancer tumor model. Boohaker and colleagues found that CT20p is amphiphilic. It can be encapsulated in polymeric nanoparticles, modifying tumor metabolism by causing an increase in mitochondrial membrane potential.<sup>82</sup> Another group focused on the small ubiquitin-like modifier 1 (SUMO1) peptidase SENP1, which reduces hypoxia and enhances chemosensitivity as a potential therapeutic target for drug-resistant testicular germ cell tumors.<sup>100</sup> Garg *et al.* also reported that PEGylated liposomes modified with a fibronectin mimetic peptide to target metastatic colon cancer cells inhibited tumor

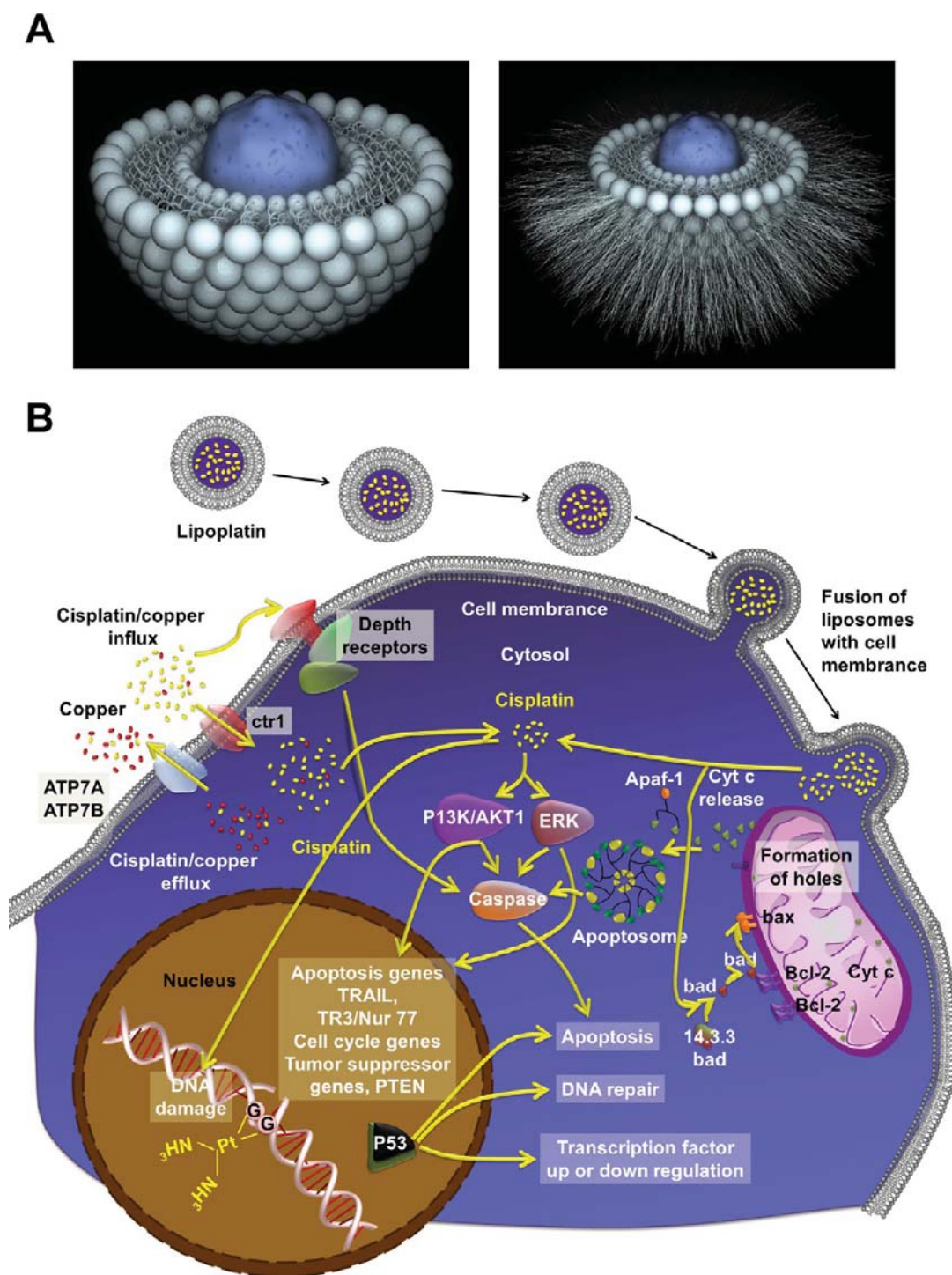


**Figure 2.** Depiction of a lipoplatin nanoparticle. (A) Cisplatin molecules are depicted as blue spheres surrounded by the lipid bilayer with hair-like PEGylated lipids protruding from the outer surface. These images were produced by François Caillaud, CNRS/SAGASCIENCE. (B) Penetration of lipoplatin nanoparticles through the cell membrane of tumor cells. Lipoplatin nanoparticles once inside the tumor cell mass can fuse with the cell membrane because of the presence of the fusogenic lipid DPPG in their lipid bilayer; an alternative mechanism proposed is that lipoplatin is taken up by endocytosis by tumor cells. These processes occurring at the cell membrane level are promoted by the lipid shell of the nanoparticles (disguised as nutrients).<sup>142,143</sup> Adapted from Boulikas, *et al.*, *Cancer Ther.* 2007, 5, 551–376. Used with permission.<sup>144</sup>

growth, reduced tumor metastasis, and stimulated drug internalization.<sup>101</sup> By targeting metabolism in resistant tumor cells, nanotechnology exhibits significant antitumor efficacy by inducing apoptosis in both sensitive and resistant cancer cells.

**nDDPs That Regulate Protein Trafficking and Degradation.** Autophagy begins with the formation of double-membrane vesicles (autophagosomes), which then fuse with lysosomes, where the sequestered contents undergo degradation and recycling, eliminating

misfolded proteins and damaged organelles.<sup>102,103</sup> The critically important process of autophagy, which is a mechanism of cell survival in the presence of genomic injury, oxidant stress, nutrient deprivation, hypoxia, inflammation, and viral/bacterial infection, has been recently recognized as important for conferring resistance to cancer treatment. Moreover, it was found that autophagy protects tumors from drug-treated apoptosis and aids survival and recovery with chemotherapeutic drug treatment. Modulation of autophagy dysfunction was found to resensitize resistant cancer cells to anticancer therapy.<sup>104–106</sup> Unlike cisplatin, which mainly causes cell death by inducing apoptosis, other platinum compounds have been shown to kill cells *via* autophagy.<sup>107</sup>

Fullerene C<sub>60</sub> (a spherical carbon structure) is a chemotherapeutic sensitizer that causes authentic autophagy at noncytotoxic concentrations.<sup>108</sup> These nanoparticles have been reported to induce autophagy and sensitize resistant cells to chemotherapy when combined with platinum drugs, killing both drug-sensitive and drug-resistant cancer cells, a novel therapeutic approach to circumvent drug resistance through modifying intracellular metabolism.<sup>109</sup>

#### RECENTLY DEVELOPED PT-TETHER NDDPS TO TREAT DRUG-RESISTANT CANCER WITH ABNORMAL MEMBRANE PROTEIN TRAFFICKING

A number of nanoparticles have recently been produced to conjugate with platinum. The process of designing Pt-tether nanoparticles includes tuning their shape and size in order to avoid disturbing the abnormal membrane protein in resistant cells. Surface modifications are also made, including various coatings and charges to increase hydrophilicity, which can alter the pharmacokinetics of platinum-based drugs. As it is difficult to entrap cisplatin in polymeric sustained-release nanoparticles (due to its small cross-section), Dhar *et al.* generated a platinum(IV) complex (*c,t,c*-[Pt-(NH<sub>3</sub>)<sub>2</sub>(O<sub>2</sub>CCH<sub>2</sub>CH<sub>2</sub>COOH)<sub>2</sub>Cl<sub>2</sub>]) as a prodrug that can be intracellularly processed into cisplatin. This release of cisplatin is achieved by reduction of the platinum(IV) complex by endogenous reductants and loss of the axial ligands. The prodrug has increased hydrophobicity and offers a position (pendant carboxylic acids) on the axial ligands for conjugation to a nanocarrier for efficient delivery, for example, by reaction with terminal amines (Figure 3A).<sup>110–113</sup>

Based on this chemistry, a series of Pt(IV)-tethered nanoparticles has been produced including single-walled carbon nanotubes,<sup>114</sup> gold nanoparticles,<sup>115</sup> PLGA-PEG nanoparticles,<sup>110,116</sup> peptides,<sup>117</sup> and aptamers,<sup>111</sup> providing good examples of both active platinum(II) derivative development and nDDPs. These nanoparticles provide platinum-based drugs with true drug carriers (Figure 3A). These studies also shed light on the impact of the complex environment of platinum on drug efficacy.

Additionally, various studies have reported that several kinds of Pt(IV)-based nanoparticles have shown very promising efficacy *in vivo*, with long blood circulation time and thereby high accumulation in tumors, with low systemic toxicity and better tolerance.<sup>111,117–120</sup>

Meanwhile, researchers are working to advance the ability of nDDPs to carry platinum drugs into resistant cells, especially with nanoparticle–Pt linkers. One popular strategy is to link a nanoparticle *via* a pH-sensitive coordination bond for endosomal release. Comenge *et al.*<sup>121</sup> used gold nanoparticles to tether cisplatin with pH-sensitive linkers, without affecting the therapeutic and imaging benefits. A novel rational engineering of cisplatin nanoparticles by poly(ethylene glycol) (PEG)-functionalized poly(isobutylene maleic acid) (PEG–PIMA) copolymer can coordinate with a [*cis*-diammineplatinum(II)] moiety through the pendant carboxylate ligands in a similar fashion to the carboxylate ligands of oxaliplatin. In effect, the NP acts as a bidentate ligand (Figure 3B). This complex self-assembles into a nanoparticle, releasing cisplatin in a pH-dependent manner.

Another strategy often used is to incorporate cisplatin into the hollow interior of nanoparticles. Single-walled carbon nanotubes (SWNTs), a “long boat” delivery system, offer abundant volume to encapsulate cisplatin. It was reported that cisplatin-bearing SWNTs increased anticancer efficiency 4–6 times that of cisplatin alone, causing high concentrations locally in cells of tumor xenograft tissue.<sup>122</sup> An assessment of a series of platinum(IV) complexes based on cisplatin with increasing lipophilicity were assessed by Johnstone *et al.*, showing that the most lipophilic platinum complex displayed the highest level of encapsulation in PLGA-PEG-COOH nanoparticles.<sup>123</sup> Lian *et al.* used highly biocompatible hollow Prussian blue (HPB) nanoparticles with a hollow interior and a microporous framework to absorb cisplatin noncovalently, and these were demonstrated to exert cytotoxicity in cell culture.<sup>124</sup> Mesoporous materials containing pores with diameters between 2 and 50 nm have become popular due to their large surface area, high core volume, and tunable nanoscale pores. The matrix pore architecture makes them suitable for hosting a broad variety of compounds, and they achieve localized intracellular release of the platinum drugs to minimize the influence of abnormal membrane proteins.<sup>83,125</sup> For example, mesoporous silica materials loaded with cisplatin and transplatin demonstrated cellular internalization and synergistic cell killing (the nanoparticles themselves display cytotoxicity).<sup>125</sup> Mesoporous silica nanoparticles conjugated with folic acid have been shown to enter cells *via* folate receptor (FR)-mediated endocytosis.<sup>126</sup> When loaded with cisplatin, these targeted mesoporous silica nanoparticles only showed cytotoxicity toward cells expressing FR. While this targeting concept is attractive, relying on endocytic



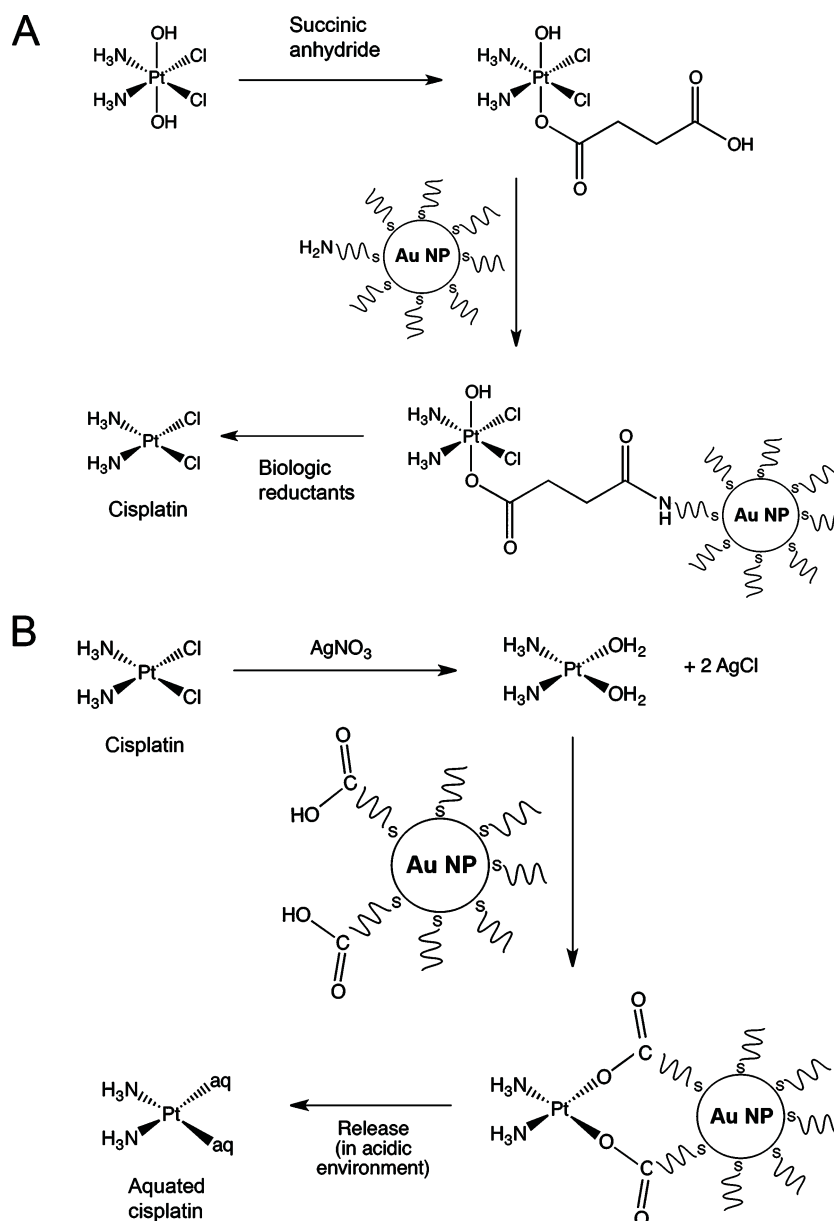


**Figure 3.** Examples of the chemical strategies used to tether cisplatin and cisplatin-like moieties to nanoparticle constructs. (A) Platinum(IV) complex *cis,trans,cis*-[PtCl<sub>2</sub>(OH)<sub>2</sub>(NH<sub>3</sub>)<sub>2</sub>] contains cisplatin in the equatorial plane along with two hydroxido ligands in the axial positions. Reaction with succinic acid produces *cis,trans,cis*-[PtCl<sub>2</sub>(OH)(O<sub>2</sub>CCH<sub>2</sub>CH<sub>2</sub>CO<sub>2</sub>H)(NH<sub>3</sub>)<sub>2</sub>]. The terminal carboxylic acid can then be conjugated to amine-functionalized nanoparticles (NPs) by amide coupling. In a biological environment, the tethered NP–platinum(IV) complex can be reduced by biological reductants such as glutathione or ascorbate. This results in the release of cisplatin, a platinum(II) complex, and the axial ligands (one of which is the NP). As such, provided that ligand exchange reactions at the platinum(IV) center do not take place, this conjugation method results in NPs that release cisplatin. (B) In this instance, cisplatin is tethered to the NP via its “leaving groups”. To achieve this chemistry, cisplatin is reacted with silver nitrate. While silver nitrate is soluble, silver chloride is highly insoluble—as silver precipitates with chloride exchanged from cisplatin, a “diaqua” species is produced. Aqua ligands are relatively unstable, and this aquation step of cisplatin (by loss of chlorido ligands) in cells is considered to be a necessary intermediate reaction before cisplatin reacts with DNA. Once the “reactive” diaqua species is produced, it is reacted with carboxylic-acid-functionalized NPs. The NP carboxylate groups coordinate with platinum(II) complex in place of the aqua ligands. In this sense, the NP acts as a very large bidentate ligand, analogous to the leaving groups of the platinum(II) drug carboplatin. Release of the platinum complex from the NP in a relatively acidic environment in theory releases the highly reactive diaqua form of cisplatin.

processing for targeting resistant cells may be limiting in cisplatin-resistant cells given their depressed endocytic rate.

Although novel chemotherapeutic nDDPs have been established every day, several problems still need careful investigation. Researchers expect nanomedicine

to resolve the problem of how to get enough of the right drug to the right place without causing side effects (from either the drug or the NPs), immune responses, or inducing resistance. A micelle-encapsulated hydrophobic platinum(II) nanomedicine displayed excellent tumor to tissue ratios and 6 times higher cellular accumulation

compared with the free platinum compound, providing a good example of not only outstanding pharmacokinetics and tumor selectivity but also specifically high cytotoxicity against tumor cells.<sup>127</sup> Harnessing the immune system capacity in order to induce antitumor response remains an important challenge. How to utilize immune response in prognosis and therapy remains unknown despite its high prevalence. A 15 kDa variable domain of *camelid* heavy-chain-only antibodies, called Nanobodies, are being explored for their ability to potentiate cancer therapy.<sup>128–130</sup> In other cases, bionanoparticles, such as antibodies peptides, etc., showed their ability to induce immune response and apoptosis.<sup>131</sup> In recent years, several nanoscale drug carriers have entered clinical trials.<sup>132</sup> Cisplatin treatment results in severe kidney toxicity, requiring patients to drink large amounts of water during treatment. However, that is not the case in NanoCarrier (Nanoplatin) trials, as the carrier's size allows it to move into and accumulate in the pancreatic tumor, instead of accumulating in the kidney.<sup>133–135</sup> A 30 nm polymer to transport chemotherapeutic drugs is currently undergoing phase II clinical trials with advanced or metastatic pancreatic cancer, doubling survival time from 5 months to more than 12.<sup>132,134,136–138</sup>

## FURTHER CHALLENGES AND PROSPECTS FOR THERAPEUTIC STRATEGIES TO COMBAT DRUG-RESISTANT CANCER

Cisplatin resistance still remains a major challenge to successful treatment of cancer. Nanotechnology is a field that has developed rapidly and provides a promising approach to chemotherapy. In addition, the properties of nDDPs, including stable and strong fluorescence, etc., also give promising opportunities to evaluate the sensitivity of imaging systems for chemotherapy.<sup>80,139,140</sup> For example, Xue *et al.* developed a self-indicating drug delivery system that visualized spatiotemporal drug release *via* tunable aggregation-induced emission by monitoring drug cargo fluorescence.<sup>141</sup> Although exciting approaches have been reported in the recent years, applications of nanotechnology to cancer treatment appear to overcome some of the limitations of traditional chemotherapy, giving hope that solutions to the problems of drug resistance can be found. To develop this approach, further study is needed in the following areas:

- (1) Abnormal membrane proteins as potential drug targets
- (2) The interaction and relationship between abnormal membrane proteins and tumor metabolism as well as the extracellular environment
- (3) The pharmacokinetics (including absorbance, distribution, metabolism, and excretion) of nanoscale drug delivery systems, especially active delivery of functionalized nanocarriers

- (4) Higher sensitivity imaging techniques with molecular specificity (as platinum-based drugs are difficult to trace)
- (5) The safety and toxicity of nanoparticles, as well as immune response

To achieve tangible therapeutic benefits from the above information, the mechanisms that cause abnormal membrane protein trafficking to develop into cisplatin resistance need to be exploited. Based on research reported so far, it can be expected that nDDPs that target abnormal membrane proteins may represent a useful approach to improving the clinical outcomes of existing platinum-based anticancer drugs.

**Conflict of Interest:** The authors declare no competing financial interest.

**Acknowledgment.** This work was financially supported in part by grants from the National Natural Science Foundation for Distinguished Young Scholars of China (No. 31225009), National Science and Technology support program (No. 2012BAF13B05), National Natural Science Foundation of China project (No. 81171455), National Key Basic Research Program of China (2009CB930200), and the Chinese Academy of Sciences (CAS) "Hundred Talents Program". This research was also partially supported by the Intramural Research Program of the National Institutes of Health, National Cancer Institute. We thank George Leiman for editorial assistance. We would also like to thank Dr. Teni Boulikas for allowing us to adapt her figure for Figure 2B. We also thank Dr. Juan Liu to advance the TOC and Figure 2.

## REFERENCES AND NOTES

1. McWhinney, S. R.; Goldberg, R. M.; McLeod, H. L. Platinum neurotoxicity pharmacogenetics. *Mol. Cancer Ther.* **2009**, *8*, 6–10.
2. Cepeda, V.; Fuertes, M. A.; Castilla, J.; Alonso, C.; Quevedo, C.; Perez, J. M. Biochemical mechanisms of cisplatin cytotoxicity. *Anticancer Agents Med. Chem.* **2007**, *7*, 3–18.
3. Paris, I.; Cappellini, G. C.; Malaguti, P.; Bassanelli, M.; Marchetti, P. Pharmacogenomics and chemotherapy. *Recent Prog. Med.* **2010**, *101*, 277–282.
4. Gottlieb, J. A.; Drewinko, B. Review of the current clinical status of platinum coordination complexes in cancer chemotherapy. *Cancer Chemother. Rep.* **1975**, *59*, 621–628.
5. Shen, D. W.; Pouliot, L. M.; Hall, M. D.; Gottesman, M. M. Cisplatin resistance: a cellular self-defense mechanism resulting from multiple epigenetic and genetic changes. *Pharmacol. Rev.* **2012**, *64*, 706–721.
6. Hall, M. D.; Okabe, M.; Shen, D. W.; Liang, X. J.; Gottesman, M. M. The role of cellular accumulation in determining sensitivity to platinum-based chemotherapy. *Annu. Rev. Pharmacol. Toxicol.* **2008**, *48*, 495–535.
7. Koberle, B.; Tomicic, M. T.; Usanova, S.; Kaina, B. Cisplatin resistance: preclinical findings and clinical implications. *Biochim. Biophys. Acta* **2010**, *1806*, 172–182.
8. Pelletier, H.; Millot, J. M.; Chauffert, B.; Manfait, M.; Genne, P.; Martin, F. Mechanisms of resistance of confluent human and rat colon cancer cells to anthracyclines: alteration of drug passive diffusion. *Cancer Res.* **1990**, *50*, 6626–6631.
9. Binks, S. P.; Dobrota, M. Kinetics and mechanism of uptake of platinum-based pharmaceuticals by the rat small intestine. *Biochem. Pharmacol.* **1990**, *40*, 1329–1336.
10. Huang, Y. Pharmacogenetics/genomics of membrane transporters in cancer chemotherapy. *Cancer Metastasis Rev.* **2007**, *26*, 183–201.
11. Ohmichi, M.; Hayakawa, J.; Tasaka, K.; Kurachi, H.; Murata, Y. Mechanisms of platinum drug resistance. *Trends Pharmacol. Sci.* **2005**, *26*, 113–116.

12. Werny, R. P.; Morin, P. J. Molecular mechanisms of platinum resistance: still searching for the Achilles' heel. *Drug Resist. Updates* **2004**, *7*, 227–232.
13. Koga, H.; Kotoh, S.; Nakashima, M.; Yokomizo, A.; Tanaka, M.; Naito, S. Accumulation of intracellular platinum is correlated with intrinsic cisplatin resistance in human bladder cancer cell lines. *Int. J. Oncol.* **2000**, *16*, 1003–1007.
14. Stordal, B.; Hamon, M.; McEneaney, V.; Roche, S.; Gillet, J. P.; O'Leary, J. J.; Gottesman, M.; Clynes, M. Resistance to paclitaxel in a cisplatin-resistant ovarian cancer cell line is mediated by P-glycoprotein. *PLoS One* **2012**, *7*, e40717.
15. Kishimoto, S.; Kawazoe, Y.; Ikeno, M.; Saitoh, M.; Nakano, Y.; Nishi, Y.; Fukushima, S.; Takeuchi, Y. Role of Na<sup>+</sup>, K<sup>+</sup>-ATPase  $\alpha$ 1 subunit in the intracellular accumulation of cisplatin. *Cancer Chemother. Pharmacol.* **2006**, *57*, 84–90.
16. Deeley, R. G.; Westlake, C.; Cole, S. P. Transmembrane transport of endo- and xenobiotics by mammalian ATP-binding cassette multidrug resistance proteins. *Physiol. Rev.* **2006**, *86*, 849–899.
17. Song, I. S.; Savaraj, N.; Siddik, Z. H.; Liu, P.; Wei, Y.; Wu, C. J.; Kuo, M. T. Role of human copper transporter Ctr1 in the transport of platinum-based antitumor agents in cisplatin-sensitive and cisplatin-resistant cells. *Mol. Cancer Ther.* **2004**, *3*, 1543–1549.
18. Samimi, G.; Varki, N. M.; Wilczynski, S.; Safaei, R.; Alberts, D. S.; Howell, S. B. Increase in expression of the copper transporter ATP7A during platinum drug-based treatment is associated with poor survival in ovarian cancer patients. *Clin. Cancer Res.* **2003**, *9*, 5853–5859.
19. More, S. S.; Akil, O.; Ianculescu, A. G.; Geier, E. G.; Lustig, L. R.; Giacomini, K. M. Role of the copper transporter, CTR1, in platinum-induced ototoxicity. *J. Neurosci.* **2010**, *30*, 9500–9509.
20. Huang, Y.; Sadee, W. Membrane transporters and channels in chemoresistance and -sensitivity of tumor cells. *Cancer Lett.* **2006**, *239*, 168–182.
21. Ejendal, K. F.; Hrycyna, C. A. Multidrug resistance and cancer: the role of the human ABC transporter ABCG2. *Curr. Protein Pept. Sci.* **2002**, *3*, 503–511.
22. Kis, O.; Robillard, K.; Chan, G. N.; Bendayan, R. The complexities of antiretroviral drug–drug interactions: role of ABC and SLC transporters. *Trends Pharmacol. Sci.* **2010**, *31*, 22–35.
23. Glavinas, H.; Krajcsi, P.; Cserepes, J.; Sarkadi, B. The role of ABC transporters in drug resistance, metabolism and toxicity. *Curr. Drug Delivery* **2004**, *1*, 27–42.
24. Gottesman, M. M.; Fojo, T.; Bates, S. E. Multidrug resistance in cancer: role of ATP-dependent transporters. *Nat. Rev. Cancer* **2002**, *2*, 48–58.
25. Fukuda, Y.; Schuetz, J. D. ABC transporters and their role in nucleoside and nucleotide drug resistance. *Biochem. Pharmacol.* **2012**, *83*, 1073–1083.
26. Fujino, H.; Saito, T.; Ogawa, S.; Kojima, J. Transporter-mediated influx and efflux mechanisms of pitavastatin, a new inhibitor of HMG-CoA reductase. *J. Pharm. Pharmacol.* **2005**, *57*, 1305–1311.
27. Marin, J. J.; Briz, O.; Monte, M. J.; Blazquez, A. G.; Macias, R. I. Genetic variants in genes involved in mechanisms of chemoresistance to anticancer drugs. *Curr. Cancer Drug Targets* **2012**, *12*, 402–438.
28. Larson, C. A.; Blair, B. G.; Safaei, R.; Howell, S. B. The role of the mammalian copper transporter 1 in the cellular accumulation of platinum-based drugs. *Mol. Pharmacol.* **2009**, *75*, 324–330.
29. Fink, D.; Nebel, S.; Aebi, S.; Nehme, A.; Howell, S. Loss of DNA mismatch repair due to knockout of MSH2 or PMS2 results in resistance to cisplatin and carboplatin. *Int. J. Oncol.* **1997**, *11*, 539–542.
30. Liang, X. J.; Yin, J. J.; Zhou, J. W.; Wang, P. C.; Taylor, B.; Cardarelli, C.; Kozar, M.; Forte, R.; Aszalos, A.; Gottesman, M. M. Changes in biophysical parameters of plasma membranes influence cisplatin resistance of sensitive and resistant epidermal carcinoma cells. *Exp. Cell Res.* **2004**, *293*, 283–291.
31. Xue, X.; You, S.; Zhang, Q.; Wu, Y.; Zou, G. Z.; Wang, P. C.; Zhao, Y. L.; Xu, Y.; Jia, L.; Zhang, X.; et al. Mitaplatin increases sensitivity of tumor cells to cisplatin by inducing mitochondrial dysfunction. *Mol. Pharmaceutics* **2012**, *9*, 634–644.
32. Liang, X. J.; Taylor, B.; Cardarelli, C.; Yin, J. J.; Annereau, J. P.; Garfield, S.; Wincovitch, S.; Szakacs, G.; Gottesman, M. M.; Aszalos, A. Different roles for K<sup>+</sup> channels in cisplatin-resistant cell lines argue against a critical role for these channels in cisplatin resistance. *Anticancer Res.* **2005**, *25*, 4113–4122.
33. Todor, I. N.; Lukyanova, N. Y.; Chekhun, V. F. The lipid content of cisplatin- and doxorubicin-resistant MCF-7 human breast cancer cells. *Exp. Oncol.* **2012**, *34*, 97–100.
34. Michelakis, E. D.; Webster, L.; Mackey, J. R. Dichloroacetate (DCA) as a potential metabolic-targeting therapy for cancer. *Br. J. Cancer* **2008**, *99*, 989–994.
35. Stacpoole, P. W. The pharmacology of dichloroacetate. *Metabolism* **1989**, *38*, 1124–1144.
36. Dhar, S.; Lippard, S. J. Mitaplatin, a potent fusion of cisplatin and the orphan drug dichloroacetate. *Proc. Natl. Acad. Sci. U.S.A.* **2009**, *106*, 22199–22204.
37. Xiao, H.; Yan, L.; Zhang, Y.; Qi, R.; Li, W.; Wang, R.; Liu, S.; Huang, Y.; Li, Y.; Jing, X. A dual-targeting hybrid platinum(IV) prodrug for enhancing efficacy. *Chem. Commun.* **2012**, *48*, 10730–10732.
38. Yadav, S.; van Vlerken, L. E.; Little, S. R.; Amiji, M. M. Evaluations of combination MDR-1 gene silencing and paclitaxel administration in biodegradable polymeric nanoparticle formulations to overcome multidrug resistance in cancer cells. *Cancer Chemother. Pharmacol.* **2009**, *63*, 711–722.
39. Kievit, F. M.; Wang, F. Y.; Fang, C.; Mok, H.; Wang, K.; Silber, J. R.; Ellenbogen, R. G.; Zhang, M. Doxorubicin loaded iron oxide nanoparticles overcome multidrug resistance in cancer *in vitro*. *J. Controlled Release* **2011**, *152*, 76–83.
40. Huang, Z.; Huang, Y. The change of intracellular pH is involved in the cisplatin-resistance of human lung adenocarcinoma A549/DDP cells. *Cancer Invest.* **2005**, *23*, 26–32.
41. Murakami, T.; Shibuya, I.; Ise, T.; Chen, Z. S.; Akiyama, S.; Nakagawa, M.; Izumi, H.; Nakamura, T.; Matsuo, K.; Yamada, Y.; et al. Elevated expression of vacuolar proton pump genes and cellular pH in cisplatin resistance. *Int. J. Cancer* **2001**, *93*, 869–874.
42. Laurencot, C. M.; Kennedy, K. A. Influence of pH on the cytotoxicity of cisplatin in EMT6 mouse mammary tumor cells. *Oncol. Res.* **1995**, *7*, 371–379.
43. Yanishevsky, R. M.; Stein, G. H. Regulation of the cell cycle in eukaryotic cells. *Int. Rev. Cytol.* **1981**, *69*, 223–259.
44. Robinson, A. C.; Collins, J. F.; Donachie, W. D. Prokaryotic and eukaryotic cell-cycle proteins. *Nature* **1987**, *328*, 766.
45. Peeper, D. S.; van der Eb, A. J.; Zantema, A. The G1/S cell-cycle checkpoint in eukaryotic cells. *Biochim. Biophys. Acta* **1994**, *1198*, 215–230.
46. Lin, W.; Arthur, G. Phospholipids are synthesized in the G2/M phase of the cell cycle. *Int. J. Biochem. Cell Biol.* **2007**, *39*, 597–605.
47. Jackowski, S. Coordination of membrane phospholipid synthesis with the cell cycle. *J. Biol. Chem.* **1994**, *269*, 3858–3867.
48. Hunter, T. Regulation of the eukaryotic cell cycle. Introduction. *Ciba Found. Symp.* **1992**, *170*, 1–6.
49. Nigg, E. A. Cyclin-dependent protein kinases: key regulators of the eukaryotic cell cycle. *Bioessays* **1995**, *17*, 471–480.
50. Hoyt, M. A. Eliminating all obstacles: regulated proteolysis in the eukaryotic cell cycle. *Cell* **1997**, *91*, 149–151.
51. Owa, T.; Yoshino, H.; Yoshimatsu, K.; Nagasu, T. Cell cycle regulation in the G1 phase: a promising target for the development of new chemotherapeutic anticancer agents. *Curr. Med. Chem.* **2001**, *8*, 1487–1503.
52. Shen, H.; Perez, R. E.; Davaadelger, B.; Maki, C. G. Two 4N cell-cycle arrests contribute to cisplatin-resistance. *PLoS One* **2013**, *8*, e59848.

53. Eastman, A. The mechanism of action of cisplatin: from adducts to apoptosis. In *Cisplatin: chemistry and biochemistry of a leading anticancer drug*; Lippert, B., Ed.; Verlag Helvetica Chimica Acta: Switzerland, 1999; pp 111–134.
54. Shah, M. A.; Schwartz, G. K. Cell cycle-mediated drug resistance: an emerging concept in cancer therapy. *Clin. Cancer Res.* **2001**, *7*, 2168–2181.
55. Pouliot, L. M.; Chen, Y. C.; Bai, J.; Guha, R.; Martin, S. E.; Gottesman, M. M.; Hall, M. D. Cisplatin sensitivity mediated by WEE1 and CHK1 is mediated by miR-155 and the miR-15 family. *Cancer Res.* **2012**, *72*, 5945–5955.
56. Ling, X.; Wen, L.; Zhou, Y. Role of mitochondrial translocation of telomerase in hepatocellular carcinoma cells with multidrug resistance. *Int. J. Med. Sci.* **2012**, *9*, 545–554.
57. Hirai, H.; Iwasawa, Y.; Okada, M.; Arai, T.; Nishibata, T.; Kobayashi, M.; Kimura, T.; Kaneko, N.; Ohtani, J.; Yamanaka, K.; et al. Small-molecule inhibition of Wee1 kinase by MK-1775 selectively sensitizes p53-deficient tumor cells to DNA-damaging agents. *Mol. Cancer Ther.* **2009**, *8*, 2992–3000.
58. Komizu, Y.; Ueoka, H.; Goto, K.; Ueoka, R. Remarkable inhibitory effects of hybrid liposomes on growth of human colon cancer cells through induction of cell cycle arrest along with apoptosis. *Int. J. Nanomed.* **2011**, *6*, 1913–1920.
59. Yang, X. Q.; Zhang, Z. M.; Wang, D.; Wang, G.; Zeng, L. L.; Yang, Z. Z. nm23-H1-siRNA enhances the chemosensitivity to liposome-encapsulated paclitaxel in lung adenocarcinoma cells *in vitro*. *Zhonghua Zhongliu Zazhi* **2011**, *33*, 405–409.
60. Ruan, F.; Xie, X. K.; Liu, S. Y. Inhibitory effects of survivin antisense oligonucleotide on drug-resistant human ovarian cancer cell COC1/DDP. *Aizheng* **2004**, *23*, 896–899.
61. Roa, W.; Zhang, X.; Guo, L.; Shaw, A.; Hu, X.; Xiong, Y.; Gulavita, S.; Patel, S.; Sun, X.; Chen, J.; et al. Gold nanoparticle sensitize radiotherapy of prostate cancer cells by regulation of the cell cycle. *Nanotechnology* **2009**, *20*, 375101.
62. Lange, T. S.; Kim, K. K.; Singh, R. K.; Strongin, R. M.; McCourt, C. K.; Brard, L. Iron(III)-salophene: an organometallic compound with selective cytotoxic and antiproliferative properties in platinum-resistant ovarian cancer cells. *PLoS One* **2008**, *3*, e2303.
63. Eom, H. J.; Choi, J. p38 MAPK activation, DNA damage, cell cycle arrest and apoptosis as mechanisms of toxicity of silver nanoparticles in Jurkat T cells. *Environ. Sci. Technol.* **2010**, *44*, 8337–8342.
64. Asharani, P. V.; Sethu, S.; Lim, H. K.; Balaji, G.; Valiyaveetil, S.; Hande, M. P. Differential regulation of intracellular factors mediating cell cycle, DNA repair and inflammation following exposure to silver nanoparticles in human cells. *Genome Integr.* **2012**, *3*, 2.
65. Wang, C. H.; Shih, W. C.; Chang, H. C.; Kuo, Y. Y.; Hung, W. C.; Ong, T. G.; Li, W. S. Preparation and characterization of amino-linked heterocyclic carbene palladium, gold, and silver complexes and their use as anticancer agents that act by triggering apoptotic cell death. *J. Med. Chem.* **2011**, *54*, 5245–5249.
66. Casaluca, F.; Sgambato, A.; Maione, P.; Ciardiello, F.; Gridelli, C. Emerging mitotic inhibitors for non-small cell carcinoma. *Expert Opin. Emerging Drugs* **2013**, *18*, 97–107.
67. Cui, M.; Naczynski, D. J.; Zevon, M.; Griffith, C. K.; Sheihet, L.; Povontud-Fuentes, I.; Chen, S.; Roth, C. M.; Moghe, P. V. Multifunctional albumin nanoparticles as combination drug carriers for intra-tumoral chemotherapy. *Adv. Healthcare Mater.* **2013**, *2*, 1236–1245.
68. Sasidharan, A.; Chandran, P.; Menon, D.; Raman, S.; Nair, S.; Koyakutty, M. Rapid dissolution of ZnO nanocrystals in acidic cancer microenvironment leading to preferential apoptosis. *Nanoscale* **2011**, *3*, 3657–3669.
69. Coronello, M.; Marcon, G.; Carotti, S.; Caciagli, B.; Mini, E.; Mazzei, T.; Orioli, P.; Messori, L. Cytotoxicity, DNA damage, and cell cycle perturbations induced by two representative gold(III) complexes in human leukemic cells with different cisplatin sensitivity. *Oncol. Res.* **2000**, *12*, 361–370.
70. Blagosklonny, M. V.; Robey, R.; Bates, S.; Fojo, T. Pretreatment with DNA-damaging agents permits selective killing of checkpoint-deficient cells by microtubule-active drugs. *J. Clin. Invest.* **2000**, *105*, 533–539.
71. Shi, J.; Votruba, A. R.; Farokhzad, O. C.; Langer, R. Nanotechnology in drug delivery and tissue engineering: from discovery to applications. *Nano Lett.* **2010**, *10*, 3223–3230.
72. Talevi, A.; Gantner, M. E.; Ruiz, M. E. Applications of nanosystems to anticancer drug therapy (part I. nanogels, nanospheres, nanocapsules). *Recent Pat. Anticancer Drug Discovery* **2012** Epub ahead of print.
73. Ruiz, M. E.; Gantner, M. E.; Talevi, A. Applications of nanosystems to anticancer drug therapy (part II. dendrimers, micelles, lipid-based nanosystems). *Recent Pat. Anticancer Drug Discovery* **2013** Epub ahead of print.
74. Jabir, N. R.; Tabrez, S.; Ashraf, G. M.; Shakil, S.; Damanhour, G. A.; Kamal, M. A. Nanotechnology-based approaches in anticancer research. *Int. J. Nanomed.* **2012**, *7*, 4391–4408.
75. Goncalves, A. S.; Macedo, A. S.; Souto, E. B. Therapeutic nanosystems for oncology nanomedicine. *Clin. Transl. Oncol.* **2012**, *14*, 883–890.
76. Kratz, F.; Warnecke, A. Finding the optimal balance: challenges of improving conventional cancer chemotherapy using suitable combinations with nano-sized drug delivery systems. *J. Controlled Release* **2012**, *164*, 221–235.
77. Cheng, J.; Meziani, M. J.; Sun, Y. P.; Cheng, S. H. Poly(ethylene glycol)-conjugated multi-walled carbon nanotubes as an efficient drug carrier for overcoming multidrug resistance. *Toxicol. Appl. Pharmacol.* **2011**, *250*, 184–193.
78. Haley, B.; Frenkel, E. Nanoparticles for drug delivery in cancer treatment. *Urol. Oncol.* **2008**, *26*, 57–64.
79. Arayne, M. S.; Sultana, N. Review: nanoparticles in drug delivery for the treatment of cancer. *Pak. J. Pharm. Sci.* **2006**, *19*, 258–268.
80. Liang, X. J.; Meng, H.; Wang, Y.; He, H.; Meng, J.; Lu, J.; Wang, P. C.; Zhao, Y.; Gao, X.; Sun, B.; et al. Metallofullerene nanoparticles circumvent tumor resistance to cisplatin by reactivating endocytosis. *Proc. Natl. Acad. Sci. U. S. A.* **2010**, *107*, 7449–7454.
81. Singhal, S. S.; Yadav, S.; Singhal, J.; Sahu, M.; Sehrawat, A.; Awasthi, S. Diminished drug transport and augmented radiation sensitivity caused by loss of RLIP76. *FEBS Lett.* **2008**, *582*, 3408–3414.
82. Boohaker, R. J.; Zhang, G.; Lee, M. W.; Nemec, K. N.; Santra, S.; Perez, J. M.; Khaled, A. R. Rational development of a cytotoxic peptide to trigger cell death. *Mol. Pharmaceutics* **2012**, *9*, 2080–2093.
83. Taratula, O.; Garbuzenko, O. B.; Chen, A. M.; Minko, T. Innovative strategy for treatment of lung cancer: targeted nanotechnology-based inhalation co-delivery of anticancer drugs and siRNA. *J. Drug Target* **2011**, *19*, 900–914.
84. Nosko, M. M.; Pivnyuk, V. M.; Solyanik, G. I.; Kulik, G. I.; Todor, I. N.; Momot, V. Y.; Melnikov, O. R.; Ponomareva, O. V.; Chekhun, V. F. Biodistribution analysis of cisplatin in liposomal form in animals with cisplatin-resistant and cisplatin-sensitive carcinoma. *Exp. Oncol.* **2010**, *32*, 40–43.
85. dos Santos Giuberti, C.; de Oliveira Reis, E. C.; Ribeiro Rocha, T. G.; Leite, E. A.; Lacerda, R. G.; Ramaldes, G. A.; de Oliveira, M. C. Study of the pilot production process of long-circulating and pH-sensitive liposomes containing cisplatin. *J. Liposome Res.* **2011**, *21*, 60–69.
86. Zalba, S.; Garrido, M. J. Liposomes, a promising strategy for clinical application of platinum derivatives. *Expert Opin. Drug Delivery* **2013**, *10*, 829–844.



87. Lucas, X.; Simon, S.; Schubert, R.; Gunther, S. Discovery of the inhibitory effect of a phosphatidylinositol derivative on P-glycoprotein by virtual screening followed by in vitro cellular studies. *PLoS One* **2013**, *8*, e60679.
88. Yefimova, S. L.; Kurilchenko, I. Y.; Tkacheva, T. N.; Rozhkov, V. A.; Sorokin, A. V.; Lukianova, N. Y.; Bezdenzhnykh, N. A.; Malyukin, Y. V.; Chekhun, V. F. Comparative study of dye-loaded liposome accumulation in sensitive and resistant human breast cancer cells. *Exp. Oncol.* **2012**, *34*, 101–106.
89. Chen, M.; Chen, J.; Hou, T.; Fang, Y.; Sun, W.; Hu, R.; Cai, B. Effect of phospholipid composition on pharmaceutical properties and anti-tumor activity of stealth liposomes containing brucine. *Zhongguo Zhongyao Zazhi* **2011**, *36*, 864–867.
90. Krieger, M. L.; Eckstein, N.; Schneider, V.; Koch, M.; Royer, H. D.; Jaehde, U.; Bendas, G. Overcoming cisplatin resistance of ovarian cancer cells by targeted liposomes in vitro. *Int. J. Pharm.* **2010**, *389*, 10–17.
91. Ye, S.; Yang, W.; Wang, Y.; Ou, W.; Ma, Q.; Yu, C.; Ren, J.; Zhong, G.; Shi, H.; Yuan, Z.; et al. Cationic liposome-mediated nitric oxide synthase gene therapy enhances the antitumor effects of cisplatin in lung cancer. *Int. J. Mol. Med.* **2013**, *31*, 33–42.
92. Farhat, F. S.; Temraz, S.; Kattan, J.; Ibrahim, K.; Bitar, N.; Haddad, N.; Jaloul, R.; Hatoum, H. A.; Nsouli, G.; Shamseddine, A. I. A phase II study of lipoplatin (liposomal cisplatin)/vinorelbine combination in HER-2/neu-negative metastatic breast cancer. *Clin. Breast Cancer* **2011**, *11*, 384–389.
93. Canta, A.; Chiorazzi, A.; Carozzi, V.; Meregalli, C.; Oggioni, N.; Sala, B.; Crippa, L.; Avezza, F.; Forestieri, D.; Rotella, G.; et al. In vivo comparative study of the cytotoxicity of a liposomal formulation of cisplatin (lipoplatin). *Cancer Chemother. Pharmacol.* **2011**, *68*, 1001–1008.
94. Devarajan, P.; Tarabishi, R.; Mishra, J.; Ma, Q.; Kourvetaris, A.; Vougiouka, M.; Boulikas, T. Low renal toxicity of lipoplatin compared to cisplatin in animals. *Anticancer Res.* **2004**, *24*, 2193–2200.
95. Arienti, C.; Tesei, A.; Ravaoli, A.; Ratta, M.; Carloni, S.; Mangianti, S.; Ulivi, P.; Nicoletti, S.; Amadori, D.; Zoli, W. Activity of lipoplatin in tumor and in normal cells in vitro. *Anticancer Drugs* **2008**, *19*, 983–990.
96. Chen, C. J.; Chin, J. E.; Ueda, K.; Clark, D. P.; Pastan, I.; Gottesman, M. M.; Roninson, I. B. Internal duplication and homology with bacterial transport proteins in the mdr1 (P-glycoprotein) gene from multidrug-resistant human cells. *Cell* **1986**, *47*, 381–389.
97. Thiebaut, F.; Tsuruo, T.; Hamada, H.; Gottesman, M. M.; Pastan, I.; Willingham, M. C. Cellular localization of the multidrug-resistance gene product P-glycoprotein in normal human tissues. *Proc. Natl. Acad. Sci. U.S.A.* **1987**, *84*, 7735–7738.
98. Batrakova, E. V.; Li, S.; Vinogradov, S. V.; Alakhov, V. Y.; Miller, D. W.; Kabanov, A. V. Mechanism of pluronic effect on P-glycoprotein efflux system in blood-brain barrier: contributions of energy depletion and membrane fluidization. *J. Pharmacol. Exp. Ther.* **2001**, *299*, 483–493.
99. Batrakova, E. V.; Li, S.; Li, Y.; Alakhov, V. Y.; Kabanov, A. V. Effect of pluronic P85 on ATPase activity of drug efflux transporters. *Pharm. Res.* **2004**, *21*, 2226–2233.
100. Wu, Y. C.; Ling, T. Y.; Lu, S. H.; Kuo, H. C.; Ho, H. N.; Yeh, S. D.; Shen, C. N.; Huang, Y. H. Chemotherapeutic sensitivity of testicular germ cell tumors under hypoxic conditions is negatively regulated by SENP1-controlled sumoylation of OCT4. *Cancer Res.* **2012**, *72*, 4963–4973.
101. Garg, A.; Tisdale, A. W.; Haidari, E.; Kokkoli, E. Targeting colon cancer cells using PEGylated liposomes modified with a fibronectin-mimetic peptide. *Int. J. Pharm.* **2009**, *366*, 201–210.
102. Codogno, P.; Meijer, A. J. Autophagy and signaling: their role in cell survival and cell death. *Cell Death Differ.* **2005**, *12* (Suppl 2), 1509–1518.
103. Levine, B.; Yuan, J. Autophagy in cell death: an innocent convict? *J. Clin. Invest.* **2005**, *115*, 2679–2688.
104. Ren, J. H.; He, W. S.; Nong, L.; Zhu, Q. Y.; Hu, K.; Zhang, R. G.; Huang, L. L.; Zhu, F.; Wu, G. Acquired cisplatin resistance in human lung adenocarcinoma cells is associated with enhanced autophagy. *Cancer Biother. Radiopharm.* **2010**, *25*, 75–80.
105. Sirichanchuen, B.; Pengsuparp, T.; Chanvorachote, P. Long-term cisplatin exposure impairs autophagy and causes cisplatin resistance in human lung cancer cells. *Mol. Cell. Biochem.* **2012**, *364*, 11–18.
106. Chen, S.; Rehman, S. K.; Zhang, W.; Wen, A.; Yao, L.; Zhang, J. Autophagy is a therapeutic target in anticancer drug resistance. *Biochim. Biophys. Acta* **2010**, *1806*, 220–229.
107. Bednarski, P. J.; Korpis, K.; Westendorf, A. F.; Perfahl, S.; Grunert, R. Effects of light-activated diazido-PtIV complexes on cancer cells in vitro. *Philos. Trans. R. Soc., A* **2013**, *371*, 20120118.
108. Zhang, Q.; Yang, W.; Man, N.; Zheng, F.; Shen, Y.; Sun, K.; Li, Y.; Wen, L. P. Autophagy-mediated chemosensitization in cancer cells by fullerene C60 nanocrystal. *Autophagy* **2009**, *5*, 1107–1117.
109. Wei, P.; Zhang, L.; Lu, Y.; Man, N.; Wen, L. C60(Nd) nanoparticles enhance chemotherapeutic susceptibility of cancer cells by modulation of autophagy. *Nanotechnology* **2010**, *21*, 495101.
110. Dhar, S.; Gu, F. X.; Langer, R.; Farokhzad, O. C.; Lippard, S. J. Targeted delivery of cisplatin to prostate cancer cells by aptamer functionalized Pt(IV) prodrug-PLGA-PEG nanoparticles. *Proc. Natl. Acad. Sci. U.S.A.* **2008**, *105*, 17356–17361.
111. Dhar, S.; Kolishetti, N.; Lippard, S. J.; Farokhzad, O. C. Targeted delivery of a cisplatin prodrug for safer and more effective prostate cancer therapy in vivo. *Proc. Natl. Acad. Sci. U.S.A.* **2011**, *108*, 1850–1855.
112. Wilson, J. J.; Lippard, S. J. Synthesis, characterization, and cytotoxicity of platinum(IV) carbamate complexes. *Inorg. Chem.* **2011**, *50*, 3103–3105.
113. Wilson, J. J.; Lippard, S. J. Modulation of ligand fluorescence by the Pt(II)/Pt(IV) redox couple. *Inorg. Chim. Acta* **2012**, *389*, 77–84.
114. Dhar, S.; Liu, Z.; Thomale, J.; Dai, H.; Lippard, S. J. Targeted single-wall carbon nanotube-mediated Pt(IV) prodrug delivery using folate as a homing device. *J. Am. Chem. Soc.* **2008**, *130*, 11467–11476.
115. Dhar, S.; Daniel, W. L.; Giljohann, D. A.; Mirkin, C. A.; Lippard, S. J. Polyvalent oligonucleotide gold nanoparticle conjugates as delivery vehicles for platinum(IV) warheads. *J. Am. Chem. Soc.* **2009**, *131*, 14652–14653.
116. Graf, N.; Bielenberg, D. R.; Kolishetti, N.; Muus, C.; Banyard, J.; Farokhzad, O. C.; Lippard, S. J.  $\alpha_v\beta_3$  Integrin-targeted PLGA-PEG nanoparticles for enhanced anti-tumor efficacy of a Pt(IV) prodrug. *ACS Nano* **2012**, *6*, 4530–4539.
117. Mukhopadhyay, S.; Barnes, C. M.; Haskel, A.; Short, S. M.; Barnes, K. R.; Lippard, S. J. Conjugated platinum(IV)-peptide complexes for targeting angiogenic tumor vasculature. *Bioconjugate Chem.* **2008**, *19*, 39–49.
118. Yang, J.; Sun, X.; Mao, W.; Sui, M.; Tang, J.; Shen, Y. Conjugate of Pt(IV)-histone deacetylase inhibitor as a prodrug for cancer chemotherapy. *Mol. Pharmaceutics* **2012**, *9*, 2793–2800.
119. Yang, J.; Liu, W.; Sui, M.; Tang, J.; Shen, Y. Platinum (IV)-coordinate polymers as intracellular reduction-responsive backbone-type conjugates for cancer drug delivery. *Biomaterials* **2011**, *32*, 9136–9143.
120. Wang, R.; Hu, X.; Wu, S.; Xiao, H.; Cai, H.; Xie, Z.; Huang, Y.; Jing, X. Biological characterization of folate-decorated biodegradable polymer-platinum(II) complex micelles. *Mol. Pharmaceutics* **2012**, *9*, 3200–3208.
121. Comenge, J.; Sotelo, C.; Romero, F.; Gallego, O.; Barnadas, A.; Parada, T. G.; Dominguez, F.; Puentes, V. F. Detoxifying antitumoral drugs via nanoconjugation: the case of gold nanoparticles and cisplatin. *PLoS One* **2012**, *7*, e47562.
122. Ajima, K.; Murakami, T.; Mizoguchi, Y.; Tsuchida, K.; Ichihashi, T.; Iijima, S.; Yudasaka, M. Enhancement of in vivo anticancer effects of cisplatin by incorporation inside

- single-wall carbon nanohorns. *ACS Nano* **2008**, *2*, 2057–2064.
123. Johnstone, T. C.; Lippard, S. J. The effect of ligand lipophilicity on the nanoparticle encapsulation of Pt(IV) prodrugs. *Inorg. Chem.* **2013**, *52*, 9915–9920.
124. Lian, H. Y.; Hu, M.; Liu, C. H.; Yamauchi, Y.; Wu, K. C. Highly biocompatible, hollow coordination polymer nanoparticles as cisplatin carriers for efficient intracellular drug delivery. *Chem. Commun.* **2012**, *48*, 5151–5153.
125. Tao, Z.; Toms, B.; Goodisman, J.; Asefa, T. Mesoporous silica microparticles enhance the cytotoxicity of anticancer platinum drugs. *ACS Nano* **2010**, *4*, 789–794.
126. Morelli, C.; Maris, P.; Sisci, D.; Perrotta, E.; Brunelli, E.; Perrotta, I.; Panno, M. L.; Tagarelli, A.; Versace, C.; Casula, M. F.; *et al.* PEG-templated mesoporous silica nanoparticles exclusively target cancer cells. *Nanoscale* **2011**, *3*, 3198–3207.
127. Jadhav, V. B.; Jun, Y. J.; Song, J. H.; Park, M. K.; Oh, J. H.; Chae, S. W.; Kim, I. S.; Choi, S. J.; Lee, H. J.; Sohn, Y. S. A novel micelle-encapsulated platinum(II) anticancer agent. *J. Controlled Release* **2010**, *147*, 144–150.
128. Shoaie-Hassani, A.; Mortazavi-Tabatabaei, S. A.; Sharif, S.; Madadi, S.; Rezaei-Khaligh, H.; Verdi, J. Recombinant lambda bacteriophage displaying nanobody towards third domain of HER-2 epitope inhibits proliferation of breast carcinoma SKBR-3 cell line. *Arch. Immunol. Ther. Exp.* **2013**, *61*, 75–83.
129. Tijink, B. M.; Laeremans, T.; Budde, M.; Stigter-van Walsum, M.; Dreier, T.; de Haard, H. J.; Leemans, C. R.; van Dongen, G. A. Improved tumor targeting of anti-epidermal growth factor receptor Nanobodies through albumin binding: taking advantage of modular Nanobody technology. *Mol. Cancer Ther.* **2008**, *7*, 2288–2297.
130. Oliveira, S.; Heukers, R.; Sornkom, J.; Kok, R. J.; van Bergen En Henegouwen, P. M. Targeting tumors with nanobodies for cancer imaging and therapy. *J. Controlled Release* **2013**, *172*, 607–617.
131. Chudecka-Glaz, A.; Rzepka-Gorska, I. Evaluation of serum levels of sCD30L ligand in patients with ovarian cancer in terms of selected clinico-pathological factors. *Contemp. Hematol./Oncol.* **2012**, *16*, 520–525.
132. Bourzac, K. Nanotechnology: carrying drugs. *Nature* **2012**, *491*, 58–60.
133. Endo, K.; Ueno, T.; Kondo, S.; Wakisaka, N.; Muro, S.; Ito, M.; Kataoka, K.; Kato, Y.; Yoshizaki, T. Tumor-targeted chemotherapy with the nanopolymer-based drug NC-6004 for oral squamous cell carcinoma. *Cancer Sci.* **2013**, *104*, 369–374.
134. Baba, M.; Matsumoto, Y.; Kashio, A.; Cabral, H.; Nishiyama, N.; Kataoka, K.; Yamasoba, T. Micellization of cisplatin (NC-6004) reduces its ototoxicity in guinea pigs. *J. Controlled Release* **2012**, *157*, 112–117.
135. Uchino, H.; Matsumura, Y.; Negishi, T.; Koizumi, F.; Hayashi, T.; Honda, T.; Nishiyama, N.; Kataoka, K.; Naito, S.; Kakizoe, T. Cisplatin-incorporating polymeric micelles (NC-6004) can reduce nephrotoxicity and neurotoxicity of cisplatin in rats. *Br. J. Cancer* **2005**, *93*, 678–687.
136. Takahashi, R.; Ishiwatari, T. Preparation of helical gold nanowires on surfactant tubules. *Chem. Commun.* **2004**, 1406140–1406147.
137. Nishiyama, N.; Kataoka, K. [Development of polymeric micelles for the delivery of antitumor agents]. *Gan To Kagaku Ryoho* **2009**, *36*, 357–361.
138. Murakami, M.; Cabral, H.; Matsumoto, Y.; Wu, S.; Kano, M. R.; Yamori, T.; Nishiyama, N.; Kataoka, K. Improving drug potency and efficacy by nanocarrier-mediated subcellular targeting. *Sci. Transl. Med.* **2011**, *3*, 64ra2.
139. Huo, S.; Ma, H.; Huang, K.; Liu, J.; Wei, T.; Jin, S.; Zhang, J.; He, S.; Liang, X. J. Superior penetration and retention behavior of 50 nm gold nanoparticles in tumors. *Cancer Res.* **2013**, *73*, 319–330.
140. Zhao, Y.; Zhang, X.; Xue, X.; Li, Z.; Chen, F.; Li, S.; Kumar, A.; Zou, G.; Liang, X. J. High throughput detection of human neutrophil peptides from serum, saliva, and tear by anthrax lethal factor-modified nanoparticles. *ACS Appl. Mater. Interfaces* **2013**, *5*, 8267–8272.
141. Xue, X.; Zhao, Y.; Dai, L.; Zhang, X.; Hao, X.; Zhang, C.; Huo, S.; Liu, J.; Liu, C.; Kumar, A.; *et al.* Spatiotemporal drug release visualized through a drug delivery system with tunable aggregation-induced emission. *Adv. Mater.* **2013**, *10.1002/adma.201302365*.
142. Boulikas, T. Clinical overview on lipoplatin: a successful liposomal formulation of cisplatin. *Expert Opin. Invest. Drugs* **2009**, *18*, 1197–1218.
143. Stathopoulos, G. P.; Boulikas, T. Lipoplatin formulation review article. *J. Drug Delivery* **2012**, *2012*, 581363.
144. Boulikas, T.; Pantos, A.; Bellis, E.; Christofis, P. Designing platinum compounds in cancer: structures and mechanisms. *Cancer Ther.* **2007**, *5*, 537–583.

# Recombinant Immunotoxin Therapy of Solid Tumors: Challenges and Strategies

Liang Shan<sup>1</sup>, Yuanyi Liu<sup>2</sup>, Paul Wang<sup>1\*</sup>

<sup>1</sup>Molecular Imaging Laboratory, Department of Radiology, Howard University, Washington DC; <sup>2</sup>Angimmune LLC, Rockville, MD

*Journal of Basic & Clinical Medicine 2013, 2(2):1-6*

## Abstract

Immunotoxins are a group of protein-based therapeutics, basically comprising two functional moieties: one is the antibody or antibody Fv fragment that allows the immunotoxin to bind specifically to target cells; another is the plant or bacterial toxin that kills the cells upon internalization. Immunotoxins have several unique features which are superior to conventional chemotherapeutics, including high specificity, extraordinary potency, and no known drug resistance. Development of immunotoxins evolves with time and technology, but significant progress has been achieved in the past 20 years after introduction of recombinant DNA technique and generation of the first single-chain variable fragment of monoclonal antibodies. Since then, more than 1,000 recombinant immunotoxins have been generated against cancer. However, most success in immunotoxin therapy has been achieved against hematological malignancies, several issues persist to be significant barriers for effective therapy of human solid tumors. Further development of immunotoxins will largely focus on the improvement of penetration capability to solid tumor mass and elimination of immunogenicity occurred when given repeatedly to patients. Promising strategies may include construction of recombinant antibody fragments with higher binding affinity and stability, elimination of immunodominant T- and B-cell epitopes of toxins, modification of immunotoxins with macromolecules like poly(ethylene glycol) and liposomes, and generation of immunotoxins with humanized antibody fragments and human endogenous cytotoxic enzymes. In this paper, we briefly reviewed the evolution of immunotoxin development and then discussed the challenges of immunotoxin therapy for human solid tumors and the potential strategies we may seek to overcome the challenges.

**Keywords:** Recombinant immunotoxin, cancer therapy, solid tumor, challenges, strategies

## Introduction

In the last decade of the 19th century, Paul Ehrlich postulated that if a compound could be made that selectively targeted against a disease-causing organism, then a toxin for that organism could be delivered along with the agent of selectivity and he further created the term “antibody” for such products (1, 2). With great efforts of about one century, scientists have not only confirmed the presence

of antibody but also unraveled its structure and function. Introduction of hybridoma technology by Kohler and Milstein in 1975 made it possible to produce monoclonal antibodies (MAbs) in a large scale (3). More recent development of recombinant DNA techniques provoked the interest of scientists to generate engineered antibody fragments as well as cytotoxic toxins (4, 5). Because of these technical achievements, antibody-based therapy has become one of the fastest growing fields in tumor therapy in recent years (6, 7).

In general, naked MAbs are rarely potent enough against cancer by themselves, they are more often used through linking cytotoxic chemical drugs or protein toxins. The former is usually called antibody-drug conjugates (ADCs), while the latter is known as immunotoxins (ITs). ADCs are generated by conjugating a MAb with a cytotoxic drug through a crosslinking reagent, while ITs are prepared by chemically conjugating an antibody or genetically fusing fragments of an antibody with a toxin, mostly from plants or bacteria such as ricin, saporin, *Pseudomonas* exotoxin A (PE), and *Diphtheria* toxin (DT) (8-10). Both ADCs and ITs are designed based on the concept that selective accumulation of cytotoxic agents at the tumor site and within the tumor cells can be achieved through the antibody specificity by targeting a specific antigen highly expressed by tumor cells, thereby improving therapeutic efficacy, while minimizing side effects induced by cytotoxic agents (11, 12). Since there have already had many excellent reviews on various aspects of ADCs, we focused in this review on the progress of IT development, and the major challenges we are facing and the potential strategies we may seek in the IT therapy of human solid tumors.

## Evolution of IT Development

ITs are basically composed of two functional moieties: one is a MAb or Fv portions of an antibody; another is a plant or bacterial toxin. MAbs are known to be the most specific agent against an antigen expressed by cancer cells, while the toxin part is among the most potent agents against cancer cells. One single IT molecule can inactivate over 200 ribosomes or elongation factor-2 molecules per minute and is potent enough to kill a cell as compared to  $10^4$ - $10^5$  molecules of a chemotherapeutic drug that are needed to kill one cell (13).

Development of ITs evolves with time and technology (5). The first generation of ITs was generated by coupling a native toxin with a MAb through a crosslinking reagent that forms disulfide bonds between the toxin and antibody moieties. However, native toxins induce severe side effects when given to humans due to their non-specific binding to normal cells. Native toxins are commonly composed of three domains: one is the receptor binding or cell recognition domain that enables the toxin to bind to the cell surface; one is the translocation domain that helps translocation of the A chain into cytosol; and the third one is the catalytic domain (also called activity domain or A chain) that exerts cytotoxic effects on cells upon translocation to the cytosol compartment (14,

Accepted in October 20, 2013

\*Correspondence author: Paul Wang, Molecular Imaging Laboratory, Department of Radiology, Howard University

2041 Georgia Ave, NW, Washington DC 20060, USA.

Tel: 202-865-3760, Fax: 202-865-3722

E-mail address: pwang@howard.edu

15). The binding domains of different toxins recognize various receptors ubiquitously on normal cells. The non-specific binding compromises the specificity of ITs, and induces severe systemic side effects. Thereby, toxins were deglycosylated and the binding domain was deleted when conjugated to MAbs, which led to the development of second generation of ITs. As expected, this approach significantly reduces the non-specific toxicities of ITs, allowing more ITs to be given to humans. Although the results were encouraging, some problems for the second generation ITs persisted, including: 1) poor stability due to the chemical crosslinking between antibody and toxin moieties; 2) heterogeneous composition and reduced binding affinity caused by the random conjugation; 3) poor penetration to solid tumor mass because of the large molecular size (>190 kDa); 4) immunogenicity; and 5) limited production (5, 16).

To improve the pharmacokinetics and reduce the side effects of ITs, great efforts have then been made to generate the third generation ITs which is called recombinant ITs (RITs). Development of RITs is driven by the ability to genetically design and express the antibody fragments and toxins with recombinant DNA techniques (17-19). Generally speaking, development of RITs involves two critical steps: 1) design and construct the recombinant antibody fragments and mutated PE or DT; and 2) expression and purification of the constructed products.

Regarding the expression of RITs, yeast, bacteria, CHO cells, and insect cells are the systems most frequently used (20-22). Each system has its unique features, but the most critical requirements for an expression system are the capability to properly fold complex proteins like RITs with multiple domains, and resistance to the toxin moiety. Cheap, fast, and easy to produce and purify the products is one more requirement. Bacterial systems are generally resistant to toxins and they are currently more widely used to generate RITs. A major limitation is that bacterial systems lack the ability to efficiently fold complex proteins. RITs with multiple domains must be denatured and refolded *ex vivo* to recover the binding capability and bioactivity. This also limits the yield of RIT production using bacterial systems. Toxin-resistant cell lines such as CHO and HEK293T are also used to produce RITs, but it is labor-intensive and time-consuming to select and characterize toxin-resistant cells (23). High cost for production is another issue for cell lines. Yeasts, like *Pichia pastoris* (*P. pastoris*), could grow in a simple, inexpensive medium with a high growth rate in either a shake flask or a fermenter, making it suitable for both small and large scale production. Importantly, *P. pastoris* is capable of properly folding RITs (20, 21). Similar to mammalian cell lines, *P. pastoris* is sensitive to toxins, thus it is also essential to select toxin-resistant strains.

Since the first report on generation of variable domain fragments in 1988, more than 1,000 RITs have been developed with different systems and development of RITs is becoming one of the fast-growing fields in cancer therapy (24, 25). This is also due to the superior features of RITs over the first two generations. First, RITs have a much smaller molecular size, which permits them penetrating into the deeper region of solid tumors. Second, RITs exhibit a more desirable pharmacokinetics with reduced immunogenicity and off-target toxicity. Third, application of engineered expression systems allows large-scale production of RITs more cost-effectively, eliminating the concern on production yield for clinical use. However, there are still some challenges we have to face, especially when RITs are used to treat human solid tumors and among them are the limited penetration capability and immunogenicity of RITs.

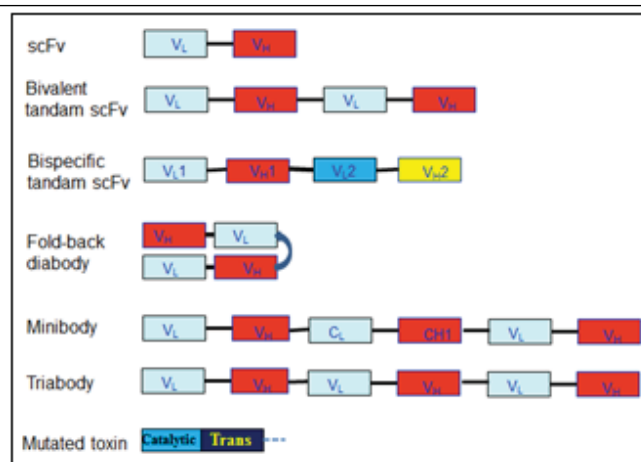


Figure 1: Constructs of different formats of recombinant antibody fragments and mutated toxin with deletion of the binding domain.  $V_L$  and  $V_H$  are the variable domains of light and heavy chains, respectively. scFv: single-chain fragment variable; Trans: translocation domain of toxin.

## Limited Penetration Capability

### 1. Molecular size, binding affinity, and binding-site barrier

Antibodies share a relatively uniform and well-characterized protein structure. They are typically composed of two large heavy chains and two small light chains, presenting a “Y”-shape. One characteristic is that antibodies have a small and extremely variable region at the two tips of “Y” that allows millions of antibodies possessing different and specific antigen binding sites (26, 27). Therefore, the smallest engineered fragment of antibodies that retains the original binding site is the scFv (25-30 kDa), which consists of a variable heavy domain ( $V_H$ ) and a variable light domain ( $V_L$ ) joined by a linker of 10 to 25 amino acid peptide (Fig. 1 and 2). The peptide linker is usually rich in glycine for flexibility and serine or threonine for solubility. Therefore, the smallest RITs generated currently are those containing one scFv. Due to the small size (~60 kDa), these small RITs exhibit markedly improved penetration capability to solid tumor mass, but they are also cleared quickly from bloodstream ( $t_{1/2} = \sim 20$  min) (28). They also have a low binding affinity due to the monovalency. The outcome is low tumor uptake and low therapeutic efficacy. More desirable pharmacokinetics has been achieved by constructing RITs using bivalent or divalent scFv (tandem scFv and diabody, 50-60 kDa), and scFv-fusion proteins (minibody, 80 kDa; scFv-Fc, 105 kDa) (29-30). Bivalent scFv is engineered by linking two scFvs with a peptide linker. This has been achieved with two formats: one is bivalent tandem scFv which is generated when the two scFvs form a single peptide chain; and another is bivalent scFv diabody which is generated by avoiding dimerization of the  $V_H$  and  $V_L$  domains from one scFv through a short linker (about five amino acids), while forcing the two scFvs to dimerize by using a long linker (about 15 amino acids) (Fig.2). Bivalent scFv RITs have a high binding affinity close to full antibodies, which are due to the increase of bivalent binding fraction and a decrease of the equilibrium dissociation constant ( $K_D$ ). Under most conditions for bivalent scFv binding, two measurable  $K_D$  exist with one for monovalent and the other for bivalent binding. The overall binding affinity of an antibody fragment is determined by the fraction of bivalent binding. Increasing the bivalent binding fraction is one approach to enhance the binding affinity, which can be achieved by optimize the primary and secondary structures (27). Wang et al.



have compared the binding affinity among different formats and shown that the bivalent fold-back format of RITs is several folds higher than bivalent tandem and monovalent scFv formats (31). Bivalent scFv RITs also have a longer circulation time ( $t_{1/2} = \sim 40$  min) than scFv RITs, but is still much shorter than antibody-toxin conjugates ( $t_{1/2} = 4-8$  hours or more). Other formats such as triabodies, tetrabodies and scFv-Fc have also been produced, but these formats are less commonly used to construct RITs because the benefit from increased binding affinity could be compromised by the increased molecular size. An alternative development is bispecific tandem scFv which is generated by linking two scFvs from two antibodies targeting different antigens (32-34). The therapeutic benefit of bispecific RITs is still unclear.

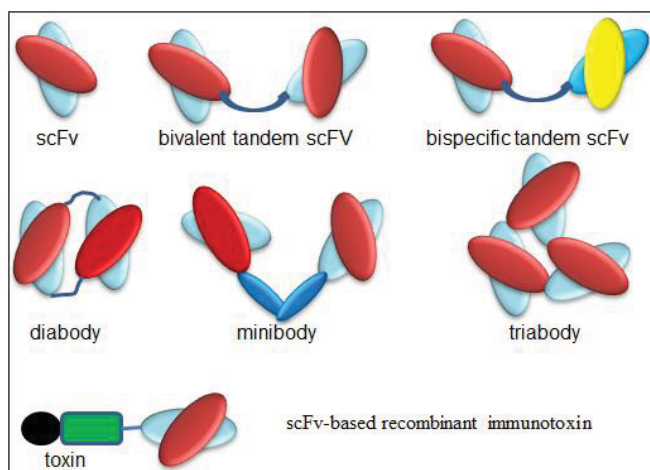


Figure 2: Carton structures of different formats of recombinant antibody fragments and representative scFv-based immunotoxin.

As pointed out above, limited transvascular diffusion of RITs into solid tumors represents a major problem for cancer therapy. Similar to naked antibodies, penetration of RITs into tumors is a process of diffusion, which is greatly affected by the molecular size and binding affinity of RITs as well as by the properties of antigen (density, distribution, and internalization rate). Decreased penetration rate following binding with antigens is referred to as the “binding-site barrier” (35-37). In general, smaller RITs and those with higher binding affinity have better penetration capabilities. Some studies have shown that the binding-site barrier could be overcome by increasing the dose, but the off-target toxicity will increase too. In this respect, increasing the stability and circulating half-life of a RIT by optimizing its structure offers an approach to enhance the penetration and accumulation of RITs in tumors.

## 2. Modifications of RITs with macromolecules

Successful delivery of drugs has been achieved with PEGylated liposomes, polymeric micelles, lipoplexes, and polyplexes (38, 39). One successful example is the liposomal doxorubicin (Doxil), the first FDA-approved nanodrug (40). Success of Doxil is based on several unrelated principles including prolonged circulation time and avoidance of the reticuloendothelial system due to the use of PEGylated liposomes, and high and stable remote loading of doxorubicin driven by a transmembrane ammonium sulfate gradient, which also allows for drug release at tumor site. Because of the enhanced permeability and retention (EPR) effect in tumors, Doxil is passively targeted to tumors and

its doxorubicin is released and becomes available to tumor cells. The EPR effect is based on the fact that the tumor vasculature is “leaky”, with an effective pore size of 200 nm to 600 nm in diameter in the endothelial lining of blood vessels (41, 42). The EPR effect allows for extravasation and accumulation of macromolecules in the interstitial space of tumors. Such accumulation is additionally affected by the virtual lack of a lymphatic system, responsible for the drainage of macromolecules from normal tissues. Such strategies have also been used to extend the half-life of RITs. Wang et al. have reported that a PEGylated chimeric toxin composed of transforming growth factor- $\alpha$  and PE exhibited an improvement in its circulation time and a decrease in its immunogenicity (43). Studies by Tsutsumi et al. have also shown that PEGylation of the RIT (anti-Tac(Fv)-PE38, LMB-2) improved its antitumor activity and reduced its toxicity and immunogenicity (44). PEGylation and coating may reduce opsonization of RITs by blood proteins, prevent interaction with blood components, and minimize the uptake by the reticuloendothelial system (45).

PEGylation or other coatings, however, may hinder drug release and drug interaction with target cells, which can be an obstacle in the realization of therapeutic response (39, 45). Attempts have been made to avoid this situation by means of shedding (i.e. a loss of the coating after arrival at the target site --- extracellular or intracellular release) (46-48). Shedding has been designed with various strategies and one effective strategy is the use of a pH-sensitive functional group as a linker between the coating and its anchor by taking advantage of the low extracellular pH (as low as 6.0) in tumors. The pH-sensitive functional group such as diorthoester, orthoester, vinyl ether, phosphoramidate, hydrazone, and thiopropionate undergoes protonation in the low pH environment, leading to hydrolysis of the sensitive bond and therefore to collapse of the particles (38, 39). Although coating and shedding approach has been well tested for delivery of chemotherapeutic drugs, there are no reports for its use in RIT therapy.

## Immunogenicity

### 1. Immunogenicity of antibody fragment and toxin moieties

IT therapy has been used successfully in patients with some types of hematological malignancies. Although easy access to tumor cells is a major factor, less human immunoreaction is another factor that is critical for the success. These patients typically have a severely compromised immune system because of the disease and previous chemotherapy. However patients with solid tumors often have a fairly healthy immune system. When RITs are given repeatedly to these patients, immunoreaction including neutralizing antibodies develops inevitably. Such a response does not necessarily cause severe side effects, but it may lead to a loss of the RIT efficacy and/or result in neutralization of the endogenous counterpart of patients (11, 49). Human immunoreaction is a major reason to stop repeated administration of RITs.

Both of the two components of RITs are immunogenic to humans, but the neutralizing antibodies are formed in patients mostly against the toxin moiety, occasionally against the mouse scFv when a mouse antibody sequence is used to construct the RITs. Reduced immunogenicity of antibody fragments is largely due to the removal of Fc region. A major intrinsic factor for the antibody's immunogenicity is the presence of carbohydrate side chains attached to the antibody via glycosylation sites conferred by

the amino acid sequence of the light and heavy chain Fv regions (50, 51).

PE and DT are the two toxins commonly used to construct RITs (15, 52, 53). PE is a 613 amino acid protein (66 kDa) originally produced by the bacterium *Pseudomonas aeruginosa*. A unique feature of PE is its resistance to various mutations without compromising its cytotoxicity. This characteristic enables PE to be modified genetically to raise its stability and lower its immunogenicity. To this end, various mutated versions of PE have been generated, and the 38 kDa and 40 kDa fragments (named PE38 and PE40, respectively) are the versions most frequently used in RIT construction. DT is a 535 amino acid protein (62 kDa) secreted by *Corynebacterium diphtheria*. Similar to PE, DT also has three functional domains, but organized in the reverse order. Except for the truncated fragments of DT486, DT389 and DT390, one modification of DT involves substitution of two amino acids at positions 390 and 525 in the C-terminal region, which results in a new molecule crossreacting material-107 (CRM-107) (54, 55). A major benefit of these mutated versions of PE and DT is the reduced non-specific toxicity to humans. For example, PE40 has been shown to be more than 100-fold less toxic than the native PE, and CRM-107 reduces the non-specific binding of native DT by 8000-fold, thus increasing the toxin's tumor-specificity of 10,000-fold (13, 55). However, the immunogenicity of these mutated toxins remains to be an issue although reduced significantly. An associated issue is that the immunogenicity to humans is determined only in clinical trials or after product launch and there is still a debate on the suitability of animal models for immunogenicity prediction during drug development because of the species-specificity of the immune response (56, 57). Most studies have shown that conventional animal models over-estimate immunogenicity in patients, making them unsuitable to predict immunogenicity in patients. However, animal models are increasingly used for selected immunogenicity studies.

## 2. Efforts on minimizing immunogenicity and next generation of RITs

To mitigate the immunogenicity, several strategies have been tested. Efforts to decrease antibody responses to ITs with cyclophosphamide, cyclosporine, or rituximab have been unsuccessful (58, 59). Interestingly, combined use of RITs with immune-modulating agents has been shown to be an approach to reduce the generation of neutralizing antibodies. Studies by Mossoba et al. have shown that induction treatment with pentostatin and cyclophosphamide before IT therapy effectively prevents the formation of neutralizing antibodies in mice and patients treated with a RIT called SS1P, which is further improved by maintenance pentostatin and cyclophosphamide therapy (60-62). Pentostatin and cyclophosphamide are two agents that could severely deplete host B and T immune cells with relative sparing of host myeloid cells, and without activity in mesothelioma. Elimination of immunodominant T- and B-cell epitopes is another strategy under studies to reduce the toxin immunogenicity (63-65). Pastan et al. have identified seven major B-cell epitope groups with 13 subgroups by using 60 monoclonal antibodies against PE38 and by mutating large surface-exposed residues to alanine (65). It has been shown that deletion of the specific hydrophilic amino acids from PE38 protein has significantly reduced its immunogenicity but still retain its full cytotoxic activity (65).

The immunogenicity problem is also addressed by developing the next or fourth generation of RITs through using humanized or human antibody fragments and human endogenous cytotoxic enzymes such as RNase, Granzyme B, and death-associated

protein kinase 2 (DAPK2) (66-68). RNase is a type of nuclease, playing critical roles in the maturation of RNA molecules as well as clearance of cellular RNA that is no longer required. Granzyme B is an immune defense protein that is secreted from the cytotoxic granules of activated cytotoxic T-cells and natural killer cells. Following the perforin-dependent translocation of Granzyme B into the cytoplasm of target cells, a proteolytic cascade can be initiated, which leads to target cell undergoing apoptosis. DAPK2 is an enzyme that belongs to the serine/threonine protein kinase family and functions as a positive mediator of apoptosis. Overproduction of DAPK2 protein has been shown to induce cell apoptosis. It is highly expected that the immunogenicity of fourth generation RITs will be minimized, but studies are still very limited and the therapeutic efficacy needs to be determined.

## Summary

Reviewing various clinical and preclinical studies, there is no doubt that RITs are one of the most promising methods for cancer therapy. At present, limited penetration capability into solid tumors and immunogenicity represent the two major barriers or challenges for RIT therapy of human solid tumors. Others such as vascular leak syndrome and hepatotoxicity are observed as dose-limiting side effects in some patients, but both are relatively rare (69, 70). Vascular leak syndrome is characterized by increased vascular permeability accompanied by extravasation of fluids and proteins, resulting in interstitial edema and organ failure. Although the pathogenesis of vascular damage is poorly understood, RITs is considered to bind with endothelium to induce a direct toxic effect or activate leukocytes to induce inflammatory cascades and disrupt endothelial cell integrity of normal blood vessels. Hepatotoxicity is a common side effect for PE-based RITs, presumably attributed to TNF-alpha release of Kupffer cells following binding with PE (71). Optimizing the inherent relationship between amino acid sequence, structure, and function will be at the heart of further optimized engineering of the antibody fragment moiety, while full humanization of the RITs will be a key for elimination of the immunogenicity.

## Acknowledgments

This work was supported in part by DoD USAMRMC W81XWH-10-1-0767 and 3G12 RR003048 from the RCMI Program Division on Research Infrastructure, National Center for Research Resources, NIH.

## References

1. Gensini GF, Conti AA, Lippi D. The contributions of Paul Ehrlich to infectious disease. *J Infect* 2007;54(3):221-4.
2. Winau F, Westphal O, Winau R. Paul Ehrlich--in search of the magic bullet. *Microbes Infect* 2004;6(8):786-9.
3. Kohler G, Milstein C. Continuous cultures of fused cells secreting antibody of predefined specificity. *Nat* 1975;256:495-7.
4. Niv R, Cohen CJ, Denkberg G, Segal D, Reiter Y. Antibody engineering for targeted therapy of cancer: recombinant Fv-immunotoxins. *Curr Pharm Biotechnol* 2001;2(1):19-46.
5. Pastan I, Hassan R, Fitzgerald DJ, Kreitman RJ. Immunotoxin treatment of cancer. *Annu Rev Med* 2007;58:221-37.
6. Sapra P, Shor B. Monoclonal antibody-based therapies in cancer: advances and challenges. *Pharmacol Ther* 2013;138:452-69.

7. Dillman RO. Cancer immunotherapy. *Cancer Biother Radiopharm* 2011;26:1-64.
8. Dosio F, Brusa P, Cattel L. Immunotoxins and anticancer drug conjugate assemblies: the role of the linkage between components. *Toxins (Basel)* 2011;3:848-83.
9. Becker N, Benhar I. Antibody-based immunotoxins for the treatment of cancer. *Antibodies* 2012;1:39-69.
10. Janthur WD, Cantoni N, Mamot C. Drug conjugates such as antibody drug conjugates (ADCs), immunotoxins and immunoliposomes challenge daily clinical practice. *Int J Mol Sci* 2012;13:16020-45.
11. Madhumathi J, Verma RS. Therapeutic targets and recent advances in protein immunotoxins. *Curr Opin Microbiol* 2012;15:300-9.
12. Risberg K, Fodstad O, Andersson Y. Immunotoxins: a promising treatment modality for metastatic melanoma? *The Ochsner J* 2012;10:193-9.
13. Li YM, Hall WA. Targeted toxins in brain tumor therapy. *Toxins (Basel)*. 2010;2(11):2645-62.
14. Pastan I, Hassan R, Fitzgerald DJ, Kreitman RJ. Immunotoxin therapy of cancer. *Nat Rev Cancer* 2006;6:559-65.
15. Adkins I, Holubova J, Kosova M, Sadilkova L. Bacteria and their toxins tamed for immunotherapy. *Curr Pharm Biotechnol* 2012;13:1446-73.
16. Litvak-Greenfeld D, Benhar I. Risks and untoward toxicities of antibody-based immunoconjugates. *Adv Drug Deliv Rev* 2012;64:1782-99.
17. Pranchevicius MC, Vieira TR. Production of recombinant immunotherapeutics for anticancer treatment: The role of bioengineering. *Bioengineered* 2013;4(5):305-12.
18. Govindan SV, Goldenberg DM. Designing immunoconjugates for cancer therapy. *Expert Opin Biol Ther* 2012;12(7):873-90.
19. Zhang F, Shan L, Liu Y, Neville D, Woo JH, Chen Y, Korotcov A, Lin S, Huang S, Sridhar R, Liang W, Wang PC. An anti-PSMA bivalent immunotoxin exhibits specificity and efficacy for prostate cancer imaging and therapy. *Adv Healthc Mater* 2013;2:736-44.
20. Liu YY, Woo JH, Neville DM. Overexpression of an anti-CD3 immunotoxin increases expression and secretion of molecular chaperone BiP/Kar2p by *Pichia pastoris*. *Appl Environ Microbiol* 2005;71:5332-40.
21. Liu YY, Woo JH, Neville DM. Targeted introduction of a diphtheria toxin resistant mutation into the chromosomal EF-2 locus of *Pichia pastoris* and expression of immunotoxin in the EF-2 mutants. *Protein Expr Purif* 2003;30:262-74.
22. Wan L, Zeng L, Chen L, Huang Q, Li S, Lu Y, Li Y, Cheng J, Lu X. Expression, purification, and refolding of a novel immunotoxin containing humanized single-chain fragment variable antibody against CTLA4 and the N-terminal fragment of human perforin. *Protein Expr Purif* 2006;48(2):307-13.
23. Liu YY, Gordienko I, Mathias A, Ma S, Thompson J, Woo JH, Neville DM Jr. Expression of an anti-CD3 single-chain immunotoxin with a truncated diphtheria toxin in a mutant CHO cell line. *Protein Expr Purif* 2000;19:304-11.
24. Bird RE, Hardman KD, Jacobson JW, Johnson S, Kaufman BM, Lee SM, Lee T, Pope SH, Riordan GS, Whitlow M. Single-chain antigen-binding proteins. *Science* 1988;242:423-6.
25. Huston JS, Levinson D, Mudgett-Hunter M, Tai MS, Novotny J, Margolies MN, Ridge RJ, Brucoleri RE, Haber E, Crea R, Oppermann H. Protein engineering of antibody binding sites: Recovery of specific activity in an anti-digoxin single-chain Fv analogue produced in *Escherichia coli*. *Proc Natl Acad Sci USA* 1988;85:5879-83.
26. Holliger P, Hudson PJ. Engineered antibody fragments and the rise of single domains. *Nat Biotechnol* 2005;23:1126-36.
27. Olafsen T, Wu AM. Antibody vectors for imaging. *Semin Nucl Med* 2010;40:167-81.
28. Bühler P, Wetterauer D, Gierschner D, Wetterauer U, Beile UE, Wolf P. Influence of structural variations on biological activity of anti-PSMA scFv and immunotoxins targeting prostate cancer. *Anticancer Res* 2010;30:3373-9.
29. Thompson J, Stavrou S, Weetall M, Hexham JM, Digan ME, Wang Z, Woo JH, Yu Y, Mathias A, Liu YY, Ma S, Gordienko I, Lake P, Neville DM Jr. Improved binding of a bivalent single-chain immunotoxin results in increased efficacy for in vivo T-cell depletion. *Protein Eng* 2001;14:1035-41.
30. Nelson AL. Antibody fragments: hope and hype. *MAbs* 2010;2:77-83.
31. Wang Z, Kim GB, Woo JH, Liu YY, Mathias A, Stavrou S, Neville DM Jr. Improvement of a recombinant anti-monkey anti-CD3 diphtheria toxin based immunotoxin by yeast display affinity maturation of the scFv. *Bioconjug Chem* 2007;18:947-55.
32. May C, Sapra P, Gerber HP. Advances in bispecific biotherapeutics for the treatment of cancer. *Biochem Pharmacol* 2012;84(9):1105-12.
33. Reichert JM. Bispecific antibodies and ADCs: Once and future kings? *MAbs* 2011;3(4):329-30.
34. Frankel AE, Woo JH. Bispecific immunotoxins. *Leuk Res* 2009;33(9):1173-4.
35. Saga T, Neumann RD, Heya T, Sato J, Kinuya S, Le N, Paik CH, Weinstein JN. Targeting cancer micrometastases with monoclonal antibodies: a binding-site barrier. *Proc Natl Acad Sci USA* 1995;92(19):8999-9003.
36. Weinstein JN, van Osdol W. Early intervention in cancer using monoclonal antibodies and other biological ligands: micropharmacology and the "binding site barrier". *Cancer Res* 1992;52(9 Suppl):2747s-51s.
37. Juweid M, Neumann R, Paik C, Perez-Bacete MJ, Sato J, van Osdol W, Weinstein JN. Micropharmacology of monoclonal antibodies in solid tumors: direct experimental evidence for a binding site barrier. *Cancer Res* 1992;52(19):5144-53.
38. Drummond DC, Zignani M, Leroux J. Current status of pH-sensitive liposomes in drug delivery. *Prog Lipid Res* 2000;39:409-60.
39. Romberg B, Hennink WE, Storm G. Sheddable coatings for long-circulating nanoparticles. *Pharm Res* 2008;25:55-71.
40. Barenholz Y. Doxil®-the first FDA-approved nano-drug: lessons learned. *J Control Release* 2012;160:117-34.
41. Maeda H, Nakamura H, Fang J. The EPR effect for macromolecular drug delivery to solid tumors: Improvement of tumor uptake, lowering of systemic toxicity, and distinct tumor imaging in vivo. *Adv Drug Deliv Rev* 2013;65:71-9.
42. Waite CL, Roth CM. Nanoscale drug delivery systems for enhanced drug penetration into solid tumors: current progress and opportunities. *Crit Rev Biomed Eng* 2012;40:21-41.
43. Wang QC, Pai LH, Debinski W, Fitzgerald DJ, Pastan I. Polyethylene glycol-modified chimeric toxin composed of transforming growth factor alpha and *Pseudomonas* exotoxin. *Cancer Res* 1993;53:4588-94.
44. Tsutsumi Y, Onda M, Nagata S, Lee B, Kreitman RJ, Pastan I. Site-specific chemical modification with polyethylene glycol of recombinant immunotoxin anti-Tac(Fv)-PE38 (LMB-2) improves antitumor activity and reduces animal toxicity and immunogenicity. *Proc Natl Acad Sci USA* 2000;97:8548-53.



45. Buse J, El-Aneed A. Properties, engineering and applications of lipid-based nanoparticle drug-delivery systems: current research and advances. *Nanomed* 2010;5:1237-60.
46. Lu T, Wang Z, Ma Y et al. Influence of polymer size, liposomal composition, surface charge, and temperature on the permeability of pH-sensitive liposomes containing lipid-anchored poly(2-ethylacrylic acid). *Int J Nanomed* 2012;7:4917-26.
47. Wehunt MP, Winschel CA, Khan AK, Guo TL, Abdrakhmanova GR, Sidorov V. Controlled drug-release system based on pH-sensitive chloride-triggerable liposomes. *J Liposome Res* 2013;23:37-46.
48. Leite EA, Souza CM, Carvalho-Júnior AD, Coelho LG, Lana AM, Cassali GD, Oliveira MC. Encapsulation of cisplatin in long-circulating and pH-sensitive liposomes improves its antitumor effect and reduces acute toxicity. *Int J Nanomed* 2012;7:5259-69.
49. Kelly RJ, Sharon E, Pastan I, Hassan R. Mesothelin-targeted agents in clinical trials and in preclinical development. *Mol Cancer Ther* 2012;11:517-25.
50. Fiona A Harding, corresponding author Marcia M Stickler, Jennifer Razo, and Robert B DuBridge. The immunogenicity of humanized and fully human antibodies: Residual immunogenicity resides in the CDR regions. *MAbs* 2010;2(3):256-65.
51. Arnold JN, Wormald MR, Sim RB, Rudd PM, Dwek RA. The impact of glycosylation on the biological function and structure of human immunoglobulins. *Annu Rev Immunol* 2007;25:21-50.
52. Antignani A, Fitzgerald D. Immunotoxins: The Role of the Toxin. *Toxins (Basel)* 2013;5(8): 1486-502.
53. Bernardes N, Chakrabarty AM, Fialho AM. Engineering of bacterial strains and their products for cancer therapy. *Appl Microbiol Biotechnol* 2013;97(12):5189-99.
54. Riedel CJ, Muraszko KM, Youle RJ. Diphtheria toxin mutant selectively kills cerebellar Purkinje neurons. *Proc Natl Acad Sci USA* 1990;87(13):5051-5.
55. Greenfield L, Johnson VG, Youle RJ. Mutations in diphtheria toxin separate binding from entry and amplify immunotoxin selectivity. *Science* 1987;238:536-9.
56. Brinks V, Jiskoot W, Schellekens H. Immunogenicity of therapeutic proteins: the use of animal models. *Pharm Res* 2011;28:2379-85.
57. Bussiere JL. Animal models as indicators of immunogenicity of therapeutic proteins in humans. *Dev Biol (Basel)* 2003;112:135-9.
58. Selvaggi K, Saria EA, Schwartz R, Vlock DR, Ackerman S, Wedel N, Kirkwood JM, Jones H, Ernstoff MS. Phase I/II study of murine monoclonal antibody-ricin A chain (Xomazyme-Mel) immunoconjugate plus cyclosporine A in patients with metastatic melanoma. *J Immunother* 1993;13:201-7.
59. Hassan R, Williams-Gould J, Watson T, Pai-Scherf L, Pastan I. Pretreatment with rituximab does not inhibit the human immune response against the immunogenic protein LMB-1. *Clin Cancer Res* 2004;10:16-8.
60. Mossoba ME, Onda M, Taylor J, Massey PR, Treadwell S, Sharon E, Hassan R, Pastan I, Fowler DH. Pentostatin plus cyclophosphamide safely and effectively prevents immunotoxin immunogenicity in murine hosts. *Clin Cancer Res* 2011;17(11):3697-705.
61. Hassan R, Miller AC, Sharon E, Thomas A, Reynolds JC, Ling A, Kreitman RJ, Miettinen MM, Steinberg SM, Fowler DH, Pastan I. Major cancer regressions in mesothelioma after treatment with an anti-mesothelin immunotoxin and immune suppression. *Sci Transl Med* 2013;5(208):208ra147.
62. Weldon JE, Xiang L, Zhang J, Beers R, Walker DA, Onda M, Hassan R, Pastan I. A recombinant immunotoxin against the tumor-associated antigen mesothelin reengineered for high activity, low off-target toxicity, and reduced antigenicity. *Mol Cancer Ther* 2013;12:48-57.
63. Liu W, Onda M, Lee B, Hassan R, Xiang L, Pastan I. Recombinant immunotoxin engineered for low immunogenicity and antigenicity by identifying and silencing human B-cell epitopes. *Proc Natl Acad Sci USA* 2012;109:11782-7.
64. Onda M, Nagata S, Fitzgerald DJ, Beers R, Fisher RJ, Vincent JJ, Lee B, Nakamura M, Hwang J, Kreitman RJ, Hassan R, Pastan I. Characterization of the B cell epitopes associated with a truncated form of *Pseudomonas* exotoxin (PE38) used to make immunotoxins for the treatment of cancer patients. *J Immunol* 2006;177:8822-34.
65. Pastan I, Onda M, Weldon J, Fitzgerald D, Kreitman R. Immunotoxins with decreased immunogenicity and improved activity. *Leuk Lymphoma* 2011;52 Suppl 2:87-90.
66. Weidle UH, Georges G, Brinkmann U. Fully human targeted cytotoxic fusion proteins: new anticancer agents on the horizon. *Cancer Genomics Proteomics*. 2012;9(3):119-33.
67. Mathew M, Verma RS. Humanized immunotoxins: a new generation of immunotoxins for targeted cancer therapy. *Cancer Sci* 2009;100(8):1359-65.
68. Rosenblum MG, Barth S. Development of novel, highly cytotoxic fusion constructs containing granzyme B: unique mechanisms and functions. *Curr Pharm Des* 2009;15(23):2676-92.
69. Liu XY, Pop LM, Schindler J, Vitetta ES. Immunotoxins constructed with chimeric, short-lived anti-CD22 monoclonal antibodies induce less vascular leak without loss of cytotoxicity. *MAbs* 2012;4:57-68.
70. Smallshaw JE, Ghetie V, Rizo J, Fulmer JR, Trahan LL, Ghetie MA, Vitetta ES. Genetic engineering of an immunotoxin to eliminate pulmonary vascular leak in mice. *Nat Biotechnol* 2003;21:387-91.
71. Rosenblum MG, Shawver LK, Marks JW, Brink J, Cheung L, Langton-Webster B. Recombinant immunotoxins directed against the c-erb-2/HER2/neu oncogene product: in vitro cytotoxicity, pharmacokinetics, and in vivo efficacy studies in xenograft models. *Clin Cancer Res* 1999;5:865-74.



Contents lists available at ScienceDirect

## Biotechnology Advances

journal homepage: [www.elsevier.com/locate/biotechadv](http://www.elsevier.com/locate/biotechadv)

Research review paper

## Techniques for physicochemical characterization of nanomaterials

Ping-Chang Lin<sup>a</sup>, Stephen Lin<sup>a</sup>, Paul C. Wang<sup>a</sup>, Rajagopalan Sridhar<sup>b,\*</sup><sup>a</sup> Laboratory of Molecular Imaging, Department of Radiology, Howard University, Washington, DC 20060, USA<sup>b</sup> Department of Radiation Oncology, Howard University, Washington, DC 20060, USA

## ARTICLE INFO

Available online xxxx

## Keywords:

Nanoparticle  
Nanomedicine  
Physicochemical properties  
Image contrast agents  
Molecular imaging

## ABSTRACT

Advances in nanotechnology have opened up a new era of diagnosis, prevention and treatment of diseases and traumatic injuries. Nanomaterials, including those with potential for clinical applications, possess novel physicochemical properties that have an impact on their physiological interactions, from the molecular level to the systemic level. There is a lack of standardized methodologies or regulatory protocols for detection or characterization of nanomaterials. This review summarizes the techniques that are commonly used to study the size, shape, surface properties, composition, purity and stability of nanomaterials, along with their advantages and disadvantages. At present there are no FDA guidelines that have been developed specifically for nanomaterial based formulations for diagnostic or therapeutic use. There is an urgent need for standardized protocols and procedures for the characterization of nanoparticles, especially those that are intended for use as theranostics.

© 2013 Published by Elsevier Inc.

## Contents

1.	Introduction . . . . .	0
2.	Overview of physicochemical characteristics . . . . .	0
2.1.	Size . . . . .	0
2.2.	Surface properties . . . . .	0
2.3.	Shape . . . . .	0
2.4.	Composition and purity . . . . .	0
2.5.	Stability . . . . .	0
2.6.	Interaction between nanomaterials and biological environments . . . . .	0
3.	Modalities for physicochemical characterization . . . . .	0
3.1.	Near-field scanning optical microscopy (NSOM) . . . . .	0
3.2.	Scanning electron microscopy (SEM) . . . . .	0
3.3.	Transmission electron microscopy (TEM) . . . . .	0
3.4.	Scanning tunneling microscopy (STM) . . . . .	0
3.5.	Atomic force microscopy (AFM) . . . . .	0
3.6.	Dynamic light scattering (DLS) . . . . .	0
3.7.	Fluorescence correlation spectroscopy (FCS) . . . . .	0
3.8.	Raman scattering (RS) . . . . .	0
3.9.	Circular dichroism (CD) . . . . .	0
3.10.	Infrared (IR) spectroscopy . . . . .	0
3.11.	Nuclear magnetic resonance (NMR) . . . . .	0
3.12.	Mass spectrometry (MS) . . . . .	0
3.13.	Zeta potential . . . . .	0
3.14.	X-ray diffraction (XRD) . . . . .	0
3.15.	Small-angle X-ray scattering (SAXS) . . . . .	0
4.	Other techniques . . . . .	0

\* Corresponding author at: Department of Radiation Oncology, Howard University, 2041 Georgia Ave., N.W., Washington, DC 20060, USA. Tel.: +1 240 416 6095; fax: +1 202 865 3722.  
E-mail address: [rsridhar@howard.edu](mailto:rsridhar@howard.edu) (R. Sridhar).

5. Characterization of nanomaterials . . . . .	0
6. Conclusion . . . . .	0
Acknowledgments . . . . .	0
References . . . . .	0

## 1. Introduction

The emerging field of nanomedicine utilizes nanomaterials to improve diagnosis, prevention and treatment of diseases (Duncan and Gaspar, 2011). According to the Nanotechnology Characterization Laboratory (NCL) at the National Cancer Institute, National Institutes of Health nanoparticles (NPs) have a size range between 1 and 100 nm (McNeil, 2005). Nanomaterials have at least one dimension in the range of sub-nanometer to 10 nm. Small molecules and certain naturally occurring biological materials are not usually referred to as nanomaterials, even though they may be in the range of 1 to 100 nm. Research on manmade nanomaterials and engineered nanomaterials in the 1 to 100 nm range has gathered momentum because of their potential for a diverse array of applications in science, technology and medicine (Webster, 2006). Some examples of nanomaterials include liposomes, dendrimers, carbon nanorods, carbon nanotubes, fullerenes, graphene derivatives, titanium oxides, gadolinium nitride nanowires, silver NPs, gold NPs, platinum NPs, magnetic NPs and quantum dots (Duncan and Gaspar, 2011; Mahajan et al., in press; Singh and Sahoo, in press; Wong et al., in press).

When a solid is split, it exposes two new surfaces; with every subsequent cut, newer surfaces emerge. As any material is broken down to very small particles, the surface area per unit mass increases dramatically. Nanomaterials are characterized by a relatively large surface area per unit mass. Since the surface area of a solid depends on its shape, e.g. a sphere has the smallest surface area per unit mass, the surface area of nanomaterials depends on the size as well as shape. Changes in size or shape of nanomaterials can affect their physicochemical and physiological properties.

The physiological interactions in the body influenced by the biodistribution, passage, phagocytosis and endocytosis of nanomaterials through tissues may differ from those of conventional medicines (Gref et al., 1994). In order to realize the full potential of nanomedicines, it is necessary to develop robust standards for characterizing the engineered/fabricated nanomaterials, for example, to provide a guidance for ensuring quality control and assessing the safety as well as toxicity of nanomaterials (Pleus, 2012). Characteristics such as molecular structure, chemical composition, melting point, boiling point, vapor pressure, flash point, pH, solubility, and water octanol partition coefficient have to be determined for nanomaterials in the same manner as they are for larger non-nanomaterials. In addition, nanomaterial characterization places special emphasis on parameters such as size/size distribution, porosity (pore size), surface area, shape, wettability, zeta potential, adsorption isotherm (adsorption potential), aggregation, distribution of conjugated moieties and impurities.

At present there are no U.S. Food and Drug Administration (FDA) guidelines developed specifically for nanomaterial based formulations for diagnostic or therapeutic use. However, the agency has issued two product-specific draft guidance documents to address the utilization of nanotechnology in the food and cosmetics industries (<http://www.fda.gov/ScienceResearch/SpecialTopics/Nanotechnology/ucm301093.htm>). This can be a stepping stone towards detection or characterization of nanomaterials, although currently there are no standardized methodologies or regulatory protocols. Still, the NCL, serving as “a national resource and knowledge base” to assist the regulatory review of nanotechnologies and the development and translation of nanoparticles and devices for clinical applications, characterizes the physicochemical properties, *in vitro* biological properties and *in vivo* compatibility of nanoparticles ([http://ncl.cancer.gov/about\\_mission.asp](http://ncl.cancer.gov/about_mission.asp)). The assay cascade protocols

at the NCL include a number of methods to investigate nanomaterials' characteristics, such as size, molecular weight, aggregation, purity, chemical composition and surface properties. The NCL protocols also include methods for determining sterility, drug release and toxicity *in vitro*, and efficacy, disposition and immunotoxicity *in vivo* ([http://ncl.cancer.gov/working\\_assay-cascade.asp](http://ncl.cancer.gov/working_assay-cascade.asp)). Similarly, the European Union has formed the unit of Registration, Evaluation, Authorization and Restriction of Chemicals, by which nanomaterials are regulated.

Many methods have been used for evaluating manufactured nanomaterials, including techniques in optical spectroscopy, electron microscopy, surface scanning, light scattering, circular dichroism, magnetic resonance, mass spectrometry, X-ray scattering and spectroscopy, and zeta-potential measurements, as well as methods in the categories of thermal techniques, centrifugation, chromatography, and electrophoresis (Sapsford et al., 2011). In this review article, we briefly describe the principles, applications, strengths and limitations of a variety of modalities commonly used to investigate the physicochemical characteristics of nanomaterials (Table 1).

## 2. Overview of physicochemical characteristics

Typically, engineered materials with dimensions in the nanometer scale are intermediates between isolated small molecules and bulk materials. Nanomaterials, which are similar to biological moieties in scale, can be used as diagnostic and therapeutic nanomedicines (Del Burgo et al., in press; Hachani et al., 2013; Kim et al., 2010). Compared to their bulk material counterparts, the distinct physicochemical properties of the nanomaterials, such as size, surface properties, shape, composition, molecular weight, identity, purity, stability and solubility, are critically relevant to particular physiological interactions (Table 2) (Patri et al., 2006). These physiological interactions may provide benefits in medical applications, including improvements in efficacy, reduction of side effects, prevention and treatment (Farokhzad and Langer, 2006; Hall et al., 2007).

Impact of nanomaterials on their physiological behaviors will influence the therapeutic efficacy and/or diagnostic accuracy of nanomedicines. In this context, it is important to understand how the different physicochemical characteristics of nanomaterials affect their *in vivo* distribution and behavior. This demands reliable and robust techniques for studying the different physicochemical characteristics of nanomaterials in general and nanomedicines in particular. The different techniques used for characterization of nanomaterials, based on their different features, are described in the following sections. A rigorous but practical approach to reliable characterization of nanomaterials is essential for quality assurance and safe, rational development of nanomedicines and theranostics (Akhter et al., 2013; Kim et al., 2013).

### 2.1. Size

In engineered nanomaterials, size is a crucial factor that regulates the circulation and navigation of nanomaterials in the bloodstream, penetration across the physiological drug barriers, site- and cell-specific localization and even induction of cellular responses (Feng, 2004; Ferrari, 2008; Jiang et al., 2008). In general, the size of a nonspherical nanomaterial is defined as an equivalent diameter of a spherical particle whose selected physical properties, e.g. diffusivity, are equivalent to those of the nanomaterial in the same environment (Powers et al., 2006; Shekunov et al., 2007). One frequently adopted example is the hydrodynamic diameter of a molecule, which is the effective size

calculated from the diffusion coefficient using the Stokes–Einstein relationship (Powers et al., 2006).

Lately there has been public and government concern about the toxicity of nanomaterials and their related adverse health effects, such as pronounced pulmonary inflammation (Horváth et al., 2013; Karlsson et al., 2009; Oberdörster, 2005). Other examples include the smaller silver NPs causing a greater apoptotic effect against certain cell lines and 20 nm silica NPs exhibiting more toxicity than negatively-charged 100 nm silica NPs (Kim et al., 2012; Park et al., 2013; Sosenkova and Egorova, 2011). Although NPs with certain chemical compositions were reported to be more toxic compared to their larger counterparts of the same composition, a consensus on the increased toxicity and putative health risks of nanomaterials may not emerge due to the lack of obvious size-related change in toxicity in other NPs, e.g. titanium oxide and iron oxides (Buzea et al., 2007; Horváth et al., 2013; Karlsson et al., 2009; Park et al., 2007; Warheit et al., 2006). The relationship of size and/or shape to nanoparticle toxicity or nanomedicine efficacy has to be investigated on a case by case basis, because of the wide differences in the behavior of different nanomaterials.

## 2.2. Surface properties

Many characteristics of nanomaterial interfaces are functions of atomic or molecular compositions of the surfaces and the physical surface structures that respond to the interactions of the nanomaterial with surrounding species (Patri et al., 2006; Powers et al., 2006). From the aspect of nanomedicine, these characteristics are considered the elements of surface properties in the environment of biological fluid (Patri et al., 2006; Powers et al., 2006). Among the different surface properties, surface composition, surface energy, wettability, surface charge and species absorbance or adhesion are commonly considered important parameters (Brodbeck et al., 2001; Patri et al., 2006; Powers et al., 2006; Ratner et al., 2004; Vertegel et al., 2004). Surface composition is intrinsically relevant to the superficial layers but not to the bulk materials. Surface energy is relevant to the dissolution, aggregation and accumulation of nanomaterial. Surface charge, with potential effect on receptor binding and physiological barrier penetration, governs the dispersion stability or aggregation of nanomaterials and is generally estimated by zeta potential. Finally, species absorbance or adhesion potentially alters the surface of nanomaterial as well as the conformation and the activity of the attached species. However, investigation of the entire spectrum of surface parameters is impractical, and prioritization of the surface parameters requires independent validation for each nanomaterial system (Powers et al., 2006; Ratner et al., 2004).

Recent studies have shown improvement of cellular and lysosome uptakes of positively-charged nanomaterials, compared with their neutral or negatively-charged counterparts (Asati et al., 2010; Baoum et al., 2010; Klesing et al., 2010; Liu et al., 2011; Luyts et al., 2013). The enhanced uptake of positively-charged NPs makes them attractive as agents for tumor drug delivery: poly(D,L-lactide-co-glycolide)-formulated NPs with cationic chitosan are useful for localized, sustained gene delivery to the alveolar epithelium (Baoum et al., 2010). However, positively-charged nanomaterials can be more toxic than their negatively-charged counterparts. The positively-charged amino-modified polystyrene-formulated NPs were cytotoxic to certain cell lines by inducing DNA damage (Liu et al., 2011). Positively-charged branched polyethyleneimine coated Ag NPs were highly toxic to certain *bacillus* species in which the NPs caused membrane damage (El Badawy et al., 2010). Cytotoxicity of positively-charged Si NP-NH<sub>2</sub> towards macrophage NR8383 cells involved effects on phagocytosis, mitochondrial disruption and the production of high levels of intracellular reactive oxygen species (Bhattacharjee et al., 2010). In contrast, the effects of surface charge on cytotoxicity and reactive oxygen species generation were enhanced in the negatively-charged silica NPs of 20 nm in size, compared with those induced by silica NPs of the same size, but weaker negative charge (Park et al., 2013). Although the connection between increased cellular uptake of positively-

charged NPs and elevated cytotoxicity was typically demonstrated in *in vitro* studies, *in vivo* evidence is less convincing (Luyts et al., 2013). The relation between surface charge/zeta potential and NP toxicity cannot be generalized (Luyts et al., 2013).

## 2.3. Shape

In addition to size and surface properties, the shape of nanomaterial can play an important role in drug delivery, degradation, transport, targeting and internalization (Champion et al., 2007; Decuzzi et al., 2009; Euliss et al., 2006; Geng et al., 2007; Gratton et al., 2008; Jiang et al., 2013; Mitragotri, 2009). Efficiency of drug delivery carriers was highly influenced by controlling the shapes of the carriers (Champion et al., 2007; Decuzzi et al., 2009), while phagocytosis of drug delivery carriers through macrophages was also dependent on carrier shape (Champion and Mitragotri, 2009). Furthermore, flow and adhesion of drug delivery carriers throughout the circulatory system and the *in vivo* circulation time of the nanomedicine can be controlled by modulating the shapes of drug-loaded nanomaterials (Doshi et al., 2010; Geng et al., 2007).

The shape of nanomaterial affects cellular uptake, biocompatibility and retention in tissues and organs (George et al., 2012; Pal et al., 2007). Additionally, the disposition and translocation of nanomaterials in the organism may be influenced by their shape, accompanying size and state of agglomeration (Powers et al., 2009). One example is an *in vitro* study of silica NPs demonstrating shape-driven agglomeration as a potential trigger in the pulmonary pathogenesis (Brown et al., 2007). Another example is the higher toxicity of dendrimer-shaped nickel NPs compared to that of the spherical ones towards zebrafish embryos (Ispas et al., 2009). Similarly, plate-shaped silver NPs were more hazardous than spherical, rod-shaped or wire shaped silver nanoparticles when tested against *Escherichia coli* and zebrafish embryos (George et al., 2012; Pal et al., 2007). Furthermore, recent studies demonstrated an asbestos-like pathogenic response when carbon nanotubes of length greater than 20 µm were delivered into the abdominal cavity of mice (Kostarelos, 2008; Poland et al., 2008; Powers et al., 2009; Takagi et al., 2008).

## 2.4. Composition and purity

A broad variety of nanomaterials are utilized in the production of approved or potential nanomedicines. These nanomaterials can be categorized by their structural types, such as NP and its derivatives, liposome, micelle, dendrimer/fleximer, virosome, emulsion, quantum dot, fullerene, carbon nanotube and hydrogel, and each type may consist of polymers, metals and metal oxides, lipids, proteins, DNA or other organic compounds (Etheridge et al., 2013; Patri et al., 2006). Composition of a nanomaterial affects transport, delivery and biodistribution. In biomedical applications of nanomaterials, there may be a need to combine two or more types of nanomaterials to form a complex such as a chelate, a conjugant or a capsule. Consequently chemical composition analysis of the nanomaterial complex is more complicated than that for a single entity (Patri et al., 2006).

There are several studies addressing toxicological concerns about NPs of different compositions (Hardman, 2006). In addition to size and shape, chemical composition is another important factor in determining toxicity of NPs (Buzea et al., 2007; Hardman, 2006). For example, TiO<sub>2</sub> induced an inflammatory neutrophil response when intratracheally instilled in rat and mouse lungs (Oberdörster, 2005; Sohaebuddin et al., 2010). In addition, cytotoxicity is generally observed in quantum dots with core metalloid complexes consisting of widely used metals such as cadmium and selenium (Hardman, 2006). Still, quantum dots can be rendered nontoxic, when core coatings are appropriately registered; alternatively, the cytotoxicity of quantum dots was only observed after degradation of their core coating *in vivo* or *in vitro* (Buzea et al., 2007; Derfus et al., 2003; Hardman, 2006).



**Table 1**

Analytical modalities for evaluation of the physicochemical characteristics of nanomaterials.

Techniques	Physicochemical characteristics analyzed	Strengths	Limitations	Refs
Dynamic light scattering (DLS)	Hydrodynamic size distribution	Non-destructive/invasive manner Rapid and more reproducible measurement Measures in any liquid media, solvent of interest Hydrodynamic sizes accurately determined for monodisperse samples Modest cost of apparatus	Insensitive correlation of size fractions with a specific composition Influence of small numbers of large particles Limit in polydisperse sample measures Limited size resolution Assumption of spherical shape samples	Brar and Verma (2011); Domingos et al. (2009); Filipe et al. (2010); Murdock et al. (2008); Pan et al. (2013); Sapsford et al. (2011); Schacher et al. (2009); Wagner et al. (2007); Zhao et al. (2013)
Fluorescence correlation spectroscopy (FCS)	Hydrodynamic dimension Binding kinetics	High spatial and temporal resolution Low sample consumption Specificity for fluorescent probes Method for studying chemical kinetics, molecular diffusion, concentration effect, and conformation dynamics Simultaneous measurement of many particles (using ELS)	Limit in fluorophore species Limited applications and inaccuracy due to lack of appropriate models	Boukari and Sackett (2008); Domingos et al. (2009); Jing and Zhu (2011); Nienhaus et al. (2013); Sapsford et al. (2011)
Zeta potential	Stability Referring to surface charge	Complementary data to IR No requirement of sample preparation Potential of detecting tissue abnormality Enhanced RS signal (SERS) Increased spatial resolution (SERS) Topological information of nanomaterials (SERS, TERS) Simultaneous fluorescence and spectroscopy measurement Nano-scaled surface analysis at ambient conditions Assessment of chemical information and interactions at nano-scaled resolution Nondestructive and prompt technique	Electro-osmotic effect Lack of precise and repeatable measurement	Choi et al. (2011); Clogston and Patri (2011); Khatun et al. (2012); Sapsford et al. (2011); Weiner et al. (1993); Xu (2008)
Raman scattering (RS) Surface enhanced Raman (SERS) Tip-enhanced Raman spectroscopy (TERS)	Hydrodynamic size and size distribution (indirect analysis) Conformation change of protein–metallic NP conjugate Structural, chemical and electronic properties	Complementary data to IR No requirement of sample preparation Potential of detecting tissue abnormality Enhanced RS signal (SERS) Increased spatial resolution (SERS) Topological information of nanomaterials (SERS, TERS) Simultaneous fluorescence and spectroscopy measurement Nano-scaled surface analysis at ambient conditions Assessment of chemical information and interactions at nano-scaled resolution Nondestructive and prompt technique	Relatively weak single compared to Rayleigh scattering Limited spatial resolution (only to micrometers) Extremely small cross section Interference of fluorescence Irreproducible measurement (SERS)	Kumar (2012); Popovic et al. (2011); Chang et al. (2012); Kattumenu et al. (2012); Kneipp et al. (2010); Kumar and Thomas (2011); Mannelli and Marco (2010); Braun et al. (2009); Lin and Chang (2007); Lucas and Riedo (2012); Sinjab et al. (2012); Xiao et al. (2010)
Near-field scanning optical microscopy (NSOM)	Size and shape of nanomaterials	Simultaneous fluorescence and spectroscopy measurement Nano-scaled surface analysis at ambient conditions Assessment of chemical information and interactions at nano-scaled resolution Nondestructive and prompt technique	Long scanning time Small specimen area analyzed Incident light intensity insufficient to excite weak fluorescent molecules Difficulty in imaging soft materials Analysis limited to the nanomaterial surface	Cuche et al. (2009); Kohli and Mittal (2011); Lin et al. (2012); Lucas and Riedo (2012); Pan et al. (2013); Park et al. (2008); Vancso et al. (2005)
Circular dichroism (CD)	Structure and conformational change of biomolecules (e.g. protein and DNA) Thermal stability	Nondestructive and prompt technique	Non-specificity of residues involved in conformational change Less sensitive than absorption methods Weak CD signal for non-chiral chromophores Challenging for analysis of molecules containing multiple chiral chromophores	Caminade et al. (2005); Ghosh et al. (2007); Huang et al. (2013b); Jiang et al. (2004); Knoppe et al. (2010); Kobayashi et al. (2011); Liu and Webster (2007); Ranjbar and Gill (2009); Ratnikova et al. (2011); Sapsford et al. (2011); Shang et al. (2007)
Mass spectroscopy (MS)	Molecular weight Composition Structure Surface properties (secondary ion MS)	High accuracy and precision in measurement High sensitivity to detection (a very small amount of sample required)	Expensive equipment Lack of complete databases for identification of molecular species Limited application to date in studying nanomaterial–bioconjugates	Gmshinski et al. (2013); Knoppe et al. (2010); Lavigne et al. (2013); Sapsford et al. (2011); Tang et al. (2010); Tiede et al. (2008)
Infrared spectroscopy (IR) Attenuated total reflection Fourier transform infrared (ATR–FTIR)	Structure and conformation of bioconjugate Surface properties (ATR–FTIR)	Fast and inexpensive measurement Minimal or no sample preparation requirement (ATR–FTIR) Improving reproducibility (ATR–FTIR) Independence of sample thickness (ATR–FTIR)	Complicated sample preparation (IR) Interference and strong absorbance of H <sub>2</sub> O (IR) Relatively low sensitivity in nanoscale analysis	Gun'ko et al. (2009); Johal (2011); Kane et al. (2009); Kazarian and Chan (2006); Liu and Webster (2007); Zak et al. (2011); Zhao et al. (2008)
Scanning electron microscopy (SEM) Environmental SEM (ESEM)	Size and size distribution Shape Aggregation Dispersion	Direct measurement of the size/size distribution and shape of nanomaterials High resolution (down to sub-nanometer) Images of biomolecules in natural state provided using ESEM	Conducting sample or coating conductive materials required Dry samples required Sample analysis in non-physiological conditions (except ESEM) Biased statistics of size distribution in heterogeneous samples Expensive equipment Cryogenic method required for most NP–bioconjugates Reduced resolution in ESEM Ultrathin samples in required	Bernier et al. (2012); Boguslavsky et al. (2011); Bootz et al. (2004); Hall et al. (2007); Jin et al. (2010); Johal (2011); Ratner et al. (2004); Sapsford et al. (2011); Tiede et al. (2008)
Transmission electron microscopy (TEM)	Size and size distribution Shape heterogeneity Aggregation Dispersion	Direct measurement of the size/size distribution and shape of nanomaterials with higher spatial resolution than SEM Several analytical methods coupled with TEM for investigation of electronic structure and chemical composition of nanomaterials	Samples in nonphysiological condition Sample damage/alternation Poor sampling Expensive equipment	Cuche et al. (2009); Domingos et al. (2009); Dominguez-Medina et al. (2012); Hall et al. (2007); Khatun et al. (2012); Pan et al. (2013); Patri et al. (2006); Schacher et al. (2009); Tiede et al. (2008); Wagner et al. (2007); Wang (2001); Williams and Carter (2009)



**Table 1** (continued)

Techniques	Physicochemical characteristics analyzed	Strengths	Limitations	Refs
Scanning tunneling microscopy (STM)	Size and size distribution Shape Structure Dispersion Aggregation	Direct measurement High spatial resolution at atomic scale	Conductive surface required Surface electronic structure and surface topography unnecessarily having a simple connection	Fleming et al. (2009); Kocum et al. (2004); Nakaya et al. (2011); Ong et al. (2013); Overgaag et al. (2008); Wang and Chu (2013)
Atomic force microscopy (AFM)	Size and size distribution Shape Structure Sorption Dispersion Aggregation Surface properties (modified AFM)	3D sample surface mapping Sub-nanoscaled topographic resolution Direct measurement of samples in dry, aqueous or ambient environment	Overestimation of lateral dimensions Poor sampling and time consuming Analysis in general limited to the exterior of nanomaterials	Domingos et al. (2009); Gmoshinski et al. (2013); Mavrocordatos et al. (2004); Parot et al. (2007); Sapsford et al. (2011); Schaefer et al. (2012); Tang et al. (2010); Tiede et al. (2008); Yang et al. (2005)
Nuclear magnetic resonance (NMR)	Size (indirect analysis) Structure Composition Purity Conformational change	Non-destructive/non-invasive method Little sample preparation	Low sensitivity Time consuming Relatively large amount of sample required Only certain nuclei NMR active	Lundqvist et al. (2005); Mullen et al. (2010); Pan et al. (2006); Patri et al. (2006); Tomalia et al. (2003); Valentini et al. (2004); Gun'ko et al. (2009); Mirau et al. (2011); Sapsford et al. (2011); Tang et al. (2010)
X-ray diffraction (XRD)	Size, shape and structure for crystalline materials	Well-established technique High spatial resolution at atomic scale	Limited applications in crystalline materials Only single conformation/binding state of sample accessible Low intensity compared to electron diffraction	Caminade et al. (2005); Cao (2004); Gun'ko et al. (2009); Sapsford et al. (2011); Zak et al. (2011); Zanchet et al. (2001); Zhao et al. (2008); Zhou et al. (2012)
Small-angle X-ray scattering (SAXS)	Size/size distribution Shape Structure	Non-destructive method Simplification of sample preparation Amorphous materials and sample in solution accessible	Relatively low resolution	Doniach (2001); Grosso et al. (2011); Hummer et al. (2012); Rao and Biswas (2009); Sapsford et al. (2011)

The presence of pharmaceutical impurities may significantly impact drug efficacy or even introduce unfavorable side effects. In general, determination of nanomaterial purity can be accomplished through

analysis of their chemical compositions. Prior to finalizing a nanomaterial's formulation and proceeding with the composition analysis, proper purification processes are required to remove any residual

**Table 2**

Physicochemical characteristics of nanomaterials and suitable evaluation modalities.

Nanomaterial characteristics	Techniques	Refs
Size/size distribution	DLS, FCS, RS, NSOM, SEM, TEM, STM, AFM, NMR, TOF-MS, XRD, SAXS, FS, UV–visible, AUC, GE, CE, FFF	Biju et al. (2010b); Bootz et al. (2004); Braun et al. (2009); Caminade et al. (2005); Domingos et al. (2009); Hall et al. (2007); Hurst et al. (2006); Jiang et al. (2004); Mavrocordatos et al. (2004); Murdock et al. (2008); Nienhaus et al. (2013); Pan et al. (2013); Powers et al. (2006); Rao and Biswas (2009); Sapsford et al. (2011); Schacher et al. (2009); Valentini et al. (2004); Wang and Chu (2013); Zanchet et al. (2001)
Surface charge	Zeta potential (ELS), ATR–FTIR, GE, CE	Choi et al. (2011); Liu and Webster (2007); Sapsford et al. (2011); Xu (2008)
Shape	NSOM, SEM, TEM, STM, AFM, XRD, SAXS, AUC	Bootz et al. (2004); Caminade et al. (2005); Hall et al. (2007); Mavrocordatos et al. (2004); Rao and Biswas (2009); Sapsford et al. (2011); Wang and Chu (2013); Zanchet et al. (2001)
Structure	TERS, CD, MS, IR, STM, AFM, RS, NMR, XRD, SAXS, FS, DSC, AUC	Bothun (2008); Caminade et al. (2005); Gmoshinski et al. (2013); Grosso et al. (2011); Gun'ko et al. (2009); Mavrocordatos et al. (2004); Mirau et al. (2011); Mullen et al. (2010); Ong et al. (2013); Popovic et al. (2011); Rao and Biswas (2009); Sapsford et al. (2011); Tomalia et al. (2003); Wang and Chu (2013); Zanchet et al. (2001)
Composition	MS, NMR	Gmoshinski et al. (2013); Mullen et al. (2010); Tomalia et al. (2003)
Purity	MS, NMR, HPLC, HDC	Liu et al. (2012); Mullen et al. (2010); Patri et al. (2006); Sapsford et al. (2011); Tang et al. (2010); Tomalia et al. (2003)
Stability	Zeta potential measurement, CD, TGA, DSC, ITC, thermophoresis, HPLC, HDC	Bothun (2008); das Neves et al. (2010); Gugulothu and Patravale (in press); Khatun et al. (2012); Patri et al. (2006); Sapsford et al. (2011)
Dispersion	ESEM, TEM, STM, AFM	Bernier et al. (2012); Bootz et al. (2004); Hall et al. (2007); Mavrocordatos et al. (2004); Sapsford et al. (2011); Wang and Chu (2013)
Surface properties	CD coupled with an enzyme-linked immunosorbent assay, time-of-flight secondary ion MS, ATR–FTIR, modified AFM, X-ray photoelectron spectroscopy	Baer (2012); Fujie et al. (2009); Guay-Bégin et al. (2011); Liu and Webster (2007); Yang and Watts (2005)
Protein corona (thickness and density) <sup>a</sup>	DLS, FCS, TEM, size exclusion chromatography, differential centrifugal sedimentation	(Milani et al. (2012); Nienhaus et al. (2013); Rahman et al. (2013); Röcker et al. (2009); Walczyk et al. (2010)
Protein corona (composition and quantify) <sup>a</sup>	Polyacrylamide GE, LC–MS/MS	(Cedervall et al. (2007); Kapralov et al. (2012); Milani et al. (2012); Monopoli et al. (2011); Rahman et al. (2013); Sacchetti et al. (2013)
Protein corona (conformation) <sup>a</sup>	CD, simulation	Gebauer et al. (2012); Laera et al. (2011); Rahman et al. (2013)
Protein corona (affinity) <sup>a</sup>	Size exclusion chromatography, SPR, ITC	Casals et al. (2010); Cedervall et al. (2007); Liu et al. (2013); Rahman et al. (2013); Tassa et al. (2009); Zhao et al. (2013)

<sup>a</sup> Courtesy of Rahman et al. (2013).

manufacturing components or side products to ensure the absence of endotoxin contamination (Crist et al., 2013).

### 2.5. Stability

Pharmaceutical stability refers to retaining the same properties for a period of time after the pharmaceutical is manufactured. Similar to conventional single-molecule pharmaceuticals, the stability of nanomedicines may be affected by one or more factors, such as temperature, moisture, solvents, pH, particle/molecular size, exposure to different types of ionizing and non-ionizing radiation, enzymatic degradation and even the presence of other excipients and impurities (Briscoe and Hage, 2009; Patri et al., 2006). The stability of nanomaterial may impact its corresponding toxicity; for instance, a number of studies have shown that quantum dot cytotoxicity might be induced during synthesis, storage or even *in vivo* by oxidative or photolytic degradation of quantum dots (Hardman, 2006).

### 2.6. Interaction between nanomaterials and biological environments

When nanomaterials are introduced into biological environments or integrated in biomaterials, many undesirable effects such as aggregation, coagulation and non-specific absorption can occur. These may be due to a variety of intermolecular interactions occurring at the interfaces of nanomaterials with biomolecules and interaction-mediating fluids (Nel et al., 2009). While the surface properties of nanomaterials in a given medium are characterized by their physicochemical properties, including chemical composition, shape, surface geometry and crystallinity, porosity, heterogeneity and hydrolytic stability, other properties, such as surface charge, dissolution, hydration, size distribution, dispersion stability, agglomeration and aggregation of nanomaterial, are mainly governed by ionic strength, pH, temperature and the presence of biological or organic macromolecules (French et al., 2009; Hull and Bowman, 2009; Nel et al., 2009; Oberdorster et al., 2005). Thus, appropriate physicochemical characterization of nanomaterials should be profiled based on different physical states of the nanomaterials, such as solution, suspension or dry powder, as well as before and after exposure to the *in vitro* or *in vivo* test environment (Hull and Bowman, 2009).

Techniques for determining the shelf life of nanomaterial formulations are essential before considering the manufacture and use of nanomedicines. For example, it is important to guard against degradation of the nanomaterials caused by moisture, oxidation and/or aggregation. In this respect, the different characterization techniques will be useful for quality assurance.

## 3. Modalities for physicochemical characterization

Characterization of conventional pharmaceuticals and nanomedicines is based on the evaluation of physicochemical properties such as molecular weight, identity, composition, purity, stability and solubility. Many techniques that are routinely applied for characterization of conventional pharmaceuticals can also be used for characterization of nanomedicines (Patri et al., 2006). Yet, several specific characteristics of nanomaterials such as size, surface composition, surface energy, surface charge and shape are critically important and need to be well investigated to better comprehend nanomaterials' behaviors *in vivo*. Addressed below are brief descriptions of modalities used to examine the specific physicochemical properties of nanomaterials, and their main strengths and limitations for nanomaterial investigation.

### 3.1. Near-field scanning optical microscopy (NSOM)

The far-field imaging resolution of a conventional optical microscope is limited by the diffraction phenomenon of illuminating light, which is specified by the Rayleigh criterion (Hartschuh, 2008; Heinzelmann and Pohl, 1994). While visible light is used in conventional optical

microscopes, any two point sources cannot be resolved if they are spatially separated by less than approximately 200 nm (Heinzelmann and Pohl, 1994). Therefore, optical microscopy is not suitable for nanostructure investigation. NSOM is a surface probe microscopy (SPM) technique that comprises concepts from both SPM and optical microscopy to surpass the far-field resolution limit (Durig et al., 1986; Hayazawa et al., 2012). Instead of equipping an objective lens, essential in a conventional microscope, NSOM permits laser light guided in optical fiber to emit through the tip aperture at close proximity to the object (Durig et al., 1986; Hayazawa et al., 2012). While the aperture radius is smaller than the light wavelength, the light emerging from the aperture becomes evanescent in the near-field distance to the object, meaning that light field is highly confined and localized at the aperture or at the object; therefore, the spatial resolution becomes a function of the aperture size, not the diffraction limit (Hayazawa et al., 2012; Heinzelmann and Pohl, 1994).

Given the advantages of an ensemble of fluorescence and spectroscopy measurements, plus high-resolution topographic information on the surface of nanomaterials, NSOM can access not only phase contrast, polarization, fluorescence and staining that are accessible by conventional optical microscopy, but also the distribution of single molecules on the surfaces of cells and interactions in protein–NP conjugates at nano-scaled spatial resolution (Hinterdorfer et al., 2012; Ianoul and Johnston, 2007; Park et al., 2008; Song et al., 2011; Vancso et al., 2005). Some tradeoffs of implementing NSOM include lengthy scanning time for high resolution images or large specimen area, low incident light intensity hindering excitation of weak fluorescent molecules, difficulty in imaging soft materials caused by the high spring constants of the optical fibers, particularly in shear-force mode, and the ability to only image surface features (Kohli and Mittal, 2011).

### 3.2. Scanning electron microscopy (SEM)

In contrast to optical microscopy, which uses light sources and glass lenses to illuminate specimens to produce magnified images, electron microscopy (EM) uses beams of accelerated electrons and electrostatic or electromagnetic lenses to generate images of much higher resolution, based on the much shorter wavelengths of electrons than visible light photons. SEM is a surface imaging method in which the incident electron beam scans across the sample surface and interacts with the sample to generate signals reflecting the atomic composition and topographic detail of the specimen surface (Hall et al., 2007; Johal, 2011; Ratner et al., 2004). The incident electrons cause emissions of elastic scattering of electrons, referring to backscattered electrons, inelastic scattering of electrons named low-energy secondary electrons, and characteristic X-ray light called cathodoluminescence from the atoms on the sample surface or near-surface material (Johal, 2011). Among these emissions, detection of the secondary electrons is the most common mode in SEM and can achieve resolution smaller than 1 nm (Johal, 2011).

The size, size distribution and shape of nanomaterials can be directly acquired from SEM; however, the process of drying and contrasting samples may cause shrinkage of the specimen and alter the characteristics of the nanomaterials (Bootz et al., 2004; Hall et al., 2007). In addition, while scanned by an electron beam, many biomolecule samples that are nonconductive specimens tend to acquire charge and insufficiently deflect the electron beam, leading to imaging faults or artifacts. Coating an ultrathin layer of electrically conducting material onto the biomolecules is often required for this sample preparation procedure (Hall et al., 2007; Suzuki, 2002). Because a cryogenic freezing method is often required in EM to image surface groups attached to NPs, the size of nanomaterial cannot be investigated in physiological conditions (Hall et al., 2007). An exception is environmental SEM (ESEM), through which samples can be imaged in their natural state without modification or preparation (Sapsford et al., 2011; Tiede et al., 2008). Because the sample chamber of ESEM is operated in a low-pressure gaseous

environment of 10–50 Torr and high humidity, the charging artifacts can be eliminated, and coating samples with a conductive material is no longer necessary (Tiede et al., 2008). Still, most of the EM techniques, including SEM, possess the disadvantage of a destructive sample preparation, prohibiting its analysis by other modalities (Gmoshinski et al., 2013). In addition, biased statistics of size-distribution of heterogeneous samples is unavoidable in SEM due to the small number of sample particles in the scanning region (Bootz et al., 2004).

### 3.3. Transmission electron microscopy (TEM)

As the most frequently used technique for characterizing nanomaterials in EM, TEM provides direct images and chemical information of nanomaterials at a spatial resolution down to the level of atomic dimensions (<1 nm) (Patri et al., 2006; Wang, 2001). In the conventional TEM mode, an incident electron beam is transmitted through a very thin foil specimen, during which the incident electrons interacting with specimen are transformed to unscattered electrons, elastically scattered electrons or inelastically scattered electrons (Williams and Carter, 2009). The magnification of TEM is mainly determined by the ratio of the distance between objective lens and the specimen and the distance between objective lens and its image plane (Williams and Carter, 2009). The scattered or unscattered electrons are focused by a series of electromagnetic lenses and then projected on a screen to generate an electron diffraction, amplitude-contrast image, a phase-contrast image or a shadow image of varying darkness according to the density of unscattered electrons (Williams and Carter, 2009).

In addition to the high spatial resolution of TEM that enhances the morphological and structural analyses of nanomaterials, a wide variety of analytical techniques can be coupled with TEM for different applications; for example, chemical analyses of electron energy loss spectroscopy and energy dispersive X-ray spectroscopy can quantitatively investigate the electronic structure and chemical composition of the nanomaterials, respectively (Patri et al., 2006; Tiede et al., 2008; Wang, 2001). Overall, both TEM and SEM can reveal the size and shape heterogeneity of nanomaterials, as well as the degrees of aggregation and dispersion. TEM has advantages over SEM in providing better spatial resolution and capability for additional analytical measurements (Hall et al., 2007). There are certain drawbacks accompanying the advantages of TEM (Williams and Carter, 2009). A significant tradeoff is that a high vacuum and thin sample section are required for electron-beam penetration in TEM measurement (Hall et al., 2007). Sample destruction and measurement in unnatural/non-physiological conditions are common to all EM techniques. In general, high-resolution EM imaging enables examination of a minute part of the specimen over a certain period of time and results in poor statistical sampling. Also, abundant artifacts are generated due to 3D specimens being probed by the 2D TEM technique in transmission view, leading to no depth sensitivity for a single TEM image. Another limitation is that specimens have to be thin enough to transmit sufficient electrons to produce images; in particular cases, the specimen thickness of less than 50 nm is required while doing high-resolution TEM or electron spectroscopy. The extensive preparation of thin specimens increases the possibility of altering sample's structure and makes TEM analysis a very time consuming process. Another big concern is that TEM specimens can be damaged or even destroyed by intense, high-voltage electron beams.

Interestingly, wet TEM can be used for determining the particle size, dispersion, aggregation/agglomeration and dynamic displacement of nanomaterials in an aqueous environment (Carlton and Ferreira, 2012; Chen and Wen, 2012; Hondow et al., 2012). In addition to adapting the function of ESEM for observing samples under partial water vapor pressure in the microscope specimen chamber, a recently developed wet scanning transmission electron microscopy (STEM) imaging system enables transmission observation of species totally submerged in a liquid phase, compared with the issues of poor contrast

and possible drifting of objects occurring in the images of the top surface of the liquid using ESEM (Bogner et al., 2005; Ponce et al., 2012). Thus, the wet mode STEM permits observation in nanoscale resolution and high contrast even through several micrometers of water, without adding contrast agents and stains (Bogner et al., 2005; de Jonge and Ross, 2011).

### 3.4. Scanning tunneling microscopy (STM)

As the earliest developed technique in the SPM family, STM uses quantum tunneling current to generate electron density images for conductive or semiconductive surfaces and biomolecules attached on conductive substrates at the atomic scale (Albrecht et al., 1988; Avouris, 1990; Binnig and Rohrer, 1983; Miles et al., 1990). Adapting the generic principle for all SPM techniques, i.e. bringing a susceptible probe in close proximity to the surface of an object measured to monitor the reactions of the probe (Chi and Röthig, 2001), the essential components of an STM include a sharp scanning tip, an xyz-piezo scanner controlling the lateral and vertical movement of the tip, a coarse control unit positioning the tip close to the sample within the tunneling range, a vibration isolation stage and feedback regulation electronics (Wiesendanger, 1994). As the tip-sample separation is maintained in the range of 4–7 Å, a small voltage applied between the scanning tip and the surface causes tunneling of electrons by which variation of the responding current can be recorded while the tip moves across the sample in the x–y plane to generate a map of charge density (Bonnell, 2001). Alternatively, keeping the responding current unchanged by adjusting the tip height through the use of feedback electronics can generate an image of tip topography across the sample (Bonnell, 2001).

As for characterization of biomolecules using STM or EM techniques, the samples are usually embedded into a matrix to preserve their original conformations, followed by coating the samples with a thin metallic layer, such as gold, before acquiring images (Kocum et al., 2004). It is impossible to image these biomolecules in their native conditions using conventional EM techniques that usually accompany a time-consuming sample preparation procedure. STM, on the other hand, can not only diminish the disadvantages of the EM techniques but also provide an image with atomic scale resolution by, for example, using a Pt–Ir tip with a very sharp end (Kocum et al., 2004). Although the high spatial resolution of STM should benefit the characterization of nanoscale biomaterials such as size, shape, structure, and states of dispersion and aggregation, only few studies using gold or carbon as substrates have been reported (Wang and Chu, 2013). The practical obstacles are mainly due to requirements of the conductive surface of the sample and detection of the surface electronic structure (Wang and Chu, 2013). Unfortunately, most biomaterials are insulating, and a simple connection of the sample's surface electronic structure with its surface topography may not necessarily exist. Still, STM is a preferred tool for investigating conductive atomic structures of, for example, carbon nanotubes, fullerenes and graphene (Wang and Chu, 2013).

### 3.5. Atomic force microscopy (AFM)

Unlike STM, AFM does not require oxide-free, electrically conductive surfaces for measurement and is a SPM imaging tool consisting of a micro-machined cantilever (typically made of silicon or silicon nitride) with a sharp tip at one end to detect the deflection of the cantilever tip caused by electrostatic and van der Waals repulsion, as well as attraction between atoms at the tip and on the measured surface (Gadegaard, 2006; Hansma et al., 1988; Marti et al., 1988; Ratner et al., 2004). The oscillating cantilever then scans over the surface of specimen to generate an image with a vertical resolution of around 0.5 nm (Tiede et al., 2008; Zhu et al., 2011). Like SEM and TEM techniques, AFM can be used for investigating the size, shape, structure, sorption, dispersion and aggregation of nanomaterials – the different scanning modes employed in AFM studies include noncontact mode



(also called static mode), contact mode and intermittent sample contact mode (also called dynamic mode and tapping mode) (Hinterdorfer et al., 2012; Mavrocordatos et al., 2004; Picas et al., 2012; Sapsford et al., 2011; Song et al., 2011). In addition to probing the sizes and shapes of nanomaterials under physiological conditions, AFM is capable of characterizing dynamics between nanomaterials in biological situations, such as observing the interaction of nanomaterials with supported lipid bilayers in real time, which is not achievable with current EM techniques (Patri et al., 2006).

AFM is gaining importance due to its capability for imaging biomaterials without causing appreciable damage to many types of native surfaces (Parot et al., 2007; Yang et al., 2005). The main strength of AFM is its capability to image a variety of biomaterials at the sub-nanometer scale in aqueous fluids (Parot et al., 2007). However, a major drawback is that the size of the cantilever tip is generally larger than the dimensions of the nanomaterials examined, leading to unfavorable overestimation of the lateral dimensions of the samples (Gmshinski et al., 2013; Tiede et al., 2008). Unlike fluorescence techniques, AFM lacks the capability of detecting or locating specific molecules; however, this disadvantage has been eliminated by recent progress in single-molecule force spectroscopy with an AFM cantilever tip carrying a ligand, a cell adhesion molecule or chemical groups, which can probe or detect single functional molecules on cell surfaces (Dufrêne and Garcia-Parajo, 2012; Francius et al., 2008).

### 3.6. Dynamic light scattering (DLS)

Several physicochemical characteristics of nanomaterials including hydrodynamic size, shape, structure, aggregation state, and biomolecular conformation can be explored using radiation scattering techniques (Inagaki et al., 2013; Sapsford et al., 2011). DLS, one of the most popular light scattering modalities, can probe the size distribution of small particles, molecules or polymers at the scale from submicron down to one nanometer in solution or suspension using a monochromatic light source, e.g. a laser (Patri et al., 2006; Sapsford et al., 2011). The principle of DLS is to monitor the temporal fluctuation of the elastic scattering intensity of light, i.e., Rayleigh scattering, induced from the Brownian motion of the particles/molecules of a size much smaller than the incident light wavelength, at a fixed scattering angle (Brar and Verma, 2011; Sapsford et al., 2011). The intensity fluctuation trace comprises a mixture of the constructive and destructive interferences of the scattered light, through which the particle size can be derived from analysis of the motion-dependent autocorrelation function using the Stokes–Einstein equation (Brar and Verma, 2011; Pons et al., 2006b; Sapsford et al., 2011).

For physicochemical characterization of nanomaterials, the main strengths of DLS include its noninvasive manner, short experiment duration (in minutes), accuracy in determining the hydrodynamic size of monodisperse samples, and capabilities of measuring diluted samples, analyzing samples in a wide range of concentrations and detecting small amounts of higher molecular weight species, along with lower apparatus costs and more reproducible measurement than other methods (Brar and Verma, 2011; Filipe et al., 2010; Lim et al., 2013). However, the functions of DLS are impacted by several disadvantages, such as difficulty in correlating size fractions with a particular composition when certain amounts of aggregates are present, dust particles interfering in the scattering intensity, and a relatively small range of particle or molecule size (1 nm–3  $\mu$ m), although the scale limitation is not really a pitfall for characterization of nanomaterials (Bootz et al., 2004; Brar and Verma, 2011; Filipe et al., 2010). In addition, DLS has limited utility for analysis of samples with heterogeneous size distributions, and resolving the dimensions of a mixed sample population varying in size less than a factor of three; moreover, DLS is unsuited to accurately measuring the sizes of non-spherical nanomaterials because spherical nature of particles is already assumed in the analysis (Bootz et al., 2004; Brar and Verma, 2011; Filipe et al., 2010; Uskokovic, 2012).

### 3.7. Fluorescence correlation spectroscopy (FCS)

Similar in function to DLS, which detects spontaneous intensity fluctuation caused by molecular diffusion, aggregation or interaction with respect to time, FCS can yield quantitative information such as diffusion coefficients, hydrodynamic radii, average concentrations and kinetic chemical reaction rates through autocorrelation analysis of temporal fluorescent variation by fitting an appropriate model (Krichevsky and Bonnet, 2002; Magde et al., 1972; Sapsford et al., 2011; Wu et al., 2008). Most FCS measurements to date are performed in an optimum detection volume defined by a diffraction-limited spot generated by the strongly focused light in confocal microscopy or two-photon excitation microscopy and thus, only few fluorophores within the illuminated region are excited to restrain a small number of molecules and a high amplitude of correlation function (Krichevsky and Bonnet, 2002; Petryayeva et al., 2013; Schwille, 2001).

Analysis of the binding kinetics between donor and receptor, for example, between nanoscale vesicles and peptides and between quantum dots and proteins, can be approached using FCS or its derivatives, such as a dual-color FCS that cross-correlates data from two different fluorescent channels simultaneously (Boukari and Sackett, 2008; Pons et al., 2006a; Rusu et al., 2004; Sapsford et al., 2011). One significant advantage of FCS over DLS or NMR is the requirement of only a small amount of fluorescent probe particles at sub- to nanomolar concentrations, specifically monitoring the probe particles and preventing interfering contribution from the medium, and probing nanomaterials' dimensions in a range of nanometers to hundreds of nanometers (Boukari and Sackett, 2008). However, retaining the advantages of FCS described above requires selection of a fluorophore with high extinction coefficient, high quantum yield, low singlet-to-triplet state transition probability and low photobleaching (Boukari and Sackett, 2008). Moreover, the lack of models also limits the application and accuracy of FCS. A recent development of FCS–NSOM, which can be applied for examining cell membranes, uses the evanescent axial excitation to constrain the fluorescent background from cytoplasm components in order to achieve an observation area in an order of magnitude below the diffraction limit, with a power density comparable to confocal FCS. (Francius et al., 2008; Vobornik et al., 2008).

### 3.8. Raman scattering (RS)

RS is a widely-used tool for structural characterization of nanomaterials and nanostructures that provides submicron spatial resolution for light-transparent material without the requirement of sample preparation, making it suitable for *in situ* experiments (Popovic et al., 2011). The principle of RS is to measure the inelastic scattering of photons possessing different frequencies from the incident light after interacting with electric dipoles of the molecule (Cantor and Schimmel, 1980). The process of RS results in frequency differences between the incident photons and the inelastically scattered photons associated with the characteristics of the molecular vibrational states, during which the inelastically scattered photons emitting frequencies lower than the incident photons refer to the Stokes lines in Raman spectrum and the inelastically scattered photons emitting frequencies higher than the incident photons are named Anti-Stokes lines (Cantor and Schimmel, 1980). RS is generally considered to be complementary to IR spectroscopy, i.e., vibrational modes that are Raman active should be IR inactive, and vice versa, for small symmetrical molecules, because Raman transitions result from nuclear motion modulating the polarizability of the molecules, rather than a net change in the dipole moment of the molecules (Cantor and Schimmel, 1980).

One of the major advantages of RS is that it is suitable for studying biological samples in aqueous solution because water molecules tend to be weak Raman scatterers. Furthermore, the detailed molecular information offered by RS can be used to investigate conformations and concentrations of tissue constituents, which demonstrates the

potential of RS for detecting tissue abnormalities (Kumar, 2012). However, while the conventional RS technique provides indirect characterization of nanomaterials, such as average size and size distribution through analysis of the spectral line broadening and shift, it lacks the spatial resolution necessary to delineate different domains for application in nanotechnology (Kattumenu et al., 2012; Popovic et al., 2011). Other downsides of conventional RS include interference of fluorescence and extremely small cross section, demanding intense laser excitation and a large amount of sample materials to provide sufficient RS signals (Chang et al., 2012). In contrast, implementation of surface enhanced Raman scattering (SERS) can strongly enhance RS signals and increase spatial resolution while the measured biomolecules are adhered to the surface of metallic structures, such as commonly used gold or silver NP colloid substrates (Lee et al., 2013a; Lin et al., 2009; Wilson and Willets, 2013). SERS can be used to (i) study surface functionalization of metallic NPs, (ii) monitor the conformational change in proteins conjugated to the metallic NPs, and (iii) track intracellular drug release from the nanoplateform and measurement of the pH in the surrounding medium (Ando et al., 2013; Huang et al., 2013a; Kneipp et al., 2010; Kumar and Thomas, 2011; Mannelli and Marco, 2010).

By adapting the concept of confining the light field in Raman near-field scanning optical microscopy to overcome diffraction-limited resolution, a recently emerging technique, tip-enhanced Raman spectroscopy (TERS), utilizes an apertureless metallic tip instead of an optical fiber to gain the surface enhancement of the Raman signals (the SERS effect) (Ando et al., 2013; Hartschuh, 2008; Hayazawa et al., 2012; Wang and Irudayaraj, 2013). In contrast to conventional RS, SERS and TERS provide topological information of the nanomaterials, in addition to their structural, chemical and electronic properties, which conventional RS provides (Lee et al., 2013b; Popovic et al., 2011). However, the lack of measurement reproducibility in SERS caused by the size and shape variation, as well as undesirable aggregation of NPs is an obstacle for *in vitro* or *in vivo* imaging applications (Xiao et al., 2010).

### 3.9. Circular dichroism (CD)

Given a chiral molecule that possesses molecular asymmetry, CD is used to characterize the structure of the molecule through the different absorptions of circularly polarized lights in left-handed direction and in right-handed direction on the asymmetric molecule (Ranjbar and Gill, 2009). In the past few decades, various types of CD-based techniques have been developed to improve the capability of assessing conformational changes in proteins and nucleic acids, secondary and tertiary structures of proteins and their thermal stability, and donor–acceptor interactions, e.g. protein–protein, protein–DNA, protein–ligand and DNA–ligand interactions (Jiang et al., 2004; Ranjbar and Gill, 2009; Sapsford et al., 2011; Shang et al., 2007). In addition, the conformational behavior of biomolecules on NPs, the structures of drug-delivery nanocarriers and the interactions of nanocarriers with biomolecules have been investigated using CD techniques (Bhogale et al., 2013; Caminade et al., 2005; Ghosh et al., 2007; Liu and Webster, 2007; Ranjbar and Gill, 2009).

Although conventional CD spectroscopy is a prompt, nondestructive tool to reveal the structure and/or conformational change of the biomolecule investigated, there are several limitations of this technique. First, CD cannot manifest the actual contribution made by any particular amino-acid residue in a protein-type biomolecule to composing a CD spectrum (Ranjbar and Gill, 2009). Second, CD spectroscopy, based on differential absorption of left and right circularly polarized radiation, is less sensitive than absorption spectroscopy by two to three orders of magnitude. Third, it is challenging to analyze CD spectra acquired in a complex of a chiral compartment adhering to a chiral receptor, which is very common in biomacromolecules and nanomaterials. And finally, conventional CD measurement exhibits weak spectra if the sample contains only non-chiral chromophores. Some of the limitations can be

eliminated by implementing different CD-based techniques, for example, fluorescence detected CD to enhance sensitivity, and magnetic CD to detect molecules that lack a chiral center (Kobayashi et al., 2011; Tanaka et al., 2005).

A number of CD-based techniques have been developed to improve biological structure measurements, such as electronic CD, magnetic CD (MCD), fluorescence detected CD, near-infrared CD, vibrational CD (VCD), HPLC–CD, stopped-flow CD and synchrotron radiation CD (Ranjbar and Gill, 2009). Some of these CD-based methods have been used to investigate nanomaterials in various circumstances/situations (Burgi, 2011). For example, the local characteristics of VCD spectra revealed the conformation of 1,1'-binaphthyl-2,2'-dithiol adhered to gold nanoclusters (Gautier and Bürgi, 2010). Additionally, MCD spectroscopy, which is complementary to UV–vis spectroscopy, for the gold(I) complex  $\text{Au}(\text{AuPPH}_3)_3^+$  in a solution phase yielded higher resolution and more features, compared with that of electronic absorption (Yao et al., 2012).

### 3.10. Infrared (IR) spectroscopy

Typically, a molecule may absorb IR radiation if it possesses a time-variant dipole moment and its oscillating frequency is the same as the frequency of incident IR light (Johal, 2011). The absorption of IR radiation transfers energy to the molecule, inducing a corresponding covalent bond stretching, bending or twisting, which, in the case of a normal mode, is described by a stationary state of molecular vibrational Hamiltonian (Cantor and Schimmel, 1980). Molecules without dipole moments, e.g. diatomic molecules  $\text{N}_2$  and  $\text{O}_2$ , do not absorb IR radiation (Johal, 2011). Generally in a molecule, the vibrations involve various coupled pairs of atoms or covalent bonds, each of which must be considered as a combination of the normal modes; therefore, the IR spectrum, illustrating absorption or transmission versus incident IR frequency, can offer a fingerprint of the structure of the molecule of interest (Cantor and Schimmel, 1980).

For nanomaterial applications, Fourier transform infrared (FTIR) spectroscopy is commonly employed to use the expression of characteristic spectral bands to reveal nanomaterial–biomolecule conjugation, e.g. proteins bound to NP surfaces, and to illustrate the conformational states of the bound proteins (Jiang et al., 2004; Perevedentseva et al., 2010; Shang et al., 2007; Tom et al., 2006). Furthermore, FTIR has also been extended to study nano-scaled materials, such as confirmation of functional molecules covalently grafted onto carbon nanotubes (Baudot et al., 2010). A recently developed technique called attenuated total reflection (ATR)–FTIR spectroscopy uses the property of total internal reflection in conjunction with IR spectroscopy to probe the structure of adsorbed/deposited species at a solid/air or solid/liquid interface, while avoiding the drawbacks of sample preparation complexity and spectral irreproducibility in conventional IR (Hind et al., 2001; Johal, 2011). In an ATR–FTIR system, the total internal reflectance, occurring within the equipped internal reflection element (IRE) crystal, which has a high refractive index at certain angles, forms evanescent waves that extend from the IRE crystal–sample interface into the sample with penetration depth of micrometers (0.5–5  $\mu\text{m}$ ), and the intensity of the evanescent waves decays exponentially from the interface (Johal, 2011). ATR–FTIR can provide IR absorption spectra to investigate, for example, changes in surface properties as well as identification of chemical properties on the polymer surface when sample on the IRE–sample interface absorbs the evanescent IR waves with frequencies matching the vibrational modes of the sample (Johal, 2011; Kazarian and Chan, 2006; Liu and Webster, 2007). Although ATR–FTIR spectroscopy can be implemented to study the surface features of nanomaterials, it is not a very sensitive surface-analysis method at nanometer scale because the penetration depth of ATR–FTIR has the same order of magnitude as the incident IR wavelength (Liu and Webster, 2007).

### 3.11. Nuclear magnetic resonance (NMR)

In contrast to imaging and diffraction techniques affording structural information at long-range order, *i.e.* the crystalline property, NMR is sensitive to the local environment to resolve the structures of amorphous materials, polymers and biomolecules that lack long-range order (Wang et al., 2001). In addition to evaluating the structures and compositions of the species, NMR spectroscopy provides tools to investigate dynamic interactions of the species in different conditions (Sapsford et al., 2011; Tiede et al., 2008) – the relaxation, molecular conformation and molecular mobility can be evaluated through different dynamic measurements using specifically designed rf and/or gradient pulse sequences (Wang et al., 2001). NMR spectroscopy has been implemented to determine several physicochemical characteristics of nanomaterials, including structure, purity and functionality in dendrimers, polymers and fullerene derivatives, as well as conformational changes occurring in the interactions between ligands and nanomaterials (Lundqvist et al., 2005; Mullen et al., 2010; Pan et al., 2006; Patri et al., 2006; Tomalia et al., 2003). Pulsed field gradient NMR has been implemented to evaluate the diffusivity of nanomaterials, through which the sizes and interactions of species under investigation can be calculated (Valentini et al., 2004).

NMR is a non-destructive/noninvasive technique that requires little sample preparation. However, the low detection sensitivity of NMR, in contrast to optical techniques, requires a relatively large amount of the sample for measurement (Sapsford et al., 2011). It can also be time consuming if a certain level of signal-to-noise ratio is necessary for spectral analysis.

Over the past few years, the method using magic angle spinning for non-solid materials named high-resolution magic angle spinning (HR-MAS) NMR has been widely adapted in the biological and biomedical fields due to its capability of generating spectra similar to high-resolution NMR for investigating tissues and cells with heterogeneous nature (Alam and Jenkins, 2012). The advantage of HR-MAS NMR for accurate characterization of the surface-attached ligands and modified surfaces has been utilized for investigating each synthetic step of the cyclo-peptide immobilized on the surface of poly(vinylidene fluoride) based NPs, and studying thermolytically produced thiol-derivatized silver clusters (Alam and Jenkins, 2012; Conte et al., 2007; Deshayes et al., 2010).

### 3.12. Mass spectrometry (MS)

MS is one of the major analytical techniques used to examine the mass, elemental composition and chemical structure of a particle or a molecule. The basic principle of MS is to distinguish charged particles with different masses based on their mass-to-charge ratios (McNaught and Wilkinson, 1997). MS provides a high degree of precision and accuracy for molecular weight determination, as well as high detection sensitivity, which only requires  $10^{-9}$  to  $10^{-21}$  mol of a sample. Several physicochemical characteristics of nanomaterials, including mass, composition and structure, can be depicted using various MS procedures, distinguished by their ion sources, separation methods and detector systems (Gmshinski et al., 2013). Among the ionization techniques coupled with MS analyzers, matrix-assisted laser desorption/ionization (MALDI) and electrospray ionization (ESI) are commonly used to ionize and volatilize the thermally-labile biomolecular derivatives instead of introducing significant fragmentation or decomposition of the molecules. Inductively coupled plasma (ICP) ionization, on the other hand, is mainly implemented in the analysis of metal-containing nanomaterials (Gmshinski et al., 2013; Tiede et al., 2008). Applications of different MS procedures for nanomaterials include using time of flight (TOF)-MS to determine the size/size distribution of nanomaterials (Powers et al., 2006), MALDI-TOF-MS to measure the molecular weights of macromolecules, polymers and dendrimers as well as to illustrate proteins binding to NPs (Patri et al., 2006; Tom et al., 2006),

ICP-MS to validate the conjugation reaction of a functionalized NP with a modified contrast agent (Endres et al., 2007), and secondary ion MS to access the elemental and molecular properties of the top layer of NPs, as well as to examine biomaterial surface properties in physiological conditions (Guo et al., 2006; Ratner et al., 2004). Although these MS techniques have been applied to the analysis of physicochemical properties of various biomolecules, the currently incomplete MS spectral databases still cause difficulty in identifying molecular species, for example, in the analysis of MALDI-TOF-MS outcome measures (Lavigne et al., 2013). Additionally, the applications of MS techniques for nanomaterials to date are constrained in nanomaterial-bioconjugate characterization, mainly due to the cost of instrumentation, sample destruction and necessary instruments generally supplied for other investigations (Sapsford et al., 2011).

### 3.13. Zeta potential

In an ionic solution, the surface of a charged particle is firmly bound to opposite charged ions, forming a thin liquid layer named the Stern layer, which is encompassed by an outer diffuse layer consisting of loosely associated ions. These two layers compose the so-called electrical double layer (Clogston and Patri, 2011). Given the tangential motion driven by an external force or Brownian motion of the charged particle, the movement of the charged particle shears ions migrating with the charge particle in the diffuse layer from ions staying with the bulk dispersant outside the layer (Clogston and Patri, 2011). The electric potential on the shear surface is called zeta potential, which is usually determined by measuring the velocity of the charged species towards the electrode in the presence of an external electric field across the sample solution (Pons et al., 2006b; Sapsford et al., 2011). The zeta potential with a value of  $\pm 30$  mV is generally chosen to infer particle stability, through which the absolute value greater than 30 mV indicates a stable condition, whereas a low zeta potential value of less than 30 mV indicates a condition towards instability, aggregation, coagulation or flocculation (Sapsford et al., 2011).

Among the methods of evaluating zeta potential, the technique of electrophoretic light scattering (ELS), which can simultaneously measure the velocities of many charged particles in liquid, is most commonly used (Doane et al., 2011; Xu, 2008). However, it still suffers the electro-osmotic effect that reduces precision and reproducibility of the measurement (Weiner et al., 1993). Although measuring the zeta potential of suspended particles after dilution reduces difficulty of light penetration into the sample solution, it is worth noting that zeta potential is a property sensitive to environmental changes including pH and ionic strength (Weiner et al., 1993; Xu, 2008). Therefore, a precise, repeatable zeta potential measurement in a diluted solution cannot reflect the true value in a concentrated suspension (Xu, 2008).

### 3.14. X-ray diffraction (XRD)

In a variety of X-ray spectroscopic modalities, XRD is a primary tool for completely resolving the tertiary structures of crystalline materials at the atomic scale (Cantor and Schimmel, 1980; Sapsford et al., 2011). The diffraction of X-ray can be simply described as the reflection of a collimated beam of X-rays incident on the crystalline planes of an examined specimen according to Bragg's law (Cantor and Schimmel, 1980). Typically, XRD, based on wide-angle elastic scattering of X-rays, is a tool for characterizing crystalline size, shape and lattice distortion by long-range order, but is limited to disordered materials (Caminade et al., 2005; Sapsford et al., 2011; Zanchet et al., 2001).

Although XRD is a well-established technique and has frequently been used to determine the material structure at the atomic scale, difficulty in growing crystals and the ability of getting results only from single conformation/binding state of the sample limit the applications of XRD technique (Cao, 2004; Sapsford et al., 2011; Zanchet et al., 2001). Another disadvantage of XRD is the low intensity of diffracted



X-rays, particularly for low atomic number materials, compared with electron diffractions (Cao, 2004). A recent X-ray diffraction study reported a new approach using femtosecond pulses from a hard-X-ray free-electron laser for structure determination, which may benefit structure determination of macromolecules that do not yield sufficient crystal size for using conventional radiation sources or are not sensitive to radiation damage (Chapman et al., 2011).

### 3.15. Small-angle X-ray scattering (SAXS)

In contrast to XRD, whose applications are limited to crystalline materials, SAXS provides information of several characteristics by examining either crystalline or amorphous materials from polymers, proteins to nanomaterials (Lipfert and Doniach, 2007; Rao and Biswas, 2009; Sapsford et al., 2011). In SAXS, a portion of an incident X-ray beam elastically scattered from the sample forms a scattering pattern on a two-dimensional flat X-ray detector perpendicular to the direction of the incident X-ray beam (Doniach, 2001; Rao and Biswas, 2009; Sapsford et al., 2011). By analyzing the intensity of the scattered X-ray collected within the scattering angle, ranging from 0.1 to 3°, SAXS can evaluate the size/size distribution, shape, orientation, and structure of a variety of polymers and nanomaterial-bioconjugate systems in solution (Doniach, 2001; Rao and Biswas, 2009; Sapsford et al., 2011).

The features of small-angle scattering in SAXS lead to the capability of studying non-repeating structures; therefore, perfect crystallized structures are not required, which simplifies sample preparation and makes SAXS a non-destructive method (Rao and Biswas, 2009). On the other hand, SAX measurements provide holistic information about the structure, which exhibits the averaged characteristics rather than local probes of individual grains (Rao and Biswas, 2009). This feature can be a disadvantage if high resolution is required. On the other hand, recent progress in SAXS can achieve higher resolution measurements by introducing synchrotron as the high-energy X-ray source (Petoukhov and Svergun, 2013; Rao and Biswas, 2009).

Other X-ray spectroscopic techniques, such as X-ray absorption spectroscopy, can yield information about chemical state and symmetries of the absorption site through analysis of the X-ray absorption near edge structure spectra, and provide structural information, including coordination numbers and inter-atomic distance to ligands and neighboring atoms from the absorbing element through investigation of the spectra of extended X-ray absorption fine structure (EXAFS) without the requirement of long-range order in the measured species (Koningsberger and Prins, 1988; Zanchet et al., 2001). Both XRD and EXAFS can provide the averaged structural information of a nanomaterial, resulting from a long-range order and a local order of samples examined, in the manner of elastic and inelastic X-ray interaction with the samples, respectively (Zanchet et al., 2001).

## 4. Other techniques

Many other commonly used spectroscopic techniques for investigating the physicochemical characteristics of nanomaterials have not been listed above. One such sample is the use of UV–visible absorbance spectroscopy to investigate the characteristics of nanomaterials including size, concentration, aggregation state and even bioconjugation when the absorption profiles of nanomaterials are distinct (Biju et al., 2010b; Jiang et al., 2004; Sapsford et al., 2011). Fluorescence spectroscopy (FS), in general, is a more effective technique for pursuing the ligand binding or conformational changes of macromolecules than CD and light absorption techniques due to its sensitivity to the environment of the chromophore, as a consequence of the targeted molecular electron remaining in the excited singlet state for a relatively long duration before de-excitation (Cantor and Schimmel, 1980). Furthermore, conjugation of an extrinsic fluorophore to the non-intrinsically fluorescent nanomaterials enables FS to determine the characteristics of

biomolecule on the NP surface, including concentration, particle size, and spacer composition (Hurst et al., 2006).

The thermal stability and the amount of the nanomaterial conjugates can be evaluated using several thermal techniques (Sapsford et al., 2011). The temperature-dependent weight change in bulk samples, such as various nanomaterial bioconjugates, can be monitored using thermal gravimetric analysis (TGA) (Gibson et al., 2007; Vaiyapuri et al., 2012). Material transitions such as melting, crystallization, glass transition and decomposition of nanomaterial-bioconjugates can be accessed through differential scanning calorimetry (DSC); therefore, subsequent analysis of DSC measurements can provide the structure and stability of the investigated material (Bothun, 2008). In addition, the stoichiometry, affinity and enthalpy derived from the interaction between nanomaterial and biomolecule can be determined using isothermal titration calorimetry (ITC) (Cedervall et al., 2007). By locally heating the sample to generate a temperature gradient, thermophoresis monitors the motion of the sample to evaluate its size and surface potential (Sapsford et al., 2011; Sperling et al., 2007). However, thermophoresis needs higher concentrations of the examined species than FCS does to ensure robust signals.

Several separation techniques are routinely used as characterization tools. Centrifugation, of course, is a conventional methodology of separating and purifying mixed materials. In the category of centrifugation techniques, analytical ultracentrifugation (AUC) can be implemented to investigate the conformation, structure, stoichiometry and self-aggregation state of nanomaterials, in addition to determining the size/size distribution, shape and molecular weight (Inagaki et al., 2013; Sapsford et al., 2011; Schaefer et al., 2012). While coupled with reverse-phase, ion-exchange-phase or size-exclusion-phase columns, the chromatography techniques, such as high-performance liquid chromatography (HPLC) and hydrodynamic chromatography (HDC), can be used for the purification of nanomaterial bioconjugates. Owning the capability of differentiating different nanomaterial bioconjugates, these chromatography techniques can exhibit the distribution of nanomaterial-to-biomolecule ratios, as well as the stability and purity of the post-products (Patri et al., 2006; Sapsford et al., 2011). Methods of electrophoresis are routinely used to partition and purify biomolecules, and gel electrophoresis (GE) and capillary electrophoresis (CE), for example, can further provide the relative and absolute hydrodynamic size and zeta potential of nanomaterials (Sapsford et al., 2011). Field flow fractionation (FFF), which utilizes an external field such as flow, thermal, electrical and magnetic fields applied to a fluid suspension or solution to separate the particles present in the fluid, has been implemented to reveal the size/size distribution and charge information of the investigated nanomaterials (Sapsford et al., 2011). Sedimentation and flow FFF can exhibit the effective mass, hydrodynamic size, density and volume of the nanomaterials investigated.

## 5. Characterization of nanomaterials

Nanomaterials commonly consist of at least two of the following units: metallic, semiconducting and organic particles or molecules (Kim et al., 2010). Additionally, nanomaterials are generally coated with polymers or biorecognition molecules to improve biocompatibility and selective targeting of biologic molecules (Kim et al., 2010). A common feature of all nanomaterials is their large ratio of surface area to volume, which may be orders of magnitude greater than that of macroscopic materials. Still, the final size and structure of nanomaterials depend on the salt and surfactant additives, reactant concentrations, reaction temperatures, and solvent conditions used during their synthesis. Stated thus, comprehension of these physicochemical properties as well as the fundamentals of the associated measuring methods is necessary before characterizing nanomaterials and developing reproducible synthesis procedures to optimize the medical application of nanomaterials.

Some nanomaterials that are nanomedicines or considered to be potential nanomedicines are generally split into several categories based

on the types of nanomaterials or the application areas, such as drug delivery, drugs and therapies, *in vivo* imaging, *in vitro* diagnostics, biomaterials and implants (Wagner et al., 2008). Regardless of what criterion is used to categorize these nanomaterials, they share a certain degree of commonality in their physicochemical characteristics within and across the categories, and the same characteristics in different nanomaterials can be visualized through the use of the same or equivalent techniques described above.

Nano-drug delivery systems aim to optimize bioavailability at particular locations over a period of time, minimizing drug toxicity, increasing drug-therapeutic index and replacing invasive administration routes with non-invasive ones (Goldberg et al., 2007; Wagner et al., 2008). Nano-drug delivery systems include liposomes, nanosuspensions, NPs, dendrimers, fullerenes, and carbon nanotubes and the drug carriers in nano-drug delivery systems can be devised by regulating the composition, size, shape and morphology (Goldberg et al., 2007; Wagner et al., 2008). In a nano-drug delivery system, the system size can influence bioavailability and circulation time in blood stream, partly resulting from the impact of surface area-to-volume ratios on the solubility of the drug delivery systems (Goldberg et al., 2007; Rabinow, 2004; Vinogradov et al., 2002). Studies showed that 10–100 nm is an optimal size for nano-drug delivery systems to mostly avoid rapid removal through extravasation or through phagocytosis (Stolnik et al., 1995; Vinogradov et al., 2002). Recent studies have demonstrated that the shape of the drug carrier plays an important role in biodistribution and cellular uptake as well as avoiding phagocytosis and prolonging circulation in blood stream (Champion and Mitragotri, 2009; Geng et al., 2007). In addition, it has been reported that the surface charge of a nano-drug delivery system affects the pharmacokinetics of drugs entrapped/adhered (Hathout et al., 2007; Law et al., 2000), while the structural difference of the delivery systems may influence drug delivery efficiency (Inokuchi et al., 2010). Among the techniques described in this article for physicochemical characterization, DLS, FCS, RS, NSOM, SEM, TEM, STM, AFM, NMR, XRD, SAXS, FS and several separation techniques are suitable for evaluating the size and size distribution of nano-drug delivery systems. NSOM, SEM, TEM, STM, AFM, XRD and SAXS are proper modalities for shape measurement, while appropriate methods for surface charge measurement include zeta potential measurement (ELS), ATR-FTIR, GE and CE. In addition, TERS, CD, MS, IR, STM, AFM, NMR, XRD, SAXS, FS and some of the thermal and separation techniques can investigate the structural properties of the nanomaterials.

Along with the development of nano-drug carriers, certain types of nanomaterials have been used to design active pharmaceuticals, such as a dendrimer-derived microbicide for preventing HIV infections and fullerenes for binding and scavenging or inactivating free radicals, which are associated with the induction of neural and cardiovascular diseases (Wagner et al., 2008). Super-paramagnetic iron-oxide NPs coated with aminosilane, for example, can be used in hyperthermia treatment of cancer by subjecting the tumor tissue to high temperatures in order to destroy neoplastic cells (Wagner et al., 2008). Magnetic NPs bound to antibodies can be specific to certain targets, e.g., stem cells, and allow sorting via magnetic field for cell therapy (Wagner et al., 2008). In addition to the physicochemical properties, including size, shape, surface charge and structure mentioned already, the stability, particularly thermal stability, of the nanomaterials plays a crucial role if nano-drugs and nano-formulations are to retain and exert consistent therapeutic efficacy. In this article, the modalities capable of characterizing the stability of nanomaterials are zeta potential measurement, CD, HPLC, HDC and several thermal techniques including TGA, DSC, ITC and thermophoresis.

Molecular diagnostics is aimed at diagnosing disease at a molecular level before symptoms manifest (Wagner et al., 2008). Compared with conventional molecular imaging agents, employment of nanomaterial-based contrast agents generally increases the signal intensity of a single particle (Rosenblum et al., 2010; Thomas et al., 2013). The strong signal generated by the nanomaterial-based contrast agents, in fact, helps

overcome the essential disadvantages of low sensitivity in MRI and limited depth penetration of optical imaging to a certain degree (Lam et al., 2013; Rosenblum et al., 2010; Thomas et al., 2013). Given the novel properties of nanomaterials, several distinct nanomaterials are commonly designed as nanoscale imaging probes, including quantum dots with specific electronic and optical properties, upconversion phosphors consisting of phosphor nanocrystals doped with rare earth metals, and super-paramagnetic iron oxide particles containing an iron oxide core of magnetite and/or maghemite encased in polysaccharide, synthetic polymer or monomer coatings, or other soft materials like dendrimers (Biju et al., 2010a; Liang et al., 2008; Rosenblum et al., 2010; Wang et al., 2011). In addition to the characteristics of conventional imaging probes, such as structure, purity and solubility, certain physicochemical properties of nanomaterial-based imaging contrast agents also have to be considered, including size, shape, composition, zeta potential and dispersion (Leung et al., 2012). Techniques that can characterize the property of purity include NMR, HPLC and HDC, while the property of composition can be characterized by MS and NMR. Furthermore, the EM- and SPM-derived techniques, such as ESEM, TEM, STM and AFM, can be implemented to characterize the dispersion of nano-based imaging probes.

Even *in vivo* nanomaterial-based imaging contrast agents are continuously under development, nanomaterial toxicity in the body has not been comprehensively studied (Chi et al., 2012). While toxicity of being a minor concern leads to various types of nanomaterials widely used in the context of *in vitro* diagnostics (Chi et al., 2012), the applications of *in vitro* diagnostics have attracted a large amount of research interests, mainly split into NP-based biomarkers and novel sensor platforms composed of nanomaterials (Chi et al., 2012; Wagner et al., 2008). Among the physicochemical characteristics, stability is a key property in the applications of biomarkers. An example is the complete replacement of organic dyes with inorganic fluorescent NPs because organic dyes in polymerase chain reaction assays and in biochips are not photostable (Chi et al., 2012; Wagner et al., 2008). While biochips with a nano-based electrical detection system are the most popular development in the field of nano-sensor platforms, the surface chemistry properties play an important role in determining the capabilities of the biochips (Chi et al., 2012; Wagner et al., 2008).

Compared to drug delivery studies, the developments of nanoscale biomaterials and implants are still in their infancy. Still, nanomaterials have been used in a wide spectrum of applications, including tissue regeneration and medical implants (Liu and Webster, 2007; Wagner et al., 2008). Nanomaterials have been considered for a variety of implant applications, such as bone substitute materials, cartilage regeneration, vascular graft endothelialization, bladder replacement, dental restoratives, neural prostheses and antibiotic materials (Liu and Webster, 2007; Wagner et al., 2008). Among the physicochemical characteristics, surface properties are of the greatest importance to understand protein-mediated cell responses since the unique surface properties of the nanomaterials can influence interactions with proteins attached to selected cell membrane receptors (Liu and Webster, 2007). Techniques that can provide surface chemical characterization and investigation of protein–nanomaterial interactions include CD coupled with an enzyme-linked immunosorbent assay, time-of-flight secondary ion MS, ATR-FTIR, modified AFM and X-ray photoelectron spectroscopy (Liu and Webster, 2007).

Protein corona is formed in a dynamic, competitive process during which proteins or enzymes present in the biological fluid adhere to the surface of nanomaterials to generate a bio-nano interface (Luyts et al., 2013; Mahmoudi et al., 2011; Nel et al., 2009). The physicochemical properties of nanomaterials influenced by protein corona include surface properties, aggregation properties and hydrodynamic size charge; in the meantime, the adhered proteins can endure conformational alternation, functionality changes, unmasking of new epitopes and alternations in avidity and affinity effects (Cedervall et al., 2007; Luyts et al., 2013; Nel et al., 2009). In contrast to using centrifugation,



a conventional method that likely disturbs protein–NP complexes, a number of methodologies, including size-exclusion chromatography gel filtration, ITC, surface plasmon resonance (SPR), have been proposed for measuring dynamic and equilibrium parameters of the protein–NP interactions and estimating the potential of NP-associated risks (Cedervall et al., 2007; Dahlin et al., 2013).

## 6. Conclusion

Given the novelty of physicochemical characteristics at the nanometer scale, nanomaterials have potential to impact physiological interactions from the molecular level to the systemic level, making the *in vivo* administration of nanomedicines an interesting research topic. The rapid development and production of nanomaterials for use as nanomedicines indicate the demand and wisdom for regulating the manufacture and use of nanomaterials. Robust techniques for characterization of nanomaterials are fundamental to regulatory guidelines for ensuring safety of nanomaterials in general and nanomedicines in particular. This article describes the essential physicochemical properties of nanomaterials, followed by an introduction to different methods that are commonly used for characterizing nanomaterials. Indeed, it is necessary to characterize the nanomaterial intended for therapeutic use in both its originally manufactured condition and after introduction into a physiological environment. The brief description of each technique, together with its strengths and limitations, provides us with a picture for selecting suitable techniques for characterization of a potential nanomedicine.

## Acknowledgments

This work was supported in part by NIH/National Institute of Minority Health Disparities G12 MD007597, and US Army Medical Research and Material Command W81XWH-10-1-0767 grants.

## References

- Akhter S, Ahmad I, Ahmad MZ, Ramazani F, Singh A, Rahman Z, et al. Nanomedicines as cancer therapeutics: current status. *Curr Cancer Drug Targets* 2013;13:362–78.
- Alam T, Jenkins J. HR-MAS NMR spectroscopy in material science. In: Farrukh M, editor. *Advanced aspects of spectroscopy*. Intech Open; 2012.
- Albrecht TR, Dovek MM, Lang CA, Grutter P, Quate CF, Kuan SWJ, et al. Imaging and modification of polymers by scanning tunneling and atomic force microscopy. *J Appl Phys* 1988;64:1178–84.
- Ando J, Yano TA, Fujita K, Kawata S. Metal nanoparticles for nano-imaging and nano-analysis. *Phys Chem Chem Phys* 2013;15:13713–22.
- Asati A, Santra S, Kaittanis C, Perez JM. Surface-charge-dependent cell localization and cytotoxicity of cerium oxide nanoparticles. *ACS Nano* 2010;4:5321–31.
- Avouris P. Atom-resolved surface chemistry using the scanning tunneling microscope. *J Phys Chem* 1990;94:2246–56.
- Baer DR. Application of surface analysis methods to nanomaterials: summary of ISO/TC 201 technical report: ISO 14187:2011 – surface chemical analysis – characterization of nanomaterials. *Surf Interface Anal* 2012;44:1305–8.
- Baoum A, Dhillon N, Buch S, Berkland C. Cationic surface modification of PLG nanoparticles offers sustained gene delivery to pulmonary epithelial cells. *J Pharm Sci* 2010;99:2413–22.
- Baudot C, Tan CM, Kong JC. FTIR spectroscopy as a tool for nano-material characterization. *Infrared Phys Technol* 2010;53:434–8.
- Bernier M-C, Besse M, Vayssade M, Morandat S, El Kirat K. Titanium dioxide nanoparticles disturb the fibronectin-mediated adhesion and spreading of pre-osteoblastic cells. *Langmuir* 2012;28:13660–7.
- Bhattacharjee S, de Haan L, Evers N, Jiang X, Marcelis A, Zuilhof H, et al. Role of surface charge and oxidative stress in cytotoxicity of organic monolayer-coated silicon nanoparticles towards macrophage NR8383 cells. *Part Fibre Toxicol* 2010;7:25.
- Bhogale A, Patel N, Mariam J, Dongre PM, Miotello A, Kothari DC. Comprehensive studies on the interaction of copper nanoparticles with bovine serum albumin using various spectroscopies. *Colloids Surf B Biointerfaces* 2013;113C:276–84.
- Biju V, Itoh T, Ishikawa M. Delivering quantum dots to cells: bioconjugated quantum dots for targeted and nonspecific extracellular and intracellular imaging. *Chem Soc Rev* 2010a;39:3031–56.
- Biju V, Mundayoor S, Omkumar RV, Anas A, Ishikawa M. Bioconjugated quantum dots for cancer research: present status, prospects and remaining issues. *Biotechnol Adv* 2010b;28:199–213.
- Binnig G, Rohrer H. Scanning tunneling microscopy. *Surf Sci* 1983;126:236–44.
- Bogner A, Thollet G, Basset D, Jouneau PH, Gauthier C. Wet STEM: a new development in environmental SEM for imaging nano-objects included in a liquid phase. *Ultramicroscopy* 2005;104:290–301.
- Boguslavsky Y, Fadida T, Talyosef Y, Lellouche J-P. Controlling the wettability properties of polyester fibers using grafted functional nanomaterials. *J Mater Chem* 2011;21:10304–10.
- Bonnell D. Scanning probe microscopy and spectroscopy: theory, techniques, and applications. Wiley-vch; 2001.
- Boottz A, Vogel V, Schubert D, Kreuter J. Comparison of scanning electron microscopy, dynamic light scattering and analytical ultracentrifugation for the sizing of poly(butyl cyanoacrylate) nanoparticles. *Eur J Pharm Biopharm* 2004;57:369–75.
- Bothun GD. Hydrophobic silver nanoparticles trapped in lipid bilayers: size distribution, bilayer phase behavior, and optical properties. *J Nanobiotechnol* 2008;6:13.
- Boukari H, Sackett DL. Fluorescence correlation spectroscopy and its application to the characterization of molecular properties and interactions. *Methods Cell Biol* 2008;84:659–78.
- Brar SK, Verma M. Measurement of nanoparticles by light-scattering techniques. *TrAC Trends Anal Chem* 2011;30:4–17.
- Braun GB, Lee SJ, Laurence T, Fera N, Fabris L, Bazan GC, et al. Generalized approach to SERS-active nanomaterials via controlled nanoparticle linking, polymer encapsulation, and small-molecule infusion. *J Phys Chem C* 2009;113:13622–9.
- Briscoe CJ, Hage DS. Factors affecting the stability of drugs and drug metabolites in biological matrices. *Bioanalysis* 2009;1:205–20.
- Brodbeck WG, Shive MS, Colton E, Nakayama Y, Matsuda T, Anderson JM. Influence of biomaterial surface chemistry on the apoptosis of adherent cells. *J Biomed Mater Res* 2001;55:661–8.
- Brown SC, Kamal M, Nasreen N, Baumuratov A, Sharma P, Antony VB, et al. Influence of shape, adhesion and simulated lung mechanics on amorphous silica nanoparticle toxicity. *Adv Powder Technol* 2007;18:69–79.
- Burgi T. Shining light at working interfaces and chiral nanoparticles. *Chim (Aarau)* 2011;65:157–67.
- Buzea C, Pacheco I, Robbie K. Nanomaterials and nanoparticles: sources and toxicity. *Biointerphases* 2007;2:MR17–71.
- Caminade A-M, Laurent R, Majoral J-P. Characterization of dendrimers. *Adv Drug Deliv Rev* 2005;57:2130–46.
- Cantor CR, Schimmel PR. Techniques for the study of biological structure and function. San Francisco: W. H. Freeman; 1980.
- Cao G. Nanostructures and nanomaterials: synthe. Imperial College Press; 2004.
- Carlton CE, Ferreira PJ. In situ TEM nanoindentation of nanoparticles. *Micron* 2012;43:1134–9.
- Casals E, Pfaller T, Duschl A, Oostingh GJ, Puentes V. Time evolution of the nanoparticle protein corona. *ACS Nano* 2010;4:3623–32.
- Cedervall T, Lynch I, Lindman S, Berggård T, Thulin E, Nilsson H, et al. Understanding the nanoparticle–protein corona using methods to quantify exchange rates and affinities of proteins for nanoparticles. *Proc Natl Acad Sci* 2007;104:2050–5.
- Champion JA, Mitragotri S. Shape induced inhibition of phagocytosis of polymer particles. *Pharm Res* 2009;26:244–9.
- Champion JA, Katare YK, Mitragotri S. Particle shape: a new design parameter for micro- and nanoscale drug delivery carriers. *J Control Release* 2007;121:3–9.
- Chang H-W, Hsu P-C, Tsai Y-C. Ag/carbon nanotubes for surface-enhanced Raman scattering. In: Kumar CSR, editor. *Raman spectroscopy for nanomaterials characterization*. Berlin Heidelberg: Springer; 2012. p. 119–35.
- Chapman HN, Fromme P, Barty A, White TA, Kirian RA, Aquila A, et al. Femtosecond X-ray protein nanocrystallography. *Nature* 2011;470:73–7.
- Chen X, Wen J. In situ wet-cell TEM observation of gold nanoparticle motion in an aqueous solution. *Nanoscale Res Lett* 2012;7:1–6.
- Chi L, Röthig C. Scanning probe microscopy of nanoclusters. Characterization of nanoparticle materials. Wiley-VCH Verlag GmbH; 2001:133–63.
- Chi X, Huang D, Zhao Z, Zhou Z, Yin Z, Gao J. Nanoprobes for in vitro diagnostics of cancer and infectious diseases. *Biomaterials* 2012;33:189–206.
- Choi J, Reipa V, Hitchins VM, Goering PL, Malinauskas RA. Physicochemical characterization and in vitro hemolysis evaluation of silver nanoparticles. *Toxicol Sci* 2011;123:133–43.
- Clogston J, Patri A. Zeta potential measurement. In: McNeil SE, editor. Characterization of nanoparticles intended for drug delivery. Humana Press; 2011. p. 63–70.
- Conte P, Carotenuto G, Piccolo A, Perlo P, Nicolais L. NMR-investigation of the mechanism of silver mercaptide thermolysis in amorphous polystyrene. *J Mater Chem* 2007;17:201–5.
- Crist RM, Grossman JH, Patri AK, Stern ST, Dobrovolskaia MA, Adisheshaiah PP, et al. Common pitfalls in nanotechnology: lessons learned from NCI's nanotechnology characterization laboratory. *Integr Biol (Camb)* 2013;5:66–73.
- Cuche A, Masenelli B, Ledoux G, Amans D, Dujardin C, Sonnefraud Y, et al. Fluorescent oxide nanoparticles adapted to active tips for near-field optics. *Nanotechnology* 2009;20:015603.
- Dahlin AB, Wittenberg NJ, Hook F, Oh SH. Promises and challenges of nanoplasmonic devices for refractometric biosensing. *Nanophotonics* 2013;2:83–101.
- das Neves J, Sarmiento B, Amiji MM, Bahia MF. Development and validation of a rapid reversed-phase HPLC method for the determination of the non-nucleoside reverse transcriptase inhibitor dapivirine from polymeric nanoparticles. *J Pharm Biomed Anal* 2010;52:167–72.
- de Jonge N, Ross FM. Electron microscopy of specimens in liquid. *Nat Nanotechnol* 2011;6:695–704.
- Decuzzi P, Pasqualini R, Arap W, Ferrari M. Intravascular delivery of particulate systems: does geometry really matter? *Pharm Res* 2009;26:235–43.

- Del Burgo LS, Hernandez RM, Orive G, Pedraz JL. Nanotherapeutic approaches for brain cancer management. *Nanomedicine* 2013. <http://dx.doi.org/10.1016/j.nano.2013.10.001>. (in press).
- Derfus AM, Chan WCW, Bhatia SN. Probing the cytotoxicity of semiconductor quantum dots. *Nano Lett* 2003;4:11–8.
- Deshayes S, Maurizot V, Clochard M-C, Berthelot T, Baudin C, Déléris G. Synthesis of specific nanoparticles for targeting tumor angiogenesis using electron-beam irradiation. *Radiat Phys Chem* 2010;79:208–13.
- Doane TL, Chuang C-H, Hill RJ, Burda C. Nanoparticle  $\zeta$ -potentials. *Acc Chem Res* 2011;45:317–26.
- Domingos RF, Baalousha MA, Ju-Nam Y, Reid MM, Tufenkji N, Lead JR, et al. Characterizing manufactured nanoparticles in the environment: multimethod determination of particle sizes. *Environ Sci Technol* 2009;43:7277–84.
- Dominguez-Medina S, McDonough S, Swanglap P, Landes CF, Link S. In situ measurement of bovine serum albumin interaction with gold nanospheres. *Langmuir* 2012;28:9131–9.
- Doniach S. Changes in biomolecular conformation seen by small angle X-ray scattering. *Chem Rev* 2001;101:1763–78.
- Doshi N, Prabhakarapandian B, Rea-Ramsey A, Pant K, Sundaram S, Mitragotri S. Flow and adhesion of drug carriers in blood vessels depend on their shape: a study using model synthetic microvascular networks. *J Control Release* 2010;146:196–200.
- Dufrene YF, Garcia-Parajo MF. Recent progress in cell surface nanoscopy: light and force in the near-field. *Nano Today* 2012;7:390–403.
- Duncan R, Gaspar R. Nanomedicine(s) under the microscope. *Mol Pharm* 2011;8:2101–41.
- Durig U, Pohl D, Rohner F. Near-field optical-scanning microscopy. *J Appl Phys* 1986;59:3318–27.
- El Badawy AM, Silva RG, Morris B, Scheckel KG, Suidan MT, Tolaymat TM. Surface charge-dependent toxicity of silver nanoparticles. *Environ Sci Technol* 2010;45:283–7.
- Endres PJ, Paunesku T, Vogt S, Meade TJ, Woloschak GE. DNA–TiO<sub>2</sub> nanoconjugates labeled with magnetic resonance contrast agents. *J Am Chem Soc* 2007;129:15760–1.
- Etheridge ML, Campbell SA, Erdman AG, Haynes CL, Wolf SM, McCullough J. The big picture on nanomedicine: the state of investigational and approved nanomedicine products. *Nanomed Nanotechnol Biol Med* 2013;9:1–14.
- Euliss LE, DuPont JA, Gratton S, DeSimone J. Imparting size, shape, and composition control of materials for nanomedicine. *Chem Soc Rev* 2006;35:1095–104.
- Farokhzad OC, Langer R. Nanomedicine: developing smarter therapeutic and diagnostic modalities. *Adv Drug Deliv Rev* 2006;58:1456–9.
- Feng SS. Nanoparticles of biodegradable polymers for new-concept chemotherapy. *Expert Rev Med Devices* 2004;1:115–25.
- Ferrari M. Nanogeometry: beyond drug delivery. *Nat Nanotechnol* 2008;3:131–2.
- Filipe V, Hawe A, Jiskoot W. Critical evaluation of nanoparticle tracking analysis (NTA) by nanosight for the measurement of nanoparticles and protein aggregates. *Pharm Res* 2010;27:796–810.
- Fleming CJ, Liu YX, Deng Z, Liu GY. Deformation and hyperfine structures of dendrimers investigated by scanning tunneling microscopy. *J Phys Chem A* 2009;113:4168–74.
- Francius G, Domenech O, Mingot-Leclercq MP, Dufrene YF. Direct observation of *Staphylococcus aureus* cell wall digestion by lysostaphin. *J Bacteriol* 2008;190:7904–9.
- French RA, Jacobson AR, Kim B, Isley SL, Penn RL, Bayeye PC. Influence of ionic strength, pH, and cation valence on aggregation kinetics of titanium dioxide nanoparticles. *Environ Sci Technol* 2009;43:1354–9.
- Fujie T, Park JY, Murata A, Estillere NC, Tria MCR, Takeoka S, et al. Hydrodynamic transformation of a freestanding polymer nanosheet induced by a thermoresponsive surface. *ACS Appl Mater Interfaces* 2009;1:1404–13.
- Gadegaard N. Atomic force microscopy in biology: technology and techniques. *Biotech Histochem* 2006;81:87–97.
- Gautier C, Bürgi T. Vibrational circular dichroism of adsorbed molecules: BINAS on gold nanoparticles†. *J Phys Chem C* 2010;114:15897–902.
- Gebauer JS, Malissek M, Simon S, Knauer SK, Maskos M, Stauber RH, et al. Impact of the nanoparticle–protein corona on colloidal stability and protein structure. *Langmuir* 2012;28:9673–9.
- Geng Y, Dalhaimer P, Cai SS, Tsai R, Tewari M, Minko T, et al. Shape effects of filaments versus spherical particles in flow and drug delivery. *Nat Nanotechnol* 2007;2:249–55.
- George S, Lin S, Ji Z, Thomas CR, Li L, Mecklenburg M, et al. Surface defects on plate-shaped silver nanoparticles contribute to its hazard potential in a fish gill cell line and zebrafish embryos. *ACS Nano* 2012;6:3745–59.
- Ghosh PS, Han G, Erdogan B, Rosado O, Krovit SA, Rotello VM. Nanoparticles featuring amino acid-functionalized side chains as DNA receptors. *Chem Biol Drug Des* 2007;70:13–8.
- Gibson JD, Khanal BP, Zubarev ER. Paclitaxel-functionalized gold nanoparticles. *J Am Chem Soc* 2007;129:11653–61.
- Gmshinski IV, Khotimchenko SA, Popov VO, Dzantiev BB, Zherdev AV, Demin VF, et al. Nanomaterials and nanotechnologies: methods of analysis and control. *Russ Chem Rev* 2013;82:48.
- Goldberg M, Langer R, Jia X. Nanostructured materials for applications in drug delivery and tissue engineering. *J Biomater Sci Polym Ed* 2007;18:241–68.
- Gratton SE, Ropp PA, Pohlhaus PD, Luft JC, Madden VJ, Napier ME, et al. The effect of particle design on cellular internalization pathways. *Proc Natl Acad Sci U S A* 2008;105:11613–8.
- Gref R, Minamitake Y, Peracchia M, Trubetskoy V, Torchilin V, Langer R. Biodegradable long-circulating polymeric nanospheres. *Science* 1994;263:1600–3.
- Grosso D, Ribot F, Boissiere C, Sanchez C. Molecular and supramolecular dynamics of hybrid organic–inorganic interfaces for the rational construction of advanced hybrid nanomaterials. *Chem Soc Rev* 2011;40:829–48.
- Guay-Bégin A-A, Chevallier P, Faucher L, Turgeon S, Fortin M-A. Surface modification of gadolinium oxide thin films and nanoparticles using poly(ethylene glycol)-phosphate. *Langmuir* 2011;28:774–82.
- Gugulothu D, Patravale V. Stability-indicating HPLC method for arteether and application to nanoparticles of arteether. *J Chromatogr Sci* 2013. <http://dx.doi.org/10.1093/chromsci/bmt125>. (in press).
- Gun'ko V, Blitz J, Zarko V, Turov V, Pakhlov E, Oranska O, et al. Structural and adsorption characteristics and catalytic activity of titania and titania-containing nanomaterials. *J Colloid Interface Sci* 2009;330:125–37.
- Guo Z, Ganawi AA, Liu Q, He L. Nanomaterials in mass spectrometry ionization and prospects for biological application. *Anal Bioanal Chem* 2006;384:584–92.
- Hachani R, Lowdell M, Birchall M, Thanh NT. Tracking stem cells in tissue-engineered organs using magnetic nanoparticles. *Nanoscale* 2013;5:11362–72. <http://dx.doi.org/10.1039/c3nr03861k>.
- Hall JB, Dobrovolskaia MA, Patri AK, McNeil SE. Characterization of nanoparticles for therapeutics. *Nanomedicine (London)* 2007;2:789–803.
- Hansma PK, Elings VB, Marti O, Bracker CE. Scanning tunneling microscopy and atomic force microscopy: application to biology and technology. *Science* 1988;242:209–16.
- Hardman R. A toxicologic review of quantum dots: toxicity depends on physicochemical and environmental factors. *Environ Health Perspect* 2006;114:165–72.
- Hartschuh A. Tip-enhanced near-field optical microscopy. *Angew Chem Int Ed* 2008;47:8178–91.
- Hathout RM, Mansour S, Mortada ND, Guinedi AS. Liposomes as an ocular delivery system for acetazolamide: in vitro and in vivo studies. *AAPS PharmSciTech* 2007;8:1.
- Hayazawa N, Tarun A, Taguchi A, Furusawa K. Tip-enhanced Raman spectroscopy. In: Kumar CSR, editor. *Raman spectroscopy for nanomaterials characterization*. Berlin Heidelberg: Springer; 2012. p. 445–76.
- Heinzelmann H, Pohl DW. Scanning near-field optical microscopy. *Appl Phys A* 1994;59:89–101.
- Hind AR, Bhargava SK, McKinnon A. At the solid/liquid interface: FTIR/ATR—the tool of choice. *Adv Colloid Interface Sci* 2001;93:91–114.
- Hinterdorfer P, Garcia-Parajo MF, Dufrene YF. Single-molecule imaging of cell surfaces using near-field nanoscopy. *Acc Chem Res* 2012;45:327–36.
- Hondow N, Wang P, Brydson R, Holton M, Rees P, Summers H. TEM analysis of nanoparticle dispersions with application towards the quantification of in vitro cellular uptake. *Journal of physics: conference series*. IOP Publishing; 2012:012020.
- Horváth L, Magrez A, Burghard M, Kern K, Forró L, Schwaller B. Evaluation of the toxicity of graphene derivatives on cells of the lung luminal surface. *Carbon* 2013;64:45–60.
- Huang J, Zong C, Shen H, Cao Y, Ren B, Zhang Z. Tracking the intracellular drug release from graphene oxide using surface-enhanced Raman spectroscopy. *Nanoscale* 2013a;5:10591–8.
- Huang R, Carney RP, Stellacci F, Lau BLT. Protein–nanoparticle interactions: the effects of surface compositional and structural heterogeneity are scale dependent. *Nanoscale* 2013b;5:6928–35.
- Hull M, Bowman D. Nanotechnology environmental health and safety. Risks, regulation and management; 2009 [Access Online via Elsevier].
- Hummer DR, Heaney PJ, Post JE. In situ observations of particle size evolution during the hydrothermal crystallization of TiO<sub>2</sub>: a time-resolved synchrotron SAXS and WAXS study. *J Cryst Growth* 2012;344:51–8.
- Hurst SJ, Lytton-Jean AKR, Mirkin CA. Maximizing DNA loading on a range of gold nanoparticle sizes. *Anal Chem* 2006;78:8313–8.
- Ianoul A, Johnston LJ. Near-field scanning optical microscopy to identify membrane microdomains. *Methods Mol Biol* 2007;400:469–80.
- Inagaki S, Ghirlando R, Grishammer R. Biophysical characterization of membrane proteins in nanodiscs. *Methods* 2013;59:287–300.
- Inokuchi Y, Hironaka K, Fujisawa T, Tozuka Y, Tsuruma K, Shimazawa M, et al. Physicochemical properties affecting retinal drug/coumarin-6 delivery from nanocarrier systems via eyedrop administration. *Invest Ophthalmol Vis Sci* 2010;51:3162–70.
- Ispas C, Andreescu D, Patel A, Goia DV, Andreescu S, Wallace KN. Toxicity and developmental defects of different sizes and shape nickel nanoparticles in zebrafish. *Environ Sci Technol* 2009;43:6349–56.
- Jiang X, Jiang J, Jin Y, Wang E, Dong S. Effect of colloidal gold size on the conformational changes of adsorbed cytochrome c: probing by circular dichroism, UV–visible, and infrared spectroscopy. *Biomacromolecules* 2004;6:46–53.
- Jiang W, Kim BY, Rutka JT, Chan WC. Nanoparticle-mediated cellular response is size-dependent. *Nat Nanotechnol* 2008;3:145–50.
- Jiang X, Qu W, Pan D, Ren Y, Williford JM, Cui H, et al. Plasmid-templated shape control of condensed DNA-block copolymer nanoparticles. *Adv Mater* 2013;25:227–32.
- Jin H, Wang N, Xu L, Hou S. Synthesis and conductivity of cerium oxide nanoparticles. *Mater Lett* 2010;64:1254–6.
- Jing B, Zhu Y. Disruption of supported lipid bilayers by semihydrophobic nanoparticles. *J Am Chem Soc* 2011;133:10983–9.
- Johal MS. Understanding nanomaterials. Boca Raton: CRC Press; 2011.
- Kane SR, Ashby PD, Pruitt LA. ATR–FTIR as a thickness measurement technique for hydrated polymer-on-polymer coatings. *J Biomed Mater Res B Appl Biomater* 2009;91:613–20.
- Kapralov AA, Feng WH, Amoscato AA, Yanamala N, Balasubramanian K, Winnica DE, et al. Adsorption of surfactant lipids by single-walled carbon nanotubes in mouse lung upon pharyngeal aspiration. *ACS Nano* 2012;6:4147–56.
- Karlsson HL, Gustafsson J, Cronholm P, Möller L. Size-dependent toxicity of metal oxide particles—a comparison between nano- and micrometer size. *Toxicol Lett* 2009;188:112–8.
- Kattumenu R, Lee C, Bliznyuk V, Singamaneni S. Micro-Raman spectroscopy of nanostructures. In: Kumar CSR, editor. *Raman spectroscopy for nanomaterials characterization*. Berlin Heidelberg: Springer; 2012. p. 417–44.
- Kazarian SG, Chan KL. Applications of ATR–FTIR spectroscopic imaging to biomedical samples. *Biochim Biophys Acta* 2006;1758:858–67.



- Khatun Z, Nurunnabi M, Cho KJ, Lee Y-k. Oral delivery of near-infrared quantum dot loaded micelles for noninvasive biomedical imaging. *ACS Appl Mater Interfaces* 2012;4:3880–7.
- Kim BY, Rutka JT, Chan WC. Nanomedicine. *N Engl J Med* 2010;363:2434–43.
- Kim TH, Kim M, Park HS, Shin US, Gong MS, Kim HW. Size-dependent cellular toxicity of silver nanoparticles. *J Biomed Mater Res A* 2012;100:1033–43.
- Kim TH, Lee S, Chen X. Nanotheranostics for personalized medicine. *Expert Rev Mol Diagn* 2013;13:257–69.
- Klesing J, Wiehe A, Gitter B, Gräfe S, Eppel M. Positively charged calcium phosphate/polymer nanoparticles for photodynamic therapy. *J Mater Sci Mater Med* 2010;21:887–92.
- Kneipp J, Kneipp H, Wittig B, Kneipp K. Novel optical nanosensors for probing and imaging live cells. *Nanomed Nanotechnol Biol Med* 2010;6:214–26.
- Knoppe S, Dharmaratne AC, Schreiner E, Dass A, Bürgi T. Ligand exchange reactions on Au<sub>38</sub> and Au<sub>40</sub> clusters: a combined circular dichroism and mass spectrometry study. *J Am Chem Soc* 2010;132:16783–9.
- Kobayashi N, Muranaka A, Mack J. Circular dichroism and magnetic circular dichroism spectroscopy for organic chemists. *R Soc Chem* 2011. (ISBN : 1847558690).
- Kocum C, Cimen EK, Piskin E. Imaging of poly(NIPAA-co-MAH)-HlgG conjugate with scanning tunneling microscopy. *J Biomater Sci Polym Ed* 2004;15:1513–20.
- Kohli R, Mittal KL. Developments in surface contamination and cleaning-detection, characterization, and analysis of contaminants. William Andrew; 2011.
- Koningsberger DC, Prins R. X-ray absorption: principles, applications, techniques of EXAFS, SEXAFS, and XANES. New York: Wiley; 1988.
- Kostarelos K. The long and short of carbon nanotube toxicity. *Nat Biotechnol* 2008;26:774–6.
- Krichinsky O, Bonnet G. Fluorescence correlation spectroscopy: the technique and its applications. *Rep Prog Phys* 2002;65:251.
- Kumar CS. Raman spectroscopy for nanomaterials characterization. Springer Verlag; 2012.
- Kumar J, Thomas KG. Surface-enhanced Raman spectroscopy: investigations at the nanorod edges and dimer junctions. *J Phys Chem Lett* 2011;2:610–5.
- Laera S, Ceconce G, Rossi F, Gilliland D, Hussain R, Siligardi G, et al. Measuring protein structure and stability of protein–nanoparticle systems with synchrotron radiation circular dichroism. *Nano Lett* 2011;11:4480–4.
- Lam T, Pouliot P, Avti PK, Lesage F, Kakkak AK. Superparamagnetic iron oxide based nanopores for imaging and theranostics. *Adv Colloid Interface Sci* 2013;199–200:95–113.
- Lavigne J-P, Espinal P, Duniach-Remy C, Messad N, Pantel A, Sotto A. Mass spectrometry: a revolution in clinical microbiology? *Clin Chem Lab Med* 2013;51:257–70.
- Law SL, Huang KJ, Chiang CH. Acyclovir-containing liposomes for potential ocular delivery. Corneal penetration and absorption. *J Control Release* 2000;63:135–40.
- Lee HM, Jin SM, Kim HM, Suh YD. Single-molecule surface-enhanced Raman spectroscopy: a perspective on the current status. *Phys Chem Chem Phys* 2013a;15:5276–87.
- Lee JP, Chen D, Li X, Yoo S, Bottomley LA, El-Sayed MA. Well-organized raspberry-like Ag@Cu bimetal nanoparticles for highly reliable and reproducible surface-enhanced Raman scattering. *Nanoscale* 2013b;5:11620–4. <http://dx.doi.org/10.1039/c3nr03363e>.
- Leung K, Chopra A, Shan L, Eckelman WC, Menkens AE. Essential parameters to consider for the characterization of optical imaging probes. *Nanomedicine (Lond)* 2012;7:1101–7.
- Liang XJ, Chen C, Zhao Y, Jia L, Wang PC. Biopharmaceutics and therapeutic potential of engineered nanomaterials. *Curr Drug Metab* 2008;9:697–709.
- Lim J, Yeap SP, Che HX, Low SC. Characterization of magnetic nanoparticle by dynamic light scattering. *Nanoscale Res Lett* 2013;8:381.
- Lin Z-H, Chang H-T. Preparation of gold–tellurium hybrid nanomaterials for surface-enhanced Raman spectroscopy. *Langmuir* 2007;24:365–7.
- Lin X-M, Cui Y, Xu Y-H, Ren B, Tian Z-Q. Surface-enhanced Raman spectroscopy: substrate-related issues. *Anal Bioanal Chem* 2009;394:1729–45.
- Lin W-f, Li J-R, G-y Liu. Near-field scanning optical microscopy enables direct observation of moiré effects at the nanometer scale. *ACS Nano* 2012;6:9141–9.
- Lipfert J, Doniach S. Small-angle X-ray scattering from RNA, proteins, and protein complexes. *Annu Rev Biophys Biomol Struct* 2007;36:307–27.
- Liu H, Webster TJ. Nanomedicine for implants: a review of studies and necessary experimental tools. *Biomaterials* 2007;28:354–69.
- Liu Y, Li W, Lao F, Liu Y, Wang L, Bai R, et al. Intracellular dynamics of cationic and anionic polystyrene nanoparticles without direct interaction with mitotic spindle and chromosomes. *Biomaterials* 2011;32:8291–303.
- Liu L, Ma Y, Chen X, Xiong X, Shi S. Screening and identification of BSA bound ligands from *Pueraria lobata* flower by BSA functionalized Fe<sub>3</sub>O<sub>4</sub> magnetic nanoparticles coupled with HPLC–MS/MS. *J Chromatogr B* 2012;887–888:55–60.
- Liu W, Rose J, Plantevin S, Auffan M, Bottero J-Y, Vidaud C. Protein corona formation for nanomaterials and proteins of a similar size: hard or soft corona? *Nanoscale* 2013;5:1658–68.
- Lucas M, Riedo E. Invited review article: combining scanning probe microscopy with optical spectroscopy for applications in biology and materials science. *Rev Sci Instrum* 2012;83:061101.
- Lundqvist M, Sethson I, Jonsson B-H. Transient interaction with nanoparticles “freezes” a protein in an ensemble of metastable near-native conformations. *Biochemistry* 2005;44:10093–9.
- Luyts K, Napierska D, Nemery B, Hoet PHM. How physico-chemical characteristics of nanoparticles cause their toxicity: complex and unresolved interrelations. *Environ Sci Process Impacts* 2013;15:23–38.
- Magde D, Elson E, Webb WW. Thermodynamic fluctuations in a reacting system—measurement by fluorescence correlation spectroscopy. *Phys Rev Lett* 1972;29:705–8.
- Mahajan KD, Fan Q, Dorcena J, Ruan G, Winter JO. Magnetic quantum dots in biotechnology—synthesis and applications. *Biotechnol J* 2013. <http://dx.doi.org/10.1002/biot.201300038>. (in press).
- Mahmoudi M, Lynch I, Ejtehadi MR, Monopoli MP, Bombelli FB, Laurent S. Protein–nanoparticle interactions: opportunities and challenges. *Chem Rev* 2011;111:5610–37.
- Mannelli I, Marco MP. Recent advances in analytical and bioanalysis applications of noble metal nanorods. *Anal Bioanal Chem* 2010;398:2451–69.
- Marti O, Ribi HO, Drake B, Albrecht TR, Quate CF, Hansma PK. Atomic force microscopy of an organic monolayer. *Science* 1988;239:50–2.
- Mavrocordatos D, Pronk W, Boiler M. Analysis of environmental particles by atomic force microscopy, scanning and transmission electron microscopy. *Water Sci Technol* 2004;50:9–18.
- McNaught AD, Wilkinson A. Compendium of chemical terminology. Oxford: Blackwell Science; 1997.
- McNeil SE. Nanotechnology for the biologist. *J Leukoc Biol* 2005;78:585–94.
- Milani S, Baldelli Bombelli F, Pitek AS, Dawson KA, Rädler J. Reversible versus irreversible binding of transferrin to polystyrene nanoparticles: soft and hard corona. *ACS Nano* 2012;6:2532–41.
- Miles M, McMaster T, Carr H, Tatham A, Shewry P, Field J, et al. Scanning tunneling microscopy of biomolecules. *J Vac Sci Technol A Vac Surf Films* 1990;8:698–702.
- Mirau PA, Naik RR, Gehring P. Structure of peptides on metal oxide surfaces probed by NMR. *J Am Chem Soc* 2011;133:18243–8.
- Mitragotri S. In drug delivery, shape does matter. *Pharm Res* 2009;26:232–4.
- Monopoli MP, Walczyk D, Campbell A, Elia G, Lynch I, Baldelli Bombelli F, et al. Physical–chemical aspects of protein corona: relevance to in vitro and in vivo biological impacts of nanoparticles. *J Am Chem Soc* 2011;133:2525–34.
- Mullen DG, Fang M, Desai A, Baker JR, Orr BG, Banaszak Holl MM. A quantitative assessment of nanoparticle–ligand distributions: implications for targeted drug and imaging delivery in dendrimer conjugates. *ACS Nano* 2010;4:657–70.
- Murdock RC, Braydich-Stolle L, Schrand AM, Schlager JJ, Hussain SM. Characterization of nanomaterial dispersion in solution prior to in vitro exposure using dynamic light scattering technique. *Toxicol Sci* 2008;101:239–53.
- Nakaya M, Kuwahara Y, Aono M, Nakayama T. Nanoscale control of reversible chemical reaction between fullerene C<sub>60</sub> molecules using scanning tunneling microscope. *J Nanosci Nanotechnol* 2011;11:2829–35.
- Nel AE, Madler L, Velegol D, Xia T, Hoek EM, Somasundaran P, et al. Understanding biophysicochemical interactions at the nano–bio interface. *Nat Mater* 2009;8:543–57.
- Nienhaus GU, Maffre P, Nienhaus K. Studying the protein corona on nanoparticles by FCS. In: Sergey YT, editor. *Methods in enzymology*. Academic Press; 2013. p. 115–37.
- Oberdorster GEJ. Nanotoxicology: an emerging discipline evolving from studies of ultra-fine particles. *Environ Health Perspect* 2005;113:823–39.
- Oberdorster G, Maynard A, Donaldson K, Castranova V, Fitzpatrick J, Ausman K, et al. Principles for characterizing the potential human health effects from exposure to nanomaterials: elements of a screening strategy. *Part Fibre Toxicol* 2005;2:8.
- Ong QK, Reguera J, Silva PJ, Moglianetti M, Harkness K, Longobardi M, et al. High-resolution scanning tunneling microscopy characterization of mixed monolayer protected gold nanoparticles. *ACS Nano* 2013;7:8529–39.
- Overgaag K, Liljeroth P, Grandidier B, Vanmaekelbergh D. Scanning tunneling spectroscopy of individual PbSe quantum dots and molecular aggregates stabilized in an inert nanocrystal matrix. *ACS Nano* 2008;2:600–6.
- Pal S, Tak YK, Song JM. Does the antibacterial activity of silver nanoparticles depend on the shape of the nanoparticle? A study of the gram-negative bacterium *Escherichia coli*. *Appl Environ Microbiol* 2007;73:1712–20.
- Pan BF, Cui DX, Gao F, He R. Growth of multi-amine terminated poly(amidoamine) dendrimers on the surface of carbon nanotubes. *Nanotechnology* 2006;17:2483–9.
- Pan G-H, Barras A, Boussekey L, Qu X, Addad A, Boukherroub R. Preparation and characterization of decyl-terminated silicon nanoparticles encapsulated in lipid nanocapsules. *Langmuir* 2013;29:12688–96.
- Park S, Lee YK, Jung M, Kim KH, Chung N, Ahn EK, et al. Cellular toxicity of various inhalable metal nanoparticles on human alveolar epithelial cells. *Inhal Toxicol* 2007;19(Suppl. 1):59–65.
- Park HK, Lim YT, Kim JK, Park HG, Chung BH. Nanoscopic observation of a gold nanoparticle-conjugated protein using near-field scanning optical microscopy. *Ultramicroscopy* 2008;108:1115–9.
- Park Y-H, Bae HC, Jang Y, Jeong SH, Lee HN, Ryu W-I, et al. Effect of the size and surface charge of silica nanoparticles on cutaneous toxicity. *Mol Cell Toxicol* 2013;9:67–74.
- Parot P, Dufrène YF, Hinterdorfer P, Le Grimmelc C, Navajas D, Pellequer J-L, et al. Past, present and future of atomic force microscopy in life sciences and medicine. *J Mol Recognit* 2007;20:418–31.
- Patri A, Dobrovolskaia M, Stern S, McNeil S, Amiji M. Preclinical characterization of engineered nanoparticles intended for cancer therapeutics. *Nanotechnology for cancer therapy*. CRC Press; 2006:105–38.
- Perevedentseva E, Cai PJ, Chiu YC, Cheng CL. Characterizing protein activities on the lysozyme and nanodiamond complex prepared for bio applications. *Langmuir* 2010;27:1085–91.
- Petoukhov MV, Svergun DI. Applications of small-angle X-ray scattering to biomacromolecular solutions. *Int J Biochem Cell Biol* 2013;45:429–37.
- Petryayeva E, Algar WR, Medintz IL. Quantum dots in bioanalysis: a review of applications across various platforms for fluorescence spectroscopy and imaging. *Appl Spectrosc* 2013;67:215–52.
- Picas L, Milhiet PE, Hernandez-Borrell J. Atomic force microscopy: a versatile tool to probe the physical and chemical properties of supported membranes at the nanoscale. *Chem Phys Lipids* 2012;165:845–60.
- Pleus R. Nanotechnologies—guidance on physicochemical characterization of engineered nanoscale materials for toxicologic assessment; 2012.
- Poland CA, Duffin R, Kinloch I, Maynard A, Wallace WA, Seaton A, et al. Carbon nanotubes introduced into the abdominal cavity of mice show asbestos-like pathogenicity in a pilot study. *Nat Nanotechnol* 2008;3:423–8.

- Ponce A, Mejia-Rosales S, Jose-Yacamán M. Scanning transmission electron microscopy methods for the analysis of nanoparticles. *Methods Mol Biol* 2012;906:453–71.
- Pons T, Medintz IL, Wang X, English DS, Mattoussi H. Solution-phase single quantum dot fluorescence resonance energy transfer. *J Am Chem Soc* 2006a;128:15324–31.
- Pons T, Uyeda HT, Medintz IL, Mattoussi H. Hydrodynamic dimensions, electrophoretic mobility, and stability of hydrophilic quantum dots. *J Phys Chem B* 2006b;110:20308–16.
- Popovic ZV, Dohcevic-Mitrovic Z, Scepanovic M, Grujic-Brojin M, Askaric S, Raman scattering on nanomaterials and nanostructures. *Ann Phys* 2011;523:62–74.
- Powers KW, Brown SC, Krishna VB, Wasdo SC, Moudgil BM, Roberts SM. Research strategies for safety evaluation of nanomaterials. Part VI. Characterization of nanoscale particles for toxicological evaluation. *Toxicol Sci* 2006;90:296–303.
- Powers KW, Palazuelos M, Brown SC, Roberts SM. Characterization of nanomaterials for toxicological evaluation. In: Sahu S, Casciano D, editors. *Nanotoxicology From In Vivo and In Vitro Models to Health Risks*; 2009. p. 1–27.
- Rabinow BE. Nanosuspensions in drug delivery. *Nat Rev Drug Discov* 2004;3:785–96.
- Rahman M, Laurent S, Tawil N, Yahia LH, Mahmoudi M. Analytical methods for corona evaluations. Protein–nanoparticle interactions. Berlin Heidelberg: Springer; 2013:65–82.
- Ranjbar B, Gill P. Circular dichroism techniques: biomolecular and nanostructural analyses – a review. *Chem Biol Drug Des* 2009;74:101–20.
- Rao CNR, Biswas K. Characterization of nanomaterials by physical methods. *Annu Rev Anal Chem* 2009;435–62. [Palo Alto: Annual Reviews].
- Ratner BD, Hoffman AS, Schoen FJ, Lemons JE. Biomaterials science: an introduction to materials in medicine. Academic Press; 2004.
- Ratnikova TA, Nedumpully Govindan P, Salonen E, Ke PC. In vitro polymerization of microtubules with a fullerene derivative. *ACS Nano* 2011;5:6306–14.
- Röcker C, Pözl M, Zhang F, Parak WJ, Nienhaus GU. A quantitative fluorescence study of protein monolayer formation on colloidal nanoparticles. *Nat Nanotechnol* 2009;4:577–80.
- Rosenblum LT, Kosaka N, Mitsunaga M, Choyke PL, Kobayashi H. In vivo molecular imaging using nanomaterials: general in vivo characteristics of nano-sized reagents and applications for cancer diagnosis. *Mol Membr Biol* 2010;27:274–85.
- Rusu L, Gambhir A, McLaughlin S, Radler J. Fluorescence correlation spectroscopy studies of peptide and protein binding to phospholipid vesicles. *Biophys J* 2004;87:1044–53.
- Sacchetti C, Motamedchaboki K, Magrini A, Palmieri G, Mattei M, Bernardini S, et al. Surface polyethylene glycol conformation influences the protein corona of polyethylene glycol-modified single-walled carbon nanotubes: potential implications on biological performance. *ACS Nano* 2013;7:1974–89.
- Sapsford KE, Tyner KM, Dair BJ, Deschamps JR, Medintz IL. Analyzing nanomaterial bioconjugates: a review of current and emerging purification and characterization techniques. *Anal Chem* 2011;83:4453–88.
- Schacher F, Bethhausen E, Walther A, Schmalz H, Pergushov DV, Müller AHE. Interpolyelectrolyte complexes of dynamic multicompartment micelles. *ACS Nano* 2009;3:2095–102.
- Schaefer J, Schulze C, Marxer EE, Schaefer UF, Wohlleben W, Bakowsky U, et al. Atomic force microscopy and analytical ultracentrifugation for probing nanomaterial protein interactions. *ACS Nano* 2012;6:4603–14.
- Schwille P. Fluorescence correlation spectroscopy and its potential for intracellular applications. *Cell Biochem Biophys* 2001;34:383–408.
- Shang L, Wang Y, Jiang J, Dong S. pH-Dependent protein conformational changes in albumin: gold nanoparticle bioconjugates: a spectroscopic study. *Langmuir* 2007;23:2714–21.
- Shekunov BY, Chattopadhyay P, Tong HH, Chow AH. Particle size analysis in pharmaceuticals: principles, methods and applications. *Pharm Res* 2007;24:203–27.
- Singh A, Sahoo SK. Magnetic nanoparticles: a novel platform for cancer theranostics. *Drug Discov Today* 2013. <http://dx.doi.org/10.1016/j.drudis.2013.10.005>. (in press).
- Sinjab F, Lekprasert B, Woolley RAJ, Roberts CJ, Tang L, Nottingher I. Near-field Raman spectroscopy of biological nanomaterials by in situ laser-induced synthesis of tip-enhanced Raman spectroscopy tips. *Opt Lett* 2012;37:2256–8.
- Sohaebuddin S, Thevenot P, Baker D, Eaton J, Tang L. Nanomaterial cytotoxicity is composition, size, and cell type dependent. *Part Fibre Toxicol* 2010;7:22.
- Song Y, Zhang Z, Elsayed-Ali HE, Wang H, Henry LL, Wang Q, et al. Identification of single nanoparticles. *Nanoscale* 2011;3:31–44.
- Sosenkova L, Egorova E. The effect of particle size on the toxic action of silver nanoparticles. *Journal of Physics: Conference Series*. IOP Publishing; 2011. p. 012027.
- Sperling RA, Liedl T, Dühr S, Kudara S, Zanella M, Lin CAJ, et al. Size determination of (bio) conjugated water-soluble colloidal nanoparticles: a comparison of different techniques. *J Phys Chem C* 2007;111:11552–9.
- Stolnik S, Illum L, Davis SS. Long circulating microparticulate drug carriers. *Adv Drug Deliv Rev* 1995;16:195–214.
- Suzuki E. High-resolution scanning electron microscopy of immunogold-labelled cells by the use of thin plasma coating of osmium. *J Microsc* 2002;208:153–7.
- Takagi A, Hirose A, Nishimura T, Fukumori N, Ogata A, Ohashi N, et al. Induction of mesothelioma in p53 +/– mice; mouse by intraperitoneal application of multi-wall carbon nanotube. *J Toxicol Sci* 2008;33:105–16.
- Tanaka K, Pescitelli G, Nakanishi K, Berova N. Fluorescence detected exciton coupled circular dichroism: development of new fluorescent reporter groups for structural studies. *Monatsh Chem/Chem Mon* 2005;136:367–95.
- Tang Z, Xu B, Wu B, Germann MW, Wang G. Synthesis and structural determination of multidentate 2,3-dithiol-stabilized Au clusters. *J Am Chem Soc* 2010;132:3367–74.
- Tassa C, Duffner JL, Lewis TA, Weissleder R, Schreiber SL, Koehler AN, et al. Binding affinity and kinetic analysis of targeted small molecule-modified nanoparticles. *Bioconjug Chem* 2009;21:14–9.
- Thomas R, Park IK, Jeong YY. Magnetic iron oxide nanoparticles for multimodal imaging and therapy of cancer. *Int J Mol Sci* 2013;14:15910–30.
- Tiede K, Boxall ABA, Tear SP, Lewis J, David H, Hasselöv M. Detection and characterization of engineered nanoparticles in food and the environment. *Food Addit Contam Part A* 2008;25:795–821.
- Tom RT, Samal AK, Sreepasad TS, Pradeep T. Hemoprotein bioconjugates of gold and silver nanoparticles and gold nanorods: structure–function correlations. *Langmuir* 2006;23:1320–5.
- Tomalia DA, Huang B, Swanson DR, Brothers HM, Klimash JW. Structure control within poly(amidoamine) dendrimers: size, shape and regio-chemical mimicry of globular proteins. *Tetrahedron* 2003;59:3799–813.
- Uskokovic V. Dynamic light scattering based microelectrophoresis: main prospects and limitations. *J Disper Sci Technol* 2012;33:1762–86.
- Vaiyapuri R, Greenland BW, Rowan SJ, Colquhoun HM, Elliott JM, Hayes W. Thermoresponsive supramolecular polymer network comprising pyrene-functionalized gold nanoparticles and a chain-folding polydiimide. *Macromolecules* 2012;45:5567–74.
- Valentini M, Vaccaro A, Rehor A, Napoli A, Hubbell JA, Tirelli N. Diffusion NMR spectroscopy for the characterization of the size and interactions of colloidal matter: the case of vesicles and nanoparticles. *J Am Chem Soc* 2004;126:2142–7.
- Vancso GJ, Hillborg H, Schönherr H. Chemical composition of polymer surfaces imaged by atomic force microscopy and complementary approaches. *Polymer analysis polymer theory*. Berlin Heidelberg: Springer; 2005:55–129.
- Vertegel AA, Siegel RW, Dordick JS. Silica nanoparticle size influences the structure and enzymatic activity of adsorbed lysozyme. *Langmuir* 2004;20:6800–7.
- Vinogradov SV, Bronich TK, Kabanov AV. Nanosized cationic hydrogels for drug delivery: preparation, properties and interactions with cells. *Adv Drug Deliv Rev* 2002;54:135–47.
- Vobornik D, Banks DS, Lu Z, Fradin C, Taylor R, Johnston LJ. Fluorescence correlation spectroscopy with sub-diffraction-limited resolution using near-field optical probes. *Appl Phys Lett* 2008;93.
- Wagner AJ, Bleckmann CA, Murdock RC, Schrand AM, Schlager JJ, Hussain SM. Cellular interaction of different forms of aluminum nanoparticles in rat alveolar macrophages. *J Phys Chem B* 2007;111:7353–9.
- Wagner V, Hüsing B, Gaisser S, Bock A-K. Nanomedicine: drivers for development and possible impacts. *JRC-IPTS Eur* 2008:23494.
- Walczky D, Bombelli FB, Monopoli MP, Lynch I, Dawson KA. What the cell “sees” in bionanoscience. *J Am Chem Soc* 2010;132:5761–8.
- Wang ZL. Transmission electron microscopy and spectroscopy of nanoparticles. Characterization of nanophase materials. Wiley-VCH Verlag GmbH; 2001:37–80.
- Wang H, Chu PK. Chapter 4 – surface characterization of biomaterials. In: Amit B, Susmita B, editors. *Characterization of biomaterials*. Oxford: Academic Press; 2013. p. 105–74.
- Wang Y, Irudayaraj J. Surface-enhanced Raman spectroscopy at single-molecule scale and its implications in biology. *Philos Trans R Soc Lond B Biol Sci* 2013;368:20120026.
- Wang L-Q, Exarhos GJ, Liu J. Nuclear magnetic resonance – characterization of self-assembled nanostructural materials. Characterization of nanophase materials. Wiley-VCH Verlag GmbH; 2001:243–60.
- Wang T, Sridhar R, Korotcov A, Ting AH, Francis K, Mitchell J, et al. Synthesis of amphiphilic triblock copolymers as multidentate ligands for biocompatible coating of quantum dots. *Colloids Surf A Physicochem Eng Asp* 2011;375:147–55.
- Warheit DB, Webb TR, Sayes CM, Colvin VL, Reed KL. Pulmonary instillation studies with nanoscale TiO<sub>2</sub> rods and dots in rats: toxicity is not dependent upon particle size and surface area. *Toxicol Sci* 2006;91:227–36.
- Webster TJ. Nanomedicine: what's in a definition? *Int J Nanomedicine* 2006;1:115.
- Weiner BB, Tscharnutter WW, Fairhurst D. Zeta potential: a new approach. New York: Brookhaven Instruments Corporation; 1993.
- Wiesendanger R. Scanning probe microscopy and spectroscopy: methods and applications. Cambridge University Press; 1994.
- Williams DB, Carter CB. The transmission electron microscope. Transmission electron microscopy. Springer; 2009:3–22.
- Wilson AJ, Willets KA. Surface-enhanced Raman scattering imaging using noble metal nanoparticles. *Wiley Interdiscip Rev Nanomed Nanobiotechnol* 2013;5:180–9.
- Wong BS, Yoong SL, Jagusiak A, Panczyk T, Ho HK, Ang WH. Carbon nanotubes for delivery of small molecule drugs. *Adv Drug Deliv Rev* 2013. <http://dx.doi.org/10.1016/j.addr.2013.08.005>. (in press).
- Wu B, Chen Y, Muller JD. Fluorescence correlation spectroscopy of finite-sized particles. *Biophys J* 2008;94:2800–8.
- Xiao M, Nyagilo J, Arora V, Kulkarni P, Xu D, Sun X, et al. Gold nanotags for combined multi-colored Raman spectroscopy and x-ray computed tomography. *Nanotechnology* 2010;21:035101.
- Xu R. Progress in nanoparticles characterization: sizing and zeta potential measurement. *Particuology* 2008;6:112–5.
- Yang L, Watts DJ. Particle surface characteristics may play an important role in phytotoxicity of alumina nanoparticles. *Toxicol Lett* 2005;158:122–32.
- Yang PH, Sun XS, Chiu JF, Sun HZ, He QY. Transferrin-mediated gold nanoparticle cellular uptake. *Bioconjug Chem* 2005;16:494–6.
- Yao H, Saeki M, Sasaki A. Boronic acid-protected gold clusters capable of asymmetric induction: spectral deconvolution analysis of their electronic absorption and magnetic circular dichroism. *Langmuir* 2012;28:3995–4002.
- Zak AK, Majid W, Darroudi M, Yousefi R. Synthesis and characterization of ZnO nanoparticles prepared in gelatin media. *Mater Lett* 2011;65:70–3.
- Zanchet D, Hall BD, Ugarte D. X-ray characterization of nanoparticles. Characterization of nanophase materials. Wiley-VCH Verlag GmbH; 2001:13–36.
- Zhao Y, Qiu X, Burda C. The effects of sintering on the photocatalytic activity of N-doped TiO<sub>2</sub> nanoparticles. *Chem Mater* 2008;20:2629–36.
- Zhao T, Chen K, Gu H. Investigations on the interactions of proteins with polyampholyte-coated magnetite nanoparticles. *J Phys Chem B* 2013;117:14129–35. <http://dx.doi.org/10.1021/jp407157n>.
- Zhou C, Liu Z, Du X, Mitchell DR, Mai YW, Yan Y, et al. Hollow nitrogen-containing core/shell fibrous carbon nanomaterials as support to platinum nanocatalysts and their TEM tomography study. *Nanoscale Res Lett* 2012;7:165.
- Zhu L, Attard P, Neto C. Reliable measurements of interfacial slip by colloid probe atomic force microscopy. II. Hydrodynamic force measurements. *Langmuir* 2011;27:6712–9.

# Highly sensitive simultaneous detection of mercury and copper ions by ultrasmall fluorescent DNA–Ag nanoclusters†

Cite this: DOI: 10.1039/c3nj01019h

 Shengliang Li,<sup>‡ab</sup> Weipeng Cao,<sup>‡a</sup> Anil Kumar,<sup>a</sup> Shubin Jin,<sup>a</sup> Yuanyuan Zhao,<sup>a</sup> Chunqiu Zhang,<sup>a</sup> Guozhang Zou,<sup>a</sup> Paul C. Wang,<sup>c</sup> Feng Li<sup>\*b</sup> and Xing-Jie Liang<sup>\*a</sup>

Fluorescent metal nanoclusters (NCs) have given rise to a new class of fluorescent nanomaterials for the detection of heavy metals. Here, we design a simple, rapid and highly sensitive sensing nanosystem for the detection of  $\text{Hg}^{2+}$  and  $\text{Cu}^{2+}$  based on fluorescence quenching of ultrasmall DNA–Ag NCs. The fluorescence intensity of DNA–Ag NCs was selectively quenched by  $\text{Hg}^{2+}$  and  $\text{Cu}^{2+}$ , and the limit of detection (LOD) was found to be 5 nM and 10 nM, respectively. The technique was renewably employed by EDTA addition and successfully applied to detection of  $\text{Hg}^{2+}$  and  $\text{Cu}^{2+}$  in domestic water samples. The quantum yield (QY) of DNA–Ag NCs was significantly higher ( $\sim 30\%$ ) compared to traditional water-soluble fluorescent metal NCs. The DNA–Ag NCs detection system is potentially suitable for detecting  $\text{Hg}^{2+}$  and  $\text{Cu}^{2+}$  and monitoring water quality in a wide range of samples regulated under the Environmental Protection Agency.

 Received (in Montpellier, France)  
29th August 2013,  
Accepted 28th January 2014

DOI: 10.1039/c3nj01019h

[www.rsc.org/njc](http://www.rsc.org/njc)

## Introduction

Recently, metal nanoclusters (NCs), composed of a few to a hundred atoms within a core structure, have emerged as novel luminescent nanomaterials and have received extensive attention because of their potential use in real-time applications.<sup>1–3</sup> With sizes comparable to the Fermi wavelength of electrons, NCs exhibit unique photoluminescence properties including strong photoluminescence, high emission rates, large Stokes shifts, excellent photostability and two-photon absorption cross sections.<sup>4–7</sup> More importantly, the emission wavelength of water-soluble metal NCs can be easily tuned from blue to near-infrared by varying the type of ligand or controlling the size.<sup>8–10</sup> Owing to their ultrasmall size and attractive photoluminescence properties, metal NCs are employed as a new class of biocompatible fluorophores for applications in biological imaging and bioassays.<sup>11,12</sup>

Heavy and transition metal ions are essential for the physical activities of biological and environmental processes.<sup>13,14</sup> However, excess amounts of these metal ions are toxic and can induce a series of health and environmental problems. Mercury is one of the most toxic heavy metal ions and poses significant toxicity even after a minute exposure. Mercury damages biological systems by disrupting biological processes and can result in a variety of serious diseases.<sup>15–17</sup> Copper, the third most abundant transition metal in the human body, plays vital roles in many fundamental biological processes. However,  $\text{Cu}^{2+}$  can cause serious damage to the liver and kidney at high concentrations.<sup>18–20</sup> Thus, methods for detecting the presence of these ions are urgently needed. Although a number of effective approaches for  $\text{Hg}^{2+}$  and  $\text{Cu}^{2+}$  detection have been developed, existing methods need complex equipment or sophisticated operations.<sup>21,22</sup> Simple and sensitive methods for detecting metal ions are still required.

In this work, we report the design of a sensing system to detect  $\text{Hg}^{2+}$ . This system is based on the interaction between DNA–Ag NCs and  $\text{Hg}^{2+}$ , which causes fluorescence quenching. We also found that the DNA–Ag NCs responded not only to  $\text{Hg}^{2+}$ , but also to  $\text{Cu}^{2+}$ .  $\text{Hg}^{2+}$  caused a more obvious fluorescence change than  $\text{Cu}^{2+}$ . Further studies were carried out to investigate the detection of  $\text{Hg}^{2+}$  and  $\text{Cu}^{2+}$  in water samples. The highly sensitive and selective fluorescence quenching by  $\text{Hg}^{2+}$  and  $\text{Cu}^{2+}$  demonstrates that DNA–Ag NCs have great potential as a nano-sensing system for monitoring water quality in a wide range of samples.

<sup>a</sup> Laboratory of Nanomedicine and Nanosafety, Division of Nanomedicine and Nanobiology, National Center for Nanoscience and Technology of China, and CAS Key Laboratory for Biomedical Effects of Nanomaterials and Nanosafety, Chinese Academy of Sciences, Beijing, 100190, China. E-mail: liangxj@nanoctr.cn

<sup>b</sup> Department of Neurobiology and Anatomy, Zhongshan School of Medicine, Sun Yat-sen University, Guangzhou, China. E-mail: lifeng@mail.sysu.edu.cn

<sup>c</sup> Laboratory of Molecular Imaging, Department of Radiology, Howard University, Washington, DC 20060, USA

† Electronic supplementary information (ESI) available. See DOI: 10.1039/c3nj01019h

‡ These authors contributed equally to this work.



# Materials and methods

## Materials and reagents

All oligonucleotides were synthesized by Beijing Sunbiotech Co. Ltd (Beijing, China). The oligonucleotides were purified by desalting. Gold(III) chloride trihydrate ( $\text{HAuCl}_4 \cdot 3\text{H}_2\text{O}$ ), silver nitrate ( $\text{AgNO}_3$ ) and sodium borohydride ( $\text{NaBH}_4$ ) were purchased from Sigma-Aldrich (St Louis, USA). Ultrapure water ( $18.2 \text{ M}\Omega \text{ cm}^{-1}$ ) produced by a Milli-Q system (Millipore Co., USA) was used in all the experimental work. All chemicals used were of analytical grade.

## Synthesis of oligonucleotide-Ag NCs

Oligonucleotide-Ag NCs were prepared as described elsewhere with slight modifications.<sup>2,23</sup> Briefly, DNA (oligonucleotide sequence: 5'-ACC CGA ACC TGG GCT ACC ACC CTT AAT CCC C-3') was dissolved in deionized water to prepare a stock solution. 6  $\mu\text{L}$  of DNA (250  $\mu\text{M}$ ) and 9  $\mu\text{L}$  of  $\text{AgNO}_3$  (1 mM) were sequentially added to sodium phosphate buffer (PBS, 20 mM, pH 6.6), and the mixture was incubated at room temperature, in the dark, for 20 minutes. Freshly prepared  $\text{NaBH}_4$  solution (90  $\mu\text{M}$ ) was then added to the reaction mixture with vigorous shaking for 30 seconds. The reaction mixture was kept in the dark at room temperature for 4 hours before use.

## Characterization of DNA-Ag NCs

UV-Vis absorption spectra were recorded using a Lambda 950 UV/Vis/NIR spectrophotometer (Perkin-Elmer, USA). The fluorescence spectra were obtained in a microcell with 1 cm path length using a Perkin-Elmer LS55 luminescence spectrometer. The fluorescence lifetime of DNA-Ag NCs was measured using an Edinburgh FL 900 single-photon counting fluorescence lifetime instrument and a laser lamp (Edinburgh Instruments, Scotland). Transmission electron microscopy (TEM) imaging was performed using an FEI Tecnai F20 U-TWIN electron microscope (FEI Company, Philips, Netherlands). The size and zeta-potential distribution of DNA-Ag NCs was measured using a Zetasizer Nano ZS (Malvern, UK) at 25  $^\circ\text{C}$ . X-ray photoelectron spectroscopy (XPS) was carried out on an X-ray photoelectron spectrometer (Perkin-Elmer, PHI-5300).

## Determination of the fluorescence spectra of DNA-Ag NCs in the presence of metal ions

To explore the interaction of DNA-Ag NCs with different metal ions, 100  $\mu\text{L}$  of the as-synthesized DNA-Ag NCs were mixed with different metal ions at 1 mM. The fluorescence spectra of DNA-Ag NCs in the presence of metal ions were recorded using a luminescence spectrometer after the samples were incubated for 5 minutes.

## Detection of metal ions

The fluorescence activity of the DNA-Ag NCs was monitored over a range of  $\text{Hg}^{2+}$  and  $\text{Cu}^{2+}$  concentrations to evaluate the lowest concentration at which metal ions could be detected. For detection of mercury ions, concentrations of  $\text{Hg}^{2+}$  varying from 0 to 2  $\mu\text{M}$  were added to a solution of DNA-Ag NCs (100  $\mu\text{L}$ ) to obtain the limit of detection and metal ion response range of

the DNA-Ag NC probes. After 5 min incubation, the changes in fluorescence behavior of the  $\text{Hg}^{2+}$ -treated solutions were observed using a UV lamp and a luminescence spectrometer. The corresponding UV-Vis absorption spectra were also recorded. The same procedure was repeated for the detection of  $\text{Cu}^{2+}$ .

## Analysis of real water samples

To analyze the activity of the DNA-Ag NCs, we used the system to detect metal ions in real water samples from different sources. Spring and laboratory tap water samples were collected for analysis. For the detection procedure, we prepared the samples by spiking them with standard solutions of  $\text{Hg}^{2+}$  and  $\text{Cu}^{2+}$  (the final concentration of each ion was 1  $\mu\text{M}$ ). The protocol for detection was similar to that described above. In order to confirm the practicality of the DNA-Ag NC system, the concentrations of  $\text{Hg}^{2+}$  and  $\text{Cu}^{2+}$  in the real water samples were detected by ICP-MS.

# Results and discussion

## Synthesis and characterization

The unique optical properties of fluorescent nanoclusters have attracted attention for use in bioassays and biological imaging.<sup>1,3</sup> Here we develop a highly sensitive and selective fluorescence sensor for detecting the metal ions  $\text{Cu}^{2+}$  and  $\text{Hg}^{2+}$  based on the fluorescence quenching of DNA-Ag NCs. An oligonucleotide (a polymer consisting of 31 nucleotides) was employed as a stabilizer, and  $\text{NaBH}_4$  was used as a reducing agent in a one-step synthesis of DNA-Ag NCs.

As shown in Fig. 1a (inset), the light brown solution of DNA-Ag NCs emitted an intense red fluorescence under UV light (365 nm), and fluorescence spectrophotometer analysis showed that the emission spectrum of DNA-Ag NCs had a single broad transition maximizing at 615 nm with a large Stokes shift ( $>80 \text{ nm}$ ) while excited at 535 nm. The quantum yield (QY)

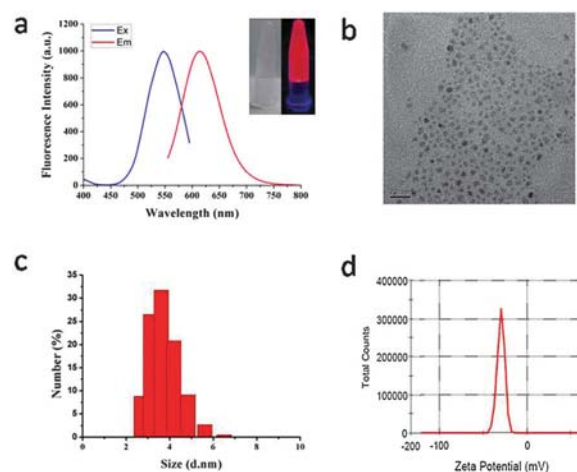


**Fig. 1** Characterization of the properties of DNA-Ag NCs. (a) Fluorescence spectrum of DNA-Ag NCs. Inset: pictures of the Ag NCs solution under normal room lighting (left) and UV irradiation (right). (b) Typical TEM image of DNA-Ag NCs. (c) The hydrodynamic diameter of DNA-Ag NCs. (d) Zeta potential distribution of the DNA-Ag NCs.

of DNA-Ag NCs was measured to be  $\sim 30\%$ , using Rhodamine B (QY = 0.95 in ethanol) as the reference. In the past, various approaches have been taken to synthesize water-soluble fluorescent metal NCs, but the QY was extremely low, in the range of  $10^{-10}$  to  $10^{-2}$ .<sup>24,25</sup> These low yields were insufficient for biomedical applications.

TEM images of DNA-Ag NCs indicate that the fluorescent nanoparticles are well dispersed and the average diameter is 3.1 nm (Fig. 1b). Energy-dispersive-X-ray spectroscopy (EDX) experiments confirmed the presence of elemental Ag in DNA-Ag NC samples (Fig. S1, ESI<sup>†</sup>). To confirm these results, dynamic light scattering (DLS) was used to show that the hydrodynamic diameter and zeta-potential of these particles are 6.5 nm and  $-29$  mV, respectively (Fig. 1c and d). The negative potential of DNA-Ag NCs implies that they possess good colloidal stability under physiological conditions.

Fluorescence lifetime measurements shed light on the underlying mechanism of fluorescence enhancement of DNA-Ag NCs. To confirm the fluorescent properties of DNA-Ag NCs, their fluorescence decay was measured. As shown in Fig. 2a, the DNA-Ag NCs possess a characteristic multi-exponential fluorescence decay that fitted well with two exponential functions, with lifetimes (fractional weights) of 5.42 ns (84.14%) and 2.6 ns (15.86%). In order to verify this result, a known fluorescein isothiocyanate (FITC) was chosen as a control for fluorescence decay measurements. The results showed that the fluorescence lifetime of FITC was 3.7 ns. In order to further confirm the mechanism of DNA-Ag NC fluorescence, X-ray photoelectron spectroscopy (XPS) measurements were carried out. As shown in Fig. 2c, the XPS spectra indicated that the DNA acted as a ligand on the surface of Ag NCs. The valence states of silver in the DNA-Ag NCs were also analyzed. The Ag 3d XPS spectrum showed that the binding energies (BE) of Ag 3d<sub>5/2</sub> and Ag 3d<sub>3/2</sub> were 367.98 eV and 373.98 eV, respectively (Fig. 2d). The BEs of Ag 3d<sub>5/2</sub> and Ag 3d<sub>3/2</sub> were close to that of Ag(0), which confirmed the formation of DNA-Ag NCs. The high luminescence of the as-synthesized DNA-Ag NCs is particularly favorable for use in biosensors.

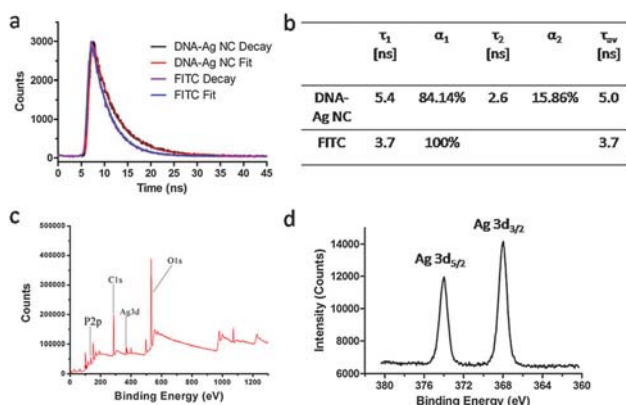


Fig. 2 (a) The fluorescence decay curves of DNA-Ag NCs and multi-exponential fits. (b) Fluorescence lifetime parameters of DNA-Ag NCs and FITC. (c) XPS spectrum of DNA-Ag NCs and (d) the expanded spectrum of Ag<sub>3d</sub>.

## Mechanism of detection of Hg<sup>2+</sup> and Cu<sup>2+</sup>

To evaluate the interaction of DNA-Ag NCs with Hg<sup>2+</sup>, DNA-Ag NCs were mixed with different concentrations of Hg<sup>2+</sup> ions. Fig. 3a displays the fluorescence emission spectra of DNA-Ag NCs as an indicator of Hg<sup>2+</sup> concentration from 0 to 1  $\mu$ M. The fluorescence intensity of the DNA-Ag NCs gradually decreased as the Hg<sup>2+</sup> concentration increased, and the emission was quenched to less than 5% in the presence of 1  $\mu$ M Hg<sup>2+</sup>. These results indicated that the fluorescence quenching effect can be developed as a DNA-Ag NC-based sensing system for detection of Hg<sup>2+</sup>. There is a good linear relationship between fluorescence quenching and the logarithm of the Hg<sup>2+</sup> concentration at low Hg<sup>2+</sup> concentrations (Fig. 3b). When the sensitivity of the DNA-Ag NC sensing system was examined, it was found that the limit of detection (LOD) of Hg<sup>2+</sup> was 5 nM. This sensitivity meets with the Hg<sup>2+</sup> detection requirement for drinking water by the U.S. Environmental Protection Agency (EPA, 10 nM) and the European Union (5 nM).

We next evaluated whether the DNA-Ag NCs can selectively detect different metal ions. We tested abundant cellular cations (Na<sup>+</sup>, K<sup>+</sup>, Mg<sup>2+</sup>, Ca<sup>2+</sup> and Al<sup>3+</sup>), essential cellular transition metal ions (Fe<sup>2+</sup>, Fe<sup>3+</sup>, Cu<sup>2+</sup>, Mn<sup>2+</sup>, Co<sup>2+</sup>, and Ni<sup>2+</sup>) and environmentally relevant heavy metal ions (Hg<sup>2+</sup>, Pb<sup>2+</sup> and Cd<sup>2+</sup>) at a concentration of 1  $\mu$ M (Fig. 3d). Only Hg<sup>2+</sup> and Cu<sup>2+</sup> caused pronounced and immediate fluorescence quenching, and Hg<sup>2+</sup> caused stronger quenching than Cu<sup>2+</sup>. Because Cu<sup>2+</sup> could interfere with the detection of Hg<sup>2+</sup> if Hg<sup>2+</sup> and Cu<sup>2+</sup> exist in the same analyte, we also studied the fluorescence responses of the DNA-Ag NCs to different concentrations of Cu<sup>2+</sup>. As shown in Fig. 4, the DNA-Ag NC sensing system showed a relationship between fluorescence intensity and Cu<sup>2+</sup> concentration. The LOD of Cu<sup>2+</sup> was estimated

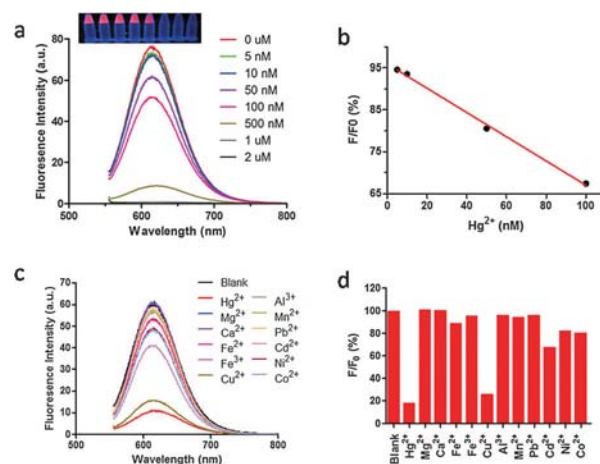


Fig. 3 (a) Fluorescence emission spectrum of DNA-Ag NCs in the presence of Hg<sup>2+</sup> concentrations increasing from 0 to 2  $\mu$ M (top to bottom, excitation at 535 nm). The inset shows an image of the Hg<sup>2+</sup>-treated DNA-Ag NCs under UV irradiation (0  $\mu$ M Hg<sup>2+</sup>, left, to 2  $\mu$ M, right). (b) Relative fluorescence intensity of DNA-Ag NCs ( $F/F_0$ , where  $F$  and  $F_0$  are the fluorescence intensities at 615 nm in the presence and absence of Hg<sup>2+</sup>, respectively) versus the logarithm of the Hg<sup>2+</sup> concentration up to 100 nM. (c) Fluorescence response of DNA-Ag NCs in the presence of different metal ions (all at 1  $\mu$ M). (d) Histogram analysis of (c).

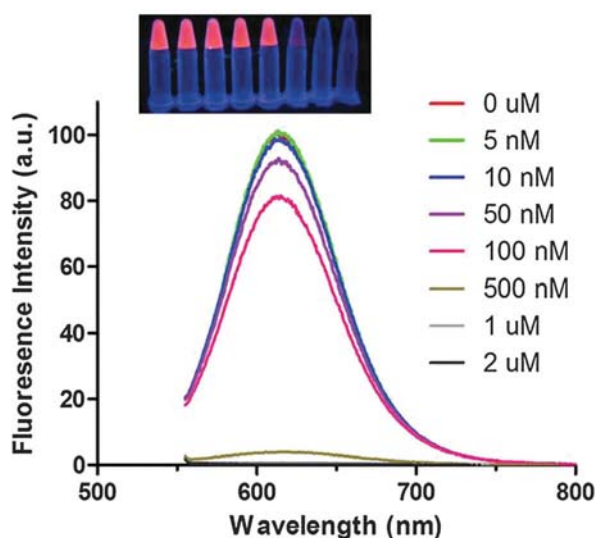


Fig. 4 Sensitivity and fluorescence response of DNA-Ag NCs toward  $\text{Cu}^{2+}$  ions. Emission spectra of DNA-Ag NCs in the presence of different concentrations of  $\text{Cu}^{2+}$  increasing from 0 to 2  $\mu\text{M}$  (top to bottom, excitation at 535 nm). The inset shows an image of the  $\text{Cu}^{2+}$ -treated DNA-Ag NCs under UV irradiation (0  $\mu\text{M}$   $\text{Cu}^{2+}$ , left, to 2  $\mu\text{M}$ , right).

to be 10 nM which met the detection requirement of the U.S. EPA (20  $\mu\text{M}$ ).<sup>26</sup> These results imply that simultaneous detection of  $\text{Hg}^{2+}$  and  $\text{Cu}^{2+}$  can easily be achieved by monitoring the fluorescence change of the DNA-Ag NCs using a UV lamp.

In order to investigate the underlying mechanism by which  $\text{Hg}^{2+}$  and  $\text{Cu}^{2+}$  quenched the fluorescence of DNA-Ag NCs, fluorescence lifetime measurements were carried out. In the presence of  $\text{Hg}^{2+}$  and  $\text{Cu}^{2+}$ , there was no distinct change in the fluorescence decay of the DNA-Ag NCs and the average fluorescence lifetime was 5.4 ns for  $\text{Hg}^{2+}$  and 5.2 ns for  $\text{Cu}^{2+}$  (Fig. S2, ESI†). XPS measurements demonstrated that  $\text{Hg}^{2+}$  and  $\text{Cu}^{2+}$  had no effect on the valence states of silver in the DNA-Ag NCs (Fig. 5b). Previous studies suggested that the fluorescence of DNA-Ag NCs could also be quenched through  $\text{Hg}^{2+}$ -mediated interparticle aggregation.<sup>27</sup> In our study, we used TEM imaging to show that the DNA-Ag NCs formed aggregates in the presence of  $\text{Hg}^{2+}$  but not  $\text{Cu}^{2+}$  (Fig. 5a).  $\text{Hg}^{2+}$  binds to thymine (T) residues in single-stranded DNA, and the interaction of  $\text{Hg}^{2+}$

with the oligonucleotides on the surface of the nanoparticles probably causes the aggregation of the DNA-Ag NCs.<sup>28–31</sup> However, our results rule out the possibility that  $\text{Hg}^{2+}$ -induced aggregation of DNA-Ag NCs is responsible for the fluorescence quenching.

We speculate that  $\text{Cu}^{2+}$  could quench the fluorescence of DNA-Ag NCs due to the specific and strong metallophilic interaction between Cu and Ag atoms in our DNA-Ag NCs. Next, we investigated the effect of the chelating agent ethylene diamine tetracetic acid (EDTA) on the ability of DNA-Ag NC to sense  $\text{Hg}^{2+}$  and  $\text{Cu}^{2+}$ . As shown in Fig. S3 (ESI†), adding EDTA to the sensor system “turned on” the fluorescence of the DNA-Ag NC- $\text{Hg}^{2+}$  and DNA-Ag NC- $\text{Cu}^{2+}$  complexes, and the fluorescence intensity of  $\text{Hg}^{2+}$  and  $\text{Cu}^{2+}$  increased to 80% and 62%, respectively, in the presence of 10  $\mu\text{M}$  EDTA (data not shown). This indicates that EDTA forms stronger complexes with  $\text{Hg}^{2+}$  than with  $\text{Cu}^{2+}$ . These results suggested that the DNA-Ag NC sensor system can be renewed by using EDTA.

In order to evaluate the potential application of DNA-Ag NCs in detecting ions in real water samples, we tested the sensitivity and specificity of the fluorescence response of  $\text{Hg}^{2+}$  and  $\text{Cu}^{2+}$  in tap water and spring water. As shown in Fig. S4 (ESI†), the real water samples did not induce fluorescence quenching of the DNA-Ag NC solution. Thus, the concentrations of  $\text{Hg}^{2+}$  and  $\text{Cu}^{2+}$  in tap water and spring water were lower than the detection limit of the DNA-Ag NCs. ICP-MS analysis was used to determine the  $\text{Hg}^{2+}$  and  $\text{Cu}^{2+}$  concentrations in the real water samples, and the data confirmed the results obtained for the DNA-Ag NC system. However, the fluorescence of DNA-Ag NCs was immediately quenched when  $\text{Hg}^{2+}$  and  $\text{Cu}^{2+}$  were added to the real water. Taken together, our data suggest that the label-free DNA-Ag NC assay system is a potential tool for  $\text{Hg}^{2+}$  and  $\text{Cu}^{2+}$  sensing in environmental samples.

## Conclusions

In summary, DNA-Ag NCs were synthesized through reduction by  $\text{NaBH}_4$  at room temperature, which markedly increased the QY of fluorescence emission. These DNA-Ag NCs are of uniform ultrasmall size and possess good photophysical properties. In the present work, we developed a simple, rapid (<5 min) and low-cost sensing system for  $\text{Hg}^{2+}$  and  $\text{Cu}^{2+}$  detection using DNA-Ag NCs. This system has unprecedented sensitivity with a limit of detection (LOD) of 5 nM and 10 nM for  $\text{Hg}^{2+}$  and  $\text{Cu}^{2+}$ , respectively. The fluorescence response of DNA-Ag NCs is remarkably specific for  $\text{Hg}^{2+}$  and  $\text{Cu}^{2+}$  in the presence of other metal ions, and thus meets the requirements of environmental and industrial monitoring applications. This novel sensing system is simple and can be easily carried out by simple mixing and incubation of the sample at room temperature. It has also been successfully applied to practical detection of  $\text{Hg}^{2+}$  and  $\text{Cu}^{2+}$  in real water samples. Because of its simplicity, rapidity and sensitivity, the DNA-Ag NC sensing system demonstrated here shows potential for monitoring water quality in developing regions.

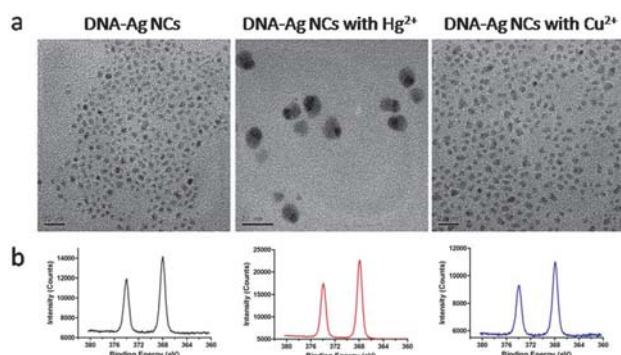


Fig. 5 TEM imaging (a) and XPS spectrum analysis (b) of DNA-Ag NCs in the absence and presence of  $\text{Hg}^{2+}$  (1  $\mu\text{M}$ ) or  $\text{Cu}^{2+}$  (1  $\mu\text{M}$ ).



## Acknowledgements

This work was supported by the Chinese Natural Science Foundation project (No. 81171455), a National Distinguished Young Scholars grant (31225009) from the National Natural Science Foundation of China, the National Key Basic Research Program of China (2009CB930200), the Chinese Academy of Sciences (CAS) "Hundred Talents Program" (07165111ZX), the CAS Knowledge Innovation Program and the State High-Tech Development Plan (2012AA020804). This work was also supported in part by NIH/NIMHD 8 G12 MD007597, and USAMRMC W81XWH-10-1-0767 grants.

## Notes and references

- H. Qian, M. Zhu, Z. Wu and R. Jin, *Acc. Chem. Res.*, 2012, **45**, 1470.
- J. Li, X. Zhong, F. Cheng, J.-R. Zhang, L.-P. Jiang and J.-J. Zhu, *Anal. Chem.*, 2012, **84**, 4140.
- X. Wu, X. He, K. Wang, C. Xie, B. Zhou and Z. Qing, *Nanoscale*, 2010, **2**, 2244.
- M. Zhu, E. Lanni, N. Garg, M. E. Bier and R. Jin, *J. Am. Chem. Soc.*, 2008, **130**, 1138.
- R. Jin, *Nanoscale*, 2010, **2**, 343.
- L. Maretti, P. S. Billone, Y. Liu and J. C. Scaiano, *J. Am. Chem. Soc.*, 2009, **131**, 13972.
- J. Xie, Y. Zheng and J. Y. Ying, *J. Am. Chem. Soc.*, 2009, **131**, 888.
- C. I. Richards, S. Choi, J.-C. Hsiang, Y. Antoku, T. Vosch, A. Bongiorno, Y.-L. Tzeng and R. M. Dickson, *J. Am. Chem. Soc.*, 2008, **130**, 5038.
- X. Le Guével, C. Spies, N. Daum, G. Jung and M. Schneider, *Nano Res.*, 2012, **5**, 379.
- J. Sharma, R. C. Rocha, M. L. Phipps, H. C. Yeh, K. A. Balatsky, D. M. Vu, A. P. Shreve, J. H. Werner and J. S. Martinez, *Nanoscale*, 2012, **4**, 4107.
- L. Shang, S. Dong and G. U. Nienhaus, *Nano Today*, 2011, **6**, 401.
- M. Zhu, E. Lanni, N. Garg, M. E. Bier and R. Jin, *J. Am. Chem. Soc.*, 2008, **130**, 1138.
- Bioinorganic Chemistry*, ed. A. X. Trautwein, Wiley-VCH, Weinheim, 1997.
- G. Aragay, J. Pons and A. Merkoci, *Chem. Rev.*, 2011, **111**, 3433.
- T. W. Clarkson and L. Magos, *CRC Crit. Rev. Toxicol.*, 2006, **36**, 609.
- M. Knecht and M. Sethi, *Anal. Bioanal. Chem.*, 2009, **394**, 33.
- T. W. Clarkson, L. Magos and G. J. N. Myers, *N. Engl. J. Med.*, 2003, **349**, 1731.
- E. L. Que, D. W. Domaille and C. J. Chang, *Chem. Rev.*, 2008, **108**, 1517–1549; M. Liu, H. Zhao, S. Chen, H. Yu, Y. Zhang and X. Quan, *Chem. Commun.*, 2011, **47**, 7749.
- Y.-W. Lin, C.-C. Huang and H.-T. Chang, *Analyst*, 2011, **136**, 863.
- Y. Guo, Z. Wang, H. Shao and X. Jiang, *Analyst*, 2012, **137**, 301.
- H. Wang, Y. Wang, J. Jin and R. Yang, *Anal. Chem.*, 2008, **80**, 9021.
- J. Wang and B. Liu, *Chem. Commun.*, 2008, 4759; M. Pramanik and A. Bhaumik, *Chem.-Eur. J.*, 2013, **19**, 8507.
- E. G. Gwinn, P. O'Neill, A. J. Guerrero, D. Bouwmeester and D. K. Fygenson, *Adv. Mater.*, 2008, **20**, 279.
- S. Link, A. Beeby, S. FitzGerald, M. A. El-Sayed, T. G. Schaaff and R. L. Whetten, *J. Phys. Chem. B*, 2002, **106**, 3410.
- T. Huang and R. W. Murray, *J. Phys. Chem. B*, 2001, **105**, 12498.
- B. Adhikari and A. Banerjee, *Chem. Mater.*, 2010, **22**, 4364.
- C. C. Huang, Z. Yang, K. H. Lee and H. T. Chang, *Angew. Chem.*, 2007, **119**, 6948.
- C.-K. Chiang, C.-C. Huang, C.-W. Liu and H.-T. Chang, *Anal. Chem.*, 2008, **80**, 3716.
- J. Du, M. Liu, X. Lou, T. Zhao, Z. Wang, Y. Xue, J. Zhao and Y. Xu, *Anal. Chem.*, 2012, **84**, 8060.
- H. Xu, X. Zhu, H. Ye, L. Yu, X. Liu and G. Chen, *Chem. Commun.*, 2011, **47**, 12158.
- Z. Zhu, L. Xu, X. Zhou, J. Qin and C. Yang, *Chem. Commun.*, 2011, **47**, 8010.

## Supporting Information

### Highly Sensitive Simultaneous Detection of Mercury and Copper Ions by Ultrasmall Fluorescent DNA-Ag Nanoclusters

Shengliang Li,<sup>a,b,\*</sup> Weipeng Cao,<sup>a,\*</sup> Anil Kumar,<sup>a</sup> Shubin Jin,<sup>a</sup> Yuanyuan Zhao,<sup>a</sup> Chunqiu Zhang,<sup>a</sup> Guozhang Zou,<sup>a</sup> Paul C. Wang,<sup>c</sup> Feng Li,<sup>b,#</sup> Xing-Jie Liang<sup>a,#</sup>

*a* Laboratory of Nanomedicine and Nanosafety, Division of Nanomedicine and Nanobiology, National Center for Nanoscience and Technology of China, and CAS Key Laboratory for Biomedical Effects of Nanomaterials and Nanosafety, Chinese Academy of Sciences, Beijing, 100190, China.

*b* Department of Neurobiology and Anatomy, Zhongshan School of Medicine, Sun Yat-sen University, Guangzhou, China

*c* Laboratory of Molecular Imaging, Department of Radiology, Howard University, Washington DC 20060, USA

*\* These authors contributed equally to this work*

*# To whom correspondence should be addressed:*

Corresponding author. (Xing-Jie Liang)

Co-corresponding authors. (Feng Li)

E-mail addresses: liangxj@nanoctr.cn (Xing-Jie Liang), lifeng@mail.sysu.edu.cn (Feng Li).

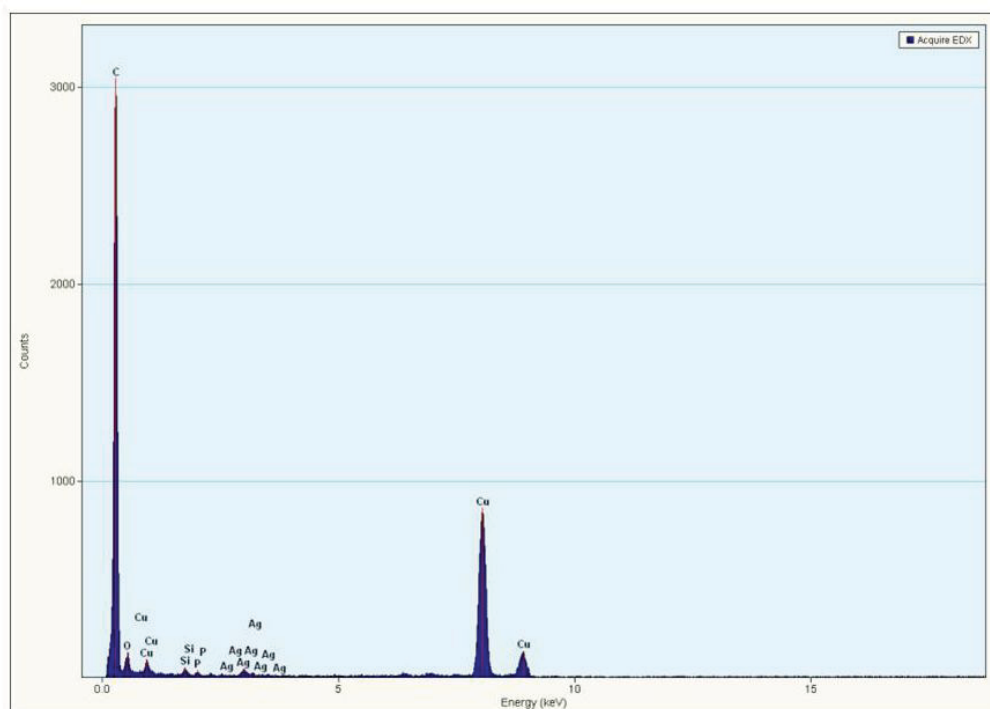
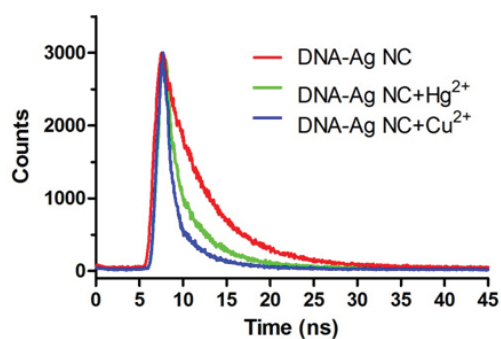


**Fig. S1** Energy-dispersive-X-ray spectroscopy (EDX) experiments confirm the presence of elemental Ag in DNA-Ag NC samples



	$\tau_1$ [ns]	$\alpha_1$	$\tau_2$ [ns]	$\alpha_2$	$\tau_{av}$ [ns]
DNA-Ag NC	5.4	84.14%	2.6	15.86%	5.0
DNA-Ag NC+Hg <sup>2+</sup>	4.2	64.87%	7.4	35.13%	5.4
DNA-Ag NC+Cu <sup>2+</sup>	3.9	43.85%	6.2	56.15%	5.2

**Fig. S2** Fluorescence decay curves of DNA-Ag NCs in the absence (red) and presence of Hg<sup>2+</sup> (1  $\mu$ M, green) and Cu<sup>2+</sup> (1  $\mu$ M, blue), and the corresponding fit curves.

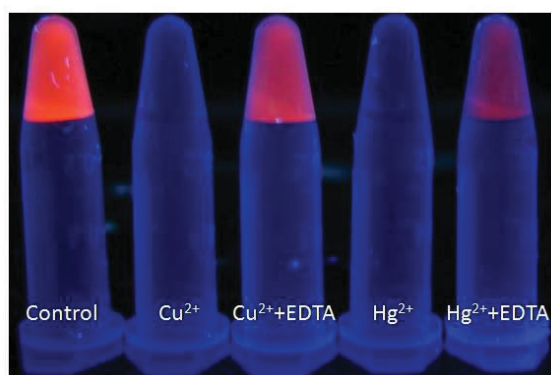


**Fig. S3** The DNA-Ag NC sensor system can be renewed using EDTA.

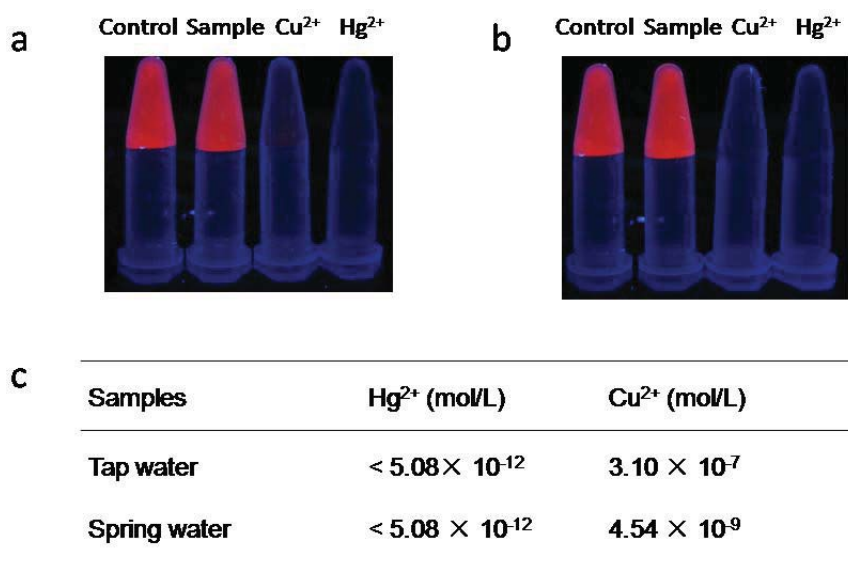


**Fig. S4** Determination of  $\text{Hg}^{2+}$  and  $\text{Cu}^{2+}$  in tap water (a) and spring water (b) samples with DNA-Ag NCs. (c) Determination of  $\text{Hg}^{2+}$  and  $\text{Cu}^{2+}$  concentrations in real water samples by ICP-MS analysis.

# Biosafe Nanoscale Pharmaceutical Adjuvant Materials

Shubin Jin<sup>1,†</sup>, Shengliang Li<sup>1,2,†</sup>, Chongxi Wang<sup>1</sup>, Juan Liu<sup>1</sup>, Xiaolong Yang<sup>1</sup>,  
Paul C. Wang<sup>3,\*</sup>, Xin Zhang<sup>4</sup>, and Xing-Jie Liang<sup>1,\*</sup>

<sup>1</sup> CAS Key Laboratory for Biological Effects of Nanomaterials and Nanosafety, National Center for Nanoscience and Technology, Beijing 100190, P. R. China

<sup>2</sup> Department of Neurobiology and Anatomy, Zhongshan School of Medicine, Sun Yat-Sen University, Guangzhou 510275, P. R. China

<sup>3</sup> Laboratory of Molecular Imaging, Department of Radiology, Howard University, Washington DC 20060, USA

<sup>4</sup> National Key Laboratory of Biochemical Engineering, Institute of Process Engineering, Chinese Academy of Sciences, Beijing 100190, P. R. China

Thanks to developments in the field of nanotechnology over the past decades, more and more biosafe nanoscale materials have become available for use as pharmaceutical adjuvants in medical research. Nanomaterials possess unique properties which could be employed to develop drug carriers with longer circulation time, higher loading capacity, better stability in physiological conditions, controlled drug release, and targeted drug delivery. In this review article, we will review recent progress in the application of representative organic, inorganic and hybrid biosafe nanoscale materials in pharmaceutical research, especially focusing on nanomaterial-based novel drug delivery systems. In addition, we briefly discuss the advantages and notable functions that make these nanomaterials suitable for the design of new medicines; the biosafety of each material discussed in this article is also highlighted to provide a comprehensive understanding of their adjuvant attributes.

**KEYWORDS:** Drug Delivery, Adjuvant Nanomaterials, Biosafe, Multifunction, Nanoparticle, Controlled Release.

## CONTENTS

Introduction . . . . .	1
Organic Nanoscale Materials Employed for Pharmaceutical Development . . . . .	6
Polymers . . . . .	6
Lipids . . . . .	11
Proteins, Peptides and Nucleic Acids . . . . .	13
Other Organic Materials . . . . .	16
Inorganic Nanoscale Materials as Potential Adjuvants in Pharmaceutics . . . . .	16
Silica . . . . .	16
Gold . . . . .	17
Other Inorganic Materials . . . . .	19
Hybrid Organic and Inorganic Nanomaterials for Pharmaceutical Application . . . . .	19
Conclusions . . . . .	20
Acknowledgments . . . . .	20
References . . . . .	20

## INTRODUCTION

Nanoscale materials, as a new class of pharmaceutical adjuvants, have provided many strategies for designing and fabricating novel medicines with a variety of advantages over conventional medicines.<sup>1–4</sup> In the past decades, numerous adjuvant materials were developed for drug delivery but few of them went further to clinical use. There are several reasons for this uncomfortable fact and we summarize these challenges in designing biosafe and efficient drug delivery systems as: (1) Inherent toxicity of adjuvant materials; (2) Drug leakage takes place before reaching the lesion; (3) The unfavorable pharmacokinetics, such as rapid elimination and poor stability in blood environment; (4) The non-targeted drug delivery *in vivo*. Therefore, the desired characteristics of pharmaceutical adjuvants are as shown in Figure 1. First, the adjuvant materials should be non-toxic as they are selected with an aim toward human health care. Meanwhile, stimulus-responsive materials that can provide controllable drug release are preferred. Drugs could be protected by the adjuvants through encapsulation, integration, or conjugation before they reach the disease

\*Authors to whom correspondence should be addressed.

Emails: [liangxj@nanoctr.cn](mailto:liangxj@nanoctr.cn), [pwang@howard.edu](mailto:pwang@howard.edu)

<sup>†</sup>These two authors are contributed equally to this work.

Received: 14 January 2014

Accepted: 30 January 2014



**Shubin Jin** is a graduate student and he is now pursuing his Ph.D. in Nanoscience and Technology at National Center for Nanoscience and Technology, China (NCNST). He received his B.E. of Biotechnology at Beijing University of Technology in 2011. Currently he is working on design and fabrication of visible drug delivery and release nanosystem.



**Shengliang Li** received his B.E. of Pharmacy at Henan University in 2009. Currently he is pursuing his medical doctor's degree in Zhongshan School of Medicine at Sun Yat-Sen University, China. And he is a joint training M.D. candidate under the guidance of Professor Xing-Jie Liang at National Center for Nanoscience and Technology, China (NCNST). His research interests focuses on functionalization and engineering of nanomaterials for nanomedicine.



**Chongxi Wang** received his B.S. of Chemical Engineering and Technology at Tianjin University in 2011. Currently he is pursuing his master's degree in Chemical Engineering at Tianjin University. And he is a joint student under the guidance of Professor Xing-Jie Liang at National Center for Nanoscience and Technology, China (NCNST). His main research interest focuses on polycations-based gene delivery system.



**Juan Liu** received her B.S. of Biopharmaceutics at Huazhong University of Science and Technology in 2011. Currently she is pursuing her Ph.D. in Physical Chemistry under the guidance of Professor Xing-Jie Liang at National Center for Nanoscience and Technology, China (NCNST). Her main research interest focuses on nanomaterial-based drug delivery systems.



**Xiaolong Yang** received his B.E. of Biotechnology at Tianjin University of Science and Technology in 2012. Currently he is pursuing his master's degree in Pharmacology at Tianjin University of Science and Technology. He is now a joint student working on nanomaterials-induced stem cell differentiation at National Center for Nanoscience and Technology, China (NCNST).





**Paul Wang** is the Director of the Molecular Imaging Laboratory and a Professor in the Department of Radiology, Howard University. Dr. Wang graduated from Fu Jen University in 1974 with a B.S. in physics. He received a Ph.D. in applied radiation physics from MIT's Nuclear Engineering Department in 1982. Dr. Wang established the Molecular Imaging Laboratory as a core facility at Howard University to promote multidisciplinary research using imaging techniques for biomedical applications. His research interests include MRI and NMR spectroscopy studies of cancer, cardiovascular and neurodegenerative diseases, multidrug interactions, and development of nanoparticles as drug delivery vehicles for targeted chemotherapy and diagnostic imaging. Dr. Wang has been a Visiting Professor at the Chinese National Center for Nanoscience and Technology since 2007. He received Howard University College of Medicine's Outstanding Faculty Researcher Award in 2008, and the Dr. M. Wharton Young Research Award in 2010.



**Xin Zhang** is Professor of Institute of Process Engineering (IPE), Chinese Academy of Sciences (CAS). She received her Ph.D. degree from University of Strasbourg. At the same year, she worked as an assistant professor at The French National Institute of Health and Medical Research. Her primary research focus is on the gene therapy, including design, synthesis and application of gene delivery vectors. The works has been published in peer-reviewed scientific journal, such as *Journal of Materials Chemistry*, *Biomaterials* and *Nano Letters*, which has been cited overall more than 400 times.



**Xing-Jie Liang** got Ph.D. at National Key Laboratory of Biomacromolecules, Institute of Biophysics at CAS. He finished his postdoc at Center for Cancer Research, NCI, NIH, and worked as a Research Fellow at Surgical Neurology Branch, NINDS. Dr. Liang worked on Molecular imaging at School of Medicine, Howard University before he became deputy director of CAS Key Laboratory for Biomedical Effects of Nanomaterials and Nanosafety, National Center for Nanoscience and Technology of China. Dr. Liang is current editorial board member of *Advances in Nano Research*, *Theranostics*, *Journal of Nanomaterials*, *Biomaterials Research*, and *Current Nanoscience*, associated editor of *Biophysics Report* and guest editor of *Biotechnology Advances*. Dr. Liang was honored with 2004, 2005, 2006 Fellows Award for Research Excellence in NIH; Special Government Allowances by Department of State, 2011;

National Distinguished Young Scholars by NSFC; and Young Pharmaceutics Scholar by CPA, 2012. Developing drug delivery strategies for prevention/treatment of AIDS and cancers are current program ongoing in Dr. Liang's lab based on understanding of basic physical-chemical and biological processes of nanomedicine.

site. After administration, adjuvants and drugs should be stable in physiological environment, avoiding from aggregation and reticuloendothelial system (RES) clearance. Surface coating and modification of drug-loaded nanoparticles, such as PEGylation, can improve their stability, resulting in a longer circulation time.<sup>5,6</sup> Finally, targeted drug delivery, both active targeting by targeting ligands and passive targeting by taking advantage of the enhanced permeability and retention (EPR) effect (an effect that nano-sized particles and macromolecule drugs tend to accumulate in tumor site rather than in normal tissue due to hypervascularity and little recovery of tumor blood/lymphatic vessels), are desired in pharmaceutical research.<sup>7,8</sup> Although nanomaterial's biosafety

remains controversial and bioeffect mechanism needs further study, their unique attributes, such as controllable size and shape,<sup>9-11</sup> alternative surface modification,<sup>12-14</sup> high surface area to volume ratio and environmentally-responsive structural deformation,<sup>15-17</sup> still attract great interest from researchers and have enabled them to design new medicines with more functions, including controlled release of drugs in specific physiological environments, targeted delivery of drugs to lesions, longer circulation time, and better loading efficiency of insoluble drugs.<sup>18-21</sup>

Higher accumulation of small anticancer drug molecules in the tumor site can be achieved by encapsulating the drug into nanocarriers, because nanoparticles show preferred retention in tumor as a result of EPR effect.<sup>22,23</sup> Targeted

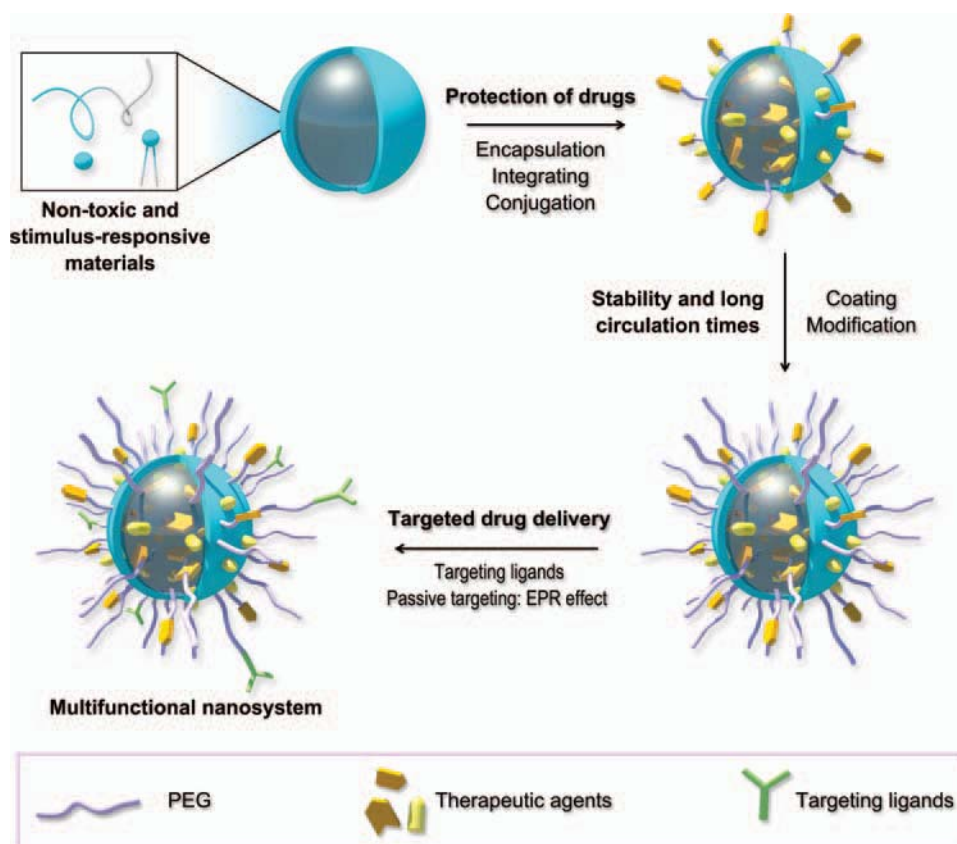


**Figure 1.** The desired characteristics of a multifunctional nanosystem composed of nanoscale pharmaceutical adjuvant materials. (A) The materials should be non-toxic to satisfy biosafety criteria and responsive to stimuli for triggered release of drugs. (B) Drugs should be carefully protected before they reach the disease site. (C) The drug vehicle should be stable in the physiological environment and resistant to clearance. (D) By conjugating with targeting ligands, active targeting can be achieved. Meanwhile, passive targeting can be realized by controlling the size of the multifunctional nanosystem.

drug delivery can be achieved by modifying the surface shell of drug-loaded nanocarriers with ligands which specifically bind to disease markers. Figure 2 illustrates the EPR effect and targeted delivery of nanoparticles, in this

case anticancer drug doxorubicin (DOX)-encapsulated micelles, *in vitro* and *in vivo*.<sup>24</sup> The non-functionalized micelles (M-Dox) showed accumulation in tumor tissue as a result of EPR effect. This nanoparticle was then

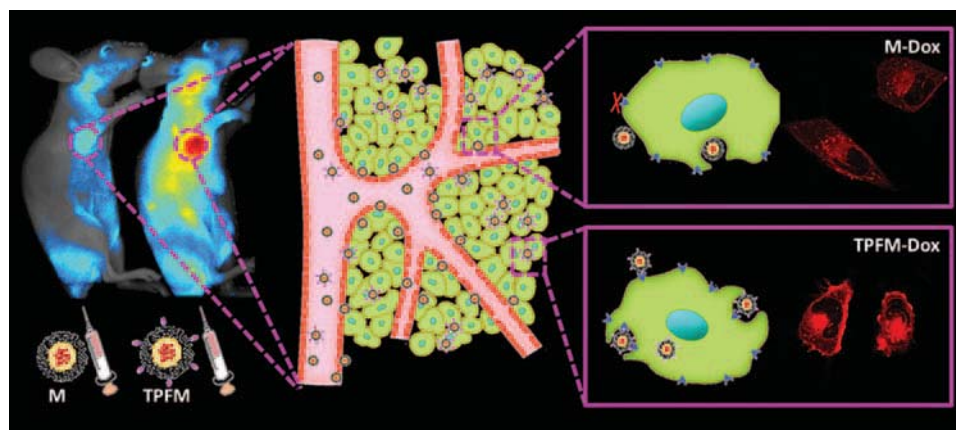


**Figure 2.** Passive and active targeting of nanoparticles. M-Dox: non-functionalized Dox-encapsulated micelle; TPFM-Dox: tumor-penetrating peptide functionalized Dox-encapsulated micelle. The shade of color in the images stands for the amount of nanoparticles in tumors and in cells. Reprinted with permission from [24], T. Wei, et al., Functionalized nanoscale micelles improve drug delivery for cancer therapy *in vitro* and *in vivo*. *Nano Lett.* 13, 2528 (2013). © 2013, American Chemical Society.

functionalized with tumor-penetrating peptide CRGDK, the receptor of which are known as neuropilin-1 (NRP-1) protein and are expressed by tumor vessel and by various human carcinoma cells.<sup>25–28</sup> The tumor-penetrating peptide functionalized micelles (TPFM-Dox) are internalized more efficiently and exhibit better accumulation and penetration in tumor. By grafting small drug molecules into nanocarriers (nanoparticles, nanorods, nanocages etc.), it is possible to realize a higher loading capacity, and also to deliver insoluble drugs.<sup>29,30</sup> Moreover, nanomaterials can be designed to release payloads triggered by environmental changes. In cancer treatment, the slightly altered acidic tumor microenvironment can be used to trigger drug release.<sup>31,32</sup> These strategies can help to optimize the biodistribution of anticancer drugs, so that more drug accumulates in the tumor while less is located in the normal organs and the anticancer efficacy is improved with less unwanted side effects. If all these features can be combined in one nanoparticle system, a delivery system could be generated which acts as a multifunctional drug delivery system.

Traditional medical research has focused on finding and screening new chemical entities (NCEs), with the aim of curing the disease with one new drug. However, this method is expensive, time consuming, and full of unknown risks; in addition, the efficiency is very low. It usually takes more than 10 years, and thousands of candidates were tested. It is possible that only one chemical entity will gain access to the market. Some of the eliminated compounds may have had better efficacy than the final winner, but severe side effect or poor biodistribution prevented them from completing the screening process. Even the winner may have fatal drawbacks, like Paclitaxel (PTX). Due to its poor solubility in water, it was first sold in a formulation employing Cremophor EL and ethanol as solvents, which caused serious side effects in patients.<sup>33</sup> It was later discovered that PTX and albumin could form nanoparticles in solution, and the efficacy was greatly improved without significant side-effects.<sup>34,35</sup> Thus, nanomaterial-based formulation can be used to increase the efficacy of chemotherapeutic agents and reduce the side-effects.

Biosafety is a major issue in the design of novel drugs and researchers must give careful consideration to this when developing nanoscale materials for medical research. The physicochemical properties of nanoparticles, such as size, shape, charge, colloidal stability, and their interaction with environmental compounds, are related to their potential toxicity.<sup>36–39</sup> When nanotechnology was first emerging in the 1980s, the biosafety of nanomaterials, including genotoxic and cytotoxic effects, toxicity to the immune system, *in vivo* biodistribution and clearance, and the long-term effects of treatment, was unclear and more studies were needed to prove that nanomaterials are biocompatible and biosafe.<sup>40,41</sup> Biodegradable and biogenic nanoscale materials, such as proteins, nucleic acids, and phospholipids, are commonly used as pharmaceutical

adjuvants. The two Food and Drug Administration (FDA) approved nanomaterial-based drug formulations, Doxil® and Abraxane®, employed organic nanomaterials (lipid in Doxil® and protein in Abraxane®).<sup>42,43</sup> However, some of them may cause immune response (especially extrinsic proteins) and should be tested before clinical use. Inorganic nanomaterials, like silica and gold, are also employed as pharmaceutical adjuvants in research because there is evidence that they are biosafe.<sup>44</sup> However, inorganic materials undergo biodegradation issue and clearance problem, and much research focusing on these two aspects has been done.<sup>45–47</sup> How does inert materials, such as gold and carbon, are degraded and cleared from body is the major concern before their clinical application. Some research work also implied that some inorganic nanomaterials would cause genomic instability, inflammatory response, and protein phosphorylation.<sup>48–50</sup> In conclusion, both organic and inorganic nanomaterials have their advantages and drawbacks when considering biosafety issue. Neither of them should be neglected when talking about biosafe nanomaterials. The concept “biosafe” in this review does not mean “no harm at all,” but indicates that the nanomaterials we talked about are with low toxicity and immunogenicity, would not cause severe damage *in vivo* at their applicable dose, and have acquired recognition as potential pharmaceutical adjuvants from most researchers.

In this article, we will review recent progress in biosafe nanomaterial-based pharmaceutical research, using representative organic, inorganic and hybrid materials as examples (Fig. 3). We also highlight the advantages and remarkable functions that make these nanomaterials ideal for use in medicine design.

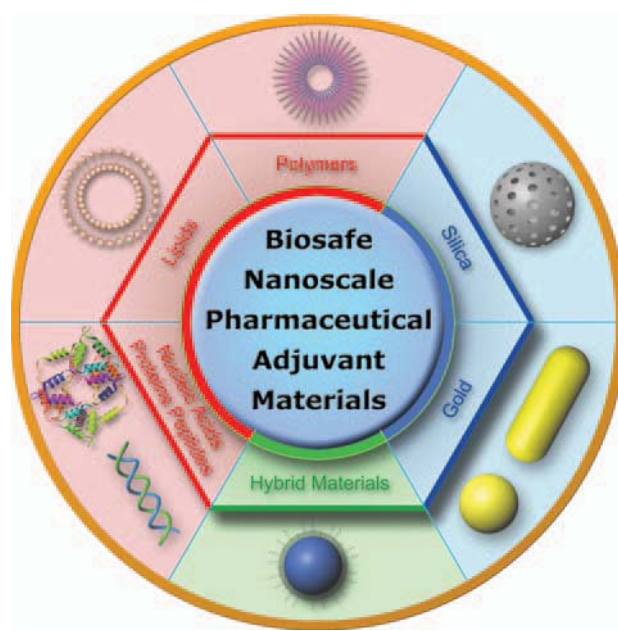


**Figure 3.** Representative biosafe nanoscale pharmaceutical adjuvant materials.



## ORGANIC NANOSCALE MATERIALS EMPLOYED FOR PHARMACEUTICAL DEVELOPMENT

### Polymers

Polymers are an important class of nanomaterial in the nanomedicine field due to their ability to encapsulate and protect cargoes and to respond to specific extrinsic stimuli.<sup>51–53</sup> They have been widely used in biomedical research, in applications such as drug delivery,<sup>54,55</sup> gene therapy,<sup>56–58</sup> cell imaging,<sup>59,60</sup> and cancer diagnosis.<sup>61</sup> Polymers can be classified into two categories, natural polymer and synthetic polymer, both of which are important pharmaceutical adjuvant materials. Chemical structures of frequently used polymers in nanomedicine design are listed in Figure 4.

### Natural Polymers

Biocompatible natural polymers have attracted great attentions of researchers, since they have many advantages such as low toxicity and biodegradability.<sup>62,63</sup> The most widely studied polymers among them are chitosan and its derivatives. And in order to achieve various functions,

many modifications have been applied on the natural polymers.<sup>64</sup>

**Chitosan.** Chitosan, a natural linear polysaccharide, has been used to synthesize nanoparticles for drug delivery and tissue engineering due to its superior biocompatibility and versatile chemical properties.<sup>65–68</sup> Chitosan nanoparticles will degrade into non-toxic compounds under the effect of lysozyme. These naturally synthesized biomaterials are biocompatible and biodegradable and are relatively easy to obtain at low cost.<sup>69</sup> Chitosan nanoparticles can also be designed to load hydrophobic agents by introducing hydrophobic molecules to chitosan. Therefore, chitosan-based nanoparticles have been employed for delivery of several protein drugs and anticancer chemical drugs, including insulin,<sup>70</sup> DOX,<sup>71</sup> cisplatin,<sup>72</sup> and docetaxel.<sup>73</sup> However, chitosan is only soluble in acidic solvents, resulting in the instability of nanoparticles in neutral or alkaline conditions.<sup>74,75</sup> Fortunately, chitosan provides chemical functional groups which make chemical modification on chitosan possible. A chemical modified chitosan, *N*-imidazolyl-*O*-carboxymethyl chitosan (IOCMCS), was introduced by Bi and co-workers to improve the solubility

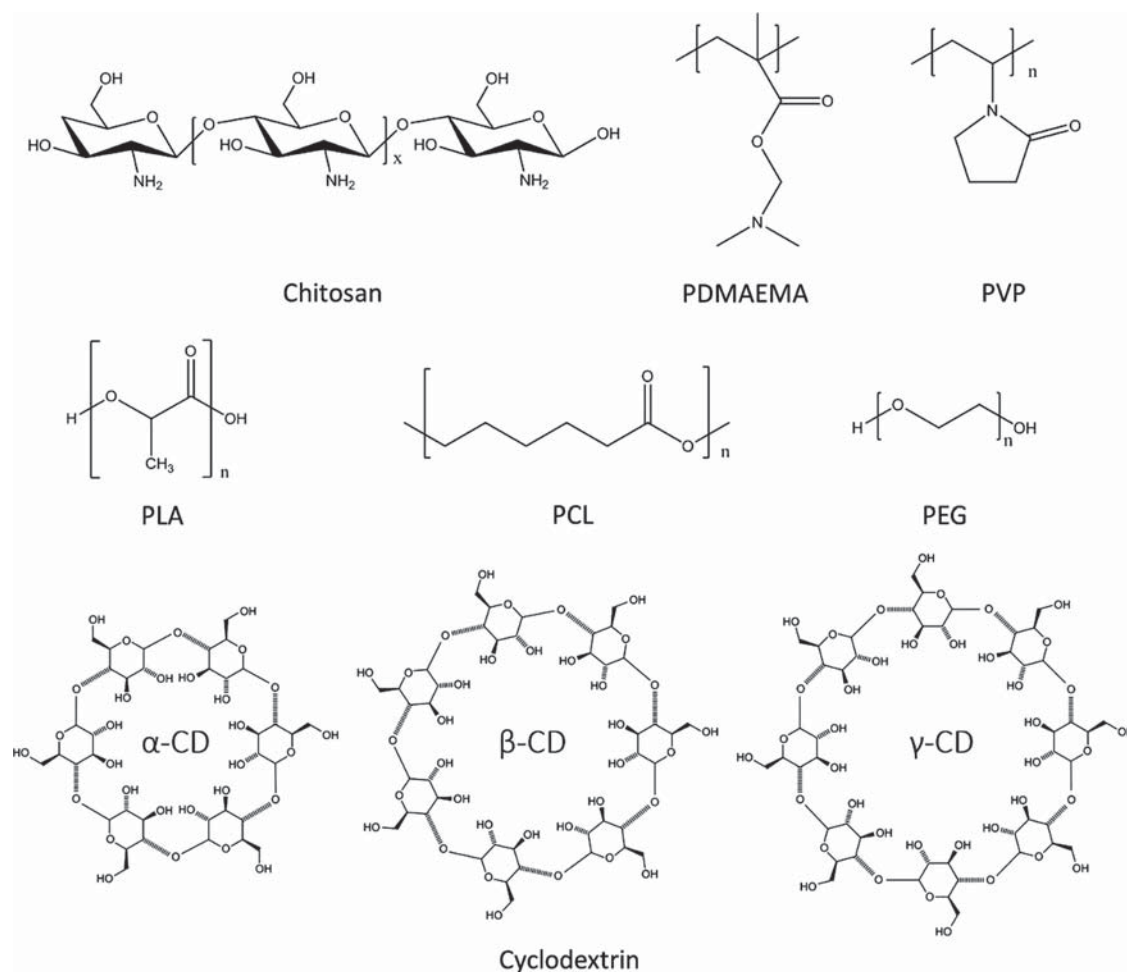


**Figure 4.** Chemical structures of representative polymers and cyclodextrins as pharmaceutical adjuvant materials.

of chitosan in water and make the IOCMCS-formed nanoparticle positively charged.<sup>76</sup> Under the N/P ratio of 5, IOCMCS could efficiently bound with plasmid DNA. It also showed higher transfection efficiency and lower cytotoxicity compared to polyethyleneimine (PEI) and Lipofectamine™ 2000. This work is one of the various successful attempts to make chemical modification of chitosan to break the obstacle of solubility and made it a promising material in the field of medicine research. Another interesting work reported by Zhang et al. recently

suggested a new application of chitosan.<sup>77</sup> A modified chitosan, *N*-octyl-*O*-sulfate chitosan (NOSC), was applied to assemble into micelle for PTX loading. According to previous report, NOSC was possible to inhibit the key drug resistance-related protein P-glycoprotein (P-gp, also known as MDR-1).<sup>78–80</sup> Thus, PTX-encapsulated NOSC micelle (PTX-M) could deliver PTX into cells bypassing P-gp. After internalization, NOSC micelle disassembled and inhibited P-gp function, improving PTX retention in cells (Fig. 5(A)). Anticancer efficacy towards HepG2

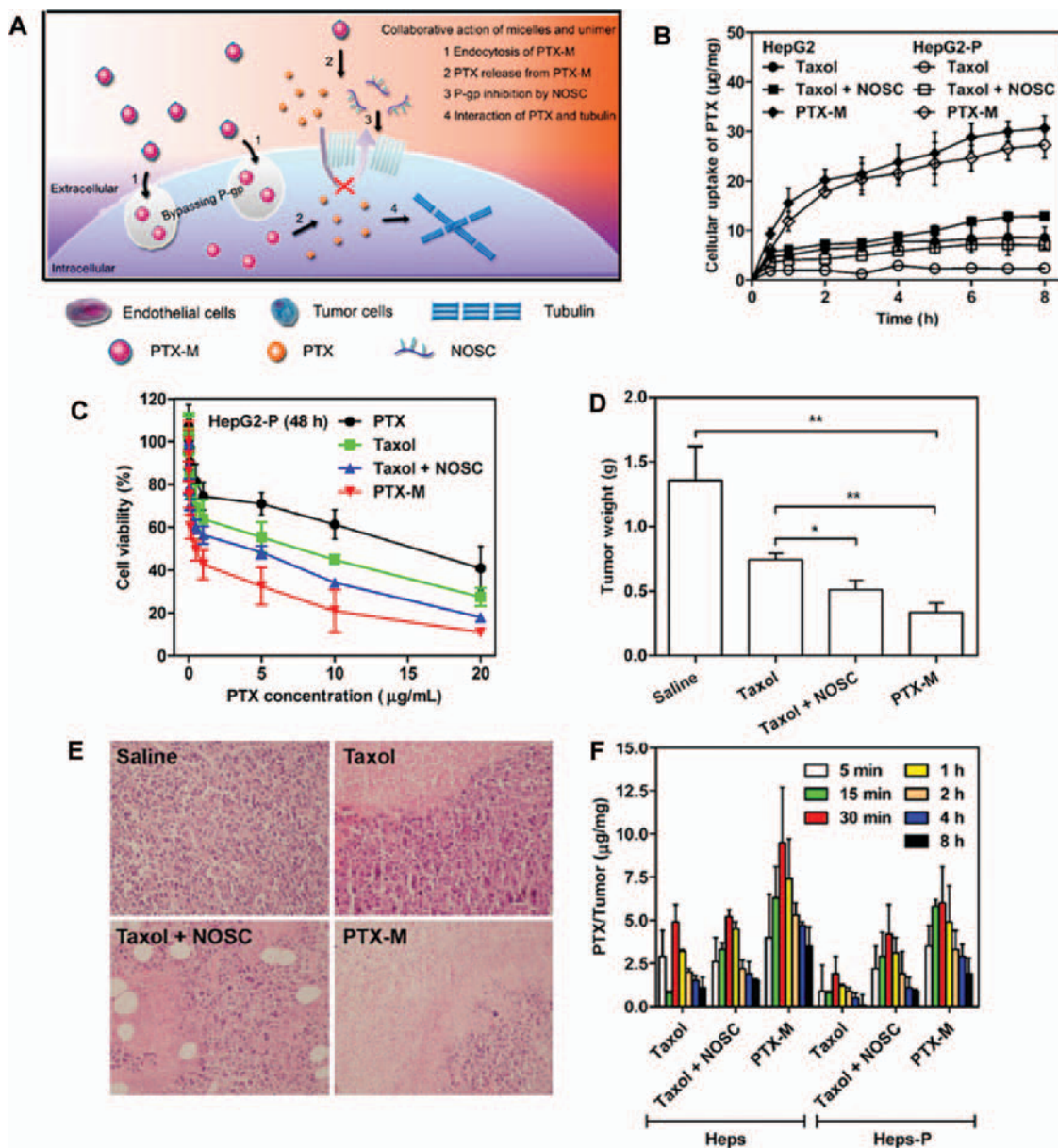


**Figure 5.** A chitosan-based micelle that can overcome drug resistance of HepG2 cells. (A) Scheme of P-gp inhibition of NOSC and P-gp bypassing of PTX. (B) Cellular uptake of different PTX formulations in HepG2 and HepG2-P cells. (C) Cytotoxicity evaluation of different PTX formulations toward HepG2-P cells after 48 h treatment. (D) Tumor weights of HepG2-P xenograft mice model after different PTX formulation treatment at day 21. (E) H&E stained tumor sections after the treatment at day 21. (F) PTX accumulation in tumor tissue after intravenous injection of different PTX formulations into Heps and Heps-P tumor-bearing mice. Reprinted with permission from [77], X. Jin, et al., Paclitaxel-loaded *N*-octyl-*O*-sulfate chitosan micelles for superior cancer therapeutic efficacy and overcoming drug resistance. *Mol. Pharm.* 11, 145 (2014). © 2014, American Chemical Society.

cell and drug resistance cell HepG2-P of different PTX formulations, including taxol (PTX dissolved in Cremophor EL and ethanol), taxol + NOSC (physical mixture of taxol and NOSC), and PTX-M, was assessed *in vitro* and *in vivo*. Cytotoxicity evaluation result indicated that PTX-M possessed the best cell killing efficacy in HepG2-P cells with the lowest half maximal inhibitory concentration (IC<sub>50</sub>) (0.55  $\mu\text{g/mL}$ ). Meanwhile, IC<sub>50</sub> of PTX was 16.39  $\mu\text{g/mL}$  (Fig. 5(C)). PTX-M also exhibited the best tumor growth inhibition efficacy *in vivo* as tumor growth was significantly controlled after PTX-M injection (Figs. 5(D), (E)). Further study of PTX accumulation in cells and tumors of different formulations revealed that PTX-M could increase the amount of PTX in cells and tumor tissues which may be a result of the dysfunction of P-gp (Figs. 5(B), (F)).

Therefore, drug resistance of HepG2-P cell was successfully overcome *in vitro* and *in vivo* by encapsulating PTX into P-gp inhibiting chitosan derivative NOSC. NOSC in this work is a P-gp inhibitor as well as a drug carrier. More interesting work could be developed basing on this material.

### Synthetic Polymers

Compared to natural ones, synthetic polymers are more designable, and can also be biocompatible by using appropriate compounds while synthesizing.<sup>81, 82</sup> The method of synthesizing can be various, such as polymerization, covalently binding, and physical assembly. Optimizing polymers to be more functional and biocompatible is now the most important research field of polymer science and attracts many scientists' attentions.<sup>83–85</sup>

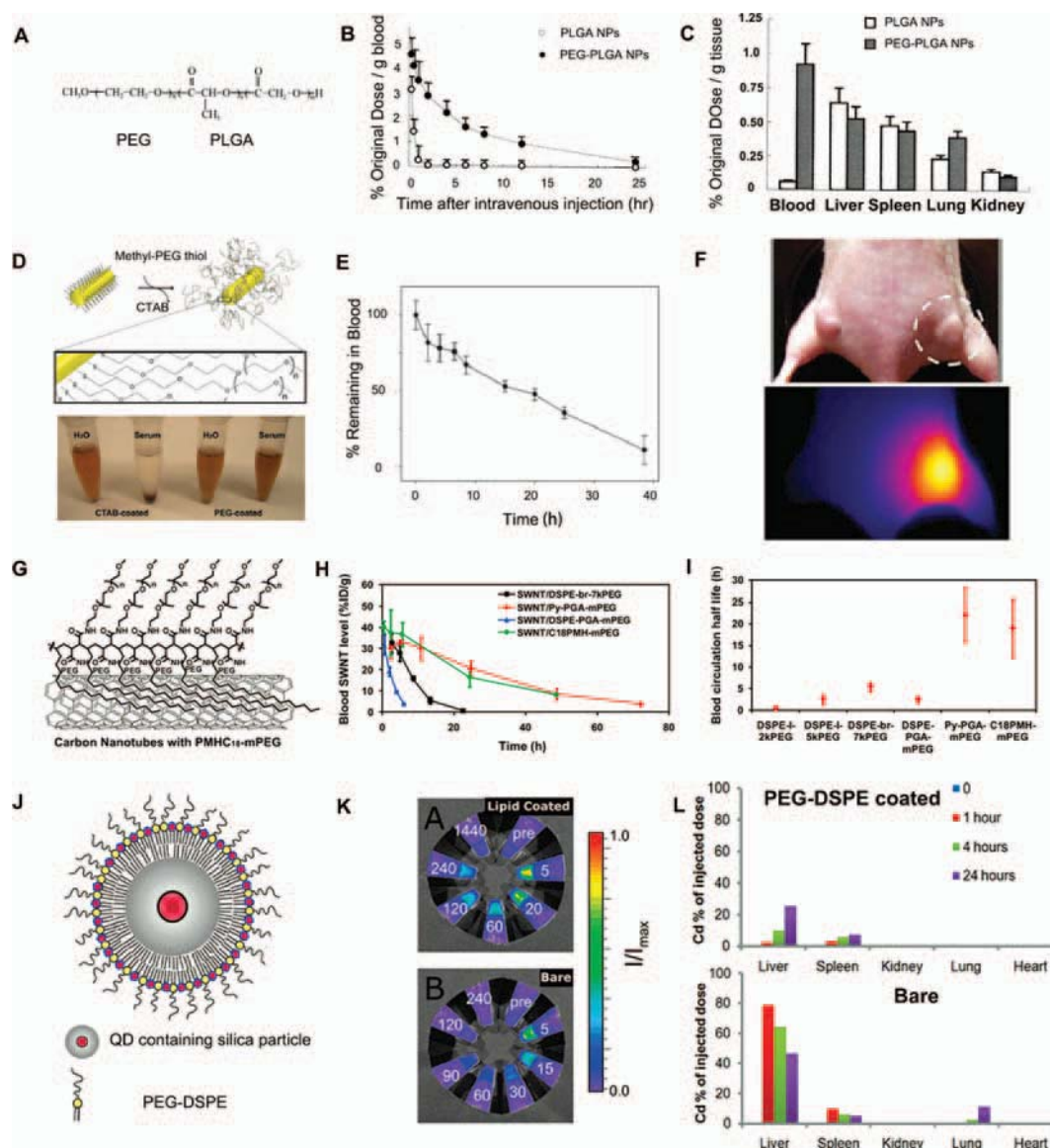
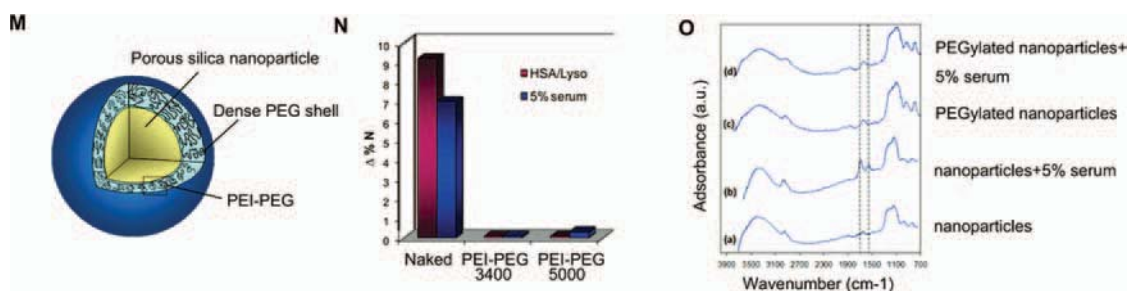


Figure 6. Continued.





**Figure 6.** PEG-protected nanoparticles with improved pharmacokinetics. (A) Structure of the PEG–PLGA copolymer. (B) Blood clearance curves of  $I^{125}$ -labeled BSA in PEG–PLGA and PLGA nanoparticles. (C) Tissue distribution of  $I^{125}$ -labeled BSA at 12 h in PEG–PLGA and PLGA nanoparticles. Reprinted with permission from [89], Y.-P. Li, et al., PEGylated PLGA nanoparticles as protein carriers: Synthesis, preparation and biodistribution in rats. *J. Control Release* 71, 203 (2001). © 2001, Elsevier. (D) Molecular schematic of PEG coating on NR surface and stability of NRs in water and serum. (E) Blood clearance curves of PEG-protected Au NRs. (F) Thermal imaging of PEG-protected Au NRs in tumor tissue 72 h post intravenous injection. Reprinted with permission from [90], G. von Maltzahn, et al., Computationally guided photothermal tumor therapy using long-circulating gold nanorod antennas. *Cancer Res.* 69, 3892 (2009). © 2009, American Association for Cancer Research. (G) SWNTs coated with PMHC18-mPEG. (H) Blood circulation curves of different PEG-coated SWNTs. (I) Blood circulation half-lives of different PEG-coated SWNTs. Reprinted with permission from [91], G. Prencipe, et al., PEG branched polymer for functionalization of nanomaterials with ultra-long blood circulation. *J. Am. Chem. Soc.* 131, 4783 (2009). © 2009, American Chemical Society. (J) Schematic representation of PEG-protected QD containing silica particle. (K) Fluorescence intensity of blood samples taken at different time points (indicated in minutes). (L) Biodistribution analysis of bare and PEG-protected particle by cadmium (Cd, a component of the QD) quantification. Reprinted with permission from [92], M. M. van Schooneveld, et al., Improved biocompatibility and pharmacokinetics of silica nanoparticles by means of a lipid coating: A multimodality investigation. *Nano Lett.* 8, 2517 (2008). © 2008, American Chemical Society. (M) Schematic structure of the PEGylated silica nanoparticle. (N) Nonspecific protein adsorption of protein on naked and PEG-protected silica nanoparticles after incubation with protein solution. (O) FTIR spectra of naked and PEG-protected silica nanoparticles after incubation with 5% serum solution. Reprinted with permission from [93], B. Thierry, et al., Electrostatic self-assembly of PEG copolymers onto porous silica nanoparticles. *Langmuir* 24, 8143 (2008). © 2008, American Chemical Society.

**PEG and Its Derivatives.** Polyethylene glycol (PEG) is another important pharmaceutical adjuvant in the nanomedicine research field. Most unmodified nanostructures, such as liposomes, micelles, and nanocrystals, usually have a high rate of uptake by the RES, leading to significant accumulation of nanomaterials in the liver and spleen.<sup>86</sup> PEGylation, the process of covalently attachment of PEG to another molecule, can increase the hydrodynamic size of nanoparticles and hinder the interaction between nanoparticles and plasma proteins, resulting in reduced immunogenicity. Nanoparticles will then show improved biocompatibility, with ultra-long circulation times and high water solubility after PEGylation.<sup>87</sup> Nowadays, many PEGylated medicines, especially PEG-liposomes and PEG-proteins, have got their FDA approval because of prolonged circulation time and reduced immunogenicity.<sup>88</sup> Figure 6 summarized several PEG-protected nanoparticles with improved pharmacokinetics. PEG was conjugated with another FDA-approved adjuvant materials, poly(lactic-co-glycolic acid) (PLGA), and reported by Pei and co-workers.<sup>89</sup>  $I^{125}$ -labeled bovine serum albumin (BSA) was loaded in PEG–PLGA and PLGA nanoparticles to trace circulation and biodistribution of two nanoparticles *in vivo*. The PEG–PLGA nanoparticle exhibited longer blood circulation time than PLGA nanoparticle. Moreover, PEG–PLGA nanoparticles remained a much higher concentration in blood than PLGA nanoparticle 12 h after intravenous injection

(Figs. 6(A)–(C)). PEG is also important surface coating agent of inorganic nanomaterials. PEG-protected gold nanorods (Au NRs) obtained by replacing CTAB with methyl-PEG thiol were stable in serum, while CTAB-protected Au NRs aggregated.<sup>90</sup> Blood clearance test showed that PEG-protected Au NRs has a very high half-life of  $\sim 17$  h. 72 h after intravenous injection, PEG–Au NRs were still visible in tumor site by thermal imaging (Figs. 6(D)–(F)). In another work, Dai et al. functionalized single-walled carbon nanotubes (SWNTs) with a branched PEG polymer, named as PMHC<sub>18</sub>-mPEG.<sup>91</sup> The blood circulation time of PEG polymer-protected SWNTs in mice upon intravenous injection was greatly prolonged ( $t_{1/2} = 22.1$  h) compared to the previous record ( $t_{1/2} = 5.4$  h). The PMHC<sub>18</sub>-mPEG was also compared with DSPE-PEG in SWNT protection *in vivo* and PMHC<sub>18</sub>-mPEG-coated SWNT showed longer half-life in blood (Figs. 6(G)–(I)). PEG holds great potential in imaging probe protection *in vivo*. Mulder et al. investigated the biocompatibility and pharmacokinetics of quantum dots (QDs, an important imaging probe) containing silica nanoparticles after PEG coating.<sup>92</sup> Both bare and PEG-coated nanoparticles were injected into mice and blood sample were obtained several minutes after injection. Then fluorescence intensity, resulting from QDs, was determined and the results showed that bare nanoparticles were rapidly cleared from blood. Meanwhile, PEG-coated nanoparticles remained in blood and exhibited fluorescence signal even

240 min post injection. Biodistribution analysis demonstrated that less PEG-coated nanoparticles were uptake by RES organ than bare nanoparticles (Figs. 6(J)–(L)). Reduced adsorption of protein on PEG corona is the main mechanism of PEG protection. Griesser et al. provide some evidence to support this viewpoint.<sup>93</sup> Nonspecific adsorption of proteins on naked and PEG-protected silica nanoparticles was determined by X-ray photoelectron spectroscopy (XPS) and Fourier transform infrared spectroscopy (FTIR) analysis, and the results confirmed that protein was hardly adsorbed by PEG-protected nanoparticles (Figs. 6(M)–(O)).

**PLA and Its Derivatives.** Poly(lactic acid) (PLA) and PLGA are the most widely used polymers as they have been approved by the FDA.<sup>94,95</sup> PLA- and PLGA-based nanocarriers were developed to deliver various drugs;<sup>96,97</sup> however, the rapid burst of cargo release without any specificity limited further *in vivo* application due to the low drug concentration at the desired site.<sup>98,99</sup> Thus, subsequent work focused on improving the specific release of drugs at the disease site by linking drug release with a specific biological process. Scientists have now successfully synthesized polymeric nanoparticles which are responsive to specific external stimuli, such as light,<sup>100</sup> temperature,<sup>101</sup> and ultrasound,<sup>102</sup> especially to inherently occurred low pH in tumor microenvironment and endosome.<sup>103</sup> Compared to

the neutral pH in healthy tissues, the lower pH in the tumor microenvironment and in endosomes can be exploited so that nanoparticles release their drug payloads in the right place.<sup>104</sup> The most widely used strategy to design pH-responsive polymeric nanoparticles is to introduce a protonation group, such as carboxylic acids and tertiary amines, into the polymer structure which can be ionized at different pH values. Another strategy to achieve pH-responsive polymeric structures is to use acid-labile functional groups which can be hydrolyzed to reveal a new hydrophilic group; the polymer then becomes water-soluble and the nanoparticle structure decomposes, thus releasing the loaded agent. For example, Fréchet et al. synthesized acetal-derivatized dextran-based particles which degraded in a pH-dependent manner (Fig. 7(A)).<sup>105</sup> At pH 7.4, the nanoparticles possessed a half-life of 360 h, as judged by measuring free dextran, but when the pH was adjusted to 5, the nanoparticles became unstable and the half-life decreased to 10 h. The ultra-long half-life at neutral pH and significantly decreased stability at acidic pH are ideal for pH-sensitive drug delivery. Nanoparticles would be extremely stable in normal tissue and response sensitively once they get to the disease site. Another merit of this approach is that both hydrophobic and hydrophilic agents were successfully encapsulated within the nanoparticles and, as dextran is biocompatible, these particles are non-toxic to cells *in vitro*.

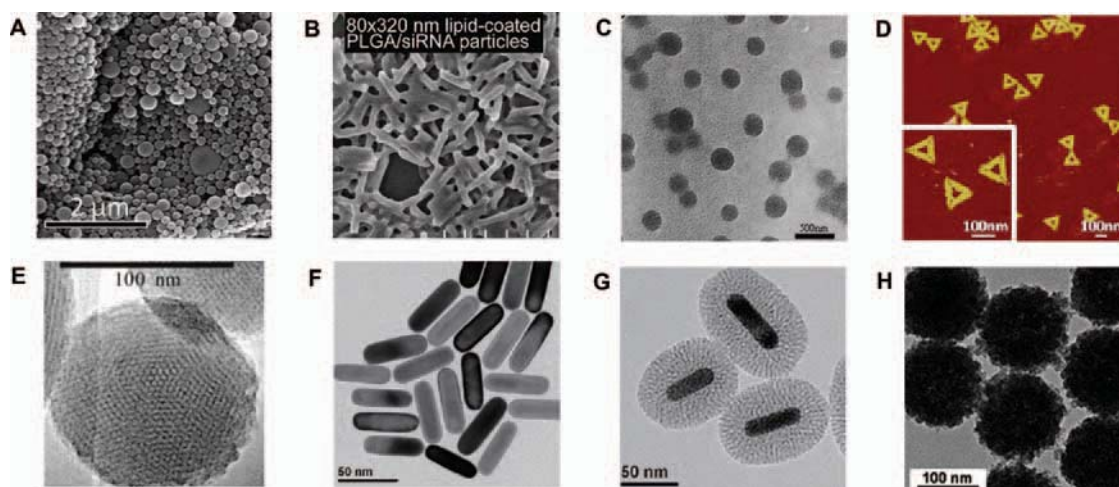


**Figure 7.** Microscope images of (A) acetal-derivatized dextran nanoparticles. Reprinted with permission from [105], E. M. Bachelder, et al., Acetal-derivatized dextran: An acid-responsive biodegradable material for therapeutic applications. *J. Am. Chem. Soc.* 130, 10494 (2008). © 2008, American Chemical Society. (B) lipid-coated PLGA/siRNA particles. Reprinted with permission from [130], W. Hasan, et al., Delivery of multiple siRNAs using lipid-coated PLGA nanoparticles for treatment of prostate cancer. *Nano Lett.* 12, 287 (2011). © 2011, American Chemical Society. (C) cisplatin-loaded milk protein nanoparticles. Reprinted with permission from [148], X. Zhen, et al., Cellular uptake, antitumor response and tumor penetration of cisplatin-loaded milk protein nanoparticles. *Biomaterials* 34, 1372 (2012). © 2012, Elsevier. (D) DNA origami nanostructures. Reprinted with permission from [173], Q. Jiang, et al., DNA origami as a carrier for circumvention of drug resistance. *J. Am. Chem. Soc.* 134, 13396 (2012). © 2012, American Chemical Society. (E) MSNs. Reprinted with permission from [191], I. Slowing, et al., Effect of surface functionalization of MCM-41-type mesoporous silica nanoparticles on the endocytosis by human cancer cells. *J. Am. Chem. Soc.* 128, 14792 (2006). © 2006, American Chemical Society. (F) Au NRs; (G) Au@SiO<sub>2</sub> nanoparticles. Reprinted with permission from [212], Z. Zhang, et al., Mesoporous silica-coated gold nanorods as a light-mediated multifunctional theranostic platform for cancer treatment. *Adv. Mater.* 24, 1418 (2012). © 2012, Wiley-VCH Verlag GmbH & Co. KGaA, Weinheim. (H) PNIPAM/AA@SiO<sub>2</sub> nanoparticles. Reprinted with permission from [227], X. Hu, et al., Multifunctional hybrid silica nanoparticles for controlled doxorubicin loading and release with thermal and pH dual response. *J. Mater. Chem. B* 1, 1109 (2013). © 2013, Royal Society of Chemistry.

**PVP and Its Derivatives.** Poly(*N*-vinylpyrrolidone) (PVP) has a lot of properties which make it an outstanding candidate as pharmaceutical adjuvant material, such as solubility in water, very low toxicity, good biocompatibility, and high complexation ability.<sup>106</sup> PVP was initially used as a blood plasma substitute and then be widely used in medicine and pharmacy.<sup>107</sup> The highly hydrated structure of PVP suppressed its interaction with immune system and made PVP a good choice as coating agent to reduce immunogenicity of nanomaterials.<sup>108</sup> The slow degradation of PVP under ultraviolet (UV) or ultrasound irradiation is another promising aspect.<sup>109</sup> It has also been reported that PVP can cause intracellular vesicular swelling and diminish the fusion of endosomes to lysosomes.<sup>110</sup> These unique features of PVP make it a good drug and gene carrier. However, the non-biodegradability of macromolecular PVP will lead to accumulation *in vivo*. To deal with this problem, PVP with molecular weight below the kidney threshold was synthesized through various methods. Saxena et al. reported a cross-linked PVP nanoparticle of size less than 100 nm which can encapsulate plasmid DNA.<sup>111</sup> The result showed these particles have high transfection efficiency both *in vitro* and *in vivo*. This synthesis method provided a low molecular weight PVP nanoparticle which was a promising vehicle for drug and gene delivery.

**Amphiphilic Copolymers.** Copolymers, especially amphiphilic copolymers, are the most common polymers in nanotechnology.<sup>112–114</sup> Amphiphilic copolymers can self-assemble into micelles or nanoparticles in aqueous solution, with a hydrophobic core inside and a hydrophilic shell outside. Each chain of the copolymer can also provide different functions, to make the particle multifunctional. For example, Guo et al. synthesized a copolymer composed of three polymers, methoxy polyethylene glycol-block-(polycaprolactone-graft-poly(2-(dimethylamino)ethyl methacrylate)) (PEG-*b*-(PCL-*g*-PDMAEMA)).<sup>115</sup> The polycaprolactone (PCL) backbone can (1) form a hydrophobic core to carry hydrophobic drugs such as PTX and DOX; (2) improve drug/gene delivery efficiency by enhancing the cellular uptake through effective interaction between the hydrophobic chains and cell membrane. The side chain poly(2-(dimethylamino)ethyl methacrylate) (PDMAEMA) is positively charged which can condense plasmid DNA and provide endosome escaping capability. As described above, PEG, the biocompatible part of backbone, forms a hydrophilic shell to protect the particle and decrease the surface positive charge. This well designed amphiphilic copolymer can self-assemble into nanoparticle and shows high gene delivery efficiency *in vitro*.

## Lipids

Lipid is a group of natural molecules including fats, sterols, fat-soluble vitamins, glycerides, phospholipids, and others. Among these lipids, phospholipids are widely employed as nanoscale pharmaceutical adjuvants in the

form of liposomes and micelles and will be highlighted in this review.<sup>116,117</sup> Phospholipids are amphiphilic compounds, with a hydrophilic polar group and a hydrophobic chain, which mimic the components of naturally occurring membrane bilayers.

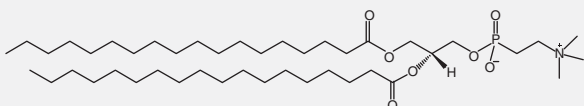
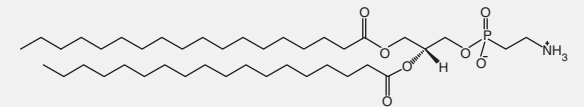
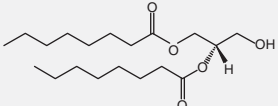
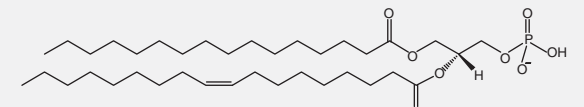
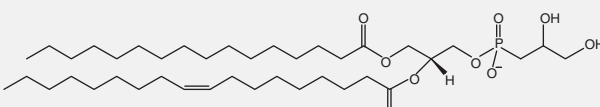
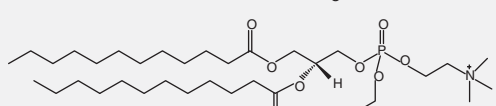
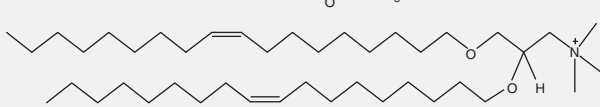
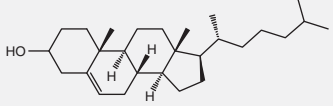
The best-known lipid-based nanostructures are liposomes, in which an internal aqueous core is separated from the bulk aqueous phase by a closed lipid bilayer shell.<sup>118</sup> Micelles, a nanostructure similar to liposomes, are usually composed of closed lipid monolayers with a fatty acid core and a polar surface, or a polar core with fatty acids on the surface (inverted micelle). Nowadays, many amphiphilic polymer-based micelles have been developed as a result of their more versatile structure and function compared to that of lipid.<sup>119,120</sup> Liposomes are capable of carrying both hydrophobic and hydrophilic drugs at the same time. The hydrophobic drugs can be integrated into the fatty acid shell while the hydrophilic drugs can be loaded into the aqueous core. In contrast, either hydrophobic or hydrophilic drugs can be encapsulated into micelles, determined by the core's polarity. Micelles are much smaller in size (1–20 nm) than liposomes (100–200 nm); however, the size of micelles is more uniform. The surface of liposomes can also be functionalized with a variety of ligands and reporters, such as antibodies,<sup>121</sup> nucleic acids,<sup>122</sup> and luminescent sensors.<sup>123</sup> The methods for liposome preparation are well developed and the process is very easy to control. Under specific conditions, amphiphilic lipids will self-assemble into liposomes. By adjusting the formulation (lipid ratio, source) and changing the synthesis conditions (temperature, solvent, ion concentration, and sonication), the size, uniformity, and stability of liposomes can be manipulated. The first FDA-approved nano-drug, known as Doxil<sup>®</sup> in the market, is a liposome loaded with the anticancer drug DOX. DOX is commonly used in the treatment of a wide range of cancers; however, the adverse side effect is life-threatening heart damage.<sup>124</sup> Using the Doxil<sup>®</sup> formulation, the drug circulation time is prolonged and more drug accumulates in the tumor site as a result of the passive targeting of liposomes to the leaky tumor vasculature.<sup>125</sup>

Lipids can also be grafted onto other nanomaterials as surface coatings for further modification, better stability, and improved biocompatibility.<sup>126,127</sup> PLGA nanoparticles are great siRNA carriers due to their stability and low toxicity.<sup>128</sup> However, the transfection efficiency of PLGA nanoparticles is low and not comparable to that of cationic lipid nanoparticles.<sup>129</sup> Thus, DeSimone et al. combined them and developed lipid-coated PLGA nanoparticles that could deliver multiple siRNAs for the treatment of prostate cancer (Fig. 7(B)).<sup>130</sup> The encapsulation efficiency was high (32–46%) and target gene expression was greatly down-regulated.

Lipids can be classified according to their surface charge: neutral lipids, anionic lipids, and cationic lipids. Cholesterol is separately introduced due to its special role



**Table I.** Structures of commonly used lipids in pharmacy research.

Lipid	Abbr.	Structure
<i>L</i> - $\alpha$ -phosphatidylcholine, hydrogenated (Soy)	HSPC	
1,2-dioctadecanoyl-sn-glycero-3-phosphoethanolamine	DSPE	
1,2-dioctanoyl-sn-glycerol	DG	
<i>L</i> - $\alpha$ -phosphatidic acid	PA	
<i>L</i> - $\alpha$ -phosphatidylglycerol	PG	
1,2-dilauroyl-sn-glycero-3-ethylphosphocholine	Ethyl PC	
1,2-di- <i>O</i> -octadecenyl 3-trimethylammonium propane	DOTMA	
Cholesterol	Chol.	

in lipid-based nanomaterials. Table I shows the commonly used lipids in pharmacy research.

### Neutral Lipids and Anionic Lipids

Neutral lipids and anionic lipids are similar in character and application. They are the main composition of conventional liposomes for pharmaceutical applications. Phosphatidylcholine (PC), phosphoethanolamine (PE), 1,2-dioctanoyl-sn-glycerol (DG), *L*- $\alpha$ -phosphatidic acid (PA), *L*- $\alpha$ -phosphatidylglycerol (PG) and their derivatives are commonly used in various liposomes. For instance, PC is a major constituent of cell membranes, which have been shown to stabilize membranes and can form a lamellar structure that is insensitive to the pH.<sup>131</sup> Due to their membrane structure and neutral or negatively charged surface, neutral and anionic liposomes can decrease the non-specific protein adsorption and remain longer in blood circulation *in vivo*. Awasthi et al. prepared PEGylated neutral and anionic liposome-encapsulated hemoglobin (LEH).<sup>132</sup> The neutral and anionic LEH showed long-lasting ability and the circulation half-life of LEH

was improved after PEGylation. Besides, neutral and anionic lipids can be modified and cooperated with other functional groups. We have recently reported a novel pH-sensitive liposome which can circumvent the DOX-resistance of cancer cells.<sup>133</sup> One way that cells develop multi-drug resistance (MDR) is by expressing high levels of certain membrane proteins, such as P-gp, which mediates efflux of intracellular drugs.<sup>79,80</sup> We developed a system to create a sudden increase in the intracellular drug level, thus killing the cell before drug export can occur. This liposome is composed of neutral lipids hydrogenated soy phosphatidylcholine (HSPC) and PEGylated 1,2-distearoyl-sn-glycero-3-phosphoethanolamine (DSPE). We loaded liposomes with ammonium bicarbonate and DOX and demonstrated that at pH 5.0, the bicarbonate ions decomposed and released CO<sub>2</sub> gas, which raised the internal pressure and ruptured the liposomes. When these liposomes reached the endosomes (pH ~ 5.0) in MDR breast cancer cells, they released all their DOX at the same time and the intracellular drug concentration reached the effective concentration immediately. Thus, resistant cells were

killed before their MDR mechanisms had time to work. This work illustrates a new strategy for designing and synthesizing pH-sensitive liposomes.

### Cationic Lipids

Cationic lipids, for example ethyl phosphocholine (ethyl PC), 1,2-di-O-octadecenyl-3-trimethylammonium propane (DOTMA), and cationic cholesterol, have cationic hydrophilic head to attract negatively charged molecules, especially nucleic acids, and form complexes. In this way, cationic lipids can be used as nucleic acid carriers and are regarded to be the most promising non-viral gene vectors.<sup>134</sup> Tenchov et al. synthesized various ethyl PCs with different hydrophobic moieties, and investigated their transfection efficiencies in human umbilical artery endothelial cells (HUAEC). The result showed that the compounds exhibited very high transfection efficiencies.<sup>135</sup> Through the investigation of liposome phase-conversion during transfection process, they found that high transfection efficiency was resulted from enhanced liposome fusion with cellular membranes. This work could be useful to assess the effect of cationic lipid carriers and for further design of new and effective gene delivery system.

### Cholesterol

Cholesterol is an essential structural constituent of animal cell membranes. The addition of cholesterol to lipid bilayers decreases its permeability to water and thus drug leakage is prevented.<sup>136</sup> Cholesterol is also incorporated into the liposome layers to increase their ordered state as it has an additional stabilizing effect.<sup>137</sup> It limits the mobility of acyl chains of phospholipids, rigidifies the membrane in the liquid-crystalline phase, and increases the mobility of these chains while in the gel phase. This character decreases the phase transition temperature of lipid membranes, a parameter that is important for the relative fluidity and mobility of lipid molecules in the bilayer. Thus, cholesterol is a regulator in lipid bilayer and plays an important role in lipid-based nanoparticles.

### Proteins, Peptides and Nucleic Acids

Proteins, peptides, and nucleic acids have many different roles in the development of nanomedicines. They can act as drugs (e.g., interferon, insulin, tesamorelin, siRNA), target ligands (e.g., aptamer, antibody, nuclear localization signal peptide), and carriers (e.g., albumin, DNA origami). As they are the most common materials in the human body, their biodegradability is in no doubt. Much higher systemic concentrations of proteins, peptides, and nucleic acids can be administered than that of inorganic nanoscale materials. As pharmaceutical adjuvants, proteins, peptides, and nucleic acids are irreplaceable because of their targeting ability. Illustrative examples of targeting ligands, including proteins, peptides, and nucleic acids, are listed in Table II. Metabolism mechanism of them is also clearly

studied, making them more advantageous than other materials. However, the disadvantage is that their structures are vulnerable and it is difficult to make modifications. Once the fine-designed structure is changed, they will lose functions and integrity. Another issue that should be addressed is the immunogenicity as immune system will be activated by exogenous proteins and DNA sequences.<sup>138</sup>

### Proteins

Self-assembled protein-based nanocages can be considered as natural drug carriers. In nature, some protein structures, such as microtubules, are assembled from multiple copies of protein subunits.<sup>139</sup> Recently, albumin, gelatin, and silk protein-based protein nanoparticles have been developed as drug delivery systems following the successful model of Abraxane®.<sup>140–142</sup> These particles are biosafe and non-antigenic; furthermore, they can realize active targeting as well as passive targeting. For example, albumin can penetrate the microvessel endothelial cells in angiogenic tumor vasculature with the assistance of the albumin-binding protein gp60 and combine with the target protein SPARC which is over-expressed in many tumors.<sup>143, 144</sup> Cao and co-workers used protein nanoparticles for active tumor targeting.<sup>145</sup> They employed human ferritin H-chain protein (FTH1) as the framework and combined it with epidermal growth factor (EGF), the ligand of EGFR, a receptor that is over-expressed in many malignant tissues.<sup>146, 147</sup> The EGF-FTH1 nanoparticles were specifically internalized by two breast cancer cell lines, MCF-7 and MDA-MB-231, but the uptake by normal epithelial MCF-10A cells was negligible. *In vivo* experiments also demonstrated the accumulation of EGF-FTH1 nanoparticles in breast tumors in a mouse xenograft model. Jiang et al. cross-linked the milk protein casein with transglutaminase to form nanoparticles, which were then loaded with cisplatin, a model anti-cancer drug (Fig. 7(C)).<sup>148</sup> In the murine xenograft model, cisplatin-loaded nanoparticles inhibited tumor growth 1.5-fold more effectively than free cisplatin and analysis of tumor sections demonstrated that the casein nanoparticles could penetrate through the tumor tissue and deliver cisplatin to cells far from the vasculature.

Collagen is another important biosafe nanomaterial that should be addressed. It is the main structural protein in animals and accounts for one third of total protein in human.<sup>149</sup> 28 types of collagen have been identified in vertebrate and 90% of the collagen in the body is type I.<sup>150, 151</sup> As collagen is the major component of the extracellular matrix (ECM), the biocompatibility of collagen is good.<sup>152–154</sup> In a recent work reported by Cai and co-workers, collagen was linked to silica nanoparticles via disulfide bond as a protein cap to protect encapsulated fluorescence probe FITC.<sup>155</sup> Silica nanoparticle is an excellent reservoir for drugs, and end-capping of them could protect encapsulated cargos, separate cargos from external environment. As a capping material, collagen has advantages in biosafety. In addition, collagen is full of sulfhydryl,

**Table II.** Examples of targeting ligands.

Category	Name	Target and indication	Refs.
Protein			
	Antibody		
	Trastuzumab (Herceptin®)	HER2/neu	[230, 231]
	Bevacizumab (Avastin®)	VEGF	[232]
	Cetuximab (Erbix®)	EGF receptor	[233, 234]
	Rituximab (Rituxan®)	CD20	[235]
	Ibritumomab tiuxetan (Zevalin®)	CD20	[236]
	Tositumomab and tositumomab (Bexxar®)	CD20	[237]
	Gemtuzumab ozogamicin (Mylotarg®)	CD33	[238]
	Alemtuzumab (Campath®)	CD52	[239]
	Others		
	Transferrin	Transferrin receptor	[240, 241]
	Low density lipoprotein	Folate receptor	[242]
	Heavy-chain ferritin	Transferrin receptor 1	[243]
Peptide	RGD	$\alpha v\beta 3$ -integrin	[244, 245]
	CRGDK	Neuropilin-1	[24]
	NGR	CD13	[246]
	SP5-52	Tumor neovasculature	[247]
	PIVO-8	Tumor angiogenesis	[248]
	PIVO-24	Tumor angiogenesis	[248]
	LyP-1	Tumor hypoxia and lymphangiogenesis	[249]
	RVG	Acetylcholine receptor	[250]
	TAT	Cell nucleus	[166, 251]
Nucleic acid: aptamer	Macugen	Vascular endothelial growth factor	[252]
	AS1411	Nucleolin	[253, 254]
	sgc8	Protein tyrosine Kinase 7	[255]
	S1.3/S2.2	Mucin 1	[256]
	TD05	Immunoglobulin $\mu$ -heavy chains	[255]
	A10	Prostate-specific membrane antigen	[257]
	TBA	$\alpha$ -thrombin	[258]
	Apt- $\alpha v\beta 3$	$\alpha v\beta 3$ integrin	[259]
	B28	HIV gp120	[260]
	A30	HER3	[261]

which are necessary to form disulfide bond that can be broke by various reducing agents, including cell-expressed glutathione.<sup>156</sup> Then, specific cargo release from nanoparticles in cytoplasm can be realized. This work subtly utilized this property and conjugated collagen with nanoparticle through disulfide bond. Redox-responsive release of cargo FITC from nanoparticles was successfully identified after adding another reducing agent, dithiothreitol (DTT), to the nanoparticle solution. Targeting moiety, lactobionic acid (LA), was also introduced to the collagen-capped nanoparticle and was demonstrated to be effective in cell-specific targeting *in vitro*. Therefore, redox-responsive release and targeted delivery were achieved in this work.

Gelatin, a derivative of collagen, has similar potential as pharmaceutical adjuvant just like collagen. It is widely used in food and pharmaceuticals as gelling agent.<sup>157</sup> Gelation would be easily triggered by increasing the temperature and suddenly cooling of gelatin solution. Nanoparticles protected by a gelatin cap could then be obtained by this method. He, Wang, and co-workers reported a work employing gelatin as a cap to protect DOX-loaded nanoparticles recently.<sup>158</sup> The gelatin cap was successfully grafted to the nanoparticles by temperature-induced gelation and stabled by glutaraldehyde mediated cross-linking. Interestingly, gelatin is a

natural pH-sensitive agent and the authors take this advantage and successfully made the gelatin-capped nanoparticles pH-sensitive. As a mixture of protein and peptide, gelatin contains many protonation groups like carboxyl and amine, making it negatively or positively charged determined by the pH value. Moreover, the isoelectric point of gelatin can be modified by removing or retaining the protonation group.<sup>159</sup> Thus, the charge of gelatin can be precisely controlled. In this work, the loaded-DOX was well-protected upon neutral pH and released from the nanoparticles once the solution was adjusted to be acidic. This pH-sensitive behavior was also confirmed *in vitro* by co-localization analysis of DOX and endosome assisted by confocal laser scanning microscopy (CLSM). DOX was first trapped in endosome, exhibiting high co-localization ratio with endosome at 5 h. Then DOX escaped from endosome and entered into cell nucleus at 12 h, indicating that gelatin cap was eliminated from the nanoparticle surface.

### Peptides

Peptide, natural outcome from protein metabolism, played a crucial role in biological activity. Accompanied by the progress of peptide synthesis, peptides are more widely used as therapeutics, targeting ligands and drug vectors.<sup>160, 161</sup> Especially, peptide presents an advanced



and rapid developing in the field of drug delivery. Compared to other drug carrier materials, peptides possess several advantages for drug delivery, including smallness, versatile structures, facile synthesis, biocompatibility, and biodegradability.<sup>162</sup>

Many studies have confirmed the potential and superiority of peptide applied as drug delivery system. For example, Divita and co-workers successfully developed a peptide-based novel method to delivery siRNA into mammalian cells.<sup>163</sup> They designed an amphiphilic peptide (CADY) of 20 residues combining aromatic tryptophan (Trp, W) and cationic arginine (Arg, R) residues. The recombinant peptide forms stable complexes with siRNA, thereby increasing the stability of the complexes forming from peptide and siRNA and improving their transfection efficiency into a wide variety of mammalian cells, notably including primary cell lines. The siRNA delivery based on the CADY peptide significantly knockdown the target gene at subnanomolar concentration of siRNA. And more importantly, the cytotoxicity results showed that the CADY peptide was non-toxic and entered cells in an endosome-independent way, delivering therapeutics into cells without enzymolysis under lysosome enzymes. CADY peptide can then be used for the delivery of unstable drugs and those whose therapeutic efficacy are compromised due to the lysosome sequestration. Meanwhile, peptides possess a great potential in the chemotherapy drug delivery. Recently, a self-assembled peptide hydrogel formed by peptide and anti-cancer drug taxol was successfully designed by Yang and co-workers.<sup>161</sup> The peptide hydrogels of taxol could markedly inhibit tumor growth and metastasis through local administration of taxol hydrogels. In addition, the peptide-based taxol hydrogels enhanced the dosage tolerance of mice to taxol by reducing the plasma concentration of taxol which is due to the local administration, and finally decreased the side effects of taxol. Peptide hydrogel can be applied for controlled and sustained release of drugs to skin tissues, which is important for wound healing, anti-inflammation, and dermatosis.

Except for drug carrier, peptide also plays an important role as functional agent in drug delivery system. Cell penetrating peptides (CPPs) and pH-sensitive peptides are two major categories of functional peptides. CPPs are a series of peptides which can facilitate cellular uptake, endosomal escape, and nuclear targeting.<sup>164, 165</sup> Tat peptide, a CPP derived from trans-activator of transcription (tat) of type I human immunodeficiency virus (HIV-1), has been widely used in drug delivery and gene transfection.<sup>166, 167</sup> Polyhistidine, as a famous example of pH-sensitive peptide, has a pKa of  $\sim 6.5$ . When the pH is turned to be below 6.5, polyhistidine would shift from hydrophobic to hydrophilic.<sup>168, 169</sup> Caruso et al. recently successfully combined these two functional peptides in one, named H4R4, and reported its application in nanoparticle-based drug delivery.<sup>170</sup> R4 stands for 4 arginines, and it is mimicking

the functional region of tat peptide which is rich of arginine (GRKKRRQRRRPQ). H4 is 4 histidines, and is the pH-sensitive part of the combined peptide. R4, like many other CPPs, is highly hydrophilic and cannot be used alone without conjugation in nanoparticle functionalization. However, conjugation makes it hard to vary the amount of CPP used.<sup>171</sup> Here H4 provides a hydrophobic part and makes H4R4 an amphiphilic peptide under neutral pH. It is simply mixed with a PEG-DOX conjugate and a poly(2-diisopropylaminoethyl methacrylate) (PDPA) homopolymer. PEG-DOX and PDPA can assemble into a nanoparticle with a hydrophilic corona and hydrophobic core, which provide space for the amphiphilic H4R4. In the acidic endosomal compartment, H4 become hydrophilic and H4R4 is released from the nanoparticle. Then, R4 could facilitate the release of PEG-DOX from endosome and its further entrance into cell nucleus. The PEG-DOX loaded in H4R4 mixed nanoparticle exhibits better endosome escape ability and higher accumulation in nucleus than that loaded in non-H4R4 mixed one, confirmed by co-localization analysis. More importantly, the cytotoxicity of the nanoparticle is tunable by adjusting the amount of H4R4 mixed. This work provides us a new sight in the application of peptides. Peptide is versatile in functions and combination of two functional peptides is easy. We may have more multifunctional drug delivery systems in peptide-involved nanoparticles.

### Nucleic Acids

Nucleic acids are considered to be fragile due to their instability in physiological environments which contain DNase and RNase. It may seem impossible that nucleic acids could be used as pharmaceutical adjuvants to carry drugs, but the opposite has proved to be true. Compared to the common linear structure, engineered DNA structures can be very stable, and have been used to build nanoparticles for the past 30 years. DNA nanostructures have great potential in the areas of molecular and cellular biophysics, energy transfer and photonics, and diagnostics.<sup>172</sup> Recently, Ding and co-workers successfully applied "origami" DNA nanostructures, made of folded nucleic acid strands, to the drug delivery field (Fig. 7(D)).<sup>173</sup> The electrostatic attraction between DOX and DNA structure was subtly used in this work. The stability issue of DNA was also settled by converting linear strands into origami nanostructure. These self-assembled, spatially addressable, DNA origami nanostructures were very stable in cell lysates, and the DOX loading efficiency was high because the drug was non-covalently bound to the DNA through intercalation. The cellular uptake of DOX was increased by this DNA origami nanostructure, resulting in a better cell killing efficiency. Meanwhile, RNA nanotechnology has achieved rapid development in biomedicine applications in recent years. A packing RNA (pRNA) of bacteriophage phi29 DNA-packaging motor is developed by Guo and coworkers to work as a highly

efficient nanovector to carry siRNA (MT-IIA) for cancer therapy.<sup>174</sup> The pRNA/siRNA can protect the siRNA from RNase and keep stable in serum. The messenger RNA (mRNA) levels of MT-IIA and its downstream gene survivin were down-regulated by this pRNA/siRNA complex, resulting in suppressed cell proliferation. Furthermore, the dimmers that were obtained by tagging the pRNA/siRNA complex with folate can be delivered cell-specifically to ovarian cancer cells which express folate receptor. From both examples we can find that stability is the major problem for nucleic acids as pharmaceutical adjuvants. If this can be settled properly, DNA and RNA have a promising future as a potent tool for drug delivery.

### Other Organic Materials

Besides polymer, lipid, protein, peptide, and nucleic acid, saccharide is another important nanoscale pharmaceutical adjuvant materials. Cyclodextrins (CDs), a family of compounds made of saccharide molecules forming a ring structure, will be introduced as an outstanding saccharide. They are produced from starch by enzymatic conversion.<sup>175</sup> CDs are composed of 5 or more  $\alpha$ -D-glucopyranoside units and typical CDs are formed by 6–8 monomers in a cone shape, known as  $\alpha$ -CD (6 monomers),  $\beta$ -CD (7 monomers), and  $\gamma$ -CD (8 monomers) (Fig. 4).<sup>176</sup> Compared to chitosan and other polymers, CDs are commonly used as one of the most versatile aids in pharmaceutical technology to enhance the aqueous solubility and chemical stability of biologically active compounds.<sup>177</sup> Especially by using guest-host chemistry, CDs can introduce the guest functional groups to the host compounds. Ma et al. conjugated  $\beta$ -CDs to a branched PEI as a host unit.<sup>178</sup> Then a guest hydrophobic polymer poly( $\beta$ -benzyl *L*-aspartate) (PBLA) was introduced to the host scaffold to mediate the assembly process. The hydrophobic core formed by PBLA serves as a nanocarrier to load hydrophobic drugs, while the positively charged hydrophilic PEI shell is capable of condensing plasmid DNA and achieve its transfection *in vitro*. In this way CDs produce a new way of assembly, and can be used as a new generation of multifunctional nanocarriers.

## INORGANIC NANOSCALE MATERIALS AS POTENTIAL ADJUVANTS IN PHARMACEUTICS

### Silica

In the past decade, silica-based nanoparticles have attracted more and more attention as pharmaceutical adjuvants.<sup>179</sup> The biocompatibility of silica nanoparticles has also been thoroughly studied in different cell lines, and there is strong evidence that they are only toxic at a high dose.<sup>180</sup> Some recent results indicated that silica nanoparticles are biocompatible in mice after serological, hematological, and histopathological examinations of blood samples and tissues.<sup>181</sup>

### Silica Nanoparticles

The most well-developed of these silica-based nanoparticles are mesoporous silica nanoparticles (MSNs) because of their tailored mesoporous structure and high surface area.<sup>182–184</sup> Mesopores can be modified with different chemical groups to be hydrophobic or hydrophilic, enabling MSNs to encapsulate a variety of drugs. Meanwhile, high surface area allows a much higher drug loading capacity compared to that of solid nanoparticles.

By preferentially manipulating the biodistribution of encapsulated pharmaceutical agents in the target organ/tissue, MSN-based systems have the potential to deliver an effective concentration of drug to the lesion at a relatively low systemic drug dose. The adverse side-effects can therefore be minimized without compromising treatment efficacy. To accomplish this goal, the surface of MSNs can be modified with a variety of functional agents, such as polymers, proteins, and stimulus-responsive groups. These surface coatings work as gatekeepers to protect the pharmaceuticals inside the pores and achieve a controlled release.<sup>185, 186</sup>  $\beta$ -CD, a saccharide which is responsive to the acidic conditions within endosomes, was employed by Zink and co-workers to work as a nanovalve in MSNs for pH-sensitive drug release.<sup>187</sup> This nanovalve is tightly closed at pH 7.4 and acidic environment is the key to open the valve and release cargos. The leak and rapid burst of drug from nanoparticles are crucial problems for drug delivery and nanovalve is a good strategy to overcome these challenges. Mesopores can be sealed under physiological condition and release drug slowly under certain stimuli. Figure 8 shows three typical nanovalve-based controlled release mechanisms. Gatekeeper molecules are covalently attached to MSNs while plug molecules are then plugged into the gatekeepers through host–guest interaction. In some work only gatekeeper molecules are employed. Initially, cargo molecules are loaded in the channels of MSNs. Drug release can be initiated in three ways:

- (1) cutting off the covalent bonds between gatekeeper molecules and MSNs;
- (2) pulling out the plug molecules by interfering host–guest interaction;
- (3) destroying gatekeeper molecules.

These mechanisms can be designed to be responsive to various stimuli, including pH, light, thermal, ultrasound, oxygen stress, and several enzymes. It is a hot pursued area to develop smart drug delivery systems with nanovalves. Reversible and precisely controlled nanovalves will be the future trend.

MSNs are also good candidates for multifunctional nanoparticles. Nanoparticle-based drug delivery systems are confronting many challenges, including uptake by the RES, interaction with serum proteins, and poor accumulation at the disease site. Thus, researchers have concentrated much effort on integrating several functions into one particle and, as a result, many MSN-based multifunctional

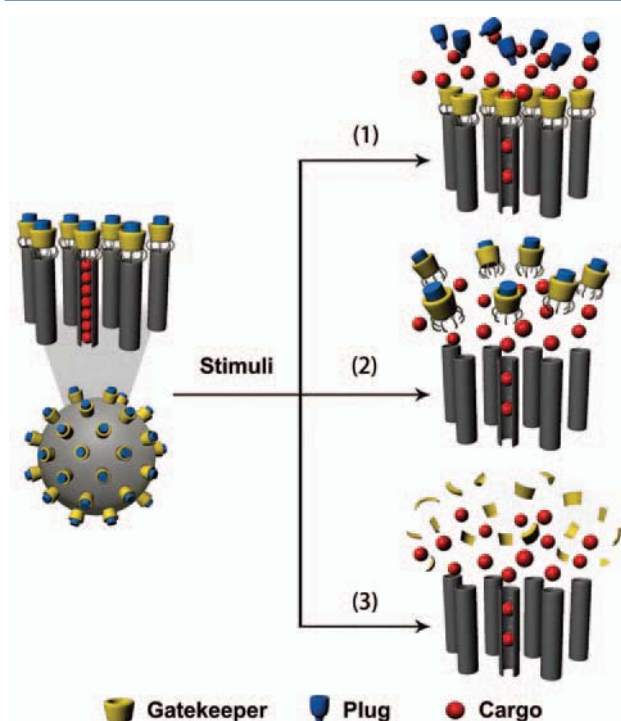


**Figure 8.** Schematic illustration of three different nanovalve-based stimuli-responsive controlled drug release mechanisms in MSNs.

nanoparticles have recently been developed.<sup>188–190</sup> Lin et al. functionalized MSNs with folate groups, the receptors of which are highly expressed in human cancer cells (Fig. 7(E)).<sup>191</sup> They demonstrated that the endocytosis of the modified nanoparticles is a receptor-mediated process and can be inhibited by free folic acid. Hyeon and co-workers reported functionalized MSNs that could be used for magnetic resonance imaging (MRI), fluorescence imaging, and drug delivery, thus combining therapeutic and diagnostic functions.<sup>192</sup> DOX was loaded into the pores and the particles were stabilized by coating with PEG to increase the circulation time. The anticancer effect of DOX-loaded nanoparticles was also observed *in vitro* and *in vivo*. In this work, both MRI and PEG coating are employed for integrated multifunction. MRI is superior than fluorescence imaging in clinical use because the latter will photobleach and the imaging depth is only a few millimeters. PEG is the best stealth delivery cover so far as introduced in the polymers section. MSN is a well-established integration platform on which multiple functions could be combined thanks to the versatility and compatibility of MSNs.

Compared to other adjuvant materials, MSNs are superior in various aspects: higher available surface area allows for more functionalization; tailored mesoporous structure provides sealed compartment for hydrophilic and hydrophobic cargos; strong adsorptive capacity results in higher drug loading; toxicity study and previous application as food additive stands for their biosafety. However,

we should also pay attention to the hydrolysis of MSNs' backbone (Si–O–Si) caused by acidic pH environment. In addition, unmodified silanol groups on MSNs will interact with red blood cell membrane and cause hemolysis.<sup>193</sup> Further modification of silanol groups and hemolysis test are needed before MSNs' intravenous injection in the pre-clinical development.

### Silica Nanotubes

Silica nanotube (SNT), a novel nanomaterial, has been developed for drug delivery,<sup>194</sup> biocatalysis,<sup>195</sup> and protein immobilization.<sup>196</sup> SNT has several advantages including large internal volume, large surface area, favorable biocompatibility, and the ability of being chemical modified.<sup>197</sup> More importantly, the size of SNT can be controlled easily.<sup>198</sup> Because of their unique physicochemical properties, SNT used as drug delivery system drew considerable attention from pharmaceuticals researchers in recently. SNT possesses the potential as effective drug delivery vehicle owing to

- (1) the large internal space of SNT can improve the drug loading capacity compared with other vectors. And the drug molecules incorporated in the inner of material cannot interact with the environment, so that the drug leakage was prevented until they reach the target destination;
- (2) SNT possesses a plentiful of hydroxide radical on the surface which lead to the high hydrophilicity of nanotubes. The drug delivered by SNT can effectively avoid the capture by the RES, and improve the bioavailability of drug molecules;
- (3) SNT can be further modified to acquire more functions through the active hydroxide radicals on the surface. Bhattacharyya and coworker reported the sol–gel template synthesized SNTs that can be applied for controlled drug delivery in which ultrasound acts as the trigger.<sup>194</sup>

In order to control drug delivery, SNTs were coated by dihydroxynaphthalene (DN) and ibuprofen was chose as a model drug. The ibuprofen loading of SNTs and DN-SNTs analyzed by thermogravimetric analysis was 46% and 25%, respectively. The release kinetics of ibuprofen from SNTs demonstrated that the drug release is heavily dependent on the ultrasound impulse *in vitro*. Fluorescent silica nanotubes prepared via sol–gel reaction were also successfully applied for plasmid DNA delivery.<sup>199</sup> This work further demonstrated that SNTs have enormous potential in biomolecule drug delivery.

### Gold

Among metal nanomaterials, those made of gold have been widely utilized in biomedical research. Gold nanomaterials have a variety of potential applications, including gene and drug delivery,<sup>200</sup> cell imaging,<sup>201</sup> phototherapy,<sup>202</sup> and colorimetric detection of biomolecules and ions.<sup>203–205</sup> Nowadays, the synthesis and modification of gold nanomaterials can be effectively manipulated, and spheroids,



rods, dodecahedra, octahedra, and cubes can be designed with a high level of precision.<sup>206</sup> The surface can also be modified with chemical functional groups, including amines, lipids, antibodies, peptides, oligonucleotides, and small molecules. In addition, the inherent non-toxicity and unique properties of gold nanomaterials, such as size- and shape-dependent cellular uptake and high surface area to volume ratio, make them excellent drug carriers.<sup>207</sup> Thus, considerable effort has been put in to develop gold nanomaterials as pharmaceutical adjuvants.

### Gold Nanoparticles

Gold nanoparticles (Au NPs) have many attributes which meet the needs of nanomedicine research. Many works have focused on the modification of Au NPs with therapeutic agents and targeting ligands. Liang and co-workers recently synthesized novel small (2 nm) Au NPs that were functionalized with a therapeutic peptide, PMI (p12), and a targeting peptide, CRGDK, which selectively binds with cancer cells through the over-expressed receptor NRP-1.<sup>208</sup> The results demonstrated that these targeting nanocarriers improve the delivery of the therapeutic p12 peptide, which is thought to activate p53, into cancer cells. When employing Au NPs as drug carriers, conjugation is commonly used for drug loading and ligand modification. The problem is that available chemical groups on the surface are limited, so it is difficult to functionalize Au NPs with both therapeutics and targeting ligands. This work employed 2 nm Au NPs, the surface area to volume ratio of which is much higher than that of commonly used Au NPs, to provide more space for drugs and functional groups.

### Gold Nanorods

The localized surface plasmon resonance (LSPR) effect is a widely utilized property of some special shaped gold nanomaterials, including nanorods, nanocages, nanoshells, and nanostars. Plasmon resonance occurs when gold nanomaterials are irradiated by light with specific wavelengths, and the luminous energy is converted into heat.<sup>209</sup> Direct killing of surrounding cells can be achieved by taking advantage of the heat released. This is called photothermal therapy. The heat released can also be further utilized to control the behavior of nanomaterials by introducing thermo-sensitive materials into them.<sup>210</sup> Therefore, many gold nanomaterial-based light-controlled drug release systems have been developed based on the LSPR effect. Moreover, the absorption of light with specific wavelengths can be utilized for *in vivo* imaging (Fig. 9).

Among these gold nanostructures with LSPR effect, Au NRs are an outstanding one due to two reasons: (1) the uniformity and size of Au NRs are easier to control than that of other materials; (2) by manipulating the aspect ratio, the LSPR maximum of Au NRs can be tuned to the near-infrared (NIR) window (700–900 nm), which is the wavelength range in which lasers can penetrate deeply through tissues.<sup>211</sup> Wu and co-workers reported promising

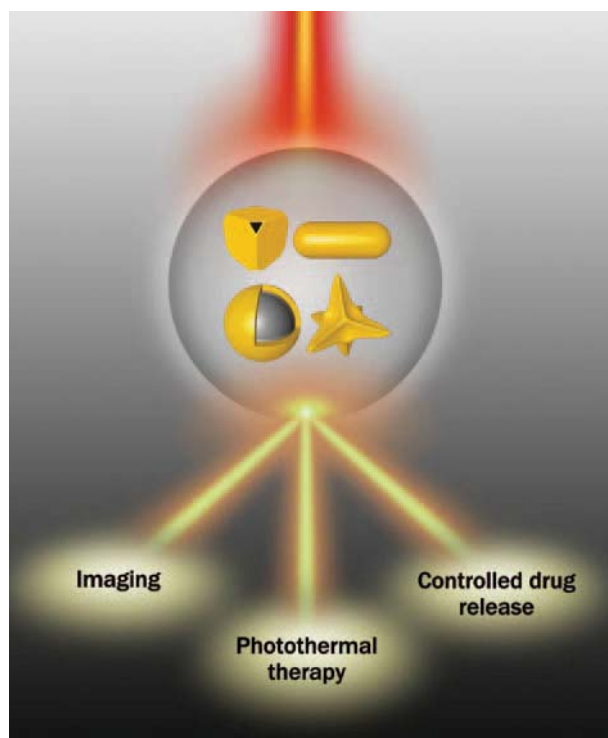


**Figure 9.** Applications of LSPR effect of gold nanostructures in pharmaceutical research.

results in this area (Figs. 7(F), (G)).<sup>212</sup> They coated light-responsive Au NRs with mesoporous silica to overcome two major disadvantages of Au NRs, namely low specific surface area and poor stability. DOX was encapsulated into the mesoporous silica shell of the Au@SiO<sub>2</sub> nanoparticles. Low intensity laser irradiation triggered drug release, while high intensity laser irradiation also triggered hyperthermia. Furthermore, the Au@SiO<sub>2</sub> nanoparticles can be visualized by two-photon microscopy, so that imaging is also successfully integrated into this platform. The advantage of Au NRs is that they can be used as drug vehicle, photothermal agent, and two-photon microscopy probe. Thus, Au NRs are an inherent multifunctional drug delivery system. However, low loading capacity and template residues caused toxicity impede their application as pharmaceutical adjuvant. This work successfully solved both challenges at the same time by mesoporous silica coating, the unique properties of Au NRs were also maintained and utilized.

Photothermal therapy is a unique application of gold nanomaterials as they are not just drug vehicles, also therapy agents. The irradiation area, time, and intensity are tunable and the killing effect is direct. Future work should focus on the targeting ability of photothermal therapy agents as the therapy efficacy is determined by the biodistribution of heat source. Moreover, gold is inert in most conditions and its degradation and clearance remains unclear. As a result, the accumulation and excretion mechanism of gold nanomaterials in cells, organs, and bodies needs further study.

### Other Gold Nanostructures

Other gold nanostructures, such as gold nanocages, gold nanoshells, and gold nanostars, are developed recently as photothermal therapy agent. Many work successfully combined photothermal therapy with imaging and drug delivery by employing these novel gold nanostructures.<sup>213, 214</sup> For, example, a NIR laser-controlled drug release system which was based on smart polymers covered gold nanocages was successfully developed by Xia et al. The smart polymer undergoes a phase transition from a hydrophilic state to a hydrophobic state when the temperature is raised above its low critical solution temperature (LCST). Once covalently anchored to the surface of gold nanocages, the smart polymer would undergo the phase transition and aggregate under the heat converted by gold nanocages after NIR laser irradiation. The pre-loaded drug, lysozyme, can therefore be released in a controllable fashion using photothermal conversion of gold nanocages. Furthermore, gold nanocages have a potential for multifunctional drug delivery system after functionalized with targeting ligands. Hollow gold nanostructures are superior in drug loading as it would be easier than that of Au NRs and Au NPs as drug will diffuse into the hollow structure when incubating with these gold nanostructures and no chemical reaction is needed. Moreover, hollow structure can provide more space compared to surface area. The biggest challenge is that the synthesis of these novel gold nanostructures is much more complicated than that of Au NRs and Au NPs. Thus, more efforts should be done to optimize the synthesis method and we believe that these gold nanostructures would become important members of gold-based nanoscale pharmaceutical adjuvant materials.

### Other Inorganic Materials

Apart from silica and gold, other inorganic nanomaterials, such as carbon,<sup>215</sup> iron,<sup>216–218</sup> and calcium,<sup>219</sup> also have been used as pharmaceutical adjuvants. Some of these have special applications in pharmaceutical adjuvant research. For example, calcium phosphate nanoparticles can work as vaccine adjuvants, inducing immunity to viruses.<sup>220</sup> Results indicated that calcium phosphate nanoparticles were more potent as vaccine adjuvant than traditional aluminium adjuvant because less inflammation was caused and high titer of antibody was induced. Graphene oxide, a novel carbon nanomaterial with monolayer structure, is promising in aromatic drug delivery via non-covalently  $\pi$ - $\pi$  stacking. SN38, a water-insoluble aromatic anticancer drug derived from camptothecin, is attached to graphene oxide by Dai and co-workers.<sup>221</sup> The obtained composite exhibited excellent water solubility while the anticancer efficacy was not compromised. Graphene oxide also showed potential in photothermal therapy, making it popular in novel medicine design.<sup>222</sup> Our previous work demonstrated that metallofullerene nanoparticles  $\text{Gd}@C_{82}(\text{OH})_{22}$ , another promising carbon-based nanomaterial, can circumvent tumor resistance to

cisplatin by reactivating endocytosis, which is a new strategy to fight with tumor drug resistance.<sup>223</sup> Further studies demonstrated that  $\text{Gd}@C_{82}(\text{OH})_{22}$  nanoparticles are inherently anticancer drug.<sup>224, 225</sup> They can inhibit pancreatic tumor metastasis by affecting matrix metalloproteinase-9 (MMP-9) function. Another potential pharmaceutical adjuvant material is superparamagnetic iron oxide nanoparticles (SPIONs) which are well-known as contrast agents.<sup>226</sup> Thus, SPIONs are appropriate for design of traceable drug delivery system. Tumor site accumulated SPIONs will enable to monitor the growth, metastasis, and location of tumor tissue. Following these established examples, inorganic nanomaterials can be used selectively to design drug vehicles with more functions.

## HYBRID ORGANIC AND INORGANIC NANOMATERIALS FOR PHARMACEUTICAL APPLICATION

Multifunctional nanoparticles, which are desired for advanced drug delivery, can be created by incorporating more than one nanomaterial into a nanostructure. These combined nanomaterials are known as hybrid nanomaterials, and they combine the advantages of each component. In another way, fatal drawbacks of one component are made up by the other one. Recently, thermal and pH dual responsive hybrid nanoparticle based on this strategy was successfully developed (Fig. 7(H)).<sup>227</sup> The hybrid nanoparticles had a  $\text{SiO}_2$  shell and a polymer core made of poly(N-isopropylacrylamide) (PNiPAM)-co-acrylic acid (AA) hydrogel, which is responsive to both heat and pH. By lowering the temperature, DOX was loaded into the nanoparticles and by manipulating the pH, DOX was rapidly released. Compared with traditional MSNs, these hybrid nanoparticles had a better uniformity and stability. Moreover, the *in vitro* results showed that these novel nanoparticles were more biocompatible and less toxic than conventional MSNs, while the anticancer efficiency was not compromised. In this work,  $\text{SiO}_2$  is employed as the drug container, but pH-responsive drug release could not be realized in pure silica system. As a result, pH-sensitive polymer is introduced as the core of the nanoparticle. This core-shell drug delivery system works like a tank:  $\text{SiO}_2$  shell is the armor, DOX is the cannonball, and PNiPAM/AA hydrogel is the fire control system. It cruises everywhere, resists attack from clearance system, and fires in the battlefield (slightly altered acidic tumor microenvironment and endosomes).

Theranostic, a new concept combines therapy and diagnostic, is emerging with the development of hybrid adjuvants.<sup>228, 229</sup> It is difficult to realize theranostic with only one adjuvant material. Therefore, hybrid adjuvants composed of more than one material are employed. For instance, after the drug-loaded nanoparticles are administered for therapeutic treatment, biodistribution of these



nanoparticles is expected to be monitored in organs and disease site. In this case, fluorescence probes or MRI contrast agents can be integrated into the drug vehicle. The labeled hybrid nanoparticles are then monitored non-invasively throughout the treatment and researchers can get more information from a single injection.

Actually, most examples we mentioned in this article are hybrid materials but only one component is discussed in detail in individual context. It is a trend to combine more functions in one nanoparticle, resulting in the widely application of hybrid nanomaterials. Although it is fascinating to design multifunctional drug delivery system with hybrid nanomaterials, there are two disadvantages under consideration in application. First, the preparation will become complicated compared to that of single-component nanoparticles, resulting in the reduction of reproducibility. Second, the drug release pathway and metabolism mechanism will be unclear after the addition of another material. Both of them are of great importance for pharmaceutical adjuvants. Therefore, every aspect of hybrid materials should be thoroughly studied.

## CONCLUSIONS

Recent progress reveals the great potential of nanoscale materials as novel pharmaceutical adjuvants. Nanomaterials are capable of transporting insoluble drugs in aqueous solution, reducing adverse side-effects, delivering dual therapeutic agents simultaneously, targeting drugs to disease lesions and controlling drug release in the desired environment. However, despite the enormous potential of nanoscale materials, considerable challenges must be addressed before they can be translated into clinical use. Pharmaceutical adjuvants must fulfill specific criteria, like biocompatibility, stability in physicochemical conditions, protection of active drugs, and low toxicity, in order to meet the requirements of the FDA. In addition, these materials should be reproducible in a scalable manner with high purity and low cost. Most reported nanomaterials are synthesized and modified in small batches. Standard protocols must be provided for industrial-scale production of nanoscale pharmaceutical adjuvant materials. Comprehensive assessment of the biosafety issues of nanomaterials, such as biocompatibility, biodegradation and biodistribution, should also be provided. Drug delivery mechanisms should be further studied for a better understanding of pharmacodynamics and pharmacokinetics of different nanocarriers. As far as we know, size, shape, charge, functional groups, and other properties of nanomaterials all have an impact on their interaction with biosystems. We need to understand the role played by each property, so that the pharmacological attributes of nanomaterials can be optimized. Nowadays, many scientists are working hard to overcome these challenges and we are sure that nanoscale materials have a bright future as pharmaceutical adjuvants.

**Acknowledgments:** This work was supported by the Chinese Natural Science Foundation project (Nos. 30970784, 81171455), a National Distinguished Young Scholars grant (31225009) from the National Natural Science Foundation of China, the National Key Basic Research Program of China (2009CB930200), the Chinese Academy of Sciences (CAS) “Hundred Talents Program” (07165111ZX), the CAS Knowledge Innovation Program and the State High-Tech Development Plan (2012AA020804). The authors also appreciate the support by the “Strategic Priority Research Program” of the Chinese Academy of Sciences, Grant No. XDA09030301. This work was also supported in part by NIH/NIMHD 8 G12 MD007597, and USAMRMC W81XWH-10-1-0767 grants.

## REFERENCES

1. P. Horcajada, T. Chalati, C. Serre, B. Gillet, C. Sebrie, T. Baati, J.F. Eubank, D. Heurtaux, P. Clayette, and C. Kreuz, Porous metal-organic-framework nanoscale carriers as a potential platform for drug delivery and imaging. *Nat. Mater.* 9, 172 (2009).
2. M. Liong, J. Lu, M. Kovochich, T. Xia, S. G. Ruehm, A. E. Nel, F. Tamanoi, and J. I. Zink, Multifunctional inorganic nanoparticles for imaging, targeting, and drug delivery. *ACS Nano* 2, 889 (2008).
3. O. C. Farokhzad and R. Langer, Impact of nanotechnology on drug delivery. *ACS Nano* 3, 16 (2009).
4. I. I. Slowing, J. L. Vivero-Escoto, C.-W. Wu, and V. S.-Y. Lin, Mesoporous silica nanoparticles as controlled release drug delivery and gene transfection carriers. *Adv. Drug Delivery Rev.* 60, 1278 (2008).
5. A. J. Cole, A. E. David, J. Wang, C. J. Galbán, and V. C. Yang, Magnetic brain tumor targeting and biodistribution of long-circulating PEG-modified, cross-linked starch-coated iron oxide nanoparticles. *Biomaterials* 32, 6291 (2011).
6. H. Otsuka, Y. Nagasaki, and K. Kataoka, PEGylated nanoparticles for biological and pharmaceutical applications. *Adv. Drug Delivery Rev.* 64, 246 (2012).
7. Y. Matsumura and H. Maeda, A new concept for macromolecular therapeutics in cancer chemotherapy: Mechanism of tumorotropic accumulation of proteins and the antitumor agent smancs. *Cancer Res.* 46, 6387 (1986).
8. H. Maeda, The enhanced permeability and retention (EPR) effect in tumor vasculature: The key role of tumor-selective macromolecular drug targeting. *Adv. Enzyme Regul.* 41, 189 (2001).
9. M. Pileni, Control of the size and shape of inorganic nanocrystals at various scales from nano to macrodomains. *J. Phys. Chem. C* 111, 9019 (2007).
10. Z.-A. Qiao, B. Guo, A. J. Binder, J. Chen, G. M. Veith, and S. Dai, Controlled synthesis of mesoporous carbon nanostructures via a “silica-assisted” strategy. *Nano Lett.* 13, 207 (2012).
11. H. S. Nalwa (ed.), Encyclopedia of Nanoscience and Nanotechnology, American Scientific Publishers, Los Angeles, CA (2004/2011), Vols. 1–25.
12. R. P. Bagwe, L. R. Hilliard, and W. Tan, Surface modification of silica nanoparticles to reduce aggregation and nonspecific binding. *Langmuir* 22, 4357 (2006).
13. Y. Zhang, N. Kohler, and M. Zhang, Surface modification of superparamagnetic magnetite nanoparticles and their intracellular uptake. *Biomaterials* 23, 1553 (2002).
14. H. S. Nalwa (ed.), Handbook of Nanostructured Materials and Nanotechnology, Academic Press, San Diego, CA (2000), Vols. 1–5.

15. K. Na, K. H. Lee, D. H. Lee, and Y. H. Bae, Biodegradable thermo-sensitive nanoparticles from poly(*L*-lactic acid)/poly(ethylene glycol) alternating multi-block copolymer for potential anti-cancer drug carrier. *Eur. J. Pharm. Sci.* 27, 115 (2006).
16. B. Yan, J.-C. Boyer, N. R. Branda, and Y. Zhao, Near-infrared light-triggered dissociation of block copolymer micelles using upconverting nanoparticles. *J. Am. Chem. Soc.* 133, 19714 (2011).
17. T. Sonia and C. P. Sharma, pH sensitive thiolated cationic hydrogel for oral insulin delivery. *J. Biomed. Nanotechnol.* 10, 642 (2014).
18. C. Y. Lai, B. G. Trewyn, D. M. Jeftinija, K. Jeftinija, S. Xu, S. Jeftinija, and V. S. Y. Lin, A mesoporous silica nanosphere-based carrier system with chemically removable CdS nanoparticle caps for stimuli-responsive controlled release of neurotransmitters and drug molecules. *J. Am. Chem. Soc.* 125, 4451 (2003).
19. S. Dhar, F. X. Gu, R. Langer, O. C. Farokhzad, and S. J. Lippard, Targeted delivery of cisplatin to prostate cancer cells by aptamer functionalized Pt (IV) prodrug-PLGA-PEG nanoparticles. *Proc. Natl. Acad. Sci. USA* 105, 17356 (2008).
20. S. Mitra, U. Gaur, P. Ghosh, and A. Maitra, Tumour targeted delivery of encapsulated dextran-doxorubicin conjugate using chitosan nanoparticles as carrier. *J. Control Release* 74, 317 (2001).
21. L. Sandiford, A. Phinikaridou, A. Protti, L. K. Meszaros, X. Cui, Y. Yan, G. Frodsham, P. A. Williamson, N. Gaddum, and R. M. Botnar, Bisphosphonate-anchored PEGylation and radiolabeling of superparamagnetic iron oxide: Long-circulating nanoparticles for *in vivo* multimodal ( $T_1$  MRI-SPECT) imaging. *ACS Nano* 7, 500 (2012).
22. I. Brigger, C. Dubernet, and P. Couvreur, Nanoparticles in cancer therapy and diagnosis. *Adv. Drug Delivery Rev.* 64, 24 (2012).
23. S. Acharya and S. K. Sahoo, PLGA nanoparticles containing various anticancer agents and tumour delivery by EPR effect. *Adv. Drug Delivery Rev.* 63, 170 (2011).
24. T. Wei, J. Liu, H. Ma, Q. Cheng, Y. Huang, J. Zhao, S. Huo, X. Xue, Z. Liang, and X.-J. Liang, Functionalized nanoscale micelles improve drug delivery for cancer therapy *in vitro* and *in vivo*. *Nano Lett.* 13, 2528 (2013).
25. J. M. Stephenson, S. Banerjee, N. K. Saxena, R. Cherian, and S. K. Banerjee, Neuropilin-1 is differentially expressed in myoepithelial cells and vascular smooth muscle cells in preneoplastic and neoplastic human breast: A possible marker for the progression of breast cancer. *Int. J. Cancer* 101, 409 (2002).
26. S. Soker, S. Takashima, H.Q. Miao, G. Neufeld, and M. Klagsbrun, Neuropilin-1 is expressed by endothelial and tumor cells as an isoform-specific receptor for vascular endothelial growth factor. *Cell* 92, 735 (1998).
27. A. M. Jubb, L. A. Strickland, S. D. Liu, J. Mak, M. Schmidt, and H. Koepfen, Neuropilin-1 expression in cancer and development. *J. Pathol.* 226, 50 (2012).
28. K. N. Sugahara, T. Teesalu, P. P. Karmali, V. R. Kotamraju, L. Agemy, O. M. Girard, D. Hanahan, R. F. Mattrey, and E. Ruoslahti, Tissue-penetrating delivery of compounds and nanoparticles into tumors. *Cancer Cell* 16, 510 (2009).
29. K. Westesen, H. Bunjes, and M. Koch, Physicochemical characterization of lipid nanoparticles and evaluation of their drug loading capacity and sustained release potential. *J. Control Release* 48, 223 (1997).
30. J. Lu, M. Liong, J. I. Zink, and F. Tamanoi, Mesoporous silica nanoparticles as a delivery system for hydrophobic anticancer drugs. *Small* 3, 1341 (2007).
31. R. van Sluis, Z. M. Bhujwalla, N. Raghunand, P. Ballesteros, J. Alvarez, S. Cerdan, J.-P. Galons, and R. J. Gillies, *In vivo* imaging of extracellular pH using  $^1\text{H}$  MRSI. *Magn. Reson. Med.* 41, 743 (1999).
32. K. Engin, D. Leeper, J. Cater, A. Thistlethwaite, L. Tupchong, and J. McFarlane, Extracellular pH distribution in human tumours. *Int. J. Hyperthermia* 11, 211 (1995).
33. R. B. Weiss, R. Donehower, P. Wiernik, T. Ohnuma, R. Gralla, D. Trump, J. Baker, Jr, D. Van Echo, D. Von Hoff, and B. Leyland-Jones, Hypersensitivity reactions from taxol. *J. Clin. Oncol.* 8, 1263 (1990).
34. M. Green, G. Manikhas, S. Orlov, B. Afanasyev, A. Makhson, P. Bhar, and M. Hawkins, Abraxane<sup>®</sup>, a novel Cremophor<sup>®</sup>-free, albumin-bound particle form of paclitaxel for the treatment of advanced non-small-cell lung cancer. *Ann. Oncol.* 17, 1263 (2006).
35. J. P. Michal, B. H. Goldstein, C. L. Birk, M. A. Rettenmaier, and J. V. Brown, III, Abraxane in the treatment of ovarian cancer: The absence of hypersensitivity reactions. *Gynecol. Oncol.* 100, 437 (2006).
36. P. Rivera-Gil, D. J. De Aberasturi, V. Wulf, B. Pelaz, P. Del Pino, Y. Zhao, J. M. De La Fuente, I. R. De Larramendi, T. Rojo, and X. J. Liang, The challenge to relate the physicochemical properties of colloidal nanoparticles to their cytotoxicity. *Acc. Chem. Res.* (2012).
37. X. Yang, A. P. Gondikas, S. M. Marinakos, M. Auffan, J. Liu, H. Hsu-Kim, and J. N. Meyer, Mechanism of silver nanoparticle toxicity is dependent on dissolved silver and surface coating in *Caenorhabditis elegans*. *Environ. Sci. Technol.* 46, 1119 (2011).
38. Y. Pan, S. Neuss, A. Leifert, M. Fischler, F. Wen, U. Simon, G. Schmid, W. Brandau, and W. Jahnke-Dechent, Size-dependent cytotoxicity of gold nanoparticles. *Small* 3, 1941 (2007).
39. D. Napierska, L. C. Thomassen, V. Rabolli, D. Lison, L. Gonzalez, M. Kirsch-Volders, J. A. Martens, and P. H. Hoet, Size-dependent cytotoxicity of monodisperse silica nanoparticles in human endothelial cells. *Small* 5, 846 (2009).
40. S. Singh and H. S. Nalwa, Nanotechnology and health safety toxicity and risk assessments of nanostructured materials on human health. *J. Nanosci. Nanotechnol.* 7, 3048 (2007).
41. Y. L. Zhao and H. S. Nalwa (eds.), Nanotoxicology: Interactions of Nanomaterials with Biological Systems, American Scientific Publishers, Los Angeles, CA (2007).
42. O. Lyass, B. Uziely, R. Ben-Yosef, D. Tzemach, N. I. Heshing, M. Lotem, G. Brufman, and A. Gabizon, Correlation of toxicity with pharmacokinetics of pegylated liposomal doxorubicin (Doxil) in metastatic breast carcinoma. *Cancer* 89, 1037 (2000).
43. E. Miele, G. P. Spinelli, E. Miele, F. Tomao, and S. Tomao, Albumin-bound formulation of paclitaxel (Abraxane<sup>®</sup> ABI-007) in the treatment of breast cancer. *Int. J. Nanomed.* 4, 99 (2009).
44. E. E. Connor, J. Mwamuka, A. Gole, C. J. Murphy, and M. D. Wyatt, Gold nanoparticles are taken up by human cells but do not cause acute cytotoxicity. *Small* 1, 325 (2005).
45. C. Zhou, M. Long, Y. Qin, X. Sun, and J. Zheng, Luminescent gold nanoparticles with efficient renal clearance. *Angew. Chem. Int. Ed.* 123, 3226 (2011).
46. J.-H. Park, L. Gu, G. von Maltzahn, E. Ruoslahti, S. N. Bhatia, and M. J. Sailor, Biodegradable luminescent porous silicon nanoparticles for *in vivo* applications. *Nat. Mater.* 8, 331 (2009).
47. T. K. Jain, M. K. Reddy, M. A. Morales, D. L. Leslie-Pelecky, and V. Labhasetwar, Biodistribution, clearance, and biocompatibility of iron oxide magnetic nanoparticles in rats. *Mol. Pharm.* 5, 316 (2008).
48. J. J. Li, S.-L. Lo, C.-T. Ng, R. L. Gurung, D. Hartono, M. P. Hande, C.-N. Ong, B.-H. Bay, and L.-Y. L. Yung, Genomic instability of gold nanoparticle treated human lung fibroblast cells. *Biomaterials* 32, 5515 (2011).
49. K. Ganguly, S. Upadhyay, M. Irmeler, S. Takenaka, K. Pukelsheim, J. Beckers, M. H. De Angelis, E. Hamelmann, T. Stoeger, and H. Schulz, Impaired resolution of inflammatory response in the lungs of JF1/Msf mice following carbon nanoparticle instillation. *Respir. Res.* 12, 1 (2011).
50. Y. Ge, M. Bruno, K. Wallace, W. Winnik, and R. Y. Prasad, Proteome profiling reveals potential toxicity and detoxification pathways following exposure of BEAS-2B cells to engineered nanoparticle titanium dioxide. *Proteomics* 11, 2406 (2011).

51. S. Sershen, S. Westcott, N. Halas, and J. West, Temperature-sensitive polymer-nanoshell composites for photothermally modulated drug delivery. *J. Biomed. Mater. Res.* 51, 293 (2000).
52. Y. Bae, S. Fukushima, A. Harada, and K. Kataoka, Design of environment-sensitive supramolecular assemblies for intracellular drug delivery: Polymeric micelles that are responsive to intracellular pH change. *Angew. Chem. Int. Ed.* 42, 4640 (2003).
53. N. Fomina, C. McFearn, M. Sermsakdi, O. Edigin, and A. Almutairi, UV and near-IR triggered release from polymeric nanoparticles. *J. Am. Chem. Soc.* 132, 9540 (2010).
54. K. S. Soppimath, T. M. Aminabhavi, A. R. Kulkarni, and W. E. Rudzinski, Biodegradable polymeric nanoparticles as drug delivery devices. *J. Control Release* 70, 1 (2001).
55. L. Y. Qiu and Y. H. Bae, Polymer architecture and drug delivery. *Pharm. Res.* 23, 1 (2006).
56. D. G. Anderson, W. Peng, A. Akinc, N. Hossain, A. Kohn, R. Padera, R. Langer, and J. A. Sawicki, A polymer library approach to suicide gene therapy for cancer. *Proc. Natl. Acad. Sci. USA* 101, 16028 (2004).
57. J. M. Bennis, J.-S. Choi, R. I. Mahato, J.-S. Park, and S. W. Kim, pH-sensitive cationic polymer gene delivery vehicle: *N*-Ac-poly (*L*-histidine)-graft-poly (*L*-lysine) comb shaped polymer. *Bioconjugate Chem.* 11, 637 (2000).
58. G. Tiram, A. Scomparin, P. Ofek, and R. Satchi-Fainaro, Interfering cancer with polymeric siRNA nanomedicines. *J. Biomed. Nanotechnol.* 10, 50 (2014).
59. H. M. Xiong, Y. Xu, Q. G. Ren, and Y. Y. Xia, Stable aqueous ZnO@polymer core-shell nanoparticles with tunable photoluminescence and their application in cell imaging. *J. Am. Chem. Soc.* 130, 7522 (2008).
60. K. Li, J. Pan, S. S. Feng, A. W. Wu, K. Y. Pu, Y. Liu, and B. Liu, Generic strategy of preparing fluorescent conjugated-polymer-loaded poly(DL-lactide-co-glycolide) nanoparticles for targeted cell imaging. *Adv. Funct. Mater.* 19, 3535 (2009).
61. A. S. Wadajkar, J. U. Menon, and K. T. Nguyen, Polymer-coated magnetic nanoparticles for cancer diagnosis and therapy. *Rev. Nanosci. Nanotechnol.* 1, 284 (2012).
62. J. M. Dang and K. W. Leong, Natural polymers for gene delivery and tissue engineering. *Adv. Drug Delivery Rev.* 58, 487 (2006).
63. L. S. Nair and C. T. Laurencin, Biodegradable polymers as biomaterials. *Prog. Polym. Sci.* 32, 762 (2007).
64. J. Zhang, W. Xia, P. Liu, Q. Cheng, T. Tah, W. Gu, and B. Li, Chitosan modification and pharmaceutical/biomedical applications. *Mar. Drugs* 8, 1962 (2010).
65. J. H. Park, G. Saravanakumar, K. Kim, and I. C. Kwon, Targeted delivery of low molecular drugs using chitosan and its derivatives. *Adv. Drug Delivery Rev.* 62, 28 (2010).
66. P. J. VandeVord, H. W. Matthew, S. P. DeSilva, L. Mayton, B. Wu, and P. H. Wooley, Evaluation of the biocompatibility of a chitosan scaffold in mice. *J. Biomed. Mater. Res.* 59, 585 (2002).
67. J. P. Kumar, L. Lakshmi, V. Jyothsna, D. Balaji, S. Saravanan, A. Moorthi and N. Selvamurugan, Synthesis and characterization of diopside particles and their suitability along with chitosan matrix for bone tissue engineering *in vitro* and *in vivo*. *J. Biomed. Nanotechnol.* 10, 970 (2014).
68. S. P. Victor, W. Paul, and C. P. Sharma, Chitosan self-aggregates and micelles in drug delivery. *J. Nanopharm. Drug Deliv.* 1, 193 (2013).
69. T. Kean and M. Thanou, Biodegradation, biodistribution and toxicity of chitosan. *Adv. Drug Delivery Rev.* 62, 3 (2010).
70. Z. Ma, T. M. Lim, and L.-Y. Lim, Pharmacological activity of peroral chitosan-insulin nanoparticles in diabetic rats. *Int. J. Pharm.* 293, 271 (2005).
71. K. A. Janes, M. P. Fresneau, A. Marazuela, A. Fabra, and M. A. J. Alonso, Chitosan nanoparticles as delivery systems for doxorubicin. *J. Control Release* 73, 255 (2001).
72. J.-H. Kim, Y.-S. Kim, K. Park, S. Lee, H. Y. Nam, K. H. Min, H. G. Jo, J. H. Park, K. Choi, and S. Y. Jeong, Antitumor efficacy of cisplatin-loaded glycol chitosan nanoparticles in tumor-bearing mice. *J. Control. Release* 127, 41 (2008).
73. H.-Y. Hwang, I.-S. Kim, I. C. Kwon, and Y.-H. Kim, Tumor targetability and antitumor effect of docetaxel-loaded hydrophobically modified glycol chitosan nanoparticles. *J. Control Release* 128, 23 (2008).
74. T. H. Kim, I. K. Park, J. W. Nah, Y. J. Choi, and C. S. Cho, Galactosylated chitosan/DNA nanoparticles prepared using water-soluble chitosan as a gene carrier. *Biomaterials* 25, 3783 (2004).
75. C. Qin, Y. Du, L. Xiao, Z. Li, and X. Gao, Enzymic preparation of water-soluble chitosan and their antitumor activity. *Int. J. Biol. Macromol.* 31, 111 (2002).
76. B. Shi, Z. Shen, H. Zhang, J. Bi, and S. Dai, Exploring *N*-imidazolyl-*O*-carboxymethyl chitosan for high performance gene delivery. *Biomacromolecules* 13, 146 (2011).
77. X. Jin, R. Mo, Y. Ding, W. Zheng, and C. Zhang, Paclitaxel-loaded *N*-octyl-*O*-sulfate chitosan micelles for superior cancer therapeutic efficacy and overcoming drug resistance. *Mol. Pharm.* 11, 145 (2014).
78. C. Zhang, G. Qu, Y. Sun, X. Wu, Z. Yao, Q. Guo, Q. Ding, S. Yuan, Z. Shen, and Q. Ping, Pharmacokinetics, biodistribution, efficacy and safety of *N*-octyl-*O*-sulfate chitosan micelles loaded with paclitaxel. *Biomaterials* 29, 1233 (2008).
79. A. Persidis, Cancer multidrug resistance. *Nat. Biotechnol.* 17, 94 (1999).
80. S.-F. Zhou, Structure, function and regulation of *P*-glycoprotein and its clinical relevance in drug disposition. *Xenobiotica* 38, 802 (2008).
81. P. A. Gunatillake and R. Adhikari, Biodegradable synthetic polymers for tissue engineering. *Eur. Cells Mater.* 5, 1 (2003).
82. Y. Liu, C. Liu, M. Li, F. Liu, L. Feng, L. Zhang, and N. Zhang, Polymer-polymer conjugation to fabricate multi-block polymer as novel drug carriers: Poly(lactic acid)-poly(ethylene glycol)-poly(*L*-lysine) to enhance paclitaxel target delivery. *J. Biomed. Nanotechnol.* 10, 948 (2014).
83. N. Nasongkla, E. Bey, J. Ren, H. Ai, C. Khemtong, J. S. Guthi, S.-F. Chin, A. D. Sherry, D. A. Boothman, and J. Gao, Multifunctional polymeric micelles as cancer-targeted, MRI-ultrasensitive drug delivery systems. *Nano Lett.* 6, 2427 (2006).
84. P. A. Bertin, J. M. Gibbs, C. K.-F. Shen, C. S. Thaxton, W. A. Russin, C. A. Mirkin, and S. T. Nguyen, Multifunctional polymeric nanoparticles from diverse bioactive agents. *J. Am. Chem. Soc.* 128, 4168 (2006).
85. J.-H. Kim, R. D. Burnett, and A. Gabriel, Stimuli-responsive hollow polymer nanoparticles for use as novel delivery systems. *J. Biomed. Nanotechnol.* 8, 432 (2012).
86. R. Löbenberg, L. Araujo, H. von Briesen, E. Rodgers, and J. Kreuter, Body distribution of azidothymidine bound to hexylcyanoacrylate nanoparticles after iv injection to rats. *J. Control Release* 50, 21 (1998).
87. J. V. Jokerst, T. Lobovkina, R. N. Zare, and S. S. Gambhir, Nanoparticle PEGylation for imaging and therapy. *Nanomedicine* 6, 715 (2011).
88. S. N. Alconcel, A. S. Baas, and H. D. Maynard, FDA-approved poly (ethylene glycol)-protein conjugate drugs. *Polym. Chem.* 2, 1442 (2011).
89. Y.-P. Li, Y.-Y. Pei, X.-Y. Zhang, Z.-H. Gu, Z.-H. Zhou, W.-F. Yuan, J.-J. Zhou, J.-H. Zhu, and X.-J. Gao, PEGylated PLGA nanoparticles as protein carriers: Synthesis, preparation and biodistribution in rats. *J. Control Release* 71, 203 (2001).
90. G. von Maltzahn, J.-H. Park, A. Agrawal, N. K. Bandaru, S. K. Das, M. J. Sailor, and S. N. Bhatia, Computationally guided photothermal tumor therapy using long-circulating gold nanorod antennas. *Cancer Res.* 69, 3892 (2009).



91. G. Prencipe, S. M. Tabakman, K. Welsher, Z. Liu, A. P. Goodwin, L. Zhang, J. Henry, and H. Dai, PEG branched polymer for functionalization of nanomaterials with ultralong blood circulation. *J. Am. Chem. Soc.* 131, 4783 (2009).
92. M. M. van Schooneveld, E. Vucic, R. Koole, Y. Zhou, J. Stocks, D. P. Cormode, C. Y. Tang, R. E. Gordon, K. Nicolay, and A. Meijerink, Improved biocompatibility and pharmacokinetics of silica nanoparticles by means of a lipid coating: A multimodality investigation. *Nano Lett.* 8, 2517 (2008).
93. B. Thierry, L. Zimmer, S. McNiven, K. Finnie, C. Barbei, and H. J. Griesser, Electrostatic self-assembly of PEG copolymers onto porous silica nanoparticles. *Langmuir* 24, 8143 (2008).
94. J. M. Chan, L. Zhang, K. P. Yuet, G. Liao, J.-W. Rhee, R. Langer, and O. C. Farokhzad, PLGA–lecithin–PEG core–shell nanoparticles for controlled drug delivery. *Biomaterials* 30, 1627 (2009).
95. R. A. Jain, The manufacturing techniques of various drug loaded biodegradable poly(lactide-co-glycolide) (PLGA) devices. *Biomaterials* 21, 2475 (2000).
96. P. C. Naha, H. J. Byrne, and A. K. Panda, Role of polymeric excipients on controlled release profile of Glipizide from PLGA and Eudragit RS 100 Nanoparticles. *J. Nanopharm. Drug Deliv.* 1, 74 (2013).
97. M. Durán-Lobato, I. Muñoz-Rubio, M.Á. Holgado, J. Álvarez-Fuentes, M. Fernández-Arévalo, and L. Martín-Banderas, Enhanced cellular uptake and biodistribution of a synthetic cannabinoid loaded in surface-modified poly(lactic-co-glycolic acid) nanoparticles. *J. Biomed. Nanotechnol.* 10, 1068 (2014).
98. P. Xu, E. Gullotti, L. Tong, C. B. Highley, D. R. Errabelli, T. Hasan, J.-X. Cheng, D. S. Kohane, and Y. Yeo, Intracellular drug delivery by poly (lactic-co-glycolic acid) nanoparticles, revisited. *Mol. Pharm.* 6, 190 (2008).
99. Y. Yamaguchi, M. Takenaga, A. Kitagawa, Y. Ogawa, Y. Mizushima, and R. Igarashi, Insulin-loaded biodegradable PLGA microcapsules: Initial burst release controlled by hydrophilic additives. *J. Control Release* 81, 235 (2002).
100. M. S. Yavuz, Y. Cheng, J. Chen, C. M. Cobley, Q. Zhang, M. Rycenga, J. Xie, C. Kim, K. H. Song, and A. G. Schwartz, Gold nanocages covered by smart polymers for controlled release with near-infrared light. *Nat. Mater.* 8, 935 (2009).
101. H. Wei, S.-X. Cheng, X.-Z. Zhang, and R.-X. Zhuo, Thermosensitive polymeric micelles based on poly (*N*-isopropylacrylamide) as drug carriers. *Prog. Polym. Sci.* 34, 893 (2009).
102. H. J. Kim, H. Matsuda, H. Zhou, and I. Honma, Ultrasound-triggered smart drug release from a poly(dimethylsiloxane)–mesoporous silica composite. *Adv. Mater.* 18, 3083 (2006).
103. M. Quesada, C. Muniesa, and P. Botella, Hybrid PLGA–organosilica nanoparticles with redox-sensitive molecular gates. *Chem. Mater.* 25, 2597 (2013).
104. M. J. Geisow and W. H. Evans, pH in the endosome: Measurements during pinocytosis and receptor-mediated endocytosis. *Exp. Cell. Res.* 150, 36 (1984).
105. E. M. Bachelder, T. T. Beaudette, K. E. Broaders, J. Dashe, and J. M. J. Freichet, Acetal-derivatized dextran: An acid-responsive biodegradable material for therapeutic applications. *J. Am. Chem. Soc.* 130, 10494 (2008).
106. X. Hu, Y. Ji, M. Wang, F. Miao, H. Ma, H. Shen, and N. Jia, Water-soluble and biocompatible MnO@PVP nanoparticles for MR imaging *in vitro* and *in vivo*. *J. Biomed. Nanotechnol.* 9, 976 (2013).
107. F. Fischer and S. Bauer, Polyvinylpyrrolidon. Ein tausendsassa in der chemie. *Chem. unserer Zeit* 43, 376 (2009).
108. X. Zhi, H. Fang, C. Bao, G. Shen, J. Zhang, K. Wang, S. Guo, T. Wan, and D. Cui, The immunotoxicity of graphene oxides and the effect of PVP-coating. *Biomaterials* 34, 5254 (2013).
109. T. Aarthi, M. Shaama, and G. Madras, Degradation of water soluble polymers under combined ultrasonic and ultraviolet radiation. *Ind. Eng. Chem. Res.* 46, 6204 (2007).
110. K. Ciftci and R. J. Levy, Enhanced plasmid DNA transfection with lysosomotropic agents in cultured fibroblasts. *Int. J. Pharm.* 218, 81 (2001).
111. A. Saxena, S. Mozumdar, and A. K. Johri, Ultra-low sized cross-linked polyvinylpyrrolidone nanoparticles as non-viral vectors for *in vivo* gene delivery. *Biomaterials* 27, 5596 (2006).
112. R. J. Hickey, A. S. Haynes, J. M. Kikkawa, and S.-J. Park, Controlling the self-assembly structure of magnetic nanoparticles and amphiphilic block-copolymers: From micelles to vesicles. *J. Am. Chem. Soc.* 133, 1517 (2011).
113. H. Wang, Y. Zhao, Y. Wu, Y.-I. Hu, K. Nan, G. Nie, and H. Chen, Enhanced anti-tumor efficacy by co-delivery of doxorubicin and paclitaxel with amphiphilic methoxy PEG-PLGA copolymer nanoparticles. *Biomaterials* 32, 8281 (2011).
114. Z. L. Tyrrell, Y. Shen, and M. Radosz, Fabrication of micellar nanoparticles for drug delivery through the self-assembly of block copolymers. *Prog. Polym. Sci.* 35, 1128 (2010).
115. S. Guo, Y. Huang, T. Wei, W. Zhang, W. Wang, D. Lin, X. Zhang, A. Kumar, Q. Du, and X. J. Liang, Amphiphilic and biodegradable methoxy polyethylene glycol-block-(polycaprolactone-graft-poly(2-(dimethylamino) ethyl methacrylate)) as an effective gene carrier. *Biomaterials* 32, 879 (2011).
116. S. Li, B. Goins, L. Zhang, and A. Bao, Novel multifunctional theranostic liposome drug delivery system: Construction, characterization, and multimodality MR, near-infrared fluorescent, and nuclear imaging. *Bioconjugate Chem.* 23, 1322 (2012).
117. R. Hu, W.-C. Law, G. Lin, L. Ye, J. Liu, J. Liu, J. L. Reynolds, and K.-T. Yong, PEGylated phospholipid micelle-encapsulated near-infrared PbS quantum dots for *in vitro* and *in vivo* bioimaging. *Theranostics* 2, 723 (2012).
118. W. T. Al-Jamal and K. Kostarelos, Liposomes: From a clinically established drug delivery system to a nanoparticle platform for theranostic nanomedicine. *Acc. Chem. Res.* 44, 1094 (2011).
119. X. Li, Y. Qian, T. Liu, X. Hu, G. Zhang, Y. You, and S. Liu, Amphiphilic multiarm star block copolymer-based multifunctional unimolecular micelles for cancer targeted drug delivery and MR imaging. *Biomaterials* 32, 6595 (2011).
120. J. Bigot, B. Charleux, G. Cooke, F. Delattre, D. Fournier, J. Lyskawa, L. Sambe, F. Stoffelbach, and P. Woisel, Tetrathiafulvalene end-functionalized poly(*N*-isopropylacrylamide): A new class of amphiphilic polymer for the creation of multistimuli responsive micelles. *J. Am. Chem. Soc.* 132, 10796 (2010).
121. I. Ahmad, M. Longenecker, J. Samuel, and T. M. Allen, Antibody-targeted delivery of doxorubicin entrapped in sterically stabilized liposomes can eradicate lung cancer in mice. *Cancer Res.* 53, 1484 (1993).
122. Z. Cao, R. Tong, A. Mishra, W. Xu, G. C. Wong, J. Cheng, and Y. Lu, Reversible Cell-specific drug delivery with Aptamer-functionalized liposomes. *Angew. Chem. Int. Ed.* 48, 6494 (2009).
123. W. T. Al-Jamal, K. T. Al-Jamal, P. H. Bomans, P. M. Frederik, and K. Kostarelos, Functionalized-quantum-dot–liposome hybrids as multimodal nanoparticles for cancer. *Small* 4, 1406 (2008).
124. T. Simunek, M. Sterba, O. Popelova, M. Adamcova, R. Hrdina, and V. Gersl, Anthracycline-induced cardiotoxicity: Overview of studies examining the roles of oxidative stress and free cellular iron. *Pharmacol. Rep.* 61, 156 (2009).
125. Y. C. Barenholz, Doxil®—The first FDA-approved nano-drug: Lessons learned. *J. Control Release* 160, 117 (2012).
126. R. Koole, M. M. van Schooneveld, J. Hilhorst, K. Castermans, D. P. Cormode, G. J. Strijkers, C. de Mello Donegá, D. Vanmaekelbergh, A. W. Griffioen, and K. Nicolay, Paramagnetic lipid-coated silica nanoparticles with a fluorescent quantum dot core: A new contrast agent platform for multimodality imaging. *Bioconjugate Chem.* 19, 2471 (2008).
127. S. K. Messerschmidt, A. Musyanovych, M. Altvater, P. Scheurich, K. Pfizenmaier, K. Landfester, and R. E. Kontermann, Targeted

- lipid-coated nanoparticles: Delivery of tumor necrosis factor-functionalized particles to tumor cells. *J. Control Release* 137, 69 (2009).
128. G. Koby, B. Ofra, D. Dganit, and M. Marcelle, Poly(*D,L*-lactide-co-glycolide acid) nanoparticles for DNA delivery: Waiving preparation complexity and increasing efficiency. *Biopolymers* 85, 379 (2007).
  129. M. RaviKumar, S. Mohapatra, X. Kong, P. Jena, U. Bakowsky, and C. Lehrd, Cationic poly(lactide-co-glycolide) nanoparticles as efficient *in vivo* gene transfection agents. *J. Nanosci. Nanotechnol.* 4, 990 (2004).
  130. W. Hasan, K. Chu, A. Gullapalli, S. S. Dunn, E. M. Enlow, J. C. Luft, S. Tian, M. E. Napier, P. D. Pohlhaus, J. P. Rolland, and J. M. DeSimone, Delivery of multiple siRNAs using lipid-coated PLGA nanoparticles for treatment of prostate cancer. *Nano Lett.* 12, 287 (2011).
  131. D. Felnerova, J.-F. Viret, R. Glück, and C. Moser, Liposomes and virosomes as delivery systems for antigens, nucleic acids and drugs. *Curr. Opin. Biotechnol.* 15, 518 (2004).
  132. V. Awasthi, D. Garcia, R. Klipper, B. A. Goins, and W. T. Phillips, Neutral and anionic liposome-encapsulated hemoglobin: Effect of postinserted poly(ethylene glycol)-distearoylphosphatidylethanolamine on distribution and circulation kinetics. *J. Pharmacol. Exp. Ther.* 309, 241 (2004).
  133. J. Liu, H. Ma, T. Wei, and X. J. Liang, CO<sub>2</sub> gas induced drug release from pH-sensitive liposome to circumvent doxorubicin resistant cells. *Chem. Commun.* 48, 4869 (2012).
  134. P. P. Karmali and A. Chaudhuri, Cationic liposomes as non-viral carriers of gene medicines: Resolved issues, open questions, and future promises. *Med. Res. Rev.* 27, 696 (2007).
  135. B. G. Tenchov, L. Wang, R. Koynova, and R. C. MacDonald, Modulation of a membrane lipid lamellar–nonlamellar phase transition by cationic lipids: A measure for transfection efficiency. *BBA-Biomembranes* 1778, 2405 (2008).
  136. S.-C. Lee, K.-E. Lee, J.-J. Kim, and S.-H. Lim, The effect of cholesterol in the liposome bilayer on the stabilization of incorporated retinol. *J. Liposome Res.* 15, 157 (2005).
  137. C. Kirby, J. Clarke, and G. Gregoriadis, Effect of the cholesterol content of small unilamellar liposomes on their stability *in vivo* and *in vitro*. *Biochem. J.* 186, 591 (1980).
  138. H. Schellekens, Immunogenicity of therapeutic proteins: Clinical implications and future prospects. *Clin. Ther.* 24, 1720 (2002).
  139. H. Li, D. J. DeRosier, W. V. Nicholson, E. Nogales, and K. H. Downing, Microtubule structure at 8 Å resolution. *Structure* 10, 1317 (2002).
  140. D. Ding, Z. Zhu, Q. Liu, J. Wang, Y. Hu, X. Jiang, and B. Liu, Cisplatin-loaded gelatin-poly(acrylic acid) nanoparticles: Synthesis, antitumor efficiency *in vivo* and penetration in tumors. *Eur. J. Pharm. Biopharm.* 79, 142 (2011).
  141. A. O. Elzoghby, W. M. Samy, and N. A. Elgindy, Albumin-based nanoparticles as potential controlled release drug delivery systems. *J. Control Release* 157, 168 (2012).
  142. A. S. Lammel, X. Hu, S. H. Park, D. L. Kaplan, and T. R. Scheibel, Controlling silk fibroin particle features for drug delivery. *Biomaterials* 31, 4583 (2010).
  143. J. Schnitzer and P. Oh, Antibodies to SPARC inhibit albumin binding to SPARC, gp60, and microvascular endothelium. *Am. J. Physiol. Heart Circ. Physiol.* 263, H1872 (1992).
  144. T. A. John, S. M. Vogel, R. D. Minshall, K. Ridge, C. Tirupathi, and A. B. Malik, Evidence for the role of alveolar epithelial gp60 in active transalveolar albumin transport in the rat lung. *J. Physiol.* 533, 547 (2001).
  145. X. Li, L. Qiu, P. Zhu, X. Tao, T. Imanaka, J. Zhao, Y. Huang, Y. Tu, and X. Cao, Epidermal growth factor–ferritin H-chain protein nanoparticles for tumor active targeting. *Small* 8, 2505 (2012).
  146. A. J. Wong, S. H. Bigner, D. D. Bigner, K. W. Kinzler, S. R. Hamilton, and B. Vogelstein, Increased expression of the epidermal growth factor receptor gene in malignant gliomas is invariably associated with gene amplification. *Proc. Natl. Acad. Sci. USA* 84, 6899 (1987).
  147. A. Destro, G. Ceresoli, M. Falleni, P. Zucali, E. Morenghi, P. Bianchi, C. Pellegrini, N. Cordani, V. Vaira, and M. Alloisio, EGFR overexpression in malignant pleural mesothelioma: An immunohistochemical and molecular study with clinicopathological correlations. *Lung Cancer* 51, 207 (2006).
  148. X. Zhen, X. Wang, C. Xie, W. Wu, and X. Jiang, Cellular uptake, antitumor response and tumor penetration of cisplatin-loaded milk protein nanoparticles. *Biomaterials* 34, 1372 (2012).
  149. M. D. Shoulders and R. T. Raines, Collagen structure and stability. *Annu. Rev. Biochem.* 78, 929 (2009).
  150. K. E. Kadler, C. Baldock, J. Bella, and R. P. Boot-Handford, Collagens at a glance. *J. Cell Sci.* 120, 1955 (2007).
  151. G. Veit, B. Kobbe, D. R. Keene, M. Paulsson, M. Koch, and R. Wagener, Collagen XXVIII, a novel von Willebrand factor A domain-containing protein with many imperfections in the collagenous domain. *J. Biol. Chem.* 281, 3494 (2006).
  152. Z. Wang, C. Zhang, and L. Xie, Biosafety evaluation of collagen-based bone repairing material. *Sheng Wu Yi Xue Gong Cheng Xue Za Zhi* 30, 105 (2013).
  153. U. Takeda, M. Odaki, M. Yokota, H. Sasaki, T. Niizato, H. Kawaoto, H. Watanabe, T. Ito, N. Ishiwatari, and H. Hayasaka, Acute and subacute toxicity studies on collagen wound dressing (CAS) in mice and rats. *J. Toxicol. Sci.* 7, 63 (1982).
  154. C. Peng, Z.-A. Zhu, G.-L. Li, D.-C. Sun, J.-G. Li, Z.-Y. Qiu, C.-L. Hu, Z.-H. Liu, H.-B. Sheng, and F.-Z. Cui, Enhancement of bone healing in rabbit ulnar critical bone defect by injectable nano-hydroxyapatite/collagen/(calcium sulfate hemihydrate) mixed with autogenous bone marrow. *J. Biomater. Tissue Eng.* 3, 534 (2013).
  155. Z. Luo, K. Cai, Y. Hu, L. Zhao, P. Liu, L. Duan, and W. Yang, Mesoporous Silica nanoparticles end-capped with collagen: Redox-responsive nanoreservoirs for targeted drug delivery. *Angew. Chem. Int. Ed.* 50, 640 (2011).
  156. H. Kim, S. Kim, C. Park, H. Lee, H.J. Park, and C. Kim, Glutathione-induced intracellular release of guests from mesoporous silica nanocontainers with cyclodextrin gatekeepers. *Adv. Mater.* 22, 4280 (2010).
  157. K. B. Djagny, Z. Wang, and S. Xu, Gelatin: A valuable protein for food and pharmaceutical industries: Review. *Crit. Rev. Food Sci. Nutr.* 41, 481 (2001).
  158. Z. Zou, D. He, X. He, K. Wang, X. Yang, Z. Qing, and Q. Zhou, Natural gelatin capped mesoporous silica nanoparticles for intracellular Acid-triggered drug delivery. *Langmuir* 29, 12804 (2013).
  159. S. Young, M. Wong, Y. Tabata, and A. G. Mikos, Gelatin as a delivery vehicle for the controlled release of bioactive molecules. *J. Control Release* 109, 256 (2005).
  160. M. Larché and D. C. Wraith, Peptide-based therapeutic vaccines for allergic and autoimmune diseases. *Nat. Med.* 11, S69 (2005).
  161. H. Wang, J. Wei, C. Yang, H. Zhao, D. Li, Z. Yin, and Z. Yang, The inhibition of tumor growth and metastasis by self-assembled nanofibers of taxol. *Biomaterials* 33, 5848 (2012).
  162. X.-X. Zhang, H. S. Eden, and X. Chen, Peptides in cancer nanomedicine: Drug carriers, targeting ligands and protease substrates. *J. Control Release* 159, 2 (2012).
  163. L. Crombez, G. Aldrian-Herrada, K. Konate, Q. N. Nguyen, G. K. McMaster, R. Brasseur, F. Heitz, and G. Divita, A new potent secondary amphipathic cell-penetrating peptide for siRNA delivery into mammalian cells. *Mol. Ther.* 17, 95 (2008).
  164. I. Nakase, Y. Konishi, M. Ueda, H. Saji, and S. Futaki, Accumulation of arginine-rich cell-penetrating peptides in tumors and the potential for anticancer drug delivery *in vivo*. *J. Control Release* 159, 181 (2012).
  165. K. Melikov and L. Chernomordik, Arginine-rich cell penetrating peptides: From endosomal uptake to nuclear delivery. *Cell. Mol. Life Sci.* 62, 2739 (2005).



166. V. P. Torchilin, R. Rammohan, V. Weissig, and T. S. Levchenko, TAT peptide on the surface of liposomes affords their efficient intracellular delivery even at low temperature and in the presence of metabolic inhibitors. *Proc. Natl. Acad. Sci. USA* 98, 8786 (2001).
167. V. P. Torchilin, T. S. Levchenko, R. Rammohan, N. Volodina, B. Papahadjopoulos-Sternberg, and G. G. D'Souza, Cell transfection *in vitro* and *in vivo* with nontoxic TAT peptide-liposome-DNA complexes. *Proc. Natl. Acad. Sci. USA* 100, 1972 (2003).
168. D. Putnam, C. A. Gentry, D. W. Pack, and R. Langer, Polymer-based gene delivery with low cytotoxicity by a unique balance of side-chain termini. *Proc. Natl. Acad. Sci. USA* 98, 1200 (2001).
169. J. Du and S. P. Armes, pH-responsive vesicles based on a hydrolytically self-cross-linkable copolymer. *J. Am. Chem. Soc.* 127, 12800 (2005).
170. K. Liang, J. J. Richardson, H. Ejima, G. K. Such, J. Cui, and F. Caruso, Peptide-tunable drug cytotoxicity via one-step assembled polymer nanoparticles. *Adv. Mater.* (2013), 10.1002/adma.201305002.
171. V. A. Sethuraman and Y. H. Bae, TAT peptide-based micelle system for potential active targeting of anti-cancer agents to acidic solid tumors. *J. Control Release* 118, 216 (2007).
172. A. V. Pinheiro, D. Han, W. M. Shih, and H. Yan, Challenges and opportunities for structural DNA nanotechnology. *Nat. Nanotechnol.* 6, 763 (2011).
173. Q. Jiang, C. Song, J. Nangreave, X. Liu, L. Lin, D. Qiu, Z. G. Wang, G. Zou, X. Liang, H. Yan, and B. Ding, DNA origami as a carrier for circumvention of drug resistance. *J. Am. Chem. Soc.* 134, 13396 (2012).
174. P. Tarapore, Y. Shu, P. Guo, and S.-M. Ho, Application of Phi29 motor pRNA for targeted therapeutic delivery of siRNA silencing metallothionein-IIA and survivin in ovarian cancers. *Mol. Ther.* 19, 386 (2010).
175. A. Biwer, G. Antranikian, and E. Heinzle, Enzymatic production of cyclodextrins. *Appl. Microbiol. Biotechnol.* 59, 609 (2002).
176. R. Villalonga, R. Cao, and A. Frago, Supramolecular chemistry of cyclodextrins in enzyme technology. *Chem. Rev.* 107, 3088 (2007).
177. M. E. Brewster and T. Loftsson, Cyclodextrins as pharmaceutical solubilizers. *Adv. Drug Delivery Rev.* 59, 645 (2007).
178. J. Zhang, H. Sun, and P. X. Ma, Host-guest interaction mediated polymeric assemblies: Multifunctional nanoparticles for drug and gene delivery. *ACS Nano* 4, 1049 (2010).
179. Y. Zhao, B. G. Trewyn, I. I. Slowing, and V. S.-Y. Lin, Mesoporous silica nanoparticle-based double drug delivery system for glucose-responsive controlled release of insulin and cyclic AMP. *J. Am. Chem. Soc.* 131, 8398 (2009).
180. Q. He, Z. Zhang, Y. Gao, J. Shi, and Y. Li, Intracellular localization and cytotoxicity of spherical mesoporous silica nano- and microparticles. *Small* 5, 2722 (2009).
181. J. Lu, M. Liong, Z. Li, J. I. Zink, and F. Tamanoi, Biocompatibility, biodistribution, and drug-delivery efficiency of mesoporous silica nanoparticles for cancer therapy in animals. *Small* 6, 1794 (2010).
182. Y. Zhou and M. Antonietti, A novel tailored bimodal porous silica with well-defined inverse opal microstructure and super-microporous lamellar nanostructure. *Chem. Commun.* 2564 (2003).
183. R. Takahashi, S. Sato, T. Sodesawa, M. Kawakita, and K. Ogura, High surface-area silica with controlled pore size prepared from nanocomposite of silica and citric acid. *J. Phys. Chem. B* 104, 12184 (2000).
184. W. Liang, S. He, Y. Wang, and J. Fang, Morphology and shape control of porous silica nanostructures with dual-templating approaches. *J. Nanosci. Nanotechnol.* 14, 4424 (2014).
185. J. Liu, C. Detrembleur, M.-C. De Pauw-Gillet, S. Mornet, L. V. Elst, S. Laurent, C. Jérôme, and E. Duguet, Heat-triggered drug release systems based on mesoporous silica nanoparticles filled with a maghemite core and phase-change molecules as gatekeepers. *J. Mater. Chem. B* 2, 59 (2014).
186. F. Muhammad, M. Guo, W. Qi, F. Sun, A. Wang, Y. Guo, and G. Zhu, pH-triggered controlled drug release from mesoporous silica nanoparticles via intracellular dissolution of ZnO nanolids. *J. Am. Chem. Soc.* 133, 8778 (2011).
187. H. Meng, M. Xue, T. Xia, Y. L. Zhao, F. Tamanoi, J. F. Stoddart, J. I. Zink, and A. E. Nel, Autonomous *in vitro* anticancer drug release from mesoporous silica nanoparticles by pH-sensitive nanovalves. *J. Am. Chem. Soc.* 132, 12690 (2010).
188. J. Kim, H. S. Kim, N. Lee, T. Kim, H. Kim, T. Yu, I. C. Song, W. K. Moon, and T. Hyeon, Multifunctional uniform nanoparticles composed of a magnetite nanocrystal core and a mesoporous silica shell for magnetic resonance and fluorescence imaging and for drug delivery. *Angew. Chem. Int. Ed.* 47, 8438 (2008).
189. C. P. Tsai, Y. Hung, Y. H. Chou, D. M. Huang, J. K. Hsiao, C. Chang, Y. C. Chen, and C. Y. Mou, High-contrast paramagnetic fluorescent mesoporous silica nanorods as a multifunctional cell-imaging probe. *Small* 4, 186 (2008).
190. S. H. Wu, Y. S. Lin, Y. Hung, Y. H. Chou, Y. H. Hsu, C. Chang, and C. Y. Mou, Multifunctional mesoporous silica nanoparticles for intracellular labeling and animal magnetic resonance imaging studies. *ChemBioChem.* 9, 53 (2008).
191. I. Slowing, B. G. Trewyn, and S.-Y. L. Victor, Effect of surface functionalization of MCM-41-type mesoporous silica nanoparticles on the endocytosis by human cancer cells. *J. Am. Chem. Soc.* 128, 14792 (2006).
192. J. E. Lee, N. Lee, H. Kim, J. Kim, S. H. Choi, J. H. Kim, T. Kim, I. C. Song, S. P. Park, W. K. Moon, and T. Hyeon, Uniform mesoporous dye-doped silica nanoparticles decorated with multiple magnetite nanocrystals for simultaneous enhanced magnetic resonance imaging, fluorescence imaging, and drug delivery. *J. Am. Chem. Soc.* 132, 552 (2009).
193. Y. Zhao, X. Sun, G. Zhang, B. G. Trewyn, I. I. Slowing, and V. S.-Y. Lin, Interaction of mesoporous silica nanoparticles with human red blood cell membranes: Size and surface effects. *ACS Nano* 5, 1366 (2011).
194. S. Kapoor and A. J. Bhattacharyya, Ultrasound-triggered controlled drug delivery and biosensing using silica nanotubes. *J. Phys. Chem. C* 113, 7155 (2009).
195. D. T. Mitchell, S. B. Lee, L. Trofin, N. Li, T. K. Nevanen, H. Söderlund, and C. R. Martin, Smart nanotubes for bioseparations and biocatalysis. *J. Am. Chem. Soc.* 124, 11864 (2002).
196. H.-M. Ding, L. Shao, R.-J. Liu, Q.-G. Xiao, and J.-F. Chen, Silica nanotubes for lysozyme immobilization. *J. Colloid Interface Sci.* 290, 102 (2005).
197. A. Nan, X. Bai, S. J. Son, S. B. Lee, and H. Ghandehari, Cellular uptake and cytotoxicity of silica nanotubes. *Nano Lett.* 8, 2150 (2008).
198. J. Jang and H. Yoon, Novel fabrication of size-tunable silica nanotubes using a reverse-microemulsion-mediated sol-gel method. *Adv. Mater.* 16, 799 (2004).
199. C. C. Chen, Y. C. Liu, C. H. Wu, C. C. Yeh, M. T. Su, and Y. C. Wu, Preparation of fluorescent silica nanotubes and their application in gene delivery. *Adv. Mater.* 17, 404 (2005).
200. Y. Cheng, A. C. Samia, J. D. Meyers, I. Panagopoulos, B. Fei, and C. Burda, Highly efficient drug delivery with gold nanoparticle vectors for *in vivo* photodynamic therapy of cancer. *J. Am. Chem. Soc.* 130, 10643 (2008).
201. H. He, C. Xie, and J. Ren, Nonbleaching fluorescence of gold nanoparticles and its applications in cancer cell imaging. *Anal. Chem.* 80, 5951 (2008).
202. M. P. Melancon, W. Lu, Z. Yang, R. Zhang, Z. Cheng, A. M. Elliot, J. Stafford, T. Olson, J. Z. Zhang, and C. Li, *In vitro* and *in vivo* targeting of hollow gold nanoshells directed at epidermal growth factor receptor for photothermal ablation therapy. *Mol. Cancer Ther.* 7, 1730 (2008).
203. J. J. Storhoff, A. D. Lucas, V. Garimella, Y. P. Bao, and U. R. Müller, Homogeneous detection of unamplified genomic DNA

- sequences based on colorimetric scatter of gold nanoparticle probes. *Nat. Biotechnol.* 22, 883 (2004).
204. M. Sliem, E. Ebeid, and M. Harith, Selective colorimetric detection of viral DNA sequence of hepatitis C virus genotype-4 genetic material using gold nanoparticles. *J. Biomed. Nanotechnol.* 3, 360 (2007).
  205. B. Bindhani, U. Parida, S. Biswal, A. Panigrahi, and P. Nayak, Gold nanoparticles and their biomedical applications. *Rev. Nanosci. Nanotechnol.* 2, 247 (2013).
  206. M. Grzelczak, J. Pérez-Juste, P. Mulvaney, and L. M. Liz-Marzán, Shape control in gold nanoparticle synthesis. *Chem. Soc. Rev.* 37, 1783 (2008).
  207. B. D. Chithrani, A. A. Ghazani, and W. C. W. Chan, Determining the size and shape dependence of gold nanoparticle uptake into mammalian cells. *Nano Lett.* 6, 662 (2006).
  208. A. Kumar, H. Ma, X. Zhang, K. Huang, S. Jin, J. Liu, T. Wei, W. Cao, G. Zou, and X. J. Liang, Gold nanoparticles functionalized with therapeutic and targeted peptides for cancer treatment. *Biomaterials* 33, 1180 (2011).
  209. E. B. Dickerson, E. C. Dreaden, X. Huang, I. H. El-Sayed, H. Chu, S. Pushpanketh, J. F. McDonald, and M. A. El-Sayed, Gold nanorod assisted near-infrared plasmonic photothermal therapy (PPTT) of squamous cell carcinoma in mice. *Cancer Lett.* 269, 57 (2008).
  210. T. Kawano, Y. Niidome, T. Mori, Y. Katayama, and T. Niidome, PNIPAM gel-coated gold nanorods for targeted delivery responding to a near-infrared laser. *Bioconjugate Chem.* 20, 209 (2009).
  211. P. K. Jain, K. S. Lee, I. H. El-Sayed, and M. A. El-Sayed, Calculated absorption and scattering properties of gold nanoparticles of different size, shape, and composition: Applications in biological imaging and biomedicine. *J. Phys. Chem. B* 110, 7238 (2006).
  212. Z. Zhang, L. Wang, J. Wang, X. Jiang, X. Li, Z. Hu, Y. Ji, X. Wu, and C. Chen, Mesoporous silica-coated gold nanorods as a light-mediated multifunctional theranostic platform for cancer treatment. *Adv. Mater.* 24, 1418 (2012).
  213. M. Schütz, D. Steingeweg, M. Salehi, K. Kömpe, and S. Schlücker, Hydrophilically stabilized gold nanostars as SERS labels for tissue imaging of the tumor suppressor p63 by immuno-SERS microscopy. *Chem. Commun.* 47, 4216 (2011).
  214. C. M. Cobley, L. Au, J. Chen, and Y. Xia, Targeting gold nanocages to cancer cells for photothermal destruction and drug delivery. *Expert Opin. Drug Deliv.* 7, 577 (2010).
  215. A. A. Bhirde, V. Patel, J. Gavard, G. Zhang, A. A. Sousa, A. Masedunskas, R. D. Leapman, R. Weigert, J. S. Gutkind, and J. F. Rusling, Targeted killing of cancer cells *in vivo* and *in vitro* with EGF-directed carbon nanotube-based drug delivery. *ACS Nano* 3, 307 (2009).
  216. T. K. Jain, M. A. Morales, S. K. Sahoo, D. L. Leslie-Pelecky, and V. Labhasetwar, Iron oxide nanoparticles for sustained delivery of anticancer agents. *Mol. Pharm.* 2, 194 (2005).
  217. N. Rozanova and J. Z. Zhang, Metal and magnetic nanostructures for cancer diagnosis and therapy. *Rev. Nanosci. Nanotechnol.* 2, 29 (2013).
  218. A. Kleinauskas, J.-K. Kim, G.-H. Choi, H.-T. Kim, K. Roe, and P. Juzenas, Superparamagnetic magnetite nanoparticles for cancer theranostics. *Rev. Nanosci. Nanotechnol.* 1, 271 (2012).
  219. I. Roy, S. Mitra, A. Maitra, and S. Mozumdar, Calcium phosphate nanoparticles as novel non-viral vectors for targeted gene delivery. *Int. J. Pharm.* 250, 25 (2003).
  220. Q. He, A. R. Mitchell, S. L. Johnson, C. Wagner-Bartak, T. Morcol, and S. J. Bell, Calcium phosphate nanoparticle adjuvant. *Clin. Diagn. Lab. Immunol.* 7, 899 (2000).
  221. Z. Liu, J. T. Robinson, X. Sun, and H. Dai, PEGylated nanographene oxide for delivery of water-insoluble cancer drugs. *J. Am. Chem. Soc.* 130, 10876 (2008).
  222. J. T. Robinson, S. M. Tabakman, Y. Liang, H. Wang, H. S. Casalongue, D. Vinh, and H. Dai, Ultrasmall reduced graphene oxide with high near-infrared absorbance for photothermal therapy. *J. Am. Chem. Soc.* 133, 6825 (2011).
  223. X.-J. Liang, H. Meng, Y. Wang, H. He, J. Meng, J. Lu, P. C. Wang, Y. Zhao, X. Gao, and B. Sun, Metallofullerene nanoparticles circumvent tumor resistance to cisplatin by reactivating endocytosis. *Proc. Natl. Acad. Sci. USA* 107, 7449 (2010).
  224. S.-G. Kang, G. Zhou, P. Yang, Y. Liu, B. Sun, T. Huynh, H. Meng, L. Zhao, G. Xing, and C. Chen, Molecular mechanism of pancreatic tumor metastasis inhibition by Gd@C82(OH) 22 and its implication for de novo design of nanomedicine. *Proc. Natl. Acad. Sci. USA* 109, 15431 (2012).
  225. Y. Song, J. Jin, J. Li, R. He, M. Zhang, Y. Chang, K. Chen, Y. Wang, B. Sun, and G. Xing, Gd@C82(OH)22 nanoparticles constrain macrophages migration into tumor tissue to prevent metastasis. *J. Nanosci. Nanotechnol.* 14, 4022 (2014).
  226. D. L. Thorek, A. K. Chen, J. Czupryna, and A. Tsourkas, Superparamagnetic iron oxide nanoparticle probes for molecular imaging. *Ann. Biomed. Eng.* 34, 23 (2006).
  227. X. Hu, X. Hao, Y. Wu, J. Zhang, X. Zhang, P. C. Wang, G. Zou, and X.-J. Liang, Multifunctional hybrid silica nanoparticles for controlled doxorubicin loading and release with thermal and pH dual response. *J. Mater. Chem. B* 1, 1109 (2013).
  228. B. Sumer and J. Gao, Theranostic nanomedicine for cancer. *Nanomedicine* 3, 137 (2008).
  229. T. Lammers, S. Aime, W. E. Hennink, G. Storm, and F. Kiessling, Theranostic nanomedicine. *Acc. Chem. Res.* 44, 1029 (2011).
  230. J. W. Park, K. Hong, D. B. Kirpotin, G. Colbern, R. Shalaby, J. Baselga, Y. Shao, U. B. Nielsen, J. D. Marks, and D. Moore, Anti-HER2 immunoliposomes enhanced efficacy attributable to targeted delivery. *Clin. Cancer Res.* 8, 1172 (2002).
  231. S.-J. Chiu, N. T. Ueno, and R. J. Lee, Tumor-targeted gene delivery via anti-HER2 antibody (trastuzumab, Herceptin®) conjugated polyethylenimine. *J. Control Release* 97, 357 (2004).
  232. L. M. Ellis and D. J. Hicklin, VEGF-targeted therapy: Mechanisms of anti-tumour activity. *Nat. Rev. Cancer* 8, 579 (2008).
  233. C. R. Patra, R. Bhattacharya, E. Wang, A. Katarya, J. S. Lau, S. Dutta, M. Mudders, S. Wang, S. A. Buhrow, and S. L. Safgren, Targeted delivery of gemcitabine to pancreatic adenocarcinoma using cetuximab as a targeting agent. *Cancer Res.* 68, 1970 (2008).
  234. G. Wu, R. F. Barth, W. Yang, M. Chatterjee, W. Tjarks, M. J. Ciesielski and R. A. Fenstermaker, Site-specific conjugation of boron-containing dendrimers to anti-EGF receptor monoclonal antibody cetuximab (IMC-C225) and its evaluation as a potential delivery agent for neutron capture therapy. *Bioconjugate Chem.* 15, 185 (2004).
  235. B. Borisch, I. Semac, A. Soltermann, C. Palomba, and D. Hoessli, Anti-CD20 treatments and the lymphocyte membrane: Pathology for therapy. *Verh. Dtsch. Ges. Pathol.* 85, 161 (2001).
  236. J. M. Reichert and V. E. Valge-Archer, Development trends for monoclonal antibody cancer therapeutics. *Nat. Rev. Drug Discov.* 6, 349 (2007).
  237. J. M. Pagel, A. Pantelias, N. Hedin, S. Wilbur, L. Saganic, Y. Lin, D. Axworthy, D. K. Hamlin, D. S. Wilbur, and A. K. Gopal, Evaluation of CD20, CD22, and HLA-DR targeting for radioimmunotherapy of B-cell lymphomas. *Cancer Res.* 67, 5921 (2007).
  238. E. Jager, V. H. van der Velden, J. G. te Marvelde, R. B. Walter, Z. Agur, and V. Vainstein, Targeted drug delivery by gemtuzumab ozogamicin: Mechanism-based mathematical model for treatment strategy improvement and therapy individualization. *PloS one* 6, e24265 (2011).
  239. R. Lapalombella, X. Zhao, G. Triantafyllou, B. Yu, Y. Jin, G. Lozanski, C. Cheney, N. Heerema, D. Jarjoura, and A. Lehman, A novel Raji-Burkitt's lymphoma model for preclinical and mechanistic evaluation of CD52-targeted immunotherapeutic agents. *Clin. Cancer Res.* 14, 569 (2008).

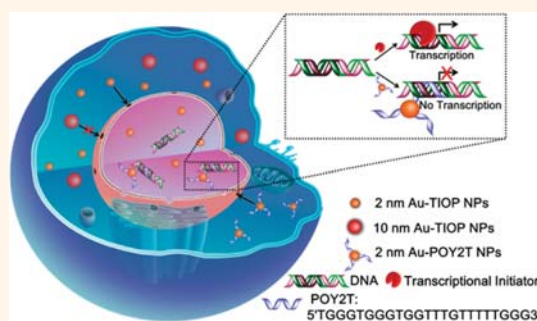
240. T. H. Kim, Y. G. Jo, H. H. Jiang, S. M. Lim, Y. S. Youn, S. Lee, X. Chen, and K. C. Lee, PEG-transferrin conjugated TRAIL (TNF-related apoptosis-inducing ligand) for therapeutic tumor targeting. *J. Control Release* 162, 422 (2012).
241. L. Han, Y. Ren, L. Long, Y. Zhong, C. Shen, P. Pu, X. Yuan, and C. Kang, Inhibition of C6 glioma *in vivo* by combination chemotherapy of implantation of polymer wafer and intracarotid perfusion of transferrin-decorated nanoparticles. *Oncol. Rep.* 27, 121 (2012).
242. P. Zhou, S. Hatzieremia, M. A. Elliott, L. Scobie, C. Crossan, A. M. Michie, T. L. Holyoake, G. W. Halbert, and H. G. Jørgensen, Uptake of synthetic low density lipoprotein by leukemic stem cells—A potential stem cell targeted drug delivery strategy. *J. Control Release* 148, 380 (2010).
243. K. Fan, C. Cao, Y. Pan, D. Lu, D. Yang, J. Feng, L. Song, M. Liang, and X. Yan, Magnetoferritin nanoparticles for targeting and visualizing tumour tissues. *Nat. Nanotechnol.* 7, 459 (2012).
244. M. H. Lee, J. Y. Kim, J. H. Han, S. Bhuniya, J. L. Sessler, C. Kang, and J. S. Kim, Direct fluorescence monitoring of the delivery and cellular uptake of a cancer-targeted RGD peptide-appended naphthalimide theragnostic prodrug. *J. Am. Chem. Soc.* 134, 12668 (2012).
245. Y. Miura, T. Takenaka, K. Toh, S. Wu, H. Nishihara, M. R. Kano, Y. Ino, T. Nomoto, Y. Matsumoto, and H. Koyama, Cyclic RGD-linked polymeric micelles for targeted delivery of platinum anticancer drugs to glioblastoma through the blood–brain tumor barrier. *ACS Nano* 7, 8583 (2013).
246. R. Bieker, T. Kessler, C. Schwöppe, T. Padró, T. Persigehl, C. Bremer, J. Dreischalück, A. Kolkmeier, W. Heindel, and R. M. Mesters, Infarction of tumor vessels by NGR-peptide-directed targeting of tissue factor: Experimental results and first-in-man experience. *Blood* 113, 5019 (2009).
247. T.-Y. Lee, C.-T. Lin, S.-Y. Kuo, D.-K. Chang, and H.-C. Wu, Peptide-mediated targeting to tumor blood vessels of lung cancer for drug delivery. *Cancer Res.* 67, 10958 (2007).
248. D.-K. Chang, C.-Y. Chiu, S.-Y. Kuo, W.-C. Lin, A. Lo, Y.-P. Wang, P.-C. Li, and H.-C. Wu, Antiangiogenic targeting liposomes increase therapeutic efficacy for solid tumors. *J. Biol. Chem.* 284, 12905 (2009).
249. Z. Yan, F. Wang, Z. Wen, C. Zhan, L. Feng, Y. Liu, X. Wei, C. Xie, and W. Lu, LyP-1-conjugated PEGylated liposomes: A carrier system for targeted therapy of lymphatic metastatic tumor. *J. Control Release* 157, 118 (2012).
250. J.-Y. Kim, W. I. Choi, Y. H. Kim, and G. Tae, Brain-targeted delivery of protein using chitosan-and RVG peptide-conjugated, pluronic-based nano-carrier. *Biomaterials* 34, 1170 (2012).
251. L. Pan, Q. He, J. Liu, Y. Chen, M. Ma, L. Zhang, and J. Shi, Nuclear-targeted drug delivery of TAT peptide-conjugated monodisperse mesoporous silica nanoparticles. *J. Am. Chem. Soc.* 134, 5722 (2012).
252. E. W. Ng, D. T. Shima, P. Calias, E. T. Cunningham, D. R. Guyer, and A. P. Adamis, Pegaptanib, a targeted anti-VEGF aptamer for ocular vascular disease. *Nat. Rev. Drug Discov.* 5, 123 (2006).
253. J. Guo, X. Gao, L. Su, H. Xia, G. Gu, Z. Pang, X. Jiang, L. Yao, J. Chen, and H. Chen, Aptamer-functionalized PEG–PLGA nanoparticles for enhanced anti-glioma drug delivery. *Biomaterials* 32, 8010 (2011).
254. Y.-A. Shieh, S.-J. Yang, M.-F. Wei, and M.-J. Shieh, Aptamer-based tumor-targeted drug delivery for photodynamic therapy. *ACS Nano* 4, 1433 (2010).
255. Y. Wu, K. Sefah, H. Liu, R. Wang, and W. Tan, DNA aptamer-micelle as an efficient detection/delivery vehicle toward cancer cells. *Proc. Natl. Acad. Sci. USA* 107, 5 (2010).
256. R. Savla, O. Taratula, O. Garbuzenko, and T. Minko, Tumor targeted quantum dot-mucin 1 aptamer-doxorubicin conjugate for imaging and treatment of cancer. *J. Control Release* 153, 16 (2011).
257. D. Kim, Y. Y. Jeong, and S. Jon, A drug-loaded aptamer-gold nanoparticle bioconjugate for combined CT imaging and therapy of prostate cancer. *ACS Nano* 4, 3689 (2010).
258. L. C. Bock, L. C. Griffin, J. A. Latham, E. H. Vermaas, and J. J. Toole, Selection of single-stranded DNA molecules that bind and inhibit human thrombin. *Nature* 355, 564 (1992).
259. A. F. Hussain, M. K. Tur, and S. Barth, An Aptamer–siRNA Chimera Silences the Eukaryotic Elongation Factor 2 Gene and Induces Apoptosis in Cancers Expressing  $\alpha v \beta 3$  Integrin. *Nucleic Acid Ther.* 23, 203 (2013).
260. C. P. Neff, J. Zhou, L. Remling, J. Kuruvilla, J. Zhang, H. Li, D. D. Smith, P. Swiderski, J. J. Rossi, and R. Akkina, An aptamer-siRNA chimera suppresses HIV-1 viral loads and protects from helper CD4+ T cell decline in humanized mice. *Sci. Transl. Med.* 3, 66ra6 (2011).
261. B. C. Chi-Hong, G. A. Chernis, V. Q. Hoang, and R. Landgraf, Inhibition of heregulin signaling by an aptamer that preferentially binds to the oligomeric form of human epidermal growth factor receptor-3. *Proc. Natl. Acad. Sci. USA* 100, 9226 (2003).

# Ultrasmall Gold Nanoparticles as Carriers for Nucleus-Based Gene Therapy Due to Size-Dependent Nuclear Entry

Shuaidong Huo,<sup>†,‡,||</sup> Shubin Jin,<sup>†,‡,||</sup> Xiaowei Ma,<sup>†,‡</sup> Xiangdong Xue,<sup>†,‡</sup> Keni Yang,<sup>†</sup> Anil Kumar,<sup>†</sup> Paul C. Wang,<sup>§</sup> Jinchao Zhang,<sup>⊥</sup> Zhongbo Hu,<sup>‡,\*</sup> and Xing-Jie Liang<sup>†,\*</sup>

<sup>†</sup>Chinese Academy of Sciences (CAS) Key Laboratory for Biological Effects of Nanomaterials and Nanosafety, National Center for Nanoscience and Technology, No.11, First North Road, Zhongguancun, Beijing, China 100190, <sup>‡</sup>University of Chinese Academy of Sciences, Beijing, China 100049, <sup>§</sup>Molecular Imaging Laboratory, Department of Radiology, Howard University, Washington D.C. 20060, United States, and <sup>⊥</sup>College of Chemistry & Environmental Science, Chemical Biology Key Laboratory of Hebei Province, Hebei University, Baoding, China. <sup>||</sup>S.H. and S.J. contributed equally to this work.

**ABSTRACT** The aim of this study was to determine the size-dependent penetration ability of gold nanoparticles and the potential application of ultrasmall gold nanoparticles for intranuclear delivery and therapy. We synthesized gold nanoparticles with diameters of 2, 6, 10, and 16 nm and compared their intracellular distribution in MCF-7 breast cancer cells. Nanoparticles smaller than 10 nm (2 and 6 nm) could enter the nucleus, whereas larger ones (10 and 16 nm) were found only in the cytoplasm. We then investigated the possibility of using ultrasmall 2 nm nanoparticles as carriers for nuclear delivery of a triplex-forming oligonucleotide (TFO) that binds to the c-myc promoter. Compared to free TFO, the nanoparticle-conjugated TFO was more effective at reducing c-myc RNA and c-myc protein, which resulted in reduced cell viability. Our result demonstrated that the entry of gold nanoparticles into the cell nucleus is critically dependent on the size of the nanoparticles. We developed a strategy for regulating gene expression, by directly delivering TFOs into the nucleus using ultrasmall gold nanoparticles. More importantly, guidelines were provided to choose appropriate nanocarriers for different biomedical purposes.



**KEYWORDS:** ultrasmall gold nanoparticles · cancer cell nucleus · size-dependent · gene regulation · cancer therapy

Nanoscale materials have been receiving increasing attention in the field of biomedicine. Understanding of the behavior of nanomaterials, especially nanoparticles (NPs), in living system is vitally important for both the design of functionalized nanoparticles and the application of some nanomaterial-based medicines already in use. Due to their superior physiochemical properties, nanomaterials exhibit excellent advantages in biomedical research, such as accumulating preferentially at sites of tumor growth or inflammation, entering cells much more rapidly through different mechanisms compared to small molecules, delivering of various payloads into their targets, and being modified conveniently to perform desirable functions.<sup>1–4</sup> For nanoparticles, one of the key parameters is size. The nanoparticle-mediated *in vivo*

and *in vitro* response is size-dependent. Previous studies showed that nanoparticles with different sizes had distinctive distributions in the organs of living mice,<sup>5–8</sup> were taken up into cells by different mechanisms,<sup>9,10</sup> and followed a size-specific pathway until they escaped from the cells.<sup>11</sup> We have previously demonstrated that smaller nanoparticles (50 nm) can penetrate deeply into tumor tissue more easily and effectively than their larger counterparts (100 nm).<sup>12</sup> Among kinds of nanoparticles, gold nanoparticles have received much attention due to their easy fabrication, controllable size and shape, tunable surface functionalization, and good biocompatibility.<sup>10,13–16</sup> In the past few years, much effort has been made to develop nanoparticle-based therapeutic approaches. The application of gold nanoparticles is continuously booming, including drug and gene

\* Address correspondence to  
huzq@gucas.ac.cn,  
liangxj@nanoctr.cn.

Received for review February 12, 2014  
and accepted May 13, 2014.

Published online  
10.1021/nn5008572

© XXXX American Chemical Society

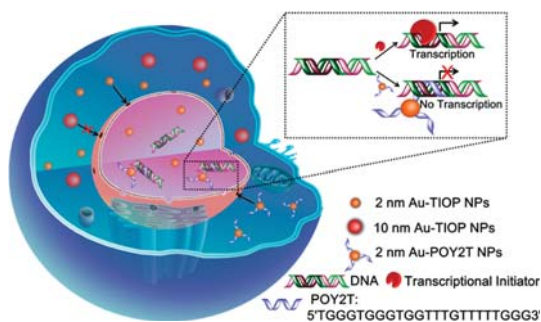


delivery vehicles, diagnostic tools, imaging agent in therapy, and biomarkers in the pharmaceutical field, etc.<sup>17–19</sup>

Nucleus is the most important organelle in regulating reproduction, growth, metabolism, and death of cells through gene expression. Controlling the nuclear-governed processes has been a major goal for nuclear-targeted therapy. However, most of the nanomaterials enter the cytoplasm exclusively. Information regarding the uptake and penetration of nanoparticles in the nucleus and their application in regulating gene expression is limited. Previously, gold nanostars were used to deliver drugs to the nucleus and induce nuclear phenotype change and apoptosis.<sup>20</sup> The use of nuclear-targeting Au NPs was also reported by Mostafa *et al.* to selectively disturb the division of cancer cells under the observation of cytokinesis arrest.<sup>21</sup> Therapeutic or reporter genes attached to magnetic nanoparticles for gene-targeting delivery via high-gradient/high-field magnets demonstrated *in vitro* transfection of a variety of cell lines.<sup>22</sup> However, nuclear targeting was indirectly achieved by conjugating nuclear targeting peptides with nanoparticles or magnetic targeting in these studies.

Gene therapy is a growing field of medicine that introduces genetic materials into the body to treat diseases.<sup>23–25</sup> Antisense (AS) gene therapy is a potentially powerful candidate for clinical treatment of various diseases, such as cancer and HIV/AIDS.<sup>23,26</sup> Triplex-forming oligonucleotides (TFOs) are known to form triplexes with specific DNA sequences, thereby interfering with gene transcription. However, due to the high activity of DNase in the cytoplasm, most TFOs are degraded before forming a triplex with the target sequence. Thus, the application of TFOs is limited. Previous studies have reported that conjugation with Au NPs can improve the stability of oligonucleotides and prevent their degradation.<sup>27–29</sup> However, none of these methods could directly deliver TFOs into the nucleus, and the therapeutic efficiency of TFOs is still maintained at a low level.

Herein, we first report using tiopronin-covered gold nanoparticles (Au-TIOP NPs) as a typical model to directly target a nucleus based on the nanoparticle's specific physiochemical properties. Tiopronin is widely used as a thiol drug with good biocompatibility.<sup>30</sup> Since the thiol groups of tiopronin can bind to the surface of nanoparticles to prevent coagulation, it is used as a stabilizing agent for metal nanoparticles.<sup>31</sup> Additionally, small molecules, peptides, or drugs can be modified to the carboxyl group of tiopronin for different biomedical applications. In this study, we find that only gold nanoparticles smaller than 10 nm (2 and 6 nm) can enter the nucleus. The larger ones (10 and 16 nm) are localized exclusively outside of the nucleus in the cytoplasm (Scheme 1). Importantly, we used the ultrasmall 2 nm Au NPs as a carrier and gene regulator



**Scheme 1.** Schematic illustration of the distribution and localization behavior of smaller (2 nm) and larger (10 nm) Au-TIOP NPs in MCF-7 cancer cells. The ultrasmall 2 nm Au-TIOP NPs were used as a carrier to enter the nucleus and deliver a TFO (POY2T) to regulate gene expression.

to deliver triplex-forming oligonucleotides into the nucleus directly. Our result shows that the expression of targeted gene was significantly down-regulated by a 2 nm Au NP–TFO complex at a concentration much lower than that of free TFOs.

## RESULTS AND DISCUSSION

**Characterization of Au-TIOP NPs with Different Sizes.** In order to investigate whether gold nanoparticles with different sizes have distinctive localization behavior and the ability to enter the nucleus in breast cancer cells, tiopronin-coated gold nanoparticles with sizes ranging from 2 to 16 nm were synthesized in this study. Tiopronin is a very well-known pharmaceutical drug used for the treatment of rheumatoid arthritis and cystinuria, and its biocompatibility is quite well-established already.<sup>23</sup> As shown in Figure S1 in Supporting Information, 2 and 6 nm Au-TIOP NPs were directly prepared by reduction of sodium borohydride with the protecting agent tiopronin. For the 10 and 16 nm Au-TIOP NPs, citrate-stabilized gold nanoparticles were first prepared, then a surface molecular ligand exchange method was used to add tiopronin.

The morphology of the as-prepared Au-TIOP NPs with different sizes is shown in Figure 1A. TEM images revealed that the gold nanoparticles have uniform spherical morphology and narrow size distribution (Figure S2 in Supporting Information). Compared with the 15 nm BBI gold nanoparticles (Figure S3 in Supporting Information), the sizes of as-prepared nanoparticles were measured and 200 NPs of each size were statistically analyzed and found to be about  $2.1 \pm 0.6$ ,  $5.6 \pm 0.8$ ,  $10.5 \pm 2.1$ , and  $15.8 \pm 2.4$  nm. In addition, the hydrodynamic diameters of the Au-TIOP NPs were measured by dynamic light scattering (DLS) and are shown in Table 1. It is reasonable that the hydrodynamic diameters were a little larger than the sizes determined by TEM, due to the different measuring principles of each method. For simplicity, the sizes of the Au-TIOP NPs are referred to as 2, 6, 10, and 16 nm in the rest of this paper. The  $\zeta$ -potentials of each size of Au-TIOP NP were analyzed using a Nano ZS



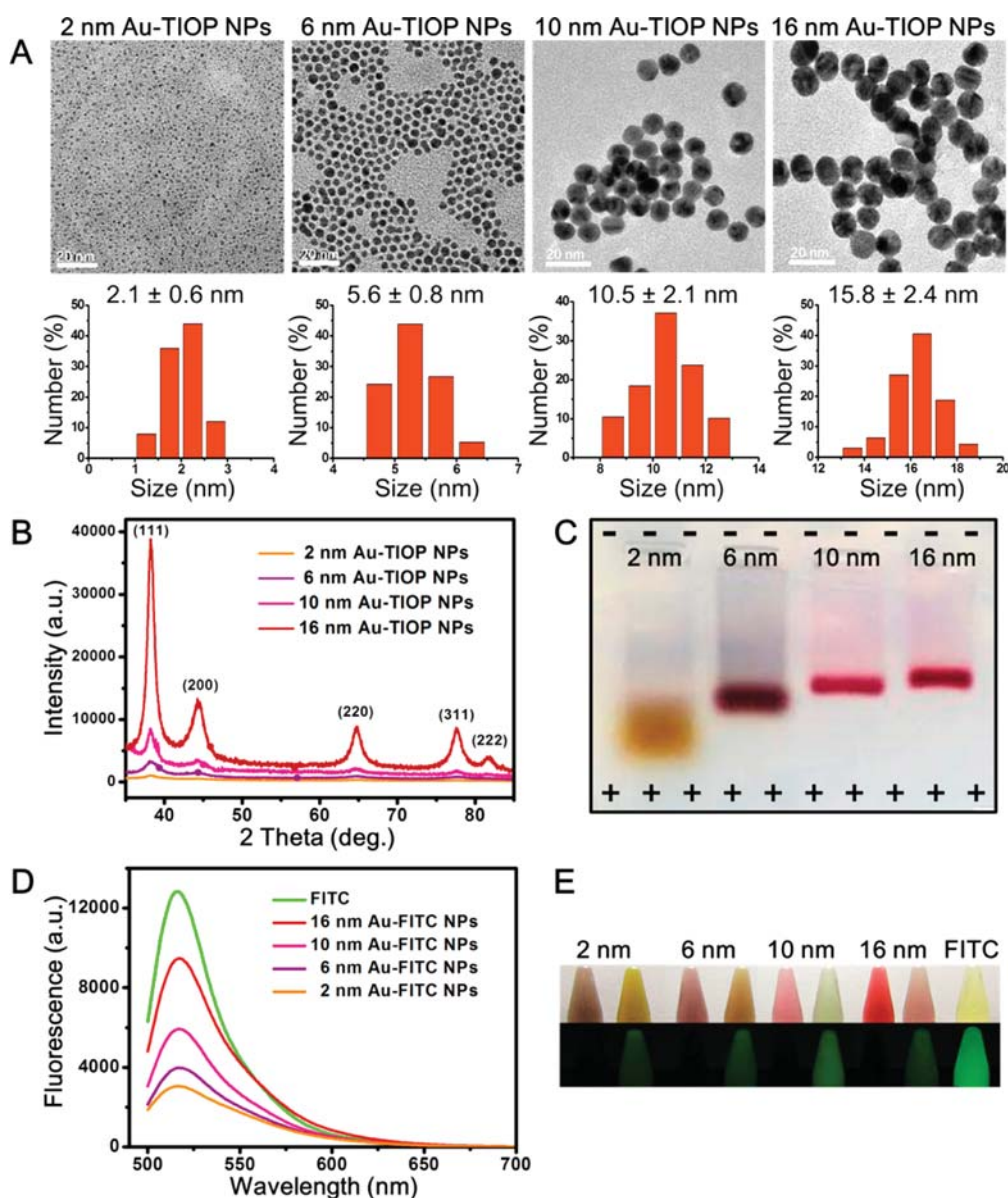


Figure 1. Characterization of 2, 6, 10, and 16 nm Au-TIOP NPs and Au-FITC NPs with different sizes. (A) TEM images and the corresponding size distribution histograms of the different sizes of Au-TIOP NPs. (B) XRD patterns of as-synthesized Au-TIOP NPs. (C) Gel shift assay of as-synthesized Au-TIOP NPs. (D) Fluorescence spectra of the as-synthesized Au-FITC NPs and free FITC. (E) Photos of as-synthesized Au-FITC NPs and free FITC under a daylight lamp and a UV lamp.

**TABLE 1. Characterization of As-Synthesized Au-TIOP NPs and Au-FITC NPs**

sample	UV-vis $\lambda_{\text{max}}$ (nm)	hydrodynamic	
		diameter (nm/PDI)	$\zeta$ -potential (mV)
2 nm Au-TIOP NPs	505	2.58/0.39	−43.9
2 nm Au-FITC NPs	456/477	4.7/0.46	−29.2
2 nm Au-POY2T NPs	507	3.6/0.40	−30.4
6 nm Au-TIOP NPs	518	6.11/0.33	−41.1
2 nm Au-FITC NPs	458/480	10.02/0.45	−28.5
10 nm Au-TIOP NPs	521	11.21/0.20	−39.1
10 nm Au-FITC NPs	458/479	15.49/0.27	−27.4
16 nm Au-TIOP NPs	525	16.8/0.31	−35.9
16 nm Au-FITC NPs	458/477	19.33/0.43	−26.7

Zetasizer and are shown in Table 1. The  $\zeta$ -potentials of Au-TIOP NPs were −43.9 mV (2 nm), −41.1 mV (6 nm), −39.1 mV (10 nm), and −35.9 mV (16 nm). All of the Au-TIOP NPs were negatively charged, and there was a minor difference (2–3.2 mV) between each pair of adjacent sizes.

X-ray diffraction (XRD) analysis was also used to characterize the four sizes of gold nanoparticles. As shown in Figure 1B, there were five primary diffraction peaks at 38.187, 44.385, 64.576, 77.567, and 81.722, which could be correspondingly indexed to the crystal planes of (111), (200), (220), (311), and (222) of Au. This result was consistent with the XRD patterns of Au with a PDF number of 04-0784 (cubic,  $a = b = c = 0.2884$  nm,

$d(111) = 0.2355$  nm). A previous report showed that the smaller the particle, the wider the corresponding XRD peak.<sup>32</sup> This has also been confirmed in this study, as shown in Figure 1B. Due to the preparation of such small nanoparticles and the reduced degree of crystallization, diffraction peaks of the Au NP samples exhibited a degree of broadening. Furthermore, according to the famous Scherrer equation,  $D = k\lambda/B \cos \theta$ ,<sup>33</sup> the calculation based on the (111) peak line width at half-maximum intensity from top to bottom roughly showed that the average sizes of the nanoparticles were about 16, 10, 6, and 2 nm. These sizes are also consistent with the results above.

Electrophoresis of colloidal gold nanoparticles was conducted not only to demonstrate the surface charge of the particles but also to determine their relative size.<sup>34</sup> As shown in Figure 1C, all of the nanoparticles with good dispersion moved toward the anode side of the electrophoresis tank, meaning that they were all negatively charged. It was also obvious that the 2 nm Au-TIOP NPs traveled the longest distance while the 16 nm Au-TIOP NPs moved the shortest distance within the same time. This can be attributed to the different resistance to the gel, which is related to the particle size. It is reasonable to assume that, since the surface charges were almost the same, the electrophoresis speed or distance traveled by the NPs was determined by their sizes.

Moreover, in order to confirm the dispersion of synthesized Au-TIOP NPs in relevant media, additional stability experiments were conducted. As shown in Figure S4 in Supporting Information, Au-TIOP NPs were well-dispersed in the relevant media in a discrete state, and the absorption peaks of each particle dispersed in different solutions also trended toward identical behaviors (for the ultrasmall size of synthesized nanoparticles, the DMEM culture medium could not be used for this test).

In summary, several methods were used to demonstrate that we successfully prepared spherical-shaped and stable Au-TIOP NPs with diameters of 2, 6, 10, and 16 nm with good PDI. As these nanoparticles differed only in size, they were used for the following studies.

**Characterization of Au-FITC NPs with Different Sizes.** In order to observe the exact distribution of the nanoparticles in cells through confocal laser scanning microscopy (CLSM), different sizes of Au-TIOP NPs were labeled with FITC. As shown in Figure S5 in Supporting Information, PEG2000 was used as a linker between particles and FITC to prevent fluorescence quenching due to the nanomaterial surface energy transfer effect.<sup>35,36</sup> The particle size and morphology of FITC-labeled gold nanoparticles can be visualized by TEM (Figure S6 in Supporting Information). As a result of the attachment of polymers to the surface of the particles, the monodispersity of the gold nanoparticles decreased and localized aggregation occurred. Furthermore,

because of the polymeric covering, the size of the nanoparticles increased (Table 1).

UV-vis absorption spectroscopy, a common method to characterize gold nanoparticles, was used to acquire the absorbance spectra of the nanoparticles before and after FITC labeling. As shown in Figure S7 in Supporting Information (a–d, black), the UV-vis absorption peak was red-shifted as the size of the Au-TIOP NPs increased. The measured absorption peaks of the 2, 6, 10, and 16 nm Au-TIOP NPs were 505, 518, 521, and 525 nm, respectively. This result was in agreement with the Mie theory.<sup>37</sup> The maximum absorption wavelength of the FITC molecule is between 490 and 495 nm, and its maximum emission wavelength is around 525–530 nm, resulting in a bright yellow-green fluorescence. After fluorescence labeling, as the red curves show (Figure S7 in Supporting Information), all four sizes of Au-TIOP NPs have large absorption peaks between 450 and 480 nm, which are similar to the absorption peak at 492 nm of free FITC. The fluorescence spectra, as shown in Figure 1D, indicated that the FITC-labeled nanoparticles also have different levels of emission and the emission peaks are all consistent with that of free FITC. As shown in Figure 1E, the color of each nanoparticle solution changed after fluorescence labeling. FITC-labeled nanoparticles also emit similar yellow-green fluorescence under ultraviolet light compared with the free FITC solution. This also proved that the prepared gold nanoparticles have fluorescent characteristics that are suitable for use in the CLSM study.

Size is a critically important factor in this study, so more than one method was used to measure the particle size to ensure the credibility of the following experiment. All the data (Figure S8 and Figure S9 in Supporting Information) are summarized in Table 1. As mentioned above, the different UV-vis absorption peaks reflect the different sizes of the gold nanoparticles. Compared with TEM images, DLS characterization gives the true hydrodynamic diameter, which reflects the real dispersed state of gold nanoparticles in solution, especially when they are surface-modified by polymers. For example, the hydrodynamic size of the 6 nm Au-TIOP NPs changed from 6.11 to 10.02 nm after FITC modification, which means that the PEG-FITC polymer added a 3–4 nm thick surface cover to the nanoparticles. The  $\zeta$ -potential changes were also observed, as shown in Table 1.

**Distribution of Au-TIOP NPs with Different Sizes in MCF-7 Cells.** Bio-TEM was conducted to observe the distribution of Au-TIOP NPs in MCF-7 cells. After treatment with different sizes of Au-TIOP NPs, cells were harvested and sectioned for bio-TEM analysis. As shown in Figure 2, 2 and 6 nm Au-TIOP NPs were located in both cytoplasm and nucleus. More importantly, they were found to be monodispersed in the cell, not aggregated. In contrast, the larger Au-TIOP NPs (10 and 16 nm) were located in

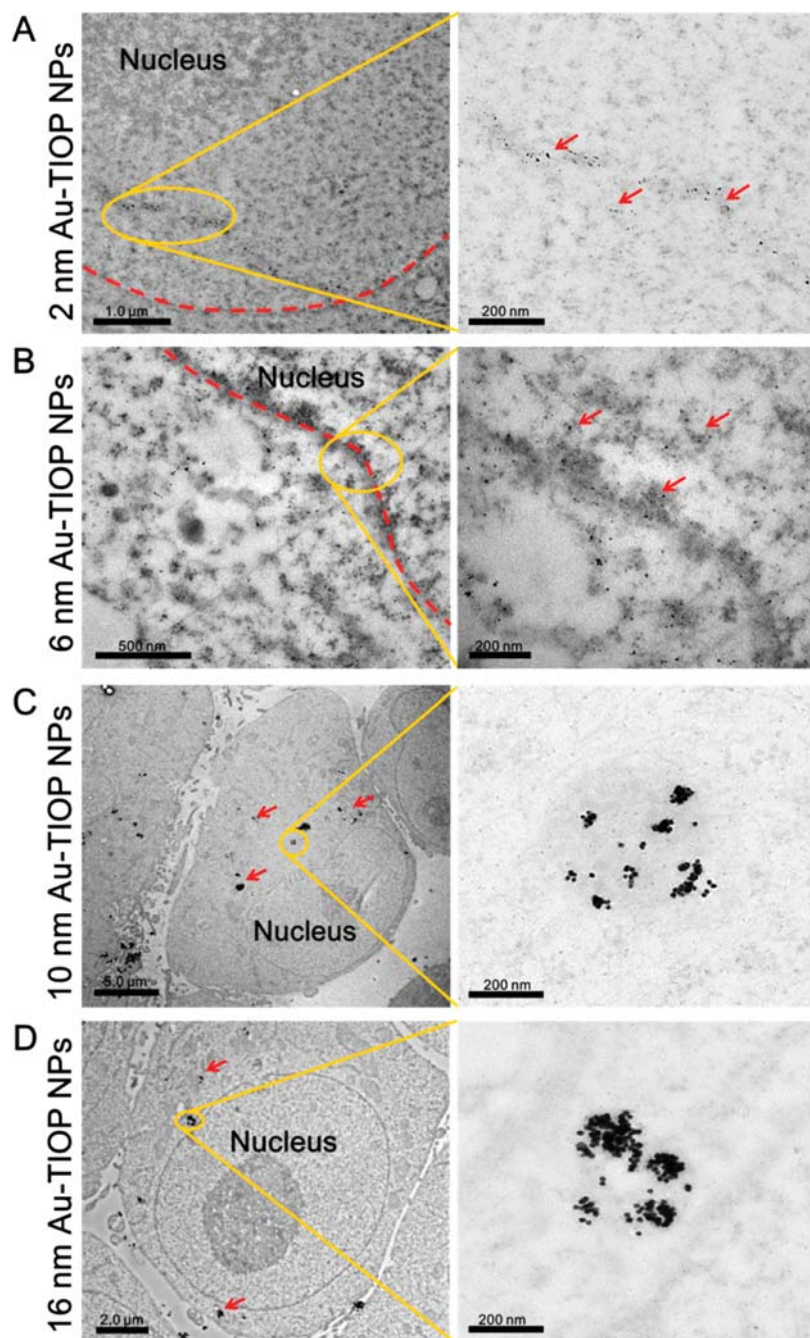


Figure 2. Bio-TEM images of the localization of 2, 6, 10, and 16 nm Au-TIOP NPs in MCF-7 cells after 24 h treatment.

the cytoplasm, and none of them entered the cell nucleus. Additionally, most of them were trapped in vesicles. We reasoned that the size-dependent nuclear distribution of the Au-TIOP NPs is related to the nuclear pore complex (NPC), which is reported to allow cargos smaller than 9 nm to enter the nucleus freely.<sup>38</sup> This hypothesis was further proved by our next experiment.

Bio-TEM results indicate that the smaller 2 and 6 nm Au-TIOP NPs have the ability to enter the nuclei of tumor cells. Thereafter, the quantitative distribution of Au-TIOP NPs in cell nucleus was determined by ICP-MS. Cell nuclei were extracted for ICP-MS analysis after

incubation for different times with various concentrations of Au-TIOP NPs. The number of NPs was then calculated according to a previously reported method.<sup>16</sup> As shown in Figure 3A(a), when cells were incubated with increasing concentrations (1 to 100 nM in particle number dose) of 2 nm Au-TIOP NPs for 24 h, the number of NPs in cells and nuclei increased and the intranuclear percentage of Au-TIOP NPs in whole cells reached about 40% when the incubation concentration was raised to 100 nM. When the incubation concentration was 100 nM, the amount of 2 nm Au-TIOP NPs in cells and nuclei also increased with



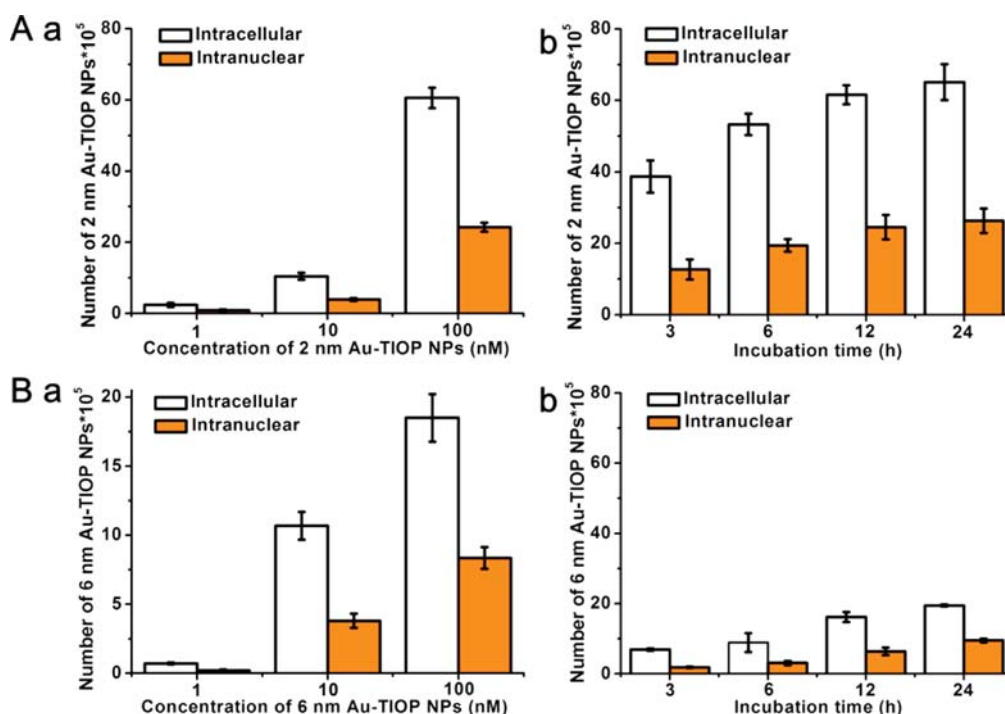


**Figure 3.** Number of 2 and 6 nm Au-TIOP NPs in cells and nuclei. (A) Number of 2 nm Au-TIOP NPs (a) after 24 h treatment at concentrations of 1, 10, and 100 nM; (b) after treatment for 3, 6, 12, and 24 h at a concentration of 100 nM. (B) Number of 6 nm Au-TIOP NPs (a) after 24 h treatment at concentrations of 1, 10, and 100 nM; (b) after treatment for 3, 6, 12, and 24 h at a concentration of 100 nM. All the volumes of Au-TIOP NPs solution added were 1 mL, and the concentration was in particle number dose.

increasing incubation time (Figure 3A(b)), which is in accordance with the result in Figure 3A(a). Similar results were obtained for 6 nm Au-TIOP NPs (Figure 3B), but a significant difference was that the number of 6 nm Au-TIOP NPs in the cells and nuclei was about 1/4 of that for cells treated with 2 nm Au-TIOP NPs under the same conditions. This also demonstrated that the smaller 2 nm Au-TIOP NPs can enter into cells and nuclei more easily and quickly than the 6 nm Au-TIOP NPs, which is consistent with the Bio-TEM images.

**Distribution of Au-FITC NPs with Different Sizes in MCF-7 Cells.** The fluorescent molecule FITC was conjugated to Au-TIOP NPs for CLSM. As shown in Figure 4, only 2 nm Au-FITC NP-treated MCF-7 cells exhibited an FITC signal (indicating the location of the nanoparticles) in both cytoplasm and nucleus. Cells treated with the other three larger nanoparticles exhibited an FITC signal in the cytoplasm only. From these results, we concluded that the 2 nm Au-FITC NPs were capable of entering the cell nucleus and 6, 10, and 16 nm Au-FITC NPs were not. This raises the question why the 6 nm nanoparticles were located in the nucleus in the TEM experiment but in the cytoplasm only in the CLSM experiment. This result could be interpreted in terms of the size increase which occurred when the Au-TIOP NPs were conjugated to FITC using PEG as a linker. The hydrodynamic diameter of the 6 nm Au-FITC NPs was actually 10.02 nm after fluorescence labeling, as shown in Table 1. This final size was larger than the 9 nm

threshold of the NPC, thus limiting the free entry of the nanoparticles into the nucleus.

#### Ultrasmall Au-TIOP NPs for Carrying DNA into the Nucleus.

Triplex-forming oligonucleotides are a kind of single-stranded DNA which can bind to the major groove of double-stranded DNA and form a triplex.<sup>39</sup> The binding between TFOs and double-stranded DNA follows the principle of Hoogsteen base pairing; therefore, a TFO can be designed to bind to a specific double-stranded DNA sequence. TFOs have been used to bind to the transcription initiation site of a target gene and inhibit its transcription, eventually silencing the gene. However, TFOs are quite vulnerable in cells and blood due to high DNase activity. High concentrations of TFOs are needed to achieve gene down-regulation. Many studies reported that DNA stability was increased significantly by conjugating the DNA with gold nanoparticles.<sup>29,40,41</sup> The high salt concentration around gold nanoparticles and steric hindrance between DNase and the conjugated DNA strand successfully protected the DNA. Thus, we decided to use our gold nanoparticles as a TFO carrier. As TFOs are only effective in the cell nucleus, we took advantage of the ability of 2 nm Au-TIOP NPs to enter the nucleus and chose 2 nm Au-TIOP NPs as the TFO carrier.

We selected a TFO named POY2T from a previous report.<sup>42</sup> POY2T is a 23 nt oligonucleotide (TGGGTGGGTGGTTTGTGTTTGGG) which can bind to the P2 promoter of the c-myc oncogene and down-regulate

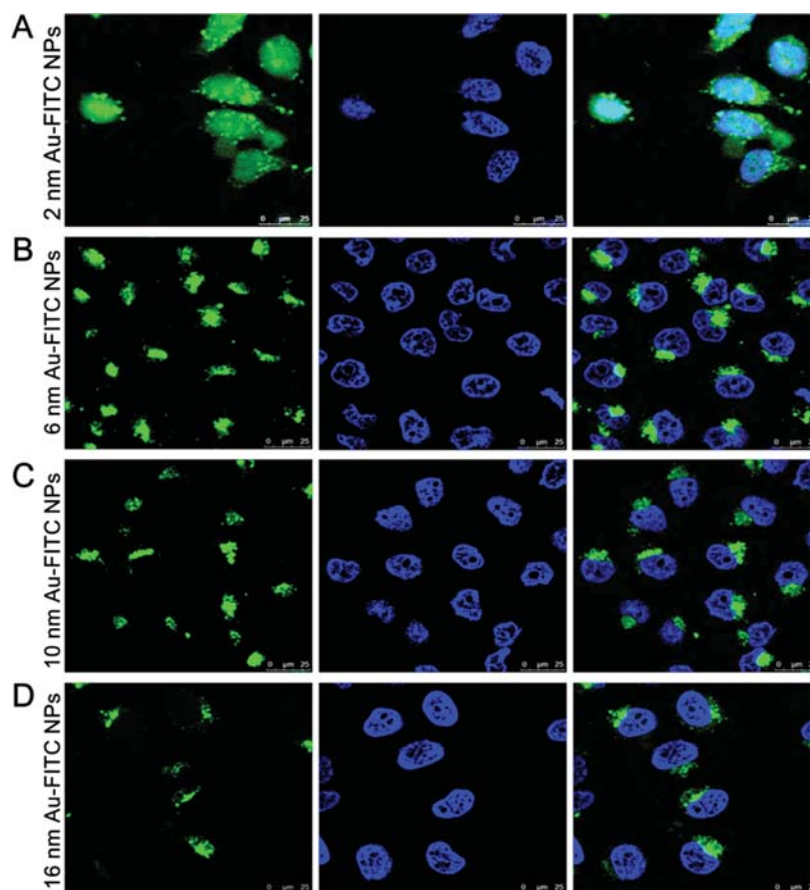


**Figure 4.** Intracellular localization of Au-FITC NPs with different sizes in MCF-7 cells observed by confocal laser scanning microscopy. MCF-7S cells were cultured in confocal dishes and incubated with Au-FITC NPs (green) of different sizes for 24 h. Cells were then washed with PBS three times, and nuclei were stained by Hoechst 33342 (blue). Cells were fixed by paraformaldehyde and observed by confocal microscopy ( $\text{ex}_{\text{FITC}} = 488 \text{ nm}$ ,  $\text{ex}_{\text{Hoechst}} = 405 \text{ nm}$ ).

c-myc expression. Figure S10 in Supporting Information shows that POY2T only inhibits cell proliferation at high concentrations (5 and  $10 \mu\text{M}$ ). In order to demonstrate the sequence-specific toxicity of POY2T, another oligonucleotide named POY2M with a scrambled sequence (GGTGTGTTGGTGGTGTGTTG) derived from POY2T was used as a control TFO sequence. It is nontoxic to MCF-7 cells at the same concentration compared with POY2T (Figure S10 in Supporting Information). We concluded that POY2T was toxic to MCF-7 cells by down-regulating c-myc gene expression and inhibiting cell proliferation.<sup>43</sup> Therefore, POY2T is an effective TFO for use in our study. 5' Amino-modified POY2T was linked to Au-TIOP NPs through the carboxyl group of tiopronin (Figure S11 in Supporting Information). The TFO-modified nanoparticles were named as Au-POY2T NPs (Figure 5A and Figure S12 in Supporting Information). MTT assays showed that Au-POY2T NPs inhibit cell viability by about 30% at a low concentration ( $1 \mu\text{M}$ ), and POY2T was not toxic at this concentration (Figure 5B). Au NPs will interfere with cell functions according to a previous report.<sup>44</sup> The potential toxicity of amino modification should also be noticed.  $\text{NH}_2$ -POY2T or Au-TIOP NPs

showed no cytotoxicity at the same concentration of  $1 \mu\text{M}$  Au-POY2T according to our result (Figure 5B), which means that the decrease in cell viability after treatment with Au-POY2T NPs was not caused by Au-TIOP NPs or amino modification of POY2T. Moreover, Au-POY2M was set as a control of Au-POY2T to rule out the interference of possible toxic materials introduced during the synthesis. The result shows that Au-POY2M was not more toxic than free POY2M, indicating that the increased toxicity of Au-POY2T NPs was not caused by the conjugating process. It is the outcome of improved stability of POY2T in culture medium and cells after conjugation with Au NPs.

Real-time PCR and Western blot analyses were conducted to determine c-myc expression after Au-POY2T NP treatment. Real-time PCR results revealed that the c-myc mRNA level was decreased to about 50% in Au-POY2T NP-treated MCF-7 cells, much lower than in the POY2T-treated cells (85%) (Figure 5C and Figure S13 in Supporting Information). Western blotting also confirmed this result. As shown in Figure 5D and Figure S14 in Supporting Information, the c-myc protein level in cells was reduced significantly after treatment with Au-POY2T NPs for 24 h, and POY2T only



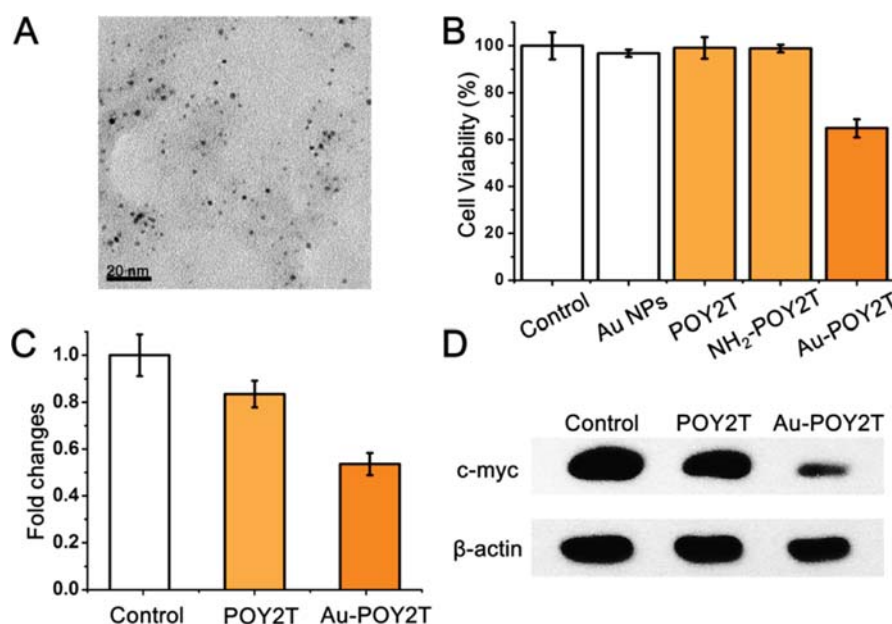


**Figure 5.** Cytotoxicity and gene regulation evaluation of Au-POY2T NPs in MCF-7 cells. (A) TEM image of as-synthesized Au-POY2T NPs. (B) Cytotoxicity evaluation of Au-POY2T NPs compared to control, Au NPs, POY2T, and NH<sub>2</sub>-POY2T (at 1  $\mu$ M in POY2T). (C) C-myc mRNA level determined by real-time PCR after 24 h treatment of 5  $\mu$ M POY2T and Au-POY2T. (D) C-myc protein level determined by Western blotting after 24 h treatment of 5  $\mu$ M POY2T and Au-POY2T.

showed weak gene silencing ability compared to Au-POY2T NPs.

Nucleus, as the center for cell proliferation regulation, plays an important role in tumor metastasis. Killing tumor cells by interfering with their gene expression in the nucleus has long been catching scientist's eyes. Antisense oligonucleotides are potential candidates for gene therapies because of their easy manipulation. Although the antisense approach is attractive, it suffers from one major disadvantage: the number of mRNA molecules in a cell is huge, which makes it difficult to completely inhibit a specific mRNA. Moreover, blocking translation of mRNA does not prevent mRNA from reproduction because of the feedback mechanisms that lead to increased mRNA transcription in antisense therapy. Triplex-forming oligonucleotides are molecules that bind to specific duplex DNA sequence and can selectively modulate the expression of genes. It is therefore a much more practical approach that directly blocks gene transcription to bring down the mRNA concentration in a more efficient and long-lasting way.<sup>45</sup>

However, the inefficient delivery of TFOs to the targeted cell greatly challenges TFOs to be used as antigene agents. Oligonucleotides have a much greater molecular mass and are polyanionic compared to small-molecule pharmaceuticals, and these make the cellular uptake of TFOs by passive diffusion inefficient. Therefore, simple addition of TFOs to culture medium could hardly reach the therapeutic concentration. Previously, cell-penetrating peptides have been used to increase the uptake of TFOs. Other ways, such as single-cell microinjection, comixture of oligonucleotides with

cationic liposomes, and electroporation, have also been tried.<sup>46–50</sup> However, none of these methods could directly deliver TFOs into the nucleus. In our method, we directly delivered TFOs using our 2 nm Au NP carriers, while avoiding the stress caused by microinjection and electroporation, etc.

Moreover, even triplex-forming oligonucleotides are successfully internalized into cells, and they do not effectively down-regulate the targeted gene. It is because unmodified oligonucleotides are prone to be degraded by endogenous DNase enzymes, resulting in little intact TFOs in the media that finally enter the nucleus. Many efforts have been made to improve the stability of triplex-forming oligonucleotides under physiological conditions. Typical approaches include modifying the nucleosides of TFO or incorporation of modified bases. However, while these modifications are carried out to achieve resistance to undesirable DNase degradation, decreased binding to the target sequence or unspecific binding happens sometimes. Gold nanoparticles have a high affinity for oligonucleotides. Our method of using ultras-small Au-TIOP NPs functionalized with amino-modified TFOs to deliver TFOs stably to cells in the culture media and the binding between gold nanoparticles and the TFOs is very selective and cooperative. Thus, not only enhanced entry of TFOs to the nucleus is achieved but also protection of oligonucleotide is achieved while keeping its specificity and high transcription inhibition efficacy. During the binding of TFO with the DNA double helix in the major groove, Au NPs and other TFOs may cause steric hindrance, but 2 nm Au NPs are even smaller than the width of the major groove (22 Å).<sup>51</sup>

Oligonucleotide is also considered to be a flexible material, and only a few TFOs are near the hybridization site. Thus, the assumed steric hindrance caused by Au NPs and other TFOs is not likely to stop hybridization of TFO with the target site effectively. Another question that should be discussed is that only one TFO in Au-POY2T takes part in the hybridization, then higher overall doses of TFO are needed theoretically. We think that the improved stability of TFO on Au NPs may be the answer to this question. Mirkin *et al.* reported that the half-life of DNA on Au NPs was prolonged by 4.3 times compared to that of free DNA.<sup>40</sup> Au NPs can protect TFOs effectively on their way from culture medium to cell nuclei, while free TFOs go unprotected. Higher TFO concentration in nuclei could then be achieved by a Au-TFO delivery system at the same treatment concentration. Slower diffusion of larger Au-TFO particles than that of free TFOs according to Stokes' law is also a problem which may makes Au-TFO work slowly. However, the diffusion speed of Au-TFO and free TFO will not be very different concerning the ultrasmall size of Au NPs. Moreover,

stability is the key in TFO-mediated gene regulation, not diffusion speed. We therefore think that slower diffusion speed will not compromise the gene regulation efficiency of Au-TFO.

## CONCLUSION

In this work, gold nanoparticles with different sizes and consistent surface properties were selected as a typical model to explore the interaction between nanoparticles and the nucleus of breast cancer cells. We used various means to systematically study the entry of Au-TIOP NPs into the cell nucleus and concluded that nuclear entry is critically dependent on size. This work presents new evidence about the entry of ultrasmall Au-TIOP NPs into the cell nucleus and provides a new strategy for regulating gene expression by delivering TFOs into the nucleus with ultrasmall gold nanoparticles. Our future work also aims at using these ultrasmall nanoparticles to realize nuclear targeting for biomedical application. More importantly, guidelines were provided to choose nanocarriers for different purposes in the field of biomedicine.

## EXPERIMENTAL SECTION

**Chemicals.** Sodium borohydride ( $\geq 98.0\%$ ), gold(III) chloride trihydrate ( $\geq 99.9\%$ ,  $\text{HAuCl}_4 \cdot 3\text{H}_2\text{O}$ ), trisodium citrate tribasic dihydrate ( $\geq 99.0\%$ ), *N*-(2-mercaptopropionyl)glycine (tiopronin), *N*-hydroxysuccinimide (98%,  $\text{NHS}$ ,  $\text{C}_4\text{H}_5\text{NO}_3$ ), *N*-(3-(dimethylamino)propyl)-*N*'-ethylcarbodiimide hydrochloride (EDC,  $\text{C}_8\text{H}_{17}\text{N}_3 \cdot \text{HCl}$ ), and fluorescein isothiocyanate isomer I ( $\geq 90\%$ , FITC,  $\text{C}_{21}\text{H}_{11}\text{NO}_5\text{S}$ ) were purchased from Sigma-Aldrich (St Louis, USA). L-(+)-Ascorbic acid (99%) was supplied by Acros (USA). Amino-modified poly(ethylene glycol) (PEG-2NH<sub>2</sub>, MW = 2000, 99%) was supplied by Beijing SeaskyBio Technology Company. Nitric acid and hydrogen peroxide (MOS grade) were provided by Beijing Chemical Reagents Institute (China). Gold stock standard solution (1000  $\mu\text{g/mL}$ ) was obtained from the National Analysis Center for Iron and Steel, China. Unless otherwise noted, all chemicals were used as received without further purification, and Milli-Q water (18.2  $\text{M}\Omega \cdot \text{cm}$ , Millipore System Inc.) was used throughout this study.

**Cell Culture.** The MCF-7 (human breast cancer cell line) cell was maintained in Dulbecco's modified Eagle's medium (DMEM) with 4.5 g/L glucose and 10% fetal bovine serum in a water-jacketed CO<sub>2</sub> incubator (Forma Series II 3110, Thermo Fisher Scientific Inc., USA) providing a humidified atmosphere containing 5% CO<sub>2</sub> at 37 °C.

**Cell Viability Assay.** MCF-7 cells were seeded at  $5 \times 10^3$  cells per well in a 96-well plate, preincubated for 24 h, then incubated with POY2T (0.1, 1, 2.5, 5, and 10  $\mu\text{M}$ ), POY2M (0.1, 1, 2.5, 5, and 10  $\mu\text{M}$ ), Au-POY2T NPs (at 1  $\mu\text{M}$  in POY2T), NH<sub>2</sub>-POY2T (at 1  $\mu\text{M}$  in POY2T), or Au-TIOP NPs (as a control of Au-POY2T NPs) for 24 h. The medium was then replaced with 100  $\mu\text{L}$  of 0.5 mg/mL MTT, and after 3 h, the MTT solution was replaced with 150  $\mu\text{L}$  of DMSO solution. The absorbance at 570 nm of each well was measured by a microplate reader (Infinite M200, Tecan, Durham, USA). The absorbance at 630 nm was also measured as a reference. Untreated cells in medium were used as control. All standard deviations were calculated from three replicates.

**Isolation of Cell Nuclei and Qualitative Determination of Au Content.** MCF-7 cells ( $10^5$ ) were seeded in 6-well plates 24 h in advance. Afterward, 1 mL of Au-TIOP NPs of 2 and 6 nm at concentrations of 1, 10, and 100 nM (in particle number dose) was added to the wells and incubated for 24 h or incubated for 3, 6, 12, and 24 h at a concentration of 100 nM. Then the cells were washed with

PBS, trypsinized, and centrifuged for 3 min at 179g. The treated cells were then resuspended in 2 mL of PBS and divided into two equal groups. One group was dissolved in aqua regia for nitrolysis and then analyzed by ICP-MS for gold element quantification. The other part was handled for cell nucleus extraction using a nuclear extraction kit (SN000, Solarbio, Shanghai, China). In brief, the sample was grinded in lysis buffer for 3 min, centrifuged at 700g for 5 min, resuspended in lysis buffer, precipitated in medium buffer, and stored in store buffer. All procedures were carried out at 4 °C quickly to keep nucleus integrity. The extracted nuclei were also analyzed by ICP-MS after nitrolysis. The percentage of Au NPs located in the cell nucleus was calculated according to the Au content in the isolated nuclei compared to that in the whole cells.

**Subcellular Localization of Au-FITC NPs.** MCF-7 cells were seeded into 35 mm glass dishes, incubated at 37 °C for 24 h, then cultured with Au-FITC NPs at a gold content concentration of 5  $\mu\text{M}$  at 37 °C for 24 h. Cells were imaged using a TCS SP2 (Leica Microsystems GmbH Wetzlar, Germany) confocal microscope. Hoechst 33342 was used to stain cell nuclei. FITC was excited by a 488 nm laser, while Hoechst 33342 was excited by a 405 nm laser.

**Bio-TEM Observation of Au-TIOP NP-Treated MCF-7 Cells.** Bio-TEM was carried out to observe the distribution of Au-TIOP NPs in treated MCF-7 cells. Briefly, MCF-7 cells were seeded in 6-well plates and incubated with 1 mL of Au-TIOP NPs at a concentration of 100 nM for 24 h, washed with PBS gently twice, and fixed overnight using 3% glutaraldehyde solution at room temperature. This was followed by secondary fixation with 1% osmium tetroxide, then dehydration in a gradient ethanol series. Cells were finally embedded in Epon resin after 3 day polymerization at 60 °C. Embedded samples were sectioned (50–60 nm in thickness) and examined under an electron microscope (HT7700, 120 kV, Hitachi, Japan). Uranyl acetate staining was not used in this study to avoid uranyl acetate precipitation interfering with the TEM observation.

**C-myc Gene Expression.** C-myc gene expression, in both mRNA and protein levels, was quantitatively determined by reverse transcriptase polymerase chain reaction (RT-PCR), real-time PCR, and Western blotting. MCF-7 cells were incubated with Au-POY2T NPs and POY2T at a POY2T concentration of 5  $\mu\text{M}$  for 24 h. For RT-PCR, total mRNA was extracted from MCF-7 cells,

and first-strand cDNA was synthesized using a PrimeScript first-strand cDNA synthesis kit (Takara, Shiga, Japan). Real-time PCR analysis of c-myc was conducted for quantitative analysis of the reduction in c-myc transcription. GAPDH was used as a reference gene. Specific forward and reverse primer sequences were as follows: c-myc fwd, 5'-TGAGGAGACACCGCCAC-3'; c-myc rev, 5'-CAACATCGATTCTCTCATCTTC-3'; GAPDH fwd, 5'-GAC-TTCAACAGCAACTCCAC-3'; GAPDH rev, 5'-TCCACCACTTG-TTGCTGTA-3'. PCR parameters were as follows: one cycle of 2 min at 95 °C, followed by 20 s at 95 °C, 20 s at 55.6 °C, and 40 s at 72 °C for 45 cycles.

For Western blotting, protein lysates from cells treated with 5  $\mu$ M POY2T and Au-POY2T for 24 h were extracted in TNE lysis buffer (0.5% NP-40, 10 mM Tris, 150 mM NaCl, 1 mM EDTA and protease inhibitors). Total protein (50 mg) was separated by 10% SDS-PAGE gel, transferred to a PVDF membrane, treated with primary rabbit monoclonal c-myc (diluted 1:1000, BS246; Bioworld Technology, Inc., Minnesota, USA), and then immunoblotted with peroxidase-conjugated secondary antibody (1:5000, zsBio, Beijing, China).

**Conflict of Interest:** The authors declare no competing financial interest.

**Acknowledgment.** This work was supported by the Chinese Natural Science Foundation project (81171455), a National Distinguished Young Scholars grant (31225009) from the National Natural Science Foundation of China, the National Key Basic Research Program of China (2009CB930200 and SS2014AA020708), the Chinese Academy of Sciences (CAS) "Hundred Talents Program" (07165111ZX), the CAS Knowledge Innovation Program and the State High-Tech Development Plan (2012AA020804). This work was also supported in part by NIH/NIMHD 8 G12 MD007597, and USAMRMC W81XWH-10-1-0767 grants. The authors also appreciate the support by the "Strategic Priority Research Program" of the Chinese Academy of Sciences (XDA09030301).

**Supporting Information Available:** Synthesis of Au-TiOP NPs and Au-FITC NPs with different sizes, characterization of Au-TiOP NPs and Au-FITC NPs with different sizes, agarose gel electrophoresis, and ICP-MS. This material is available free of charge via the Internet at <http://pubs.acs.org>.

## REFERENCES AND NOTES

- Dreaden, E. C.; Alkilany, A. M.; Huang, X. H.; Murphy, C. J.; El-Sayed, M. A. The Golden Age: Gold Nanoparticles for Biomedicine. *Chem. Soc. Rev.* **2012**, *41*, 2740–2779.
- Ghosh, P.; Han, G.; De, M.; Kim, C. K.; Rotello, V. M. Gold Nanoparticles in Delivery Applications. *Adv. Drug Delivery Rev.* **2008**, *60*, 1307–1315.
- Pissuwan, D.; Niidome, T.; Cortie, M. B. The Forthcoming Applications of Gold Nanoparticles in Drug and Gene Delivery Systems. *J. Controlled Release* **2011**, *149*, 65–71.
- Dreaden, E. C.; Mackey, M. A.; Huang, X. H.; Kang, B.; El-Sayed, M. A. Beating Cancer in Multiple Ways Using Nanogold. *Chem. Soc. Rev.* **2011**, *40*, 3391–3404.
- Huang, K. Y.; Ma, H. L.; Liu, J.; Huo, S. D.; Kumar, A.; Wei, T.; Zhang, X.; Jin, S. B.; Gan, Y. L.; Wang, P. C.; *et al.* Size-Dependent Localization and Penetration of Ultra-small Gold Nanoparticles in Cancer Cells, Multicellular Spheroids, and Tumors *in Vivo*. *ACS Nano* **2012**, *6*, 4483–4493.
- De Jong, W. H.; Hagens, W. I.; Krystek, P.; Burger, M. C.; Sips, A. J. A. M.; Geertsma, R. E. Particle Size-Dependent Organ Distribution of Gold Nanoparticles after Intravenous Administration. *Biomaterials* **2008**, *29*, 1912–1919.
- Pan, Y.; Neuss, S.; Leifert, A.; Fischler, M.; Wen, F.; Simon, U.; Schmid, G.; Brandau, W.; Jahnke-Dechent, W. Size-Dependent Cytotoxicity of Gold Nanoparticles. *Small* **2007**, *3*, 1941–1949.
- Zhang, X. D.; Wu, D.; Shen, X.; Chen, J.; Sun, Y. M.; Liu, P. X.; Liang, X. J. Size-Dependent Radiosensitization of PEG-Coated Gold Nanoparticles for Cancer Radiation Therapy. *Biomaterials* **2012**, *33*, 6408–6419.
- Lesniak, A.; Salvati, A.; Santos-Martinez, M. J.; Radomski, M. W.; Dawson, K. A.; Aberg, C. Nanoparticle Adhesion to the Cell Membrane and Its Effect on Nanoparticle Uptake Efficiency. *J. Am. Chem. Soc.* **2013**, *135*, 1438–1444.
- Jiang, W.; Kim, B. Y. S.; Rutka, J. T.; Chan, W. C. W. Nanoparticle-Mediated Cellular Response Is Size-Dependent. *Nat. Nanotechnol.* **2008**, *3*, 145–150.
- Zhu, M. T.; Li, Y. Y.; Shi, J.; Feng, W. Y.; Nie, G. J.; Zhao, Y. L. Exosomes as Extrapulmonary Signaling Conveyors for Nanoparticle-Induced Systemic Immune Activation. *Small* **2012**, *8*, 404–412.
- Huo, S. D.; Ma, H. L.; Huang, K. Y.; Liu, J.; Wei, T.; Jin, S. B.; Zhang, J. C.; He, S. T.; Liang, X. J. Superior Penetration and Retention Behavior of 50 nm Gold Nanoparticles in Tumors. *Cancer Res.* **2013**, *73*, 319–330.
- Chauhan, V. P.; Popovic, Z.; Chen, O.; Cui, J.; Fukumura, D.; Bawendi, M. G.; Jain, R. K. Fluorescent Nanorods and Nanospheres for Real-Time *In Vivo* Probing of Nanoparticle Shape-Dependent Tumor Penetration. *Angew. Chem., Int. Ed.* **2011**, *50*, 11417–11420.
- Kim, B.; Han, G.; Toley, B. J.; Kim, C.-k.; Rotello, V. M.; Forbes, N. S. Tuning Payload Delivery in Tumour Cylindroids Using Gold Nanoparticles. *Nat. Nanotechnol.* **2010**, *5*, 465–472.
- Perrault, S. D.; Walkey, C.; Jennings, T.; Fischer, H. C.; Chan, W. C. Mediating Tumor Targeting Efficiency of Nanoparticles through Design. *Nano Lett.* **2009**, *9*, 1909–1915.
- Chithrani, B. D.; Ghazani, A. A.; Chan, W. C. W. Determining the Size and Shape Dependence of Gold Nanoparticle Uptake into Mammalian Cells. *Nano Lett.* **2006**, *6*, 662–668.
- Chen, J.; Saeki, F.; Wiley, B. J.; Cang, H.; Cobb, M. J.; Li, Z.-Y.; Au, L.; Zhang, H.; Kimmey, M. B.; Li, X.; *et al.* Gold Nanocages: Bioconjugation and Their Potential Use as Optical Imaging Contrast Agents. *Nano Lett.* **2005**, *5*, 473–477.
- Hirsch, L. R.; Stafford, R. J.; Bankson, J. A.; Sershen, S. R.; Rivera, B.; Price, R. E.; Hazle, J. D.; Halas, N. J.; West, J. L. Nanoshell-Mediated Near-Infrared Thermal Therapy of Tumors under Magnetic Resonance Guidance. *Proc. Natl. Acad. Sci. U.S.A.* **2003**, *100*, 13549–13554.
- Dykman, L.; Khlebtsov, N. Gold Nanoparticles in Biomedical Applications: Recent Advances and Perspectives. *Chem. Soc. Rev.* **2012**, *41*, 2256–2282.
- Dam, D. H. M.; Lee, J. H.; Sisco, P. N.; Co, D. T.; Zhang, M.; Wasielewski, M. R.; Odom, T. W. Direct Observation of Nanoparticle–Cancer Cell Nucleus Interactions. *ACS Nano* **2012**, *6*, 3318–3326.
- Kang, B.; Mackey, M. A.; El-Sayed, M. A. Nuclear Targeting of Gold Nanoparticles in Cancer Cells Induces DNA Damage, Causing Cytokinesis Arrest and Apoptosis. *J. Am. Chem. Soc.* **2010**, *132*, 1517–1519.
- Dobson, J. Gene Therapy Progress and Prospects: Magnetic Nanoparticle-Based Gene Delivery. *Gene Ther.* **2006**, *13*, 283–287.
- Patil, S. D.; Rhodes, D. G.; Burgess, D. J. DNA-Based Therapeutics and DNA Delivery Systems: A Comprehensive Review. *AAPS J.* **2005**, *7*, E61–E77.
- McManus, M. T.; Sharp, P. A. Gene Silencing in Mammals by Small Interfering RNAs. *Nat. Rev. Genet.* **2002**, *3*, 737–747.
- Lebedeva, I.; Stein, C. A. Antisense Oligonucleotides: Promise and Reality. *Annu. Rev. Pharmacol.* **2001**, *41*, 403–419.
- Jason, T. L. H.; Koropatnick, J.; Berg, R. W. Toxicology of Antisense Therapeutics. *Toxicol. Appl. Pharmacol.* **2004**, *201*, 66–83.
- Rosi, N. L.; Giljohann, D. A.; Thaxton, C. S.; Lytton-Jean, A. K. R.; Han, M. S.; Mirkin, C. A. Oligonucleotide-Modified Gold Nanoparticles for Intracellular Gene Regulation. *Science* **2006**, *312*, 1027–1030.
- Jin, R. C.; Wu, G. S.; Li, Z.; Mirkin, C. A.; Schatz, G. C. What Controls the Melting Properties of DNA-Linked Gold Nanoparticle Assemblies? *J. Am. Chem. Soc.* **2003**, *125*, 1643–1654.
- Lytton-Jean, A. K. R.; Mirkin, C. A. A Thermodynamic Investigation into the Binding Properties of DNA Functionalized Gold Nanoparticle Probes and Molecular Fluorophore Probes. *J. Am. Chem. Soc.* **2005**, *127*, 12754–12755.
- Goldsborough, A. S.; Handley, M. D.; Dulcey, A. E.; Pluchino, K. M.; Kannan, P.; Brimacombe, K. R.; Hall, M. D.; Griffiths, G.

- Gottesman, M. M. Collateral Sensitivity of Multidrug-Resistant Cells to the Orphan Drug Tiopronin. *J. Med. Chem.* **2011**, *54*, 4987–4997.
31. Dahl, J. A.; Maddux, B. L. S.; Hutchison, J. E. Toward Greener Nanosynthesis. *Chem. Rev.* **2007**, *107*, 2228–2269.
  32. Petkov, V.; Peng, Y.; Williams, G.; Huang, B. H.; Tomalia, D.; Ren, Y. Structure of Gold Nanoparticles Suspended in Water Studied by X-ray Diffraction and Computer Simulations. *Phys. Rev. B* **2005**, *72*, 195402.
  33. Li, Z. P.; Duan, X. R.; Liu, C. H.; Du, B. A. Selective Determination of Cysteine by Resonance Light Scattering Technique Based on Self-Assembly of Gold Nanoparticles. *Anal. Biochem.* **2006**, *351*, 18–25.
  34. Albanese, A.; Chan, W. C. W. Effect of Gold Nanoparticle Aggregation on Cell Uptake and Toxicity. *ACS Nano* **2011**, *5*, 5478–5489.
  35. Ao, L. M.; Gao, F.; Pan, B. F.; He, R.; Cui, D. X. Fluoroimmunoassay for Antigen Based on Fluorescence Quenching Signal of Gold Nanoparticles. *Anal. Chem.* **2006**, *78*, 1104–1106.
  36. Loumagne, M.; Praho, R.; Nutarelli, D.; Werts, M. H. V.; Debarre, A. Fluorescence Correlation Spectroscopy Reveals Strong Fluorescence Quenching of FITC Adducts on PEGylated Gold Nanoparticles in Water and the Presence of Fluorescent Aggregates of Desorbed Thiolate Ligands. *Phys. Chem. Chem. Phys.* **2010**, *12*, 11004–11014.
  37. Foss, C. A.; Hornyak, G. L.; Stockert, J. A.; Martin, C. R. Template-Synthesized Nanoscopic Gold Particles-Optical-Spectra and the Effects of Particle-Size and Shape. *J. Phys. Chem.* **1994**, *98*, 2963–2971.
  38. Paine, P. L.; Moore, L. C.; Horowitz, S. B. Nuclear-Envelope Permeability. *Nature* **1975**, *254*, 109–114.
  39. Jain, A.; Magistri, M.; Napoli, S.; Carbone, G. M.; Catapano, C. V. Mechanisms of Triplex DNA-Mediated Inhibition of Transcription Initiation in Cells. *Biochimie* **2010**, *92*, 317–320.
  40. Seferos, D. S.; Prigodich, A. E.; Giljohann, D. A.; Patel, P. C.; Mirkin, C. A. Polyvalent DNA Nanoparticle Conjugates Stabilize Nucleic Acids. *Nano Lett.* **2009**, *9*, 308–311.
  41. Han, G.; Martin, C. T.; Rotello, V. M. Stability of Gold Nanoparticle-Bound DNA toward Biological, Physical, and Chemical Agents. *Chem. Biol. Drug Des.* **2006**, *67*, 78–82.
  42. McGuffie, E. M.; Pacheco, D.; Carbone, G. M. R.; Catapano, C. V. Antigenic and Antiproliferative Effects of a c-Myc-Targeting Phosphorothioate Triple Helix-Forming Oligonucleotide in Human Leukemia Cells. *Cancer Res.* **2000**, *60*, 3790–3799.
  43. Dang, C. V. c-Myc Target Genes Involved in Cell Growth, Apoptosis, and Metabolism. *Mol. Cell. Biol.* **1999**, *19*, 1–11.
  44. Leifert, A.; Pan, Y.; Kinkeldey, A.; Schiefer, F.; Setzler, J.; Scheel, O.; Lichtenbeld, H.; Schmid, G.; Wenzel, W.; Jahn-Dechent, W.; *et al.* Differential hERG Ion Channel Activity of Ultrasmall Gold Nanoparticles. *Proc. Natl. Acad. Sci. U.S.A.* **2013**, *110*, 8004–8009.
  45. Guntaka, R. V.; Varma, B. R.; Weber, K. T. Triplex-Forming Oligonucleotides as Modulators of Gene Expression. *Int. J. Biochem. Cell Biol.* **2003**, *35*, 22–31.
  46. Rogers, F. A.; Manoharan, M.; Rabinovitch, P.; Ward, D. C.; Glazer, P. M. Peptide Conjugates for Chromosomal Gene Targeting by Triplex-Forming Oligonucleotides. *Nucleic Acids Res.* **2004**, *32*, 6595–6604.
  47. Harris, J. D.; Lemoine, N. R. Strategies for Targeted Gene Therapy. *Trends Genet.* **1996**, *12*, 400–405.
  48. Stein, C. A.; Cheng, Y. C. Antisense Oligonucleotides as Therapeutic Agents: Is the Bullet Really Magical. *Science* **1993**, *261*, 1004–1012.
  49. Felgner, J. H.; Kumar, R.; Sridhar, C. N.; Wheeler, C. J.; Tsai, Y. J.; Border, R.; Ramsey, P.; Martin, M.; Felgner, P. L. Enhanced Gene Delivery and Mechanism Studies with a Novel Series of Cationic Lipid Formulations. *J. Biol. Chem.* **1994**, *269*, 2550–2561.
  50. Lewis, J. G.; Lin, K. Y.; Kothavale, A.; Flanagan, W. M.; Matteucci, M. D.; DePrince, R. B.; Mook, R. A.; Hendren, R. W.; Wagner, R. W. A Serum-Resistant Cytofectin for Cellular Delivery of Antisense Oligodeoxynucleotides and Plasmid DNA. *Proc. Natl. Acad. Sci. U.S.A.* **1996**, *93*, 3176–3181.
  51. Wing, R.; Drew, H.; Takano, T.; Broka, C.; Tanaka, S.; Itakura, K.; Dickerson, R. E. Crystal-Structure Analysis of a Complete Turn of B-DNA. *Nature* **1980**, *287*, 755–758.



## REVIEW

# pH-responsive mesoporous silica nanoparticles employed in controlled drug delivery systems for cancer treatment

Ke-Ni Yang<sup>1,2</sup>, Chun-Qiu Zhang<sup>2</sup>, Wei Wang<sup>1</sup>, Paul C. Wang<sup>3</sup>, Jian-Ping Zhou<sup>1</sup>, Xing-Jie Liang<sup>2</sup>

<sup>1</sup>State Key Laboratory of Natural Medicines, Department of Pharmaceutics, China Pharmaceutical University, Nanjing 210009, China; <sup>2</sup>CAS Key Laboratory for Biological Effects of Nanomaterials and Nanosafety, National Center for Nanoscience and Technology, Chinese Academy of Sciences, Beijing 100190, China; <sup>3</sup>Laboratory of Molecular Imaging, Department of Radiology, Howard University, Washington DC 20060, USA

### ABSTRACT

In the fight against cancer, controlled drug delivery systems have emerged to enhance the therapeutic efficacy and safety of anti-cancer drugs. Among these systems, mesoporous silica nanoparticles (MSNs) with a functional surface possess obvious advantages and were thus rapidly developed for cancer treatment. Many stimuli-responsive materials, such as nanoparticles, polymers, and inorganic materials, have been applied as caps and gatekeepers to control drug release from MSNs. This review presents an overview of the recent progress in the production of pH-responsive MSNs based on the pH gradient between normal tissues and the tumor microenvironment. Four main categories of gatekeepers can respond to acidic conditions. These categories will be described in detail.

### KEYWORDS

Mesoporous silica nanoparticles; pH-responsive; controlled drug release; drug delivery systems; antineoplastic protocols

## Introduction

Cancer is the leading cause of death worldwide. Conventional chemotherapy is often characterized by clinical inefficiency and serious side-effects, mainly because of the leaking out of drugs during blood circulation and nonspecific cell/tissue biodistribution. The development of nanotechnology and nanomedicine in the past decades has facilitated the development of various nanovehicles for experimental and clinical application as drug delivery systems to solve these problems<sup>1,2</sup>. Nanovehicles benefit from surface properties and nanoscales and can thus accumulate in tumor tissue effectively with grafted multiple targeting ligands for 'active targeting', while exhibiting enhanced permeability and retention effect (EPR) for 'passive targeting', which mainly improves local drug concentration and reduces nonspecific tissue biodistribution<sup>3-5</sup>. Nanovehicles can carry

a large payload of cargoes and be conveniently modified to perform desirable functions, such as controlling drug release<sup>6</sup>, improving blood circulation half-life<sup>7</sup>, increasing bioavailability, and bypassing multidrug resistance mechanism<sup>8,9</sup>.

The most commonly used nanovehicles include liposomes<sup>10</sup>, micelles<sup>11</sup>, dendrimers<sup>12</sup>, nanoparticles<sup>13</sup>, and inorganic materials<sup>14</sup>. However, several barriers block clinical translocation of these nanovehicles to a certain extent because of the premature release and early extraction before reaching the target, uncontrollable rate of release to obtain low local concentration, and inefficient cellular uptake and endosomal escape<sup>15-17</sup>. Thus, controlled drug delivery systems should be designed. In such systems, controlled drug release at special time and space on demand can be achieved with a 'zero release' effect in blood circulation to protect healthy tissues from toxic drugs and to prevent drug decomposition. Several controlled drug delivery nanovehicles based on organic platforms have been fabricated<sup>18-20</sup>. Discoveries based on inorganic materials have recently opened up new and exciting possibilities in designing controlled drug delivery systems. These materials include gold nanoparticles<sup>14</sup>, magnetic nanoparticles<sup>21</sup>, and silica nanoparticles<sup>22</sup>.

Among these inorganic materials, mesoporous silica nanoparticles

Correspondence to: Xing-Jie Liang; Jian-Ping Zhou  
E-mail: liangxj@nanoctr.cn; zhoujpcpu@126.com.

Received January 9, 2014; accepted February 10, 2014.

Available at [www.cancerbiomed.org](http://www.cancerbiomed.org)

Copyright © 2014 by Cancer Biology & Medicine



(MSNs) have aroused significant interest and rapidly developed into an important candidate for nanomedical applications since a MCM-41-type mesoporous silica material was first reported as a drug delivery system in 2001<sup>23</sup>. As shown in **Figure 1**, the simple, scalable, and cost-effective fabrication, as well as non-toxic nature, large surface area and pore volume, and high density silanol-containing surface are apparent advantages of MSNs. On one hand, the textural characteristics of MSNs increase the loading amount of anti-cancer drugs that are encapsulated in pore tunnels. On the other hand, the silanol-containing surface can be easily modified with various molecules, resulting in an enhanced profile for the pharmacokinetics and pharmacodynamics of therapeutic agents<sup>22</sup>. Moreover, the nanotunnels that encapsulate cargoes can be sealed with various gatekeepers, and such cargoes will not be released until triggered by stimuli, which offers an opportunity to design stimuli-responsive drug delivery systems for controlled release.

The stimulus can be divided into endogenous stimulus and exogenous stimulus<sup>17</sup>. Endogenous stimuli arise from the microenvironment differences between normal tissues and tumor, such as reduced intercellular/intracellular pH, higher redox potential, and increased level of certain enzymes<sup>24,25</sup>. However, exogenous stimuli are based on extracorporeal physical alterations, including temperature changes, magnetic fields, ultrasounds, as well as light and electric fields<sup>17</sup>. Among these stimuli, low pH is easy to achieve and has become the focus of numerous investigations in oncology because the extracellular pH of normal tissues and blood is approximately 7.4, whereas that in a tumor microenvironment is between 6.0 and 7.0, which is mainly caused by high glycolysis rate and high level of CO<sub>2</sub><sup>26</sup>. The pH value will drop further from the extracellular microenvironment of a tumor to intracellular organelles, such

as endosomes (pH=5.5) and lysosomes (pH<5.5). Therefore, the abnormal pH gradients combined with the advantages of MSNs provide opportunities to realize pH-responsive MSNs as controlled drug delivery systems for cancer treatment.

Many groups have reported on pH-responsive MSNs modified with various gatekeepers. The triggered release of anti-cancer drugs from nanotunnels of mesoporous materials has mainly been achieved by using polyelectrolytes, supramolecularnanovalves, pH-sensitive linkers, and acid-decomposable inorganic materials<sup>27</sup>.

In this paper, we review the recent advances in drug delivery of pH-responsive MSNs with four categories of gatekeepers for cancer treatment based on tumor microenvironment.

### pH-responsive MSNs with polyelectrolytes gatekeepers

Polyelectrolytes, which are polymers with repeating units that bear electrolyte groups, are either absorbed or covalently bonded to the surface of MSNs to serve as a mechanized stimulus-responsive release system by transformation under different pH values<sup>28</sup>. Under neutral or weakly basic conditions, the polyelectrolytes tightly wrap around the particle surface and block multiple openings. With decreasing pH value, the polyelectrolytes are triggered to go through swelling or coiling so that the cargoes are released from the unblocked pores<sup>29</sup>.

Feng *et al.*<sup>30</sup> synthesized a type of pH-responsive MSNs with polyelectrolyte multilayers (PEM) composed of poly (allylamine hydrochloride) (PAH) and sodium poly(styrene sulfonate) (PSS) using a layer-by-layer technique. A schematic illustration of the construction and release mechanism of PEM-MSNs is shown in **Figure 2A and 2B**. The PEM-MSNs with eight polymer layers

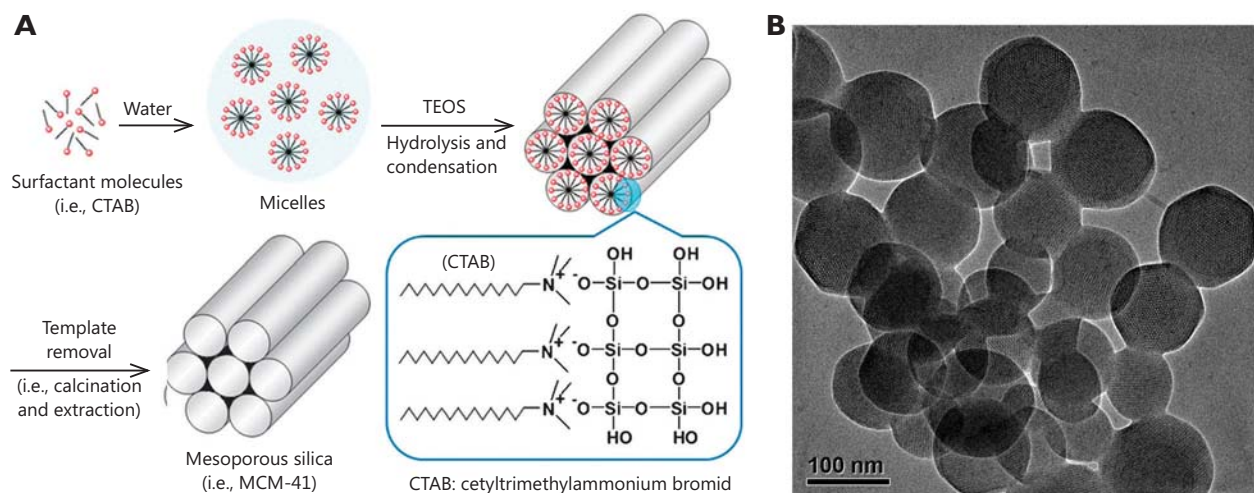


**Figure 1** Synthesis scheme for the preparation of MSNs (A) and transmission electron microscopy (TEM) images of MCM-41 (B). (**Figure 1A** is adapted from Ref. 22 with permission of The Royal Society of Chemistry).

possess maximum encapsulation efficiency, and the release of DOX is accelerated under acidic conditions with incompact PAH/PSS multilayers (**Figure 2C**). In HeLa cells, DOX-loaded PEM-MSNs are almost distributed in the cytoplasm within 6 h, and some DOX is released from carriers into the nucleus for 12 h. Meanwhile, free DOX rapidly enter cancer cells and accumulate in the nucleus within 0.5 h. Thus, DOX-loaded PEM-MSNs are internalized into endosomes/lysosomes, and then pH-triggered DOX release occurs from nanotunnels because of the low pH ( $\sim 5.0$ ) in the endosomes/lysosomes followed by the delivery of

released DOX from cytoplasm to nucleus. This process prolongs the accumulation of DOX in the nucleus to enhance the anti-cancer efficiency. Moreover, the blood profiles of DOX after intravenous injection of free DOX and DOX-loaded MSNs show different patterns (**Figure 2D**). The majority of free DOX have a rapid clearance within 2 h of administration, followed by a slow clearance phase. By contrast, DOX-loaded PEM-MSNs show low and sustained drug concentration in rat plasma up to 24 h post-injection, possibly because of the relatively high pH value of blood and the close state of PEM-MSNs. Furthermore,

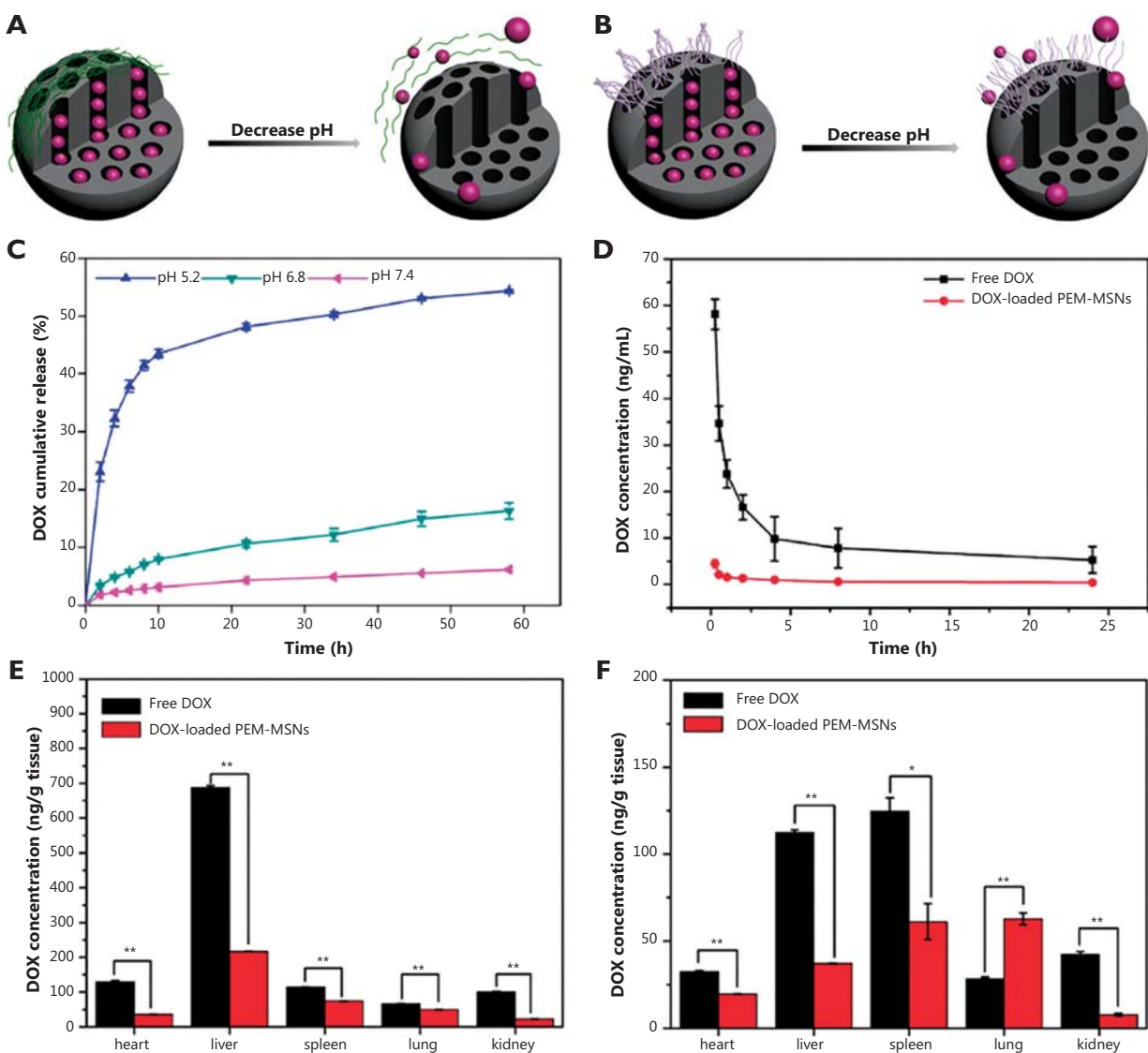


**Figure 2** Graphical representation of pH-responsive MSNs with polyelectrolyte multilayers (A) and polyelectrolyte brushes (B). Release profiles of DOX from PEM-MSNs (eight layers) in different pH media (C). DOX concentrations in plasma after DOX and DOX-loaded PEM-MSNs were injected intravenously through the vein for incremental time (D). Biodistribution of DOX in healthy SD rats at 2 h (E) and 24 h (F) after DOX and DOX-loaded PEM-MSNs at 2 mg/kg DOX equivalent were injected intravenously through the vein. \* $P < 0.05$  and \*\* $P < 0.01$  compared with free DOX group. (**Figure 2C,D,E,F** are adapted from Ref. 30 with permission from The Royal Society of Chemistry).

the determination of DOX levels in major organs, as well as the histological examination, indicates that DOX-loaded PEM-MSNs have lower systemic toxicity than free DOX (**Figure 2E,F**).

Sun *et al.*<sup>31</sup> selected poly[2-(diethylamino)ethyl methacrylate] (PDEAEMA) to functionalize the MSNs through the surface-initiated atom transfer radical polymerization of DEAEEMA. Under neutral and alkaline conditions, PDMAEMA chains are prone to aggregate together with polymer chain-chain interactions to seal the nanotunnels of MSNs. However, under acid conditions, the tertiary amine in PDEAEMA can easily obtain a proton to form quaternary ammonium. This process is followed by polymer chain stretching with the electrostatic repulsions and strong chain-solvent interaction (**Figure 2B**), which facilitates cargo release. Yang *et al.*<sup>32-36</sup> also studied the ways by which to employ polyelectrolytes as pH-responsive gatekeepers. For instance, in their pH-sensitive system of poly (glutamic acid) grafted MSNs (MSN-PLGA), the drug loading experiment was performed at pH 8.0 because of the electrostatic attraction between DOX and the nanoparticles. The drug release behavior of MSN-PLGA loaded DOX was then studied at different pH values (5.5, 6.8, and 7.4). The results indicated that MSN-PLGA had high drug loading efficiency and exhibited a significantly pH-dependent drug release behavior. This finding can be attributed to the fact that the protonation of poly (glutamic acid) with decreasing pH results in the dissociation of the electrostatic interaction between PLGA and DOX and consequently facilitates DOX release. Many other polyelectrolytes were developed as gatekeepers for designing pH-responsive MSNs, such as poly(4-vinyl pyridine)<sup>37</sup>, chitosan<sup>38,39</sup> and poly(acrylic acid)<sup>40</sup>. Thus, the weak acid tumor tissues make pH-responsive release systems suitable for the controlled release of anti-cancer drugs.

## pH-responsive MSNs with supramolecularnanovalves

The development of supramolecular chemistry enabled supramolecular assembly to be made into a 'nanovalve' machine responding to various stimuli, such as chemical, light, and electrical stimuli<sup>41</sup>. The supramolecularnanovalve, as a gatekeeper for controlling cargo release, includes an immobilized stalk molecule covalently attached to silica surface and a mobile cyclic molecule encircling the stalk via non-covalent interactions<sup>29</sup>. Under certain conditions, the binding constant between cyclic caps and stalks weakens, thus resulting in large-amplitude sliding motions of the caps and the unblocking of nanotunnels. Therefore, supramolecularnanovalves provide opportunities for MSNs to construct a pH-responsive drug delivery system for responding to weak acidic tumor tissues (**Figure 3A**).

Meng *et al.*<sup>42</sup> reported a novel MSNs delivery system based on the function of  $\beta$ -cyclodextrin ( $\beta$ -CD) nanovalves that were responsive to the acidic conditions of endosomes in cancer cells. In this system, *N*-methylbenzimidazole is chosen to serve as stalks for the optimized  $pK_a$  (5.67) (**Figure 3B**), which binds to the  $\beta$ -CD rings strongly at pH 7.4 with trapping cargoes in nanotunnels while causing dissociation with the  $\beta$ -CD caps at pH <6 in the acidifying endosomal compartment. The profiles of drug release accompanied by  $\beta$ -CD detachment from MSNs before and after acid stimuli are presented in **Figure 3C**, which shows typical pH-responsive release characteristics. To improve the rate and quantity of DOX release, the interior of the silica surface is modified with 7.5% ammonium (**Figure 3D**). In squamous carcinoma (KB-31) cells, DOX-loaded nanoparticles are taken up into the perinuclear regions efficiently within 3 h, where drug release to the nucleus is observed. The release is followed by apoptosis at 60 h, nuclear fragmentation after 80 h, and finally cell death (**Figure 3E**, left panel). However, the release profile of DOX dramatically changes after  $NH_4Cl$  treatment of KB-31 cells, in which most drugs are retained inside nanotunnels and little evidence of nuclear staining and cell death is observed (**Figure 3E**, right panel). In addition, quantitative analysis of the nuclear DOX fluorescence signal and MTS assays further confirm that the cargo release caused by lysosomal acidification is made feasible by the pH-sensitive nanovalves during *in vitro* operation.

Similarly, Du *et al.*<sup>43</sup> successfully synthesized a biocompatible pH-responsive nanovalve based on MSNs comprising  $\alpha$ -cyclodextrin ( $\alpha$ -CD) rings and *p*-anisidino linkers modified on the silica surface. Luminescence spectroscopy demonstrates that the pH-responsive system exhibits good bio-stability and no drug leakage at pH ~7.4, as well as excellent drug release performance not only in  $H_2O$  but also in cell culture medium at pH ~5.5 upon the protonation of *p*-anisidino nitrogen atoms (part of the linker). Therefore, Du *et al.* explored the applications of the  $\alpha$ -CD nanovalves based on MSNs by testing their delivery capability in different types of human cancer cells at lysosomal pH levels.

In addition, cucurbit[n]uril, the structure of which is similar to cyclodextrin, is capable of blocking the pores of MSNs as nanovalves and of preventing the cargoes from leaking out until they are detached from the stalks or positioned far away from the pore entrances by sliding under acidic stimuli<sup>41</sup>. In a typical design, Angelos *et al.*<sup>44</sup> developed supramolecularnanovalves composed of cucurbit(6)uril [CB(6)]/trisammoniumpseudorotaxanes that are attached to MSNs surfaces and encapsulate cargo molecules at neutral pH and then release the cargoes under mildly acidic conditions. Owing to the difference in the binding affinity of CB(6) with  $NH_3^+(CH_2)_6NH_3^+$  and  $NH_3^+(CH_2)_4NH_3^+$ , the CB(6)

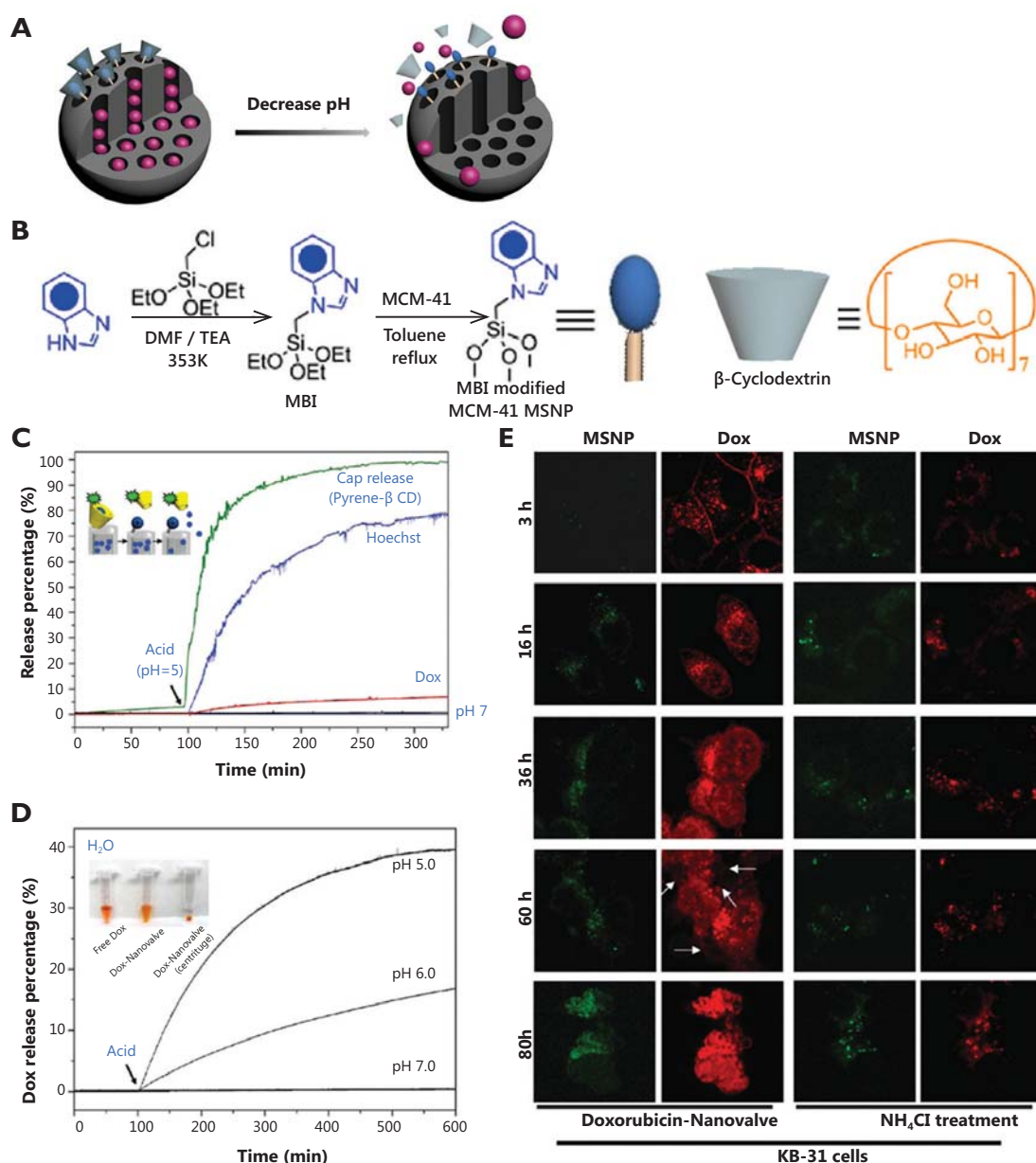


**Figure 3** Graphical representation of the pH-responsive MSNs with supramolecular nanovalves (A). Synthesis of the stalk on the surface of MSNs for further  $\beta$ -CD capping on the pore (B). Fluorescence intensity plots for the release of Hoechst dye, doxorubicin, and the pyrene-loaded cyclodextrin cap from MSNs (C) and release profiles of doxorubicin from ammonium-modified (7.5%, w/w) nanoparticles showing a faster and larger response compared with that of unmodified MSNs (D). Confocal images of KB-31 cells incubated with MSNs containing doxorubicin for the indicated times: KB-31 cancer cells effectively endocytosed the doxorubicin-loaded FITC-MSNs at 3 h. This action is followed by nuclear fragmentation after 80 h. However, with  $\text{NH}_4\text{Cl}$  treatment, most of the doxorubicin was confined to nanoparticles, such that no observable cell death occurred (E). (Figure 3B,C,D,E are adapted with permission from Ref. 42. Copyright 2010, American Chemical Society).

ring shuttles to the distal hexamethylenediammonium recognition unit once the anilinium nitrogen atom protonated, which then unblocks the pore orifice and facilitates cargo release. More importantly, the pH at which the MSNs system responds can be tuned through rational chemical modification of the stalk.

### pH-responsive MSNs with pH-sensitive linkers

The pH-sensitive linkers, such as acetal bond, hydrazine bond, and ester bond can be cleaved with decreasing pH value, thus



providing opportunities for designing pH-responsive MSNs. On one hand, the pH-sensitive linkers modified over the pore entrances of MSNs can induce bulky groups as nanogates to block the pores and control drug release (**Figure 4**). On the other hand, the pH-sensitive linkers can also be modified in the nanotunnels to bond with drugs covalently. These drugs will then be released with the cleavage effects of linkers between drugs and MSNs under acidic conditions.

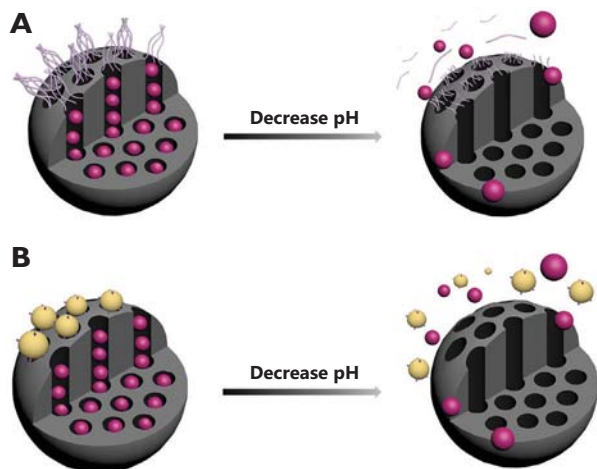


**Figure 4** Graphical representation of the pH-responsive MSNs capped with polymers (A) and nanoparticles (B) that linked to the surface of MSNs via pH-sensitive linkers.

Gao *et al.*<sup>45</sup> employed functionalized MSNs as drug reservoirs and then blocked the mesopores with polypseudorotaxanes through pH-sensitive benzoic-imine bonds hydrolyzed under very weak acidic conditions but stable at neutral basic pH because of the proper  $\pi$ - $\pi$  conjugation extent. The polypseudorotaxanes consist of poly (ethylene glycol) (PEG) and  $\alpha$ -CD, with PEG serving as the guest polymer for CD hosts and imparting *in vivo* longevity to MSNs by preventing nonspecific protein adsorptions during the circulation. Under weak acidic tumor extracellular pH ( $\sim 6.8$ ), the benzoic-imine linkages begin partially hydrolyzing to accelerate DOX release and meanwhile generate positive amino groups to facilitate internalization of particles. Subsequently, in the more acidic endosomal pH ( $\sim 5.0$ ), the increasing hydrolysis of the benzoic-imine bond would intensify the removal of the polypseudorotaxane caps and thus accelerate the release of DOX into the cytoplasm. In HepG2 cells, DOX-loaded MSNs are initially located within endosomal intracellular compartments and release drugs in the cytosol region in a sustained manner. Moreover, the different results of confocal fluorescence microscopy and cytotoxicity assay

between cells exposed to DOX-loaded MSNs at pH =6.8 and pH =7.4 again prove that enhanced tumor-specific uptake and intracellular delivery can be achieved through the inclusion of the benzoic-imine linkage.

Analogously, Liu *et al.*<sup>46</sup> reported a new pH-responsive nanogated construction by capping gold nanoparticles onto mesoporous silica through acid-labile acetal linkers (**Figure 4B**). At neutral pH, the linker remains intact, and pores are blocked by gold nanoparticles to inhibit cargo diffusion. However, at acidic pH, the hydrolysis of the acetal group removes the caps and allows release of cargoes. Aside from bulky groups capped on the outlets via pH-sensitive linkers, Lee *et al.*<sup>47</sup> conjugated DOX to the inner wall of MSNs nanochannels via liable hydrazone bonds. Through EPR effects, the Atto-647-MSN-hydrazone-DOX inherently accumulates in solid tumors of the liver. Nanoparticles then highly concentrate within endosomes and lysosomes of cancer cells. Sustained release of drug payload is observed because of the leakage of hydrazone bonds at endosomal and lysosomal pH. Moreover, apart from DOX, the pH-sensitive drug release mechanism can be applied to other anti-cancer drugs that possess functional ketones or aldehydes.

### pH-responsive MSNs with acid-decomposable inorganic gatekeepers

The common strategies used for surface functionalization include grafting organic species. However, such strategies have been limited by tedious and intricate organic synthesis steps and the lack of a clear definition of the body toxicity of dismantled pore-blocking agents. Some acidic-decomposable inorganic materials have recently been reported as gatekeepers to control drug release, offering opportunities to design promising specific carriers for therapeutic agents (**Figure 5A**).

Rim *et al.*<sup>48</sup> introduced inorganic calcium phosphate (CaP) as a novel pore blocker through the enzyme-mediated mineralization on the MSN surface, which can be dissolved in intracellular endosomes as nontoxic ions to initiate drug release. The construction of the nanoparticle involves urease functionalization of MSN surfaces and subsequent enzyme-mediated surface CaP mineralization in the presence of urea under mild conditions within a short time. For pH-controlled DOX release from mineralized MSNs, pH variation between physiological pH (pH 7.4) and low pH (pH 4.5) is employed. The results show that a large amount of DOX was released after 24 h under low pH conditions (**Figure 5B**). Furthermore, the pH-dependent dissolution kinetics of Hap-like coating support the DOX release profiles from CaP capped MSNs (**Figure 5C**), which confirms that the dissolution of pore blocks results in the opening of the pore and then triggers DOX release.



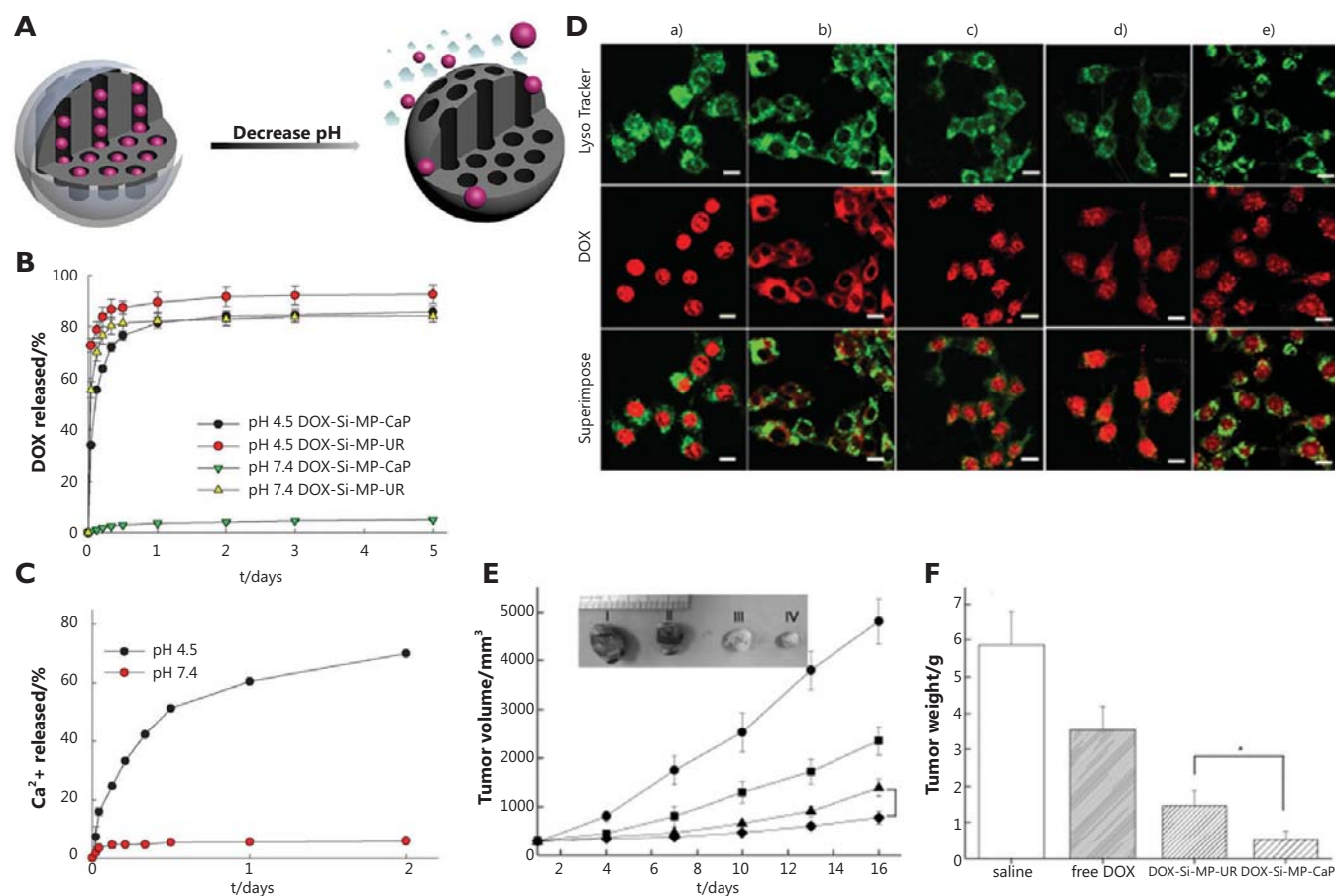


**Figure 5** (A) Graphical representation of pH-responsive MSNs with acid-decomposable inorganic gatekeepers. (B) DOX release profiles from DOX-Si-MP-UR and DOX-Si-MP-CaP under pH control. (C) Kinetics of calcium dissolution from DOX-Si-MP-CaP under pH control. (D) CLSM images of live MCF-7 cells treated with Lyso Tracker (50 nm), free DOX (5  $\mu\text{g/mL}$ ), and DOX-Si-MP-CaP (DOX = 5  $\mu\text{g/mL}$ ), thereinto, (a) free DOX for 1 h exposure; (b) DOX-Si-MP-CaP for 1 h exposure; (c) DOX-Si-MP-CaP for 5 h exposure; (d) DOX-Si-MP-UR for 1 h exposure; and (e) DOX-Si-MP-UR for 5 h exposure. (Green fluorescence is associated with Lyso Tracker; the red fluorescence is expressed by free DOX, released DOX, and DOX retained within MSNs). Scale bar: 20  $\mu\text{m}$ . (E) *In vivo* therapeutic efficacy after a single intratumoral injection of saline (●), free DOX (■), DOX-Si-MP-UR (▲), and DOX-Si-MP-CaP (◆) at a DOX-equivalent dose of 10 mg/kg. Inset: images of excised tumors at 16 days after treatment. I: saline, II: free DOX, III: DOX-Si-MP-UR, IV: DOX-Si-MP-CaP. (F) Tumor weights at 16 days after treatment. The results represent the means  $\pm$  SDs ( $n=4$ ); \* $P<0.05$ . (Figure 4B,C,D,E,F are adapted from Ref. 48 with permission of John Wiley and Sons).

In breast cancer MCF-7 cells, DOX-loaded mineralized MSNs (DOX-Si-MP-CaP) carry DOX in nanopores effectively before endocytosis, and DOX release can be facilitated in lysosomes by the dissolution of mineral coatings, followed by the DOX release and accumulation in the nucleus (Figure 5D). Moreover, the evaluation of the *in vivo* efficacy of DOX-Si-MP-CaP using xenograft models of MCF-7 human breast cancer shows that a single intratumoral administration of DOX-Si-MP-CaP is significantly more effective in tumor reduction than control groups including free DOX and DOX-Si-MP-UR (Figure 5E,F).

Muhammad *et al.*<sup>49</sup> employed acid-decomposable luminescent ZnO quantum dots (QDs) to seal the nanopores of MSNs in order to inhibit premature drug (DOX) release. After internalization into

HeLa cells, the ZnO QD lids are dissolved rapidly in the acidic intracellular compartments, followed by loaded drug release from MSNs into cytosol. In this pH-responsive drug delivery system, ZnO QDs behave as a dual-purpose entity that not only serves as a lid but also imposes a synergistic anti-tumor effect on cancer cells. Zheng *et al.*<sup>50</sup> reported a pH-responsive controlled release system via using acid-decomposable layered double hydroxides (LDHs) as inorganic nanovalves, by virtue of the electrostatic interaction of LDH nanosheets on the surface of MSNs. The preparation procedure of the pH-responsive MSNs is free from complicated organic synthesis. Guest molecules are loaded and encapsulated in neutral and released in acidic pH depending on the dissolution of LDHs. Thus, acid-decomposable inorganic materials are promising

candidates for designing pH-responsive MSNs.

## Conclusion and outlook

In this review, we highlighted the exciting research advances on pH-responsive drug delivery systems based on MSNs. Various materials can be used as gatekeepers to control drug release under acidic conditions. These materials have great potential for application in tumor therapy and for improving anti-cancer drug efficiency and decreasing side effects. However, most work is focused on *in vitro* studies<sup>51</sup>. Thus, several challenges still need to be overcome for the further advancement of the biological and biomedical applications of pH-responsive MSNs. First, the differences in the pH values between tumor microenvironment and normal tissues are minimal, making the manipulation of the stimuli-responsive drug delivery system *in vivo* via pH difficult. Second, the targeting effects of pH-responsive MSNs depending on EPR effects are low, thus causing nanoparticles accumulation in some organs, such as the heart, liver, and spleen. Upon accumulation in normal tissues, MSNs can be internalized into cells via endocytosis to trigger drug release, which may result in side effects. Third, the biodistribution, acute and chronic toxicities, changes in molecule level, long-term stability, and circulation properties of stimulus-responsive drug delivery systems need to be further investigated before implementation in clinical practice. Therefore, future work in designing stimulus-responsive MSNs will most likely be directed toward the integration of multiple stimuli strategies that can respond to two or more stimuli simultaneously and can bear targeting molecules for efficiently directing the nanoparticles to tumor tissues, with low toxicity and good pharmacokinetic profile.

## Acknowledgements

This work was supported by the Chinese Natural Science Foundation Project (Grant No. 30970784 and 81171455), a National Distinguished Young Scholars Grant (Grant No. 31225009) from the National Natural Science Foundation of China, the National Key Basic Research Program of China (Grant No. 2009CB930200), the Chinese Academy of Sciences (CAS) 'Hundred Talents Program' (Grant No. 07165111ZX), the CAS Knowledge Innovation Program, and the State High-Tech Development Plan (Grant No. 2012AA020804). The authors also appreciate the support by the 'Strategic Priority Research Program' of the Chinese Academy of Sciences (Grant No. XDA09030301). This work was also supported in part by NIH/NIMHD 8 G12 MD007597 and USAMRMC W81XWH-10-1-0767 grants.

## Conflict of interest statement

No potential conflicts of interest are disclosed.

## References

1. Nazir S, Hussain T, Ayub A, Rashid U, MacRobert AJ. Nanomaterials in combating cancer: therapeutic applications and developments. *Nanomedicine* 2014;10:19-34.
2. Farokhzad OC, Langer R. Impact of nanotechnology on drug delivery. *ACS Nano* 2009;3:16-20.
3. Maeda H. The enhanced permeability and retention (EPR) effect in tumor vasculature: the key role of tumor-selective macromolecular drug targeting. *Adv Enzyme Regul* 2001;41:189-207.
4. Cho K, Wang X, Nie S, Chen ZG, Shin DM. Therapeutic nanoparticles for drug delivery in cancer. *Clin Cancer Res* 2008;14:1310-1316.
5. Davis ME, Chen ZG, Shin DM. Nanoparticle therapeutics: an emerging treatment modality for cancer. *Nat Rev Drug Discov* 2008;7:771-782.
6. Mu L, Feng SS. A novel controlled release formulation for the anticancer drug paclitaxel (Taxol): PLGA nanoparticles containing vitamin E TPGS. *J Control Release* 2003;86:33-48.
7. Prencipe G, Tabakman SM, Welsher K, Liu Z, Goodwin AP, Zhang L, et al. PEG branched polymer for functionalization of nanomaterials with ultralong blood circulation. *J Am Chem Soc* 2009;131:4783-4787.
8. Brigger I, Dubernet C, Couvreur P. Nanoparticles in cancer therapy and diagnosis. *Adv Drug Deliv Rev* 2002;54:631-651.
9. Cuvier C, Roblot-Treupel L, Millot JM, Lizard G, Chevillard S, Manfait M, et al. Doxorubicin-loaded nanospheres bypass tumor cell multidrug resistance. *Biochem Pharmacol* 1992;44:509-517.
10. Malam Y, Loizidou M, Seifalian AM. Liposomes and nanoparticles: nanosized vehicles for drug delivery in cancer. *Trends Pharmacol Sci* 2009;30:592-599.
11. Blanco E, Kessinger CW, Sumer BD, Gao J. Multifunctional micellar nanomedicine for cancer therapy. *Exp Biol Med* (Maywood) 2009;234:123-131.
12. Nanjwade BK, Bechra HM, Derkar GK, Manvi FV, Nanjwade VK. Dendrimers: emerging polymers for drug-delivery systems. *Eur J Pharm Sci* 2009;38:185-196.
13. Liu Z, Jiao Y, Wang Y, Zhou C, Zhang Z. Polysaccharides-based nanoparticles as drug delivery systems. *Adv Drug Deliv Rev* 2008;60:1650-1662.
14. Ghosh P, Han G, De M, Kim CK, Rotello VM. Gold nanoparticles in delivery applications. *Adv Drug Deliv Rev* 2008;60:1307-1315.
15. Talelli M, Iman M, Varkouhi AK, Rijcken CJ, Schiffelers RM, Etrych T, et al. Core-crosslinked polymeric micelles

- with controlled release of covalently entrapped doxorubicin. *Biomaterials* 2010;31:7797-7804.
16. Andresen TL, Jensen SS, Jørgensen K. Advanced strategies in liposomal cancer therapy: problems and prospects of active and tumor specific drug release. *Prog Lipid Res* 2005;44:68-97.
  17. Mura S, Nicolas J, Couvreur P. Stimuli-responsive nanocarriers for drug delivery. *Nat Mater* 2013;12:991-1003.
  18. Sawant RR, Torchilin VP. Liposomes as 'smart' pharmaceutical nanocarriers. *Soft Matter* 2010;6:4026-4044.
  19. Zhang Q, Ko NR, Oh JK. Recent advances in stimuli-responsive degradable block copolymer micelles: synthesis and controlled drug delivery applications. *Chem Commun (Camb)* 2012;48:7542-7552.
  20. Kojima C. Design of stimuli-responsive dendrimers. *Expert Opin Drug Deliv* 2010;7:307-319.
  21. Yuan Q, Venkatasubramanian R, Hein S, Misra RD. A stimulus-responsive magnetic nanoparticle drug carrier: magnetite encapsulated by chitosan-grafted-copolymer. *Acta Biomater* 2008;4:1024-1037.
  22. Yang P, Gai S, Lin J. Functionalized mesoporous silica materials for controlled drug delivery. *Chem Soc Rev* 2012;41:3679-3698.
  23. Chen T, Fu J. pH-responsive nanovalves based on hollow mesoporous silica spheres for controlled release of corrosion inhibitor. *Nanotechnology* 2012;23:235605.
  24. Torchilin V. Multifunctional and stimuli-sensitive pharmaceutical nanocarriers. *Eur J Pharm Biopharm* 2009;71:431-444.
  25. Zhu L, Torchilin VP. Stimulus-responsive nanopreparations for tumor targeting. *Integr Biol (Camb)* 2013;5:96-107.
  26. Danhier F, Feron O, Préat V. To exploit the tumor microenvironment: Passive and active tumor targeting of nanocarriers for anti-cancer drug delivery. *J Control Release* 2010;148:135-146.
  27. Xing L, Zheng H, Cao Y, Che S. Coordination polymer coated mesoporous silica nanoparticles for pH-responsive drug release. *Adv Mater* 2012;24:6433-6437.
  28. Fu Q, Rao GR, Ista LK, Wu Y, Andrzejewski BP, Sklar LA, et al. Control of molecular transport through stimuli-responsive ordered mesoporous materials. *Adv Mater* 2003;15:1262-1266.
  29. Li Z, Barnes JC, Bosoy A, Stoddart JF, Zink JI. Mesoporous silica nanoparticles in biomedical applications. *Chem Soc Rev* 2012;41:2590-2605.
  30. Feng W, Zhou X, He C, Qiu K, Nie W, Chen L, et al. Polyelectrolyte multilayer functionalized mesoporous silica nanoparticles for pH-responsive drug delivery: layer thickness-dependent release profiles and biocompatibility. *J Mater Chem B* 2013;1:5886-5898.
  31. Sun JT, Hong CY, Pan CY. Fabrication of PDEAEMA-coated mesoporous silica nanoparticles and pH-responsive controlled release. *J Phys Chem C* 2010;114:12481-12486.
  32. Chang B, Sha X, Guo J, Jiao Y, Wang C, Yang W. Thermo and pH dual responsive, polymer shell coated, magnetic mesoporous silica nanoparticles for controlled drug release. *J Mater Chem* 2011;21:9239-9247.
  33. Chen Y, Yang W, Chang B, Hu H, Fang X, Sha X. In vivo distribution and antitumor activity of doxorubicin-loaded N-isopropylacrylamide-co-methacrylic acid coated mesoporous silica nanoparticles and safety evaluation. *Eur J Pharm Biopharm* 2013;85:406-412.
  34. Tang H, Guo J, Sun Y, Chang B, Ren Q, Yang W. Facile synthesis of pH sensitive polymer-coated mesoporous silica nanoparticles and their application in drug delivery. *Int J Pharm* 2011;421:388-396.
  35. Zheng J, Tian X, Sun Y, Lu D, Yang W. pH-sensitive poly(glutamic acid) grafted mesoporous silica nanoparticles for drug delivery. *Int J Pharm* 2013;450:296-303.
  36. Wen H, Guo J, Chang B, Yang W. pH-responsive composite microspheres based on magnetic mesoporous silica nanoparticle for drug delivery. *Eur J Pharm Biopharm* 2013;84:91-98.
  37. Liu R, Liao P, Liu J, Feng P. Responsive Polymer-Coated Mesoporous Silica as a pH-Sensitive Nanocarrier for Controlled Release. *Langmuir* 2011;27:3095-3099.
  38. Popat A, Liu J, Lu GQ, Qiao SZ. A pH-responsive drug delivery system based on chitosan coated mesoporous silica nanoparticles. *J Mater Chem* 2012;22:11173-11178.
  39. Hu X, Wang Y, Peng B. Chitosan-capped mesoporous silica nanoparticles as pH-responsive nanocarriers for controlled drug release. *Chem Asian J* 2014;9:319-327.
  40. Yuan L, Tang Q, Yang D, Zhang JZ, Zhang F, Hu J. Preparation of pH-responsive mesoporous silica nanoparticles and their application in controlled drug delivery. *J Phys Chem C* 2011;115:9926-9932.
  41. Yang YW. Towards biocompatible nanovalves based on mesoporous silica nanoparticles. *Med Chem Comm* 2011;2:1033-1049.
  42. Meng H, Xue M, Xia T, Zhao YL, Tamanoi F, Stoddart JF, et al. Autonomous in vitro anticancer drug release from mesoporous silica nanoparticles by pH-sensitive nanovalves. *J Am Chem Soc* 2010;132:12690-12697.
  43. Du L, Song H, Liao S. A biocompatible drug delivery nanovalve system on the surface of mesoporous nanoparticles. *Micropor Mesopor Mat* 2012;147:200-204.
  44. Angelos S, Khashab NM, Yang YW, Trabolsi A, Khatib HA, Stoddart JF, et al. pH clock-operated mechanized nanoparticles. *J Am Chem Soc* 2009;131:12912-12914.
  45. Gao Y, Yang C, Liu X, Ma R, Kong D, Shi L. A multifunctional nanocarrier based on nanogated mesoporous silica for enhanced tumor-specific uptake and intracellular delivery. *Macromol Biosci*

- 2012;12:251-259.
46. Liu R, Zhang Y, Zhao X, Agarwal A, Mueller LJ, Feng P. pH-responsive nanogated ensemble based on gold-capped mesoporous silica through an acid-labile acetal linker. *J Am Chem Soc* 2010;132:1500-1501.
  47. Lee CH, Cheng SH, Huang IP, Souris JS, Yang CS, Mou CY, et al. Intracellular pH-responsive mesoporous silica nanoparticles for the controlled release of anticancer chemotherapeutics. *Angew Chem Int Ed Engl* 2010;49:8214-8219.
  48. Rim HP, Min KH, Lee HJ, Jeong SY, Lee SC. pH-Tunable calcium phosphate covered mesoporous silica nanocontainers for intracellular controlled release of guest drugs. *Angew Chem Int Ed Engl* 2011;50:8853-8857.
  49. Muhammad F, Guo M, Qi W, Sun F, Wang A, Guo Y, et al. pH-Triggered controlled drug release from mesoporous silica nanoparticles via intracellular dissolution of ZnO nanolids. *J Am Chem Soc* 2011;133:8778-8781.
  50. Zheng Q, Hao Y, Ye P, Guo L, Wu H, Guo Q, et al. A pH-responsive controlled release system using layered double hydroxide (LDH)-capped mesoporous silica nanoparticles. *J Mater Chem B* 2013;1:1644-1648.
  51. Tang F, Li L, Chen D. Mesoporous silica nanoparticles: synthesis, biocompatibility and drug delivery. *Adv Mater* 2012;24:1504-1534.
- Cite this article as:** Yang KN, Zhang CQ, Wang W, Wang PC, Zhou JP, Liang XJ. pH-responsive mesoporous silica nanoparticles employed in controlled drug delivery systems for cancer treatment. *Cancer Biol Med* 2014;11:34-43. doi: 10.7497/j.issn.2095-3941.2014.01.003



## Appendix 7      Reprints of Abstracts

- a) Wright D, Lin S, Lin PC, Wu CS, Zhang D, Duerinckx A, Wang PC, Lee DL. **Measuring Renal Oxygenation in a Mouse Model of Volume-Dependent Hypertension using BOLD MRI.** Radiological Society of Northern America, Chicago, IL, Dec 1-6, 2013.

**Purpose:** Hypertension is closely associated with the progression of kidney damage and dysfunction. Tissue hypoxia in the hypertensive kidney contributes to the progression of kidney damage. Peroxisome proliferator activated receptor- $\alpha$  (PPAR- $\alpha$ ) is a nuclear receptor that plays an important role in reducing volume-dependent hypertension. Previous reports demonstrate that a slow pressor dose of Angiotensin II (Ang II) is a model of volume-dependent hypertension. The goal of this study was to determine the role of PPAR- $\alpha$  on renal oxygenation using blood oxygen level-dependent (BOLD) MRI in a model of volume-dependent hypertension.

**Materials and Methods:** Wild-type (WT) and PPAR- $\alpha$  knockout (KO) mice were imaged using a multiple gradient echo BOLD sequence (12 echoes from 3.2-54ms, TR=900ms) on a 9.4T MRI to measure functional changes in renal oxygenation. Imaging was performed during baseline, day 12 of Ang II (400 ng/kg/min), and 9 days after Ang II-treatment (recovery). T2\* relaxation time was measured in the cortex and medulla of the kidney.

**Results:** Cortex T2\* values were lower in KO vs WT during baseline ( $11.0 \pm 1.1$  ms vs  $13.1 \pm 1.5$  ms), day 12 of Ang II ( $11.6 \pm 1.2$  ms vs  $16.2 \pm 1.5$  ms) and 9 days after Ang II ( $12.5 \pm 0.7$  ms vs  $15.2 \pm 0.3$  ms). Medulla T2\* values were lower on day 12 of Ang II in KO ( $16.5 \pm 2.5$  ms) vs WT ( $20 \pm 1.6$  ms) mice. Medulla T2\* values were similar between KO and WT mice during baseline and the recovery period. In KO and WT mice, cortex T2\* values were lower than that of the medulla, indicative of different metabolic functions between the two tissues.

**Conclusion:** PPAR- $\alpha$  plays an important role in blood pressure regulation and renal oxygenation in the cortex and medulla of the kidney during Ang II-induced hypertension.

**Clinical Relevance Statement:** Hypertension is a risk factor for chronic kidney disease when untreated. BOLD MRI can aid in monitoring renal oxygenation changes during hypertension and determine therapeutic interventions in humans.

- b) Wang PC. **Nanoparticles as Targeted Drug Delivery Vehicles for Molecular Imaging and Chemotherapy Applications.** Taiwan Industrial Technology Research Institute, HsinChu, Taiwan. December 10, 2013.

Nanotechnology is a multidisciplinary scientific undertaking involving the creation and utilization of materials, devices, or systems on the nanometer scale. It is currently undergoing explosive development on many fronts and is expected to spark innovation and play a critical role in various biomedical applications, especially in drug delivery. Advances in nanotechnology that enable drugs to preserve their efficacy while being delivered to precise therapeutic targets are creating a host of opportunities for drug developers. By combining nanotechnology-based target-specific drug therapy with methods for early diagnosis of pathologies, we are getting closer to creating the ultimate functional drug carrier for personalized medicine. In this presentation, the molecular imaging techniques based on optical imaging and MRI will briefly be introduced. Two research studies, (1) using liposome labeled florescent dye and encapsulated MRI contrast agent as a dual probe for imaging, and (2) using metallofullerene nanoparticles to circumvent tumor resistance to cisplatin, will be presented as examples of applications of nanotechnology in imaging and therapy. Some challenges of using nanoparticles as drug delivery vehicles will also be presented.

- c) Zhang Z, Wang J, Nie X, Chen C, Wang PC. **Near Infrared Laser Mediated Targeted Tumor Thermo-chemotherapy Using Thermosensitive Polymer Coated Gold Nanoparticles.** Howard University Research Day 2014. Washington DC. April 4, 2014.

**Background:** Targeted delivery of therapeutic agents to tumors has the potential to increase efficacy while minimizing side effects. Poly(N-isopropylacrylamide) is a thermosensitive polymer that can shrink when heated in water. Combined with the photothermal effect of gold nanorods, a nanocomposite was created for the laser-mediated targeted therapy of tumors.

**Methods:** Mesoporous silica and Poly(N-isopropylacrylamide) was coated onto the surface of gold nanorods and loaded with Doxorubicin to form a nanocomposite. This was administered to breast cancer tumor bearing mice, followed by near-infrared laser irradiation of the tumor. The biodistribution of the nanocomposite was analysed using inductively coupled plasma mass spectrometry. Therapeutic efficacy was evaluated by daily size measurements and the final weight of the tumor after 14 days.

**Results:** Laser irradiation caused solution heating, which decreased the nanocomposite size and dissociated the electrostatically absorbed Doxorubicin releasing it. The accumulation of the nanocomposite and its payloads was significantly enhanced by laser irradiation. The nanocomposite with laser treatment almost completely inhibited tumor growth, which was significantly better than nanocomposite or laser treatment alone.

**Conclusions:** The photothermal and thermosensitive properties were successfully combined to facilitate laser-mediated targeted delivery of heat and doxorubicin to the tumor. The enhanced accumulation is probably due to the decreased size and increased tumor vascular permeability at elevated temperatures when the tumor was irradiated. Since the laser can be manipulated precisely and flexibly, this laser mediated nanocomposite provides a versatile platform to simultaneously deliver heat and anticancer drugs to tumor with facile control of the area, time, and dosage.

- d) Shan L, Lin S, Lin PC, Zhang Z, Liu Y, Wang PC. **Engineered Antibody Fragments and Immunotoxin for Targeted Imaging and Therapy of Prostate Cancer.** Howard University Research Day 2014. Washington DC. April 4, 2014.

**Background:** Prostate cancer is the most common malignancy and the second leading cause of cancer-related death among American men. This high mortality is mainly due to the inability to define early lesions and lack of an efficacious therapeutic technique.

**Methods:** By capitalizing upon the overexpression of prostate-specific membrane antigen (PSMA) in almost all prostate cancers and the high specificity of J591 antibody against the extracellular domain of PSMA, we engineered three antibody fragments including single-chain variable fragment (scFv), bivalent tandem scFv (biscFv), and bivalent scFv fold-back diabody (scfbDb), and further constructed a recombinant immunotoxin by fusing the diabody with a mutated diphtheria toxin moiety (DT390). The biological properties of the engineered fragments and the anti-tumor efficacy of the immunotoxin were studied in culture cells and animal models of prostate cancer.

**Results:** The binding affinity of scfbDb was 7-fold and 2.5-fold higher than that of the scFv and biscFv formats, respectively. In vitro, scfbDb efficiently mediated the entry of toxins into the PSMA-expressing LNCaP cancer cells, inducing cell apoptosis and growth arrest (IC<sub>50</sub>, ~0.57 nM). In animal models, the immunotoxin significantly inhibited the growth of LNCaP tumor xenografts, but not the growth of PSMA-negative PC-3 xenografts (0.27±0.09 vs. 0.67±0.11 g; P < 0.05). Specific tumor targeting was further confirmed with optical imaging. The data has been published in *Adv Healthc Mater* 2(5):736-44, 2013.

**Conclusions:** The engineered antibody fragments and immunotoxin could serve as a springboard to develop targeted imaging and therapeutic agents with high sensitivity and specificity against prostate cancers.

- e) Lin S, Shan L, Lin PC, Zhang Z, Gu X, Wang PC. **Construction of Transferrin Receptor-targeted Multimodality Agents for Cancer Imaging.** Howard University Research Day 2014. Washington DC. April 4, 2014.

**Background:** Transferrin receptor (TfR) is overexpressed in a wide variety of human tumors including head and neck squamous cell carcinoma (HNSCC) and breast cancer, serving as an optimal target for cancer imaging.

**Methods:** To achieve TfR-targeted imaging of tumors, we generated an optical imaging agent and further constructed a dual nanoprobe.

**Results:** Western blotting and immunocytochemistry showed TfR was overexpressed in all four HNSCC cell lines, compared with that in normal keratinocytes (OKFL). In the JHU-013 HNSCC tumor xenografts, specific accumulation of the optical imaging agent was clearly detected with optical imaging as early as 10 min and peaked at ~120 min after injection. A high fluorescent ratio of the tumor to muscle was obtained, which ranged from 1.42 to 4.15, depending on the tumor sizes. MRI and optical imaging studies showed that the dual nanoprobe could significantly enhance the image contrast of the MDA-MB-231 breast cancer xenografts. The tumor contrast enhancement in MRI exhibited a heterogeneous pattern, consistent to the pathologic heterogeneity of tumors. Pretreatment with Tf blocked the uptake of the probe reporters, indicating the specificity of the nanoprobe.

**Conclusions:** The optical imaging and the dual nanoprobe exhibited superior properties to the contrast agent of Magnevist and will be useful for detecting tumors, identifying the tumor pathologic features, and monitoring the tumor response to therapy.

- f) Wang PC. **Howard University Biomedical Core Facility.** Howard University Research Day 2014. Washington DC. April 4, 2014

The Howard Molecular Imaging Laboratory (MIL) is a university core facility to promote and support a sustainable long-term research using modern imaging technology to study the mechanism of disease processes and their response to therapy at the molecular, subcellular, cellular, and whole animal levels. The objectives of MIL are (1) to provide state-of-the-art instrumentation, technical expertise and essential services for molecular, cellular and in vivo imaging (2) to provide a broader training in biomedical imaging through methodology-centered seminars, workshops, mini-courses, and internships (3) to foster new multidisciplinary research collaborations using modern imaging techniques. The MIL has a 9.4T NMR machines for small animal imaging and MR spectroscopy studies, a Caliper Spectrum optical imaging machine, and an Olympus confocal microscope. The MIL provides expertise in imaging experiment design, and offers high resolution and high sensitivity MRI, optical imaging, and multiphoton confocal microscopy imaging services. The MIL also provides expertise and services in: development of efficient organ and intracellular targeting and amplification strategies, as well as in developing strategies for identifying suitable biomarkers, or imaginable gene products. The MIL provides assistance to develop nanoparticles with ligands to transfect cells with bioluminescent or fluorescent markers, targeted to specific receptors, proteins or biochemical pathways for in vitro and in vivo studies. Research supported by NIH/NIMHD 8 G12 MD007597, and DOD USAMRMC W81XWH-10-1-0767.

- g) Lin PC. **Assessment of chemical exchange kinetics through CPMG multiple spin-echo NMR measurements.** Howard University Research Day 2014. Washington DC. April 4, 2014.

A number of NMR spectroscopic methods possess the capability of assessing the dynamics of the ligand-receptor complex such as the kinetic rate constants. However, certain drawbacks including the titration procedure of gradually changing the concentration ratio between ligand and receptor limit the applications of these NMR methods, particularly in excluding the study of in vivo pharmacokinetics. To eliminate the disadvantage of being inaccessible to the in vivo investigation, we propose an alternative approach through use of fluorine-19 NMR spectroscopy equipped with a multiple of mixing bovine serum albumin (BSA) into a 6-fluoro-DL-tryptophan solution was selected to detect the kinetics of chemical exchange. In addition, dialysis membrane was used to separate the protein-ligand mixture from the ligand only solution, which mimics the intracellular and extracellular fluids in the body. The MSE NMR experiment was designed to measure a row of fluorine-19 signals at incrementally changed echo times to form a free induction decay, and the echo time interval in the MSE pulse sequence was adjusted to collect a series of free induction decays for examining the spin-spin T2 relaxation dispersion. A non-negative least squares algorithm was used for multiexponential T2 analysis to extract different T2 relaxation times that represent free and BSA bounded 6-fluoro-DL-tryptophan, respectively. Furthermore, quantification of free and BSA-bounded tryptophan can be achieved through individually integrating the corresponding peaks located around T2 relaxation times of 1 sec and 100-200 msec. This approach demonstrates the potential in the in vivo pharmacokinetics study.